HABILITATION À DIRIGER DES RECHERCHES

par

Pierre PUJOL

Sujet : Interactions, désordre et frustration en basses dimensions

Soutenue le 25 Novembre 2004 devant le Jury :

MM.	J. L. Barrat	
	D. Cabra	
	A. Castro-Neto	
	T. Giamarchi	Rapporteur
	P. Holdsworth	
	A. Honecker	
	T. Jolicoeur	Rapporteur
	D. Poilblanc	Rapporteur

Table des matières

Remerciements

Mes premiers remerciements vont bien sûr pour Chlöé, pour sa patience infinie avec moi et ses encouragements permanents. J'aimerais ensuite remercier Marc Magro, mon collègue et compagnon de bureau, pour sa patience aussi, ainsi que pour les nombreuses et passionnantes conversations en physique que nous avons presque au quotidien. Des remerciements très spéciaux aussi pour François Delduc, qui a méticuleusement relu ce manuscrit et qui a toujours été présent pour éclairsir mes doutes sur plusieurs sujets en physique.

Je remercie ensuite tous mes collègues du Laboratoire de Physique de l'ENS-Lyon, en particulier mes amis du groupe de théorie, grâce à qui l'ambiance au laboratoire a toujours été merveilleuse, et dont j'ai aussi beaucoup appris. Une pensée très spéciale aussi pour tous mes collègues de recherche, certains encore étudiants, d'autres des experts dans leurs sujets, et avec qui, pour certains, j'ai depuis déjà plusieurs années collaboré. L'apprentissage en physique et l'amitié qu'ils m'ont tous toujours apporté est tout simplement d'une valeur inestimable.

J'aimerais finalement remercier les rapporteurs et membres de mon jury pour avoir accepté cette tâche. Ils ont tous aussi, de façon directe pour certains, indirecte pour d'autres, contribué avec des conversations ou leurs articles à élargir mes connaissances en physique et la passion que je porte à cette discipline.

1 Curriculum Vitae

Date de naissance : 25 novembre 1968
Lieu de travail :
Laboratoire de Physique
École normale supérieure de Lyon
69364 Lyon Cedex 07, France
Telephone : (33) 04 72 72 85 19
Fax : (33) 04 72 72 87 77

1.1 Diplômes et expérience professionnelle

Diplômes :

1996 Doctorat en Physique Théorique, Université de Paris VI, "Théories Conformes et Systèmes Désordonnés", Mention Trés Honorable avec Félicitations du Jury.

1993 DEA de Physique Théorique, Université Pierre et Marie Curie (Paris VI) Mention Bien.

1991 Licenciatura en FISICA (CUM LAUDE), Université SIMON BOLIVAR (Caracas Vénézuéla).

Expérience professionnelle :

- Referee pour Physical Review Letters, Physical Review **B**, Journal of Physics **A** : Mathematical and General Physics, et Journal of Physics **C** : Condensed Matter.
- De juin 2002 à septembre 2003 : Scientifique visiteur au Département de Physique de Boston University, États Unis.
- De septembre 2002 à septembre 2003 : Scientifique détaché au CNRS, grade CR1.
- De janvier 2002 à décembre 2004 : Directeur d'un projet Procoppe de coopération avec le Département de Physique de l'Université de Braunsweig, Allemagne.
- De janvier 2001 à décembre 2004 : membre d'un projet de coopération ECOS-Sud avec le Département de Physique de l'Université de La Plata, Argentine.
- Depuis septembre 1998 : Maître de Conférences à l'École Normale Supérieure de Lyon.
- De novembre 1996 à au août 1998 : post-doctorat à la SISSA, Trieste, Italie.
- De septembre 1991 à août 1992 : Moniteur de Physique basique, Université SIMON BOLIVAR (Caracas Vénézuéla).

1.2 Liste de publications

Livres

[1] A. Alastuey, M. Magro et P. Pujol,
Méthodes théoriques en Physique,
En préparation.

[2] D. Cabra and P. Pujol
Field-theoretical methods in quantum magnetism
Chapitre du livre *Quantum Magnetism*,
Lecture Notes in Physics, Springer-Verlag Heidelberg,
U. Schollwöck, J. Richter, D. Farnell and R. Bishop Eds.

Articles de revues arbitrées :

[1] C. Castelnovo, C. Chamon, C. Mudry and P. Pujol
The quantum three-coloring dimer model and its line of critical points that is interrupted by quantum glassiness
preprint *cond-mat/0410562.*

[2] D.C. Cabra, M.D. Grynberg, P.C.W. Holdsworth, A. Honecker, P. Pujol, J. Richter, D. Schmalfuss, J. Schulenburg,
Quantum kagome antiferromagnet in a magnetic field : Low-lying non-magnetic excitations versus valence-bond crystal order
preprint *cond-mat/0404279.*

[3] C. Castelnovo, P. Pujol, and C. Chamon,
Dynamical obstruction in a constrained system and its realization in lattices of superconducting devices
Phys. Rev. **B 69**, 104529, 2004,
article sélectionné par les éditeurs pour paraître dans *Virtual Journal of Applications of Superconductivity*, Avril 2004.

[4] P. Pujol and J. Rech,
Site-centered impurities in quantum spin chains
Phys. Rev. **B 66**, 104401, 2002.

[5] D.C. Cabra, M.D. Grynberg, P.C.W. Holdsworth and P. Pujol,
From classical to quantum Kagome antiferromagnet in a magnetic field
Phys. Rev. **B 65**, 094418, 2002.

[6] D.C. Cabra, A. De Martino, P. Pujol and P. Simon,
Hubbard ladders in a magnetic field
Europhys. Lett. , **57** (3), 402, 2002.

[7] A. Honecker, M. Picco and P. Pujol
Nishimori point in the 2D +/- J random-bond Ising model
Phys. Rev. Lett. **87**, 047201, 2001.

[8] D.C. Cabra, A. De Martino, A. Honecker, P. Pujol and P. Simon,
Emergence of Irrationality : Magnetization Plateaux in Modulated Hubbard Chains
Phys. Rev. **B 63**, 094406, 2001.

[9] D.C. Cabra, A. De Martino, M. Grynberg, S. Peysson and P. Pujol,
Random bond XXZ chains with modulated couplings
Phys. Rev. Lett. **85**, 4791, 2000.

[10] D.C. Cabra, A. De Martino, A. Honecker, P. Pujol and P. Simon,
Doping-dependent magnetization plateaux in p-merized Hubbard chains
Phys. Lett. **A 268**, 418, 2000.

[11] D.C. Cabra, A. Honecker and P. Pujol,
Magnetic Properties of Zig-Zag Ladders
Eur. Phys. J. **B 13**, 55, 2000.

[12] D.C. Cabra, A. Honecker and P. Pujol,
Magnetization Plateaux in N-Leg Spin Ladders
Phys. Rev. **B 58**, pp. 6241, 1998.

[13] D.C. Cabra, P. Pujol and C. von Reichenbach,
Non-Abelian Bosonization and Haldane's Conjecture
Phys. Rev. **B 58**, pp. 65, 1998.

[14] D.C. Cabra, A. Honecker and P. Pujol,
Magnetization Curves of Antiferromagnetic Heisemberg Spin-1/2 Ladders
Phys. Rev. Lett. **79**, pp. 5126, 1997.

[15] D.C. Cabra, A. Honecker, G. Mussardo and P. Pujol,
A Non-Perturbative Approach to the Random-Bond Ising Model
Jour. Phys. A : Math. Gen. **30**, pp. 8415, 1997.

[16] V. Dotsenko, M. Picco and P. Pujol,
Randomly coupled minimal models
Phys. Lett. **B** vol 383, pp. 287, 1996.

[17] P. Pujol,
Effect of randomness in many coupled Potts models
Europhys. Lett., **35** (4), pp. 283, 1996.

[18] Vik. Dotsenko, V. Dotsenko, M. Picco and P. Pujol,
Renormalization Group Solution For The Two-Dimensional Random Bond Potts Model With Broken Replica Symmetry
Europhys. Lett. **32** (1995) 425.

[19] V. Dotsenko, M. Picco and P. Pujol,
Renormalisation group calculations of correlation functions for the 2D random bond Ising and Potts models
Nucl.Phys. **B455** (1995) 701.

[20] V. Dotsenko, M. Picco and P. Pujol,
Spin-spin critical point correlation functions for the 2D random bond Ising and Potts models
Phys.Lett. **B347** (1995) 113.

Articles de conférences

[1] D.C. Cabra, M.D. Grynberg and P. Pujol
Ground states of quantum kagome antiferromagnets in a magnetic field
Contribution to the Japanese-French symposium on "Quantum magnetism in spin, charge and orbital systems", Paris, Octobre 2003.

[2] P. Pujol,
Magnetic properties of quasi-one-dimensional strongly correlated systems,
Contribution to the proceedings of the "XXIV International Colloquium on Group Theoretical Methods in Physics", Paris, juillet 2002.

[3] A. Honecker, J. L. Jacobsen, M. Picco and P. Pujol,
Nishimori point in random-bond Ising and Potts models in 2D,
cond-mat/0112069. Contribution to the proceedings of the "NATO Adevnaced Research Workshop on Statistical Field Theories", Como, Italie, Juin 2001.

[4] D.C. Cabra, M. Grynberg, A. Honecker and P. Pujol,
Magnetization Plateaux in Quasi-One-Dimensional Strongly Correlated Electron Systems : A Brief Review,
Contribution to "XXIV International Workshop on Condensed Matter Theories", Buenos Aires, Argentine, septembre 2000.

[5] V. Dotsenko, M. Picco and P. Pujol,
Correlation functions for the 2D random bonds Potts Models,
Nucl. Phys. **B** (Proc. Suppl.) 45A, 145 (1996)
Proccedings of the Trieste Conference on Recent Developments in Statistical Mechanics and Quantum Field Theory, Avril 1995

[6] U. Percoco, P. Pujol. and V. Villalba,
Quantum effects associated with scalar particles in two dimensional accelerated frames of reference.
Proceedings of the 6th. Marcel Grossman Meeting on General Relativity, 1992. World Scientific Publishing. pp. 597-599.

Thèses

- Théories Conformes et Systèmes Désordonnés, thèse de doctorat, Université de Paris VI, Octobre 4 1996.
- Creación de partículas en sistemas de referencia acelerados, Thèse de “licenciatura”, 1991, Universidad SIMON BOLIVAR.

1.3 Enseignement, encadrement et examination d'étudiants

1.3.1 Examination d'étudiants

- 20 Novembre 2003 : Jury de thèse de R. Santachiara, sujet : "Etude des phénomènes critiques à l'aide des théories des champs conformes : des systèmes désordonnés aux théories parafermioniques", LPTHE, Paris.

1.3.2 Encadrement d'étudiants

- 2004 : Encadrement du Stage de D.E.A. de Physique Théorique Rhône-Alpin de Kay-Uwe Giering.
- 2001 : Encadrement avec D. Carpentier du Stage de D.E.A. de Physique Statistique et Phénomènes non linéaires de Fabien Leonforte.
- 2000 : Encadrement du Stage de D.E.A. de Physique Statistique et Phénomènes non linéaires de Bénédicte Dujardin.
- 2000 : Encadrement du Stage de maîtrise de Jerome Rech.

1.3.3 Enseignement

- De 1999 à 2001 : Cours de "Méthodes Théoriques en Physique" au D.E.A. de Physique Statistique et Phénomènes non linéaires.
- Depuis 2000 : Cours de "Supraconductivité et Superfluidité" au Mastère de Sciences de la Matière. Ideé et élaboration du cours et de sont programme, créés et proposés pour la première fois au Magistère/Mastère des Sciences de la Matière.
- Depuis 2004 : Cours de "Mécanique Quantique Avancée" au Mastère de Sciences de la Matière.
- 2000 et 2001 : Cours d'"Électromagnétisme" dans la préparation à l'Agrégation de Physique.
- 2003 : Tutorats de "Théorie des Champs" et "Mécanique Quantique Avancée" au D.E.A. de Physique Théorique.
- Depuis 2003 : Tutorats de "Mécanique Quantique" au Magistère de Sciences de la Matière.
- De 1998 à 2001 : Travaux dirigés de "Mécanique Analytique" au Magistère de Sciences de la Matière.
- Depuis 1998 : Travaux Pratiques de Physique Générale de premiére et deuxième année du Magistère de Sciences de la Matière.
- Depuis 1998 : Corrections de leçons, d'épreuves blanches et tutorats dans la préparation à l'Agrégation de Physique et de Chimie-option Physique.
- De 1991 à 1992 : Cous d'"Électromagnétisme" élémentaire, en première année de l'Université SIMON BOLIVAR (Caracas Vénézuéla).

2 Activité scientifique

2.1 Systèmes fortement corrélés en basses dimensions

Ces dernières années ont connu un très grand développement de la théorie des systèmes fortement corrélés avec de nombreux résultats analytiques, numériques et expérimentaux. Le paradigme majeur dans ce domaine reste la compréhension du phénomène de supraconductivité à hautes températures. Ce problème s'est avéré très compliqué à aborder du fait de la très grande variété de mécanismes qui se produisent dans les matériaux susceptibles de donner lieu à ce phénomène et de la nature hautement non perturbative de certains effets. Il existe cependant des modèles, qui ont aussi leur contrepartie dans la réalité expérimentale, beaucoup plus simples à étudier d'un point de vue théorique.

Les systèmes antiferromagnétiques en une ou deux dimensions sont peut-être dans ce sens les plus intéressants à étudier. Les chaînes et les échelles de spins, dont nous allons parler dans la suite, présentent déjà une phénoménologie très riche, tels que l'effet entier/semi-entier de Haldane dans les propriétés de l'état fondamental des chaînes anitiferromagnétiques de Heisenberg de spin S, ou les excitations de spins 1/2 (spinons) dans le modèle de Heisenberg de spin 1/2. Les effets exotiques liés aux propriétés de l'état fondamental et aux excitations de basses énergie se complètent avec un comportement tout aussi intéressant en présence d'un champ magnétique, comme nous allons le voir. En effet, les échelles de spins présentent, dans certains cas que nous allons spécifier, des plateaux dans leur courbe d'aimantation dans des positions bien précises. La valeur de l'aimantation pour laquelle se produit ce plateau dépend uniquement du nombre de chaînes qui composent l'échelle. Au delà de cette propriété qui peut avoir des applications industrielles importantes, cet effet est aussi le reflet de la nature complexe et intéressante des états fondamentaux de ces systèmes magnétiques fortement corrélés.

La situation est encore plus complexe quand des degrés de liberté de charge sont présents. Prenons comme exemple de base le modèle de Hubbard unidimensionnel qui correspond à des électrons (avec spin 1/2) sur une chaîne discrète et en interaction de courte portée (plus proches voisins). Il est bien connu que ce modèle présente le phénomène exotique de séparation de spin et de charge, où des excitation "transportant" uniquement du spin sans charge, ou de la charge sans spin peuvent coexister avec des vitesses de déplacement différentes. Quand le nombre d'électrons correspond exactement au nombre de sites de la chaîne (demi-remplissage du fait du spin 1/2 des électrons), les degrés de liberté de charge ont un gap dans le spectre d'excitation et, à grandes échelles de distances, ou à très basses températures, seuls les degrés de liberté de spins seront visibles et produiront un comportement équivalent à celui d'un modèle de Heisenberg de spins 1/2. La présence d'un champ magnétique complique encore d'avantage les choses. Comme nous allons le voir, on peut trouver des situations où les degrés de

liberté de charge et/ou de spin ont un gap pour des valeurs précises du remplissage (nombre total d'électrons) et de l'aimantation (différence entre les nombres de spins 'up' et 'down'). Bien que ce type d'effet soit facile à observer dans des chaînes simples, mais avec une périodicité non-triviale du réseau (dimérisation ou polymérisation), ainsi que dans les échelles formées de plusieurs chaînes, son étude analytique et numérique est difficile à réaliser.

Nous allons ensuite discuter les effets d'un certain type d'impuretés dans les chaînes de spins, qui, comme nous le verrons, donnent lieu aussi à la présence de plateaux dont la position dépend cette fois-ci de la concentration en impuretés. Il est remarquable que des propriétés universelles à aimantation nulle, caractéristiques d'un grand nombre de types de désordre, coexistent avec des propriétés hautement non-universelles et intrinsèques à la nature microscopique des impuretés qui sont présentes. Ces résultats sont tout aussi intéressants dans le domaine de la conductivité de particules en interactions, l'analogie entre les systèmes chaînes de spin - particules en interaction se faisant via la relation susceptibilité magnétique - densité d'états qui est une conséquence immédiate de la transformation de Jordan-Wigner que nous allons décrire plus loin.

Pour finir ce chapitre sur les propriétés quantiques des systèmes fortement corrélés nous allons aborder partiellement le vaste domaine des systèmes bidimensionnels. Plus particulièrement, les systèmes que nous allons étudier sont des systèmes frustrés, dont l'étude comprend plusieurs intérêts. Tout d'abord, un certain type de systèmes frustrés que nous allons décrire présente, du moins en l'absence de fluctuations quantiques, des excitations fractionnaires, relativement facile à mettre en évidence en une dimension, mais beaucoup moins en deux dimensions. Il est intéressant de voir si les fluctuations quantiques, préservent la nature déconfinée de ces excitations, ou si au contraire elles introduisent une interaction effective qui confine de telles excitations dans des 'particules' plus traditionnelles, comme par exemple deux spinons qui forment un magnon. Une autre question, reliée à la première et tout aussi intéressante, et de savoir si la grande dégénérescence de l'état de plus basse énergie, typique des systèmes frustrés, sera levée par les fluctuations quantiques et dans ce cas quelle sera la nature de l'état fondamental. De ce point de vue, ce dernier volet de l'étude des systèmes fortement corrélés propose comme but plus ambitieux de donner une compréhension des systèmes bidimensionnels, en général plus difficiles à aborder d'un point de vue théorique.

2.1.1 Chaînes et échelles de spins

Les modèles de spins quantiques en basses dimensions sont peut-être les systèmes fortement corrélés les plus simples où l'on retrouve cependant toute la richesse des phénomènes exotiques que l'on a dans ce domaine de la matière condensée. Prenons comme exemple le plus simple, une chaîne de spins S quel-

conque, dont le Hamiltonien est donné par :

$$H = J \sum_i \vec{S}_i . \vec{S}_{i+1} \; ; \; \vec{S}^2 = S(S+1) \tag{1}$$

où J est positif. En 1983, Haldane [1] a conjecturé que si S est entier, l'état fondamental de ce système est unique et séparé par un "gap" des états excités, alors que si S est un semi-entier, le système n'a pas de gap (bien que l'état fondamental soit toujours unique). La solution exacte par ansatz de Bethe [2] du cas $S = 1/2$ et les évidences numériques et expérimentales obtenues sur divers cas pour $S = 1,\ 3/2,\ 2$ [3] semblent confirmer cette conjecture. Sans entrer dans les détails techniques, nous présentons ici un tableau qui nous montre le comportement à basses températures des diverses quantités physiques, mesurables expérimentalement, en présence ou non d'un gap dans le spectre d'excitations.

	gap	pas de gap
Fonctions de corrélation à grandes distances	$< S(0)S(x) > \rightarrow \lvert x\rvert^{-\alpha} e^{-x/\xi}$	$< S(0)S(x) > \rightarrow \lvert x\rvert^{-\alpha}$
Chaleur spécifique à basses températures	$C(T) \sim T e^{-\Delta T}$	$C(T) \sim T$
Susceptibilité magnétique à basses températures	$\chi(T) \sim e^{-\Delta T}$	$\chi(T) \sim \chi_0 \neq 0$

Cette conjecture remarquable de Haldane a été ensuite généralisée pour les échelles de spins [4]. Si l'on construit une échelle de spins en prenant une bande infinie du réseau carré de N colonnes de spins S couplés entre plus proches voisins, alors si le produit SN est entier, le spectre a un gap, et si SN est semi-entier, le spectre n'a pas de gap.

Le résultat de Haldane se base sur une description en termes du modèle Sigma non-linéaire que l'on obtient dans la limite de S grand. Comme nous le savons, le modèle Sigma non-linéaire est donné par l'action Euclidienne :

$$S = \frac{1}{2g} \int d^2x \, (\partial_\mu \vec{n})^2 \tag{2}$$

où $\vec{n}$ est un vecteur unitaire. Une analyse par le groupe de renormalisation nous montre que, à grandes échelles, le système est gouverné par le régime de couplage fort $g \rightarrow \infty$, qui peut s'interpréter comme un comportement à haute température d'un modèle classique bi-dimensionnel avec des corrélations à courte portée. ce phénomène de création dynamique de masse, provenant des fluctuations quantiques, implique, entre autres, la présence d'un gap dans le système. L'action

effective obtenue par Haldane contient un terme supplémentaire qui s'écrit sous la forme :

$$i\theta S_{WZ} = \frac{i\theta}{8\pi} \int d^2x \epsilon_{\mu\nu} \left(\partial_\mu \vec{n} \times \partial_\nu \vec{n}\right) .\vec{n}$$

c'est un terme topologique. En effet, S_{WZ} est l'index de Pontryagin d'une application de S^2 sur elle même et peut prendre comme valeur un nombre entier arbitraire. Pour S entier, ce terme ne joue aucun rôle dans le calcul de la fonction de partition, car il ne donnera lieu qu'à des phases triviales, et le modèle sera tout simplement décrit par l'action (2), avec les conséquences que cela implique. En revanche, pour S semi-entier, le terme topologique donnera lieu à des signes (-) dans le calcul de la fonction de partition et le comportement sera très différent. Pour ne citer que l'argument le plus simple, si l'on suppose que le modèle en présence du terme topologique décrit le comportement à grandes échelles de toutes les chaînes de spin semi-entier, la solution exacte dont nous disposons pour $S = 1/2$ nous dit alors que toutes les chaînes de spins semi-entiers n'auront pas de gap dans leur spectre d'excitations.

Dans le premier article inclus dans ce chapitre, nous proposons une approche différente pour s'attaquer à ce problème. Nous utilisons une représentation des opérateurs de spin S en termes de $2S$ couleurs différentes de fermions. Pour chaque site de la chaîne, les opérateurs de spin peuvent être construits en termes d'opérateurs de création et annihilation des fermions :

$$\vec{S}_x = C^\dagger_{\alpha i x} \frac{\vec{\sigma}_{\alpha\beta}}{2} C_{\beta i x}, \tag{3}$$

où $\vec{\sigma}$ sont les matrices de Pauli et $i = 1..2S$ Il faut imposer des contraintes sur ces fermions, qui assurent que des fermions sont présents sur chaque site, et que les états physiques soient des singulets de couleur :

$$\begin{aligned} \sum_i \quad & C^\dagger_{\alpha i x} C_{\alpha i x} |phys> = 2S|phys> \\ \sum_{ij} \quad & C^\dagger_{\alpha i x} \tau^a_{ij} C_{\alpha j y} |phys> = 0, \end{aligned} \tag{4}$$

où τ^a sont les générateurs de $SU(2S)$. La théorie effective résultant de la bosonisation de ce système correspond à un modèle de Wess-Zumino-Novikov-Witten (WZNW) avec symétrie $SU(2)$ et niveau $2S$, plus des perturbations.

$$S_{eff} = S_{SU(2)_{2S}} + \int d^2x \left(\alpha \; Tr \; (\Phi^{(1)}) + \beta \; \vec{J}_R.\vec{J}_R\right) \tag{5}$$

Le dernier terme correspond au produit des composantes chirales des courants de Kac-Moody et correspond à une perturbation marginale, dans le sens du groupe de renormalisation. Le premier est la trace de l'opérateur primaire dans la représentation adjointe de $SU(2)$ et correspond à une perturbation pertinente. Nous

rappelons que, pour un modèle de WZNW $SU(2)_k$, nous pouvons construire à partir de l'algèbre de Kac-Moody générée par les courants une algèbre de Virasoro de charge centrale $c = \frac{3k}{k+2}$. Les représentations de plus haut poids de cette algèbre de Virasoro sont classifiées par les représentations du groupe $SU(2)$ et sont données par des champs de dimensions $h = \overline{h} = \frac{j(j+1)}{k+2}$, $j \leq k/2$. On voit donc que, bien que le terme correspondant à $j = 1$

$$Tr\ (\Phi^{(1)})$$

n'existe pas pour $k = 1$ (la chaîne de spin 1/2), il est bien présent pour $k > 1$ et donne lieu à une perturbation pertinente. En conséquence, le flot de renormalisation sera non-trivial, et si des points fixes non-triviaux sont présents dans celui-ci, ils sont non-perturbatifs et une simple analyse par le groupe de renormalisation ne nous donnera certainement pas les informations nécessaires à comprendre le comportement du système. L'idée consiste alors à utiliser une équivalence au niveau des espace de Hilbert de cette théorie avec celle du produit d'une théorie de champ scalaire, à symétrie $U(1)$ et d'un théorie parafermionique avec symétrie Z_{2S}, que l'on connaît par la construction des théories quotient en théorie conforme. Le point important est que les termes de perturbation, qui se décomposent en termes de d'opérateurs du secteur bosonique et parafermionique, donne lieu entre autres à la présence, sans aucun couplage à des opérateurs du secteur $U(1)$, du premier opérateur thermique du secteur parafermionique Z_{2S}. Sans entrer dans les détails techniques qui peuvent être retrouvés dans l'article qui suit, nous nous limitons à dire que, comme la théorie Z_{2S} perturbée par le premier opérateur thermique est massive et intégrable, nous pouvons donc formellement intégrer sur ces degrés de liberté parafermionique et obtenir une action effective pour le champ scalaire, dont la forme est fixée sans ambiguïté par les symétries du système. Celle-ci correspond à l'action d'un champ massif pour le cas de S entier, alors que pour S semi-entier nous retrouvons l'action d'un modèle de WZNW de niveau 1, avec une perturbation marginale non-pertinente qui introduira au plus des corrections logarithmiques dans certaines fonctions de corrélations, comme pour le cas $S = 1/2$ [1].

L'intérêt de cette méthode est d'abord qu'elle ne repose pas sur une approximation de S grand, et met en évidence clairement que le comportement d'une chaîne de spin S semi-entier est le même que celui de $S = 1/2$ pour toute valeur de S. Par ailleurs, il est possible de comprendre plus facilement pourquoi en introduisant des termes supplémentaires dans le modèle microscopique, tels que $\sum_i (\vec{S_i}.\vec{S_{i+1}})^2$ et un réglage fin des paramètres on peut obtenir une criticalité différente, correspondant au modèle de WZNW $SU(2)_{2S}$. La présence de dimérisation, ou d'une faible anisotropie du type XXZ peut aussi être étudiée plus facilement dans cette nouvelle description de théorie des champs.

[1] Pour un certain rayon de compactification, la théorie du champ scalaire possède en fait une symétrie $SU(2)$ étendue, et le modèle est équivalent à un modèle de WZNW $SU(2)_1$.

Imaginons maintenant que nous introduisons une chaîne de spins comme celles que nous venons de décrire dans un champ magnétique H selon la direction z. Pour les chaînes de spins semi-entier, l'état fondamental pour $H = 0$ est un singulet qui est donc d'aimantation nulle. Il existe cependant des états avec aimantation $M = \frac{<S^z>}{<S^z>_{max}} = \epsilon$ infinitésimale qui ont une énergie supérieure mais infiniment proche de celle du fondamental (dans la limite de taille infinie). Pour toute valeur de H non-nulle, le système "choisira" alors comme état fondamental un état d'aimantation non-nulle. En fait, la courbe d'aimantation M contre H sera une fonction monotone croissante et continue jusqu'à la valeur $M = 1$ obtenue pour $H = H_{sat}$.

Si maintenant nous considérons une chaîne de spins entiers, comme l'état fondamental pour $H = 0$ est séparé du reste des état par un gap non nul, il faudra atteindre une valeur de champ magnétique non nulle avant d'obtenir un état fondamental avec une aimantation non nulle. La courbe d'aimantation présentera alors un plateau pour $M = 0$. Une fois que le système a atteint une aimantation non nulle (pour un H suffisamment grand), en général la courbe d'aimantation sera alors monotone et continue comme pour le cas des spins semi-entiers. Un modèle assez représentatif est la chaîne XXZ de spins 1/2, dont le Hamiltonien est donné par :

$$H_{XXZ} = J \sum_i \left(S_i^x S_{i+1}^x + S_i^y S_{i+1}^y + \Delta S_i^z S_{i+1}^z + H S_i^z \right) \ ; \ J > 0 \tag{6}$$

Ce système est intégrable et ses propriétés à grandes échelles et basses températures peuvent être obtenues de façon exacte. Le diagramme de phases H *vs.* Δ est représenté dans le deuxième article de cette section. Pour $\Delta > 1$ la courbe d'aimantation présente un plateau d'aimantation pour $M = 0$ qui traduit la présence d'un gap dans le spectre d'excitations. Dans ce cas, il faut un champ magnétique $H > H_{gap}$ pour aimanter la chaîne, qui, une fois aimantée, sera dans une phase sans gap. Dans la phase sans gap, y compris pour $\Delta > 1$, le comportement à grandes échelles est donné par une théorie conforme correspondant à un champ scalaire $c = 1$, dont le rayon de compactification dépend de M et de Δ.

Cette transition à $\Delta = 1$ entre le régime non-massif et massif peut être vue comme une transition conducteur isolant en termes de fermions en interaction. Nous pouvons en effet comprendre ce phénomène en utilisant la transformation de Jordan-Wigner pour les spin 1/2, donnée par la correspondance entre les opérateur de spin et des opérateur fermioniques :

$$S_i^z = \psi_i^\dagger \psi_i - \frac{1}{2} \ ; \ S_i^+ = \psi_i^\dagger \ e^{i\pi \sum_{j=1}^{i-1} \psi_j^\dagger \psi_j} \tag{7}$$

On vérifie alors que le cas $\Delta = 0$ correspond au cas de fermions libre alors que un Δ non nul correspond à des interaction entre fermions sur des sites voisins.

L'ouverture d'un gap pour $\Delta = 1$ peut donc s'interpréter comme une transition de Mott, due aux interactions, contrairement à un gap de bande créé, par exemple, par une modulation de la constante de couplage. Le système donné par le Hamiltonien

$$H_{dim} = \sum_i (J + (-1)^i \delta J) \left(S_i^x S_{i+1}^x + S_i^y S_{i+1}^y + \Delta S_i^z S_{i+1}^z \right) \tag{8}$$

a un gap pour $M = 0$ même pour $\Delta = 0$ que l'on peut comprendre facilement en étudiant la structure de bandes (deux bandes dans le cas présent) séparés par un gap. La bosonisation abélienne nous permet alors de faire le lien avec la théorie de champ scalaire mentionnée plus haut, et de donner une vision unificatrice des deux phénomènes de gap. En effet, la théorie bosonique effective d'un champ compactifié que l'on obtient dans le cas général est donnée par l'action :

$$S = \int d^2x \left[(\partial_\mu \Phi)^2 + \lambda \, cos \left(\frac{n\Phi}{R} \right) \right] \tag{9}$$

avec $n = 1$ pour le cas dimérisé et $n = 2$ pour le cas invariant par translation mais avec $\Delta \neq 0$.

L'intérêt de la technique de bosonisation abélienne réside dans le fait que l'on peut étendre cette analyse à des cas plus complexes, tels que les chaînes de spins. Comme nous le montrons dans le deuxième article présenté ici, nous pouvons en effet anticiper la présence de gap de spin dans des échelles de spins même pour des valeurs de l'aimantation non nulle. Nous étudions les conditions pour que se produise un gap dans le spectre, et donc un plateau d'aimantation, pour des valeurs arbitraires de l'aimantation. Le principal résultat est que ces plateaux surviennent pour des valeurs de l'aimantation particulières, que l'on peut résumer par la formule suivante : Si N est le nombre chaînes couplées, S la valeur du spin dans chaque site et l la périodicité du réseau (*i. e.* $l = 2$ pour le cas dimérisé par exemple) alors :

$$lSN\,(1 - M) \in \mathbb{Z} \tag{10}$$

La figure (1) montre la courbe d'aimantation d'une échelle à trois pattes formées de spins 1/2. Un plateau à $M = 1/3$, comme le prédit (10) y est clairement visible. Ce résultat peut être considéré comme la généralisation de la conjecture de Haldane faite pour les chaînes de spins ainsi que son extension aux échelles mentionnées plus haut. De façon plus précise, les degrés de libertés effectifs, présents à grandes échelles, ne correspondent qu'à une partie de ceux initiaux, que l'on peut, pour des chaînes de spins 1/2, représenter par $\{\Phi_i\}$; $i = 1..N$. L'action effective à grandes échelles correspond en fait à celle de (9) pour un seul champ $\Phi_D = \sum_i \Phi_i$, mais dont la présence d'un opérateur $cos(n\Phi_D)$ (avec $n = 2$) est régie par la valeur de l'aimantation.

Si certains cas persistent à échapper à la règle (10), tels que les plateaux induits par la frustration que l'on peut trouver dans les couplages anti-ferromagnétiques

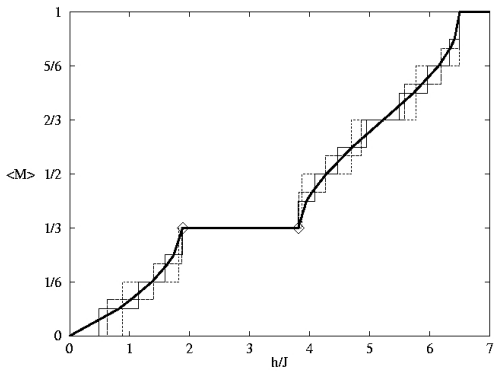

FIG. 1 – Courbe d'aimantation pour une échelle de spins 1/2 formée de trois chaînes. Elle a été obtenue à partir de résultats numériques pour des systèmes de taille finie. la ligne solide correspond à la limite de taille infinie.

entres chaînes avec conditions aux bords périodiques ou les couplages en "zigzag" [5], ce résultat englobe la grande majorité des cas. Il provient d'une dérivation simple et intuitive faite dans l'article présenté ci-dessous et correspond à l'aboutissement de la caractérisation des propriétés magnétiques des chaînes de spins dans les conditions les plus générales.

Références

[1] F. D. M. Haldane, Phys. Rev. Lett. **50**, 1153 (1983) ; Phys. Lett. **93 A**, 464 (1983).

[2] R. J. Baxter, Ann. Phys. (N. Y.) **70**, 193 (1972) ; L. D. Fadeev and L. A. Takhtajan, Phys. Lett. **85 A**, 375 (1981).

[3] K. Hallberg, X. Q. G. Wang, P. Horsch, and A. Moreo, Phys. Rev. Lett. **76**, 4955 (1996) ; G. E. Granroth, M. W. Meisel, M. Chaparala, Th. Jolicoeur, B. H. Ward, and D. R. Talham, Phys. Rev. Lett. **77**, 1616 (1996).

[4] G. Sierra, *Lectures Notes in Physics, vol.478, eds. G. Sierra , and M.A. Martin-Delgado, Springer-Verlag (1997).*

[5] D.C. Cabra, A. Honecker and P. Pujol, Eur. Phys. J. **B 13**, 55, 2000.

Non-Abelian bosonization and Haldane's conjecture

D. C. Cabra
Departamento de Física, Universidad Nacional de la Plata, C.C. 67, (1900) La Plata, Argentina and Facultad de Ingeniería, Universidad Nacional de Lomas de Zamora, Cno. de Cintura y Juan XXIII, (1832) Lomas de Zamora, Argentina

P. Pujol
International School for Advanced Studies, Via Beirut 2-4, 34014 Trieste, Italy

C. von Reichenbach
Departamento de Física, Universidad Nacional de la Plata, C.C. 67, (1900) La Plata, Argentina
(Received 26 March 1998)

We study the long-wavelength limit of a spin S Heisenberg antiferromagnetic chain. The fermionic Lagrangian obtained corresponds to a perturbed level $2S$ $SU(2)$ Wess-Zumino-Witten (WZW) model. This effective theory is then mapped into a compact $U(1)$ boson interacting with Z_{2S} parafermions. The analysis of this effective theory allows us to show that when S is an integer there is a mass gap to all excitations, whereas this gap vanishes in the half-odd-integer spin case and the $SU(2)_{2S}$ WZW model flows towards the $SU(2)_1$ stable fixed point. This gives a field theory treatment of the so-called Haldane's conjecture for arbitrary values of the spin S. [S0163-1829(98)04726-2]

I. INTRODUCTION

In 1983 Haldane conjectured that in the case of integer spin, the spin S quantum Heisenberg antiferromagnetic (HAF) chain had a unique disordered ground state with a finite excitation gap, while the same model had no excitation gap when S was a half odd integer.[1] Using a mapping to the nonlinear σ model, valid in the large-S limit, the origin of the difference has been identified as being due to an extra topological ''Θ term'' in the effective σ-model Lagrangian for systems with a half integer S.[1] This clearly suggests that the origin of this difference is nonperturbative. Although Haldane's predictions were based on large-S arguments, it is known that this conjecture is consistent with the Bethe ansatz exact solution that is available for $S=\frac{1}{2}$,[2] and experimental, numerical, and theoretical studies almost confirmed its validity for $S=1$.[3] For the higher half-odd-integer spin, the ground state is either degenerate or has a massless excitation[4] that suggests, but does not prove, critical correlations. In Ref. 5, massless behavior in $S=\frac{3}{2}$ has been tested numerically (see also Ref. 6). Recent experimental evidence of the existence of the Haldane gap for $S=2$ HAF chains has been found in the study of the compound $MnCl_3(bipy)$.[7]

Bosonization techniques have been extensively used in the study of spin chains (see Ref. 8 for a review on the subject and references therein). The starting point consists of the mapping of the original problem, in terms of spin variables, to the problem of fermionic variables with additional constraints (that are necessary for the two systems to be equivalent) and then bosonize the resulting system. In Ref. 9, the HAF model was formulated as a certain limit of the Hubbard model. By using a bosonization technique and a renormalization-group analysis, they found an effective theory for the low-energy physics of $S=\frac{1}{2}$ and the limit of large-S spin chains. In Ref. 10 another approach was used that relies on the fact that the spin S HAF chain can be represented as $2S$ spin-$\frac{1}{2}$ chains for large ferromagnetic coupling. In a recent paper[11] the issue of implementing explicitly the above-mentioned additional constraints within the path-integral approach was taken up, and a reconfirmation of Haldane's conjecture was obtained for large values of the spin S by using non-Abelian bosonization techniques.

In this paper we study the effective low-energy theory in terms of a fermionic coset model that corresponds to the level $2S$ $SU(2)$ Wess-Zumino-Witten (WZW) theory[12,13] following Ref. 11, and map it onto a coupled system of a compact $U(1)$ boson and Z_{2S} parafermions (PF's). The analysis of the phase diagrams of Z_{2S} models together with the knowledge of their operator product algebra provide us with the elements to establish the difference between integer and half integer spin chains.

We would like to stress that our analysis does not rely on a large-S approximation, but is valid for all values of S.

II. COSET MODEL

Let us briefly review the work of Ref. 11: The spin S HAF model can be written in terms of fermionic operators $C_{\alpha ix}$, with $\alpha=\uparrow,\downarrow; i=1,\ldots,2S$. α, i and x are spin, color, and site indices, respectively. The spin S operator on one site x is represented by

$$\vec{S}_x = C^{\dagger}_{\alpha ix}\frac{\vec{\sigma}_{\alpha\beta}}{2}C_{\beta ix}, \tag{1}$$

where $\vec{\sigma}_{\alpha\beta}$ are the Pauli matrices. In order to correctly represent the spin S chain, the physical states must satisfy

$$\begin{aligned}\sum_i C^{\dagger}_{\alpha ix}C_{\alpha ix}|phys\rangle &= 2S|phys\rangle,\\ \sum_{ij} C^{\dagger}_{\alpha ix}\tau^a_{ij}C_{\alpha jy}|phys\rangle &= 0,\end{aligned} \tag{2}$$

where τ^a are the $SU(2S)$ generators. The first constraint imposes the condition that allows only one spin per site, whereas the second one states that the physical states must be color singlets.

The Heisenberg Hamiltonian

$$H=\sum_{\langle xy\rangle}\vec{S}_x\cdot\vec{S}_y \tag{3}$$

can be expressed in terms of the fermionic operators introduced above as

$$H=-\frac{1}{2}\sum_{\langle xy\rangle}C^\dagger_{\alpha ix}C_{\alpha jy}C^\dagger_{\beta jy}C_{\beta ix}+\text{const}, \tag{4}$$

which has a local $SU(2S)\times U(1)$ invariance. This quartic interaction can be rewritten by introducing an auxiliary field B as

$$H=\frac{1}{2}\sum_{\langle xy\rangle}(B^{ij}_{xy}C^\dagger_{\alpha ix}C_{\alpha jy}+\text{H.c.}+\overline{B}^{ji}_{yx}B^{ij}_{xy}). \tag{5}$$

In the mean-field approximation B is a constant $2S\times 2S$ matrix, and H can be diagonalized. As we will see below, it is important to consider the quantum fluctuations around this point.

To obtain an effective low-energy theory, we keep the operators $C(k)$ with k near the Fermi surface $\pm\pi/2a$. We can then write

$$\frac{1}{\sqrt{a}}C_{\alpha ix}=e^{(i\pi/2a)x}\Psi_{R\alpha i}(x)+e^{(-i\pi/2ax)}\Psi_{L\alpha i}(x), \tag{6}$$

where $1/\sqrt{a}$ appears for dimensional reasons and $\Psi_{R,L\alpha i}(x)$ are slowly varying on the lattice scale.

We also expand the field B as

$$B_{xy}=B_0e^{aV_{xy}}\simeq B_0(1+aV_{xy}), \tag{7}$$

define $A_1\equiv\frac{1}{2}(V_{xy}-V^\dagger_{xy})$, and $R_{xy}\equiv\frac{1}{2}(V_{xy}+V^\dagger_{xy})$. These fields correspond to the quantum fluctuations around the mean-field configuration. To ensure the correctness of our procedure, we have to integrate them out in an exact way.

When substituted back into the Hamiltonian, the expansion (7) leads to a quadratic integral in R_{xy} that can be performed exactly to give

$$H=B_0[-i\Psi^\dagger_{Ri}(\delta_{ij}\partial_x+A^1_{ij})\Psi_{Rj}+i\Psi^\dagger_{Li}(\delta_{ij}\partial_x+A^1_{ij})\Psi_{Lj}]+\tfrac{1}{4}(\Psi^\dagger_{Li}\Psi_{Rj}-\Psi^\dagger_{Ri}\Psi_{Lj})^2. \tag{8}$$

The effective Lagrangian is obtained by introducing a Lagrange multiplier A_0 in the Lie algebra of $U(2S)$, together with the use of the identity

$$\delta[\overline{\Psi}_i\Psi_j]=\lim_{\lambda_2\to\infty}e^{-\lambda_2\int d^2x(\overline{\Psi}_i\Psi_j)^2}, \tag{9}$$

in order to implement the constraints (2) (see Ref. 11 for details). The effective Lagrangian then reads

$$L=\overline{\Psi}\gamma^\mu iD_\mu\Psi-\lambda_1(i\overline{\Psi}_i\gamma_5\Psi_j)^2-\lambda_2(i\overline{\Psi}_i\Psi_j)^2, \tag{10}$$

where $D_\mu=\partial_\mu-ia_\mu+B_\mu$, and we have decomposed, for later convenience, the field A_μ into a $U(1)$ field a_μ and a $SU(2S)$ field B_μ.

The Lagrangian can be rewritten as

$$L=\overline{\Psi}_{i\alpha}\gamma^\mu i(\partial_\mu-ia_\mu\delta_{ij}\delta_{\alpha\beta}+B^{ij}_\mu\delta_{\alpha\beta})\Psi_{j\beta}+4(\lambda_1+\lambda_2)\vec{J}_R\cdot\vec{J}_L+(\lambda_1+\lambda_2)j_Rj_L-(\lambda_1-\lambda_2)(\Psi^\dagger_{Ri\alpha}\Psi_{Lj\alpha}\Psi^\dagger_{Rj\beta}\Psi_{Li\beta}+\text{H.c.}), \tag{11}$$

where $\vec{J}_{R,L}=\Psi^\dagger_{R,Li\alpha}\vec{\sigma}_{\alpha\beta}/2\Psi_{R,Li\beta}$, $j_{R,L}=i\Psi^\dagger_{R,Li\alpha}\Psi_{R,Li\alpha}$ are $SU(2)_{2S}$ and $U(1)$ currents, respectively.

The first term in the Lagrangian (11) corresponds to the fermionic coset version of the level $2S$ $SU(2)$ WZW theory[14] as was already observed in Ref. 11. In this context the original spin operator corresponds to the fundamental field of the WZW model. The third term can be absorbed by a redefinition of the $U(1)$ gauge field a_μ.

Thus, we have to deal with the second and last terms in Eq. (11) that can be expressed as

$$\Delta\mathcal{L}=(\lambda_1-\lambda_2)(g_{\alpha\beta}g_{\beta\alpha}+\text{H.c.})+4(\lambda_1+\lambda_2)\vec{J}_R\cdot\vec{J}_L, \tag{12}$$

where $g\equiv\Psi^\dagger_{Ri}\Psi_{Li}$ is the spin-$\frac{1}{2}$ primary field of the $SU(2)_{2S}$ WZW theory, $\Phi^{(1/2)}$, with conformal dimensions $h=\overline{h}=3/[8(S+1)]$. The first term in Eq. (12) corresponds to the spin 1 affine primary $\Phi^{(1)}$ with conformal dimensions $h=\overline{h}=1/(S+1)$, so we can write

$$\Delta\mathcal{L}=-4\ (\lambda_1-\lambda_2)\text{tr}\,\Phi^{(1)}+4(\lambda_1+\lambda_2)\vec{J}_R\cdot\vec{J}_L. \tag{13}$$

The $S=\frac{1}{2}$ case is simpler, as has been discussed in Refs. 9 and 11, since affine (Kac-Moody) selection rules forbid the appearance of the relevant operator $\Phi^{(1)}$. We then have an effective massless theory in accordance with Haldane's predictions. The second term in Eq. (13) is marginally irrelevant since $\lambda_1+\lambda_2$ is positive, and gives the well-known logarithmic corrections to correlators.

For higher spins, we have to consider the interaction term (13) and we also have to include all other terms that will be radiatively generated. We then need the operator product expansion (OPE) coefficients among the different components of $\Phi^{(1)}$ that have been computed in Ref. 15. The OPE coefficients are nonvanishing if the so-called ''fusion rules'' are nonvanishing. In the level k $SU(2)$ WZW theory they are given by[16]

$$\Phi^{(j)}_{m,\overline{m}}\times\Phi^{(j')}_{m',\overline{m}'}=\sum_{n=|j-j'|}^{min(j+j',k-j-j')}\Phi^{(n)}_{m+m',\overline{m+m'}}. \tag{14}$$

We will use that[15,17]

$$SU(2)_k\equiv Z_k\,\square\,U(1) \tag{15}$$

in the sense that the Hilbert spaces of the two theories coincide. We will exploit this equivalence to derive an effective low-energy action for the spin S HAF chain. Indeed, it was shown in Ref. 15 that the primary fields of the $SU(2)_k$ WZW theory are related to the primaries of the Z_k parafermion theory and the $U(1)$ vertex operators. They are connected by the relation

$$\Phi^{(j)}_{m,\bar{m}}(z,\bar{z}) = \phi^{(2j)}_{2m,2\bar{m}}(z,\bar{z}) : e^{i/\sqrt{2S}[m\varphi(z)+\bar{m}\bar{\varphi}(\bar{z})]} :, \quad (16)$$

where the Φ fields are the invariant fields of the $SU(2)_k$ WZW theory, the ϕ fields are the Z_k PF primaries, and φ and $\bar{\varphi}$ are the holomorphic and antiholomorphic components of a compact massless free boson field. In the same way, the currents are related as

$$J^+_R(z) = (2S)^{1/2}\psi_1(z) : \exp\left(\frac{i}{\sqrt{2S}}\varphi(z)\right) :,$$

$$J^0_R(z) = (2S)^{1/2}\partial_z\varphi(z), \quad (17)$$

where ψ_1 is the first parafermionic field. (A similar relation holds for the left-handed currents.)

Using this equivalence we can express the relevant perturbation term (13) as

$$\begin{aligned}\Delta\mathcal{L} = &-4(\lambda_1-\lambda_2)(\phi^{(2)}_{0,0} + \phi^{(2)}_{2,-2} : e^{i/\sqrt{2S}[\varphi(z)-\bar{\varphi}(\bar{z})]} : \\ &+ \phi^{(2)}_{-2,2} : e^{-i/\sqrt{2S}[\varphi(z)-\bar{\varphi}(\bar{z})]} :) + 4S(\lambda_1+\lambda_2) \\ &\times(\psi_1\bar{\psi}^\dagger_1 : e^{i/\sqrt{2S}[\varphi(z)-\bar{\varphi}(\bar{z})]} : + \text{H.c.}), \end{aligned} \quad (18)$$

where we absorbed the derivative part of the $U(1)$ field coming from Eq. (17) into a redefinition of the constant in front of the unperturbed Lagrangian. The first term corresponds to the first ''thermal'' field of the PF theory, $\phi^{(2)}_{0,0} = \epsilon_1$, with conformal dimensions $h = \bar{h} = 1/(1+S)$, while the second and third terms correspond to the $p=2$ disorder operator in the PF theory, $\phi^{(2)}_{2,-2} = \mu_2$ and its adjoint $\phi^{(2)}_{-2,2} = \mu_2^\dagger$, with dimensions $d_2 = \bar{d}_2 = (S-1)/[2S(S+1)]$.

Including all the operators that are radiatively generated, we get three ''families'' of perturbations:

(1) The thermal operator ϵ_1 and all the members of its subalgebra (higher thermal operators). As shown in Ref. 18, the Z_{2S} PF theory perturbed by ϵ_1 flows into a massive regime, irrespectively of the sign of the coupling. Assuming that, as for the Z_2 case, due to the sign of the coupling $\lambda_1 - \lambda_2$ in Eq. (18) the theory is driven into a low-temperature ordered phase, we have that vacuum expectation values (v.e.v.'s) of disorder operators μ_j, vanish for $j \neq 2S\,mod(2S)$ as well as v.e.v.'s of the parafermionic fields $\langle\psi_k\bar{\psi}^\dagger_k\rangle = 0$, for $2k \neq 2S\,mod(2S)$.

(2) The family of the disorder operator (with the corresponding vertex operators) given by

$$\sum_{k=1}^{[S]} \mu_{2k} : e^{ik/\sqrt{2S}[\varphi(z)-\bar{\varphi}(\bar{z})]} : + \text{H.c.},$$

where $[S]$ means integer part of S. Note that μ_{2S} corresponds to the identity operator and then for S integer, this family contains the single vertex operator

$$: e^{iS/\sqrt{2S}[\varphi(z)-\bar{\varphi}(\bar{z})]} : + \text{H.c.} \quad (19)$$

(3) The family of the parafermionic fields:

$$\sum_{k=1}^{2S} \psi_k(z)\bar{\psi}^\dagger_k(\bar{z}) : e^{ik/\sqrt{2S}[\varphi(z)-\bar{\varphi}(\bar{z})]} : + \text{H.c.}$$

Note that the system is invariant under the extended $Z_{2S} \times \tilde{Z}_{2S}$ transformation

$$\mu_p \to w^{p(m-n)}\mu_p; \quad \psi_p\bar{\psi}^\dagger_p \to w^{2p(m-n)}\psi_p\bar{\psi}^\dagger_p;$$

$$\varphi \to \varphi - \frac{\sqrt{2}\pi m}{\sqrt{S}}; \quad \bar{\varphi} \to \bar{\varphi} - \frac{\sqrt{2}\pi n}{\sqrt{S}}, \quad (20)$$

with $w = \exp(\pi i/S)$ and $m,n \in Z$.

Since the parafermionic sector is massive, the effective theory for large scales can be obtained by integrating out these degrees of freedom. Since this massive sector is driven into the phase where Eq. (20) is unbroken, we can obtain the most general effective action for the remaining $U(1)$ field, where only the vertex operators invariant under Eq. (20) will be allowed to appear. We get

$$\begin{aligned} Z_{eff} = \int \mathcal{D}\phi\, \exp\Bigg[&- \int K_S(\partial_\mu\phi)^2 \\ &+ \alpha_S \int \cos\left(\frac{2S}{\sqrt{2S}}(\varphi - \bar{\varphi})\right) + \cdots \Bigg], \end{aligned} \quad (21)$$

for the S half integer, and

$$\begin{aligned} Z_{eff} = \int \mathcal{D}\phi\, \exp\Bigg[&- \int K_S(\partial_\mu\phi)^2 \\ &+ \beta_S \int \cos\left(\frac{S}{\sqrt{2S}}(\varphi - \bar{\varphi})\right) \\ &+ \alpha_S \int \cos\left(\frac{2S}{\sqrt{2S}}(\varphi - \bar{\varphi})\right) + \cdots \Bigg], \end{aligned} \quad (22)$$

for the S integer. Here the dots simply mean higher powers of the perturbing vertex operators and K_S is an effective constant arising from the OPE of vertex and parafermionic operators in the process of integration of the massive degrees of freedom. We immediately notice that, for the integer S, there is an extra vertex operator coming from Eq. (19) that is not present for the half integer S, and, as we will see, this difference between integer and half integer effective actions is crucial.

Using Eqs. (1) and (6), we can write the continuum expression of the original spin operator $\vec{S}(x)$ as

$$\vec{S}(x) = \vec{J}_R + \vec{J}_L + (-1)^x \text{tr}[\vec{\sigma}/2(\Phi^{(1/2)} + \Phi^{(1/2)\dagger})]. \quad (23)$$

One way to see whether the system is gapped or not is to study the behavior of the spin-spin correlation function at large scales. Since our original $SU(2)$ WZW model is perturbed, correlation functions of the fundamental field will contain supplementary operators coming from the OPE between $\Phi^{(1/2)}$ and the perturbing fields. With the help of the fusion rules (14) it is easy to see that, for example, the effective alternating z component of the spin operator containing the scalar field will be given by

$$\sum_{k \leq 2S,\ k odd} a_k\ \mu_k : e^{ik/2\sqrt{2S}[\varphi(z)-\bar{\varphi}(\bar{z})]} : + \text{H.c.}, \quad (24)$$

where only odd k fields appear in the sum. Let us now consider separately the case of the half integer and the integer S: For the S half integer, the operator $\Phi^{(S)}$ is present in Eq. (24), and we can easily check that (since μ_{2S} corresponds to the identity) this operator is simply given by

$$e^{iS/\sqrt{2S}(\varphi-\bar{\varphi})}+\text{H.c.}$$

The other operators in the series contain parafermionic disorder operators whose correlators will decay exponentially to zero at large scales. Thus, considering only the Gaussian part of Eq. (21), we can show that the spin-correlation functions at large scales behave like

$$\begin{aligned}\langle S_z(x)S_z(y)\rangle &\sim(-1)^{(x-y)}|x-y|^{-2SK_S},\\ \langle S_+(x)S_-(y)\rangle &\sim(-1)^{(x-y)}|x-y|^{-1/(2SK_S)}.\end{aligned}\tag{25}$$

The fact that the $SU(2)$ symmetry is unbroken at all scales then fixes the value of K_S to be

$$K_S=1/(2S).\tag{26}$$

For this value of K_S one can show that the perturbing operator in (21) is marginally irrelevant.

We conclude then that the large scale behavior of half integer spin chains is given by the level 1 $SU(2)$ WZW model with logarithmic corrections as for the spin-$\frac{1}{2}$ chain. This confirms the scenario suggested by Affleck (see, for example, Ref. 8) where a perturbed $SU(2)_{2S}$ WZW model flows to its stable IR fixed point, the $SU(2)_1$. An interesting extension of this analysis is to add an arbitrary dimerization to the chain. In the context of the WZW approach this corresponds to the addition of the field $tr\ \Phi^{(1/2)}+\text{H.c.}\propto\mu_1:e^{i/2\sqrt{2S}[\varphi(z)-\bar{\varphi}(z)]}:+\text{H.c.}$ in the perturbing terms.[8] Reproducing the same arguments as above, we see that this term has the effect of making the operator $\cos[S/\sqrt{2S}(\varphi-\bar{\varphi})]$ appear in the effective action (21). Using Eq. (26), we see now that this operator is highly relevant, and so will produce a gap in the excitation spectrum unless a fine tuning of the parameters is performed.

Let us now consider integer spins S. Since the series (24) for the effective spin operator contains only half integer spins j (odd k's), all the operators in the series will contain nontrivial parafermionic operators. Then all the terms in the spin-spin correlation function will decay exponentially to zero with the distance indicating the presence of a gap in the excitation spectrum, thus confirming Haldane's conjecture. This is our main result.

A possible modification consists in the addition of dimerization to the system (that again corresponds to the inclusion of the field $tr\ \Phi^{(1/2)}$ as a perturbation). Then, also integer spin j terms (even k's) will be generated [as indicated by the fusion rules (14)] in the effective spin operator and in particular the vertex operator (19), which is the only candidate for a power-law decay of the spin-spin correlators. However, as for the (dimerized) half integer spin case, the presence in Eq. (22) of the (relevant) first vertex operator prevents the system from being massless (this situation is similar to the one encountered in Ref. 19, in the context of Abelian bosonization), indicating again that a fine tuning of the dimerization parameter has to be performed to get a massless regime.

We have presented the continuum limit of the spin S antiferromagnetic Heisenberg chain in terms of a parafermion conformal field theory interacting with a compact $U(1)$ boson. After integrating out the massive parafermions, we have shown that HAF chains with half-odd-integer spins have a massless spectrum while those with integer spin have a gap to all excitations, in complete accordance with Haldane's conjecture.

It has been shown by using a mapping to the σ model that a dimerized spin S chain should have $2S+1$ massless points in the dimerization parameter space.[9] This result was shown to be valid for large S and a detailed treatment of dimerization within the present approach could help to extend this result for small values of the spin.

ACKNOWLEDGMENTS

We are grateful to F. Alcaraz, P. Dorey, V. S. Dotsenko, A. Lugo, V. A. Fateev, A. Honecker, M. Picco, and V. Rittenberg for useful discussions. D.C.C. thanks CONICET and Fundación Antorchas for financial support. C.v.R. was supported by CONICET, Argentina.

[1] F. D. M. Haldane, Phys. Rev. Lett. **50**, 1153 (1983); Phys. Lett. **93A**, 464 (1983).
[2] R. J. Baxter, Ann. Phys. (N.Y.) **70**, 193 (1972); **70**, 323 (1972); L. D. Fadeev and L. A. Takhtajan, Phys. Lett. **85A**, 375 (1981).
[3] M. Hagiwara, K. Katsumata, I. Affleck, B. I. Halperin, and J. P. Renard, Phys. Rev. Lett. **65**, 3181 (1990); M. Takahashi, *ibid.* **62**, 2313 (1989); O. Golinelli, T. Jolicoeur, and R. Lacaze, Phys. Rev. B **50**, 3037 (1994).
[4] E. Lieb, T. Schultz, and D. Mattis, Ann. Phys. (Leipzig) **16**, 407 (1961); I. Affleck and E. Lieb, Lett. Math. Phys. **12**, 57 (1986).
[5] T. Ziman and H. J. Schulz, Phys. Rev. Lett. **59**, 140 (1987).
[6] K. Hallberg, X. Q. G. Wang, P. Horsch, and A. Moreo, Phys. Rev. Lett. **76**, 4955 (1996).
[7] G. E. Granroth, M. W. Meisel, M. Chaparala, Th. Jolicoeur, B. H. Ward, and D. R. Talham, Phys. Rev. Lett. **77**, 1616 (1996).
[8] I. Affleck, in *Fields, Strings and Critical Phenomena*, Les Houches, Session XLIX, edited by E. Brezin and J. Zinn-Justin (North-Holland, Amsterdam, 1988).
[9] I. Affleck and F. D. M. Haldane, Phys. Rev. B **36**, 5291 (1987).
[10] H. J. Schulz, Phys. Rev. B **34**, 6372 (1986).
[11] C. Itoi and H. Mukaida, J. Phys. A **27**, 4695 (1994).
[12] E. Witten, Commun. Math. Phys. **94**, 455 (1984).
[13] V. G. Knizknik and A. B. Zamolodchikov, Nucl. Phys. B **247**, 83 (1984).
[14] S. G. Naculich and H. J. Schnitzer, Nucl. Phys. B **347**, 687 (1990).
[15] A. B. Zamolodchikov and V. A. Fateev, Zh. Éksp. Teor. Fiz. **89**, 380 (1985) [Sov. Phys. JETP **62**, 215 (1985)].
[16] D. Gepner and E. Witten, Nucl. Phys. B **278**, 493 (1986).
[17] D. Gepner and Z. Qiu, Nucl. Phys. B: Field Theory Stat. Syst. **285**[FS19], 423 (1987).
[18] V. A. Fateev, Int. J. Mod. Phys. A **12**, 2109 (1991).
[19] H. J. Schulz, cond-mat/9605075 (unpublished).

Magnetization plateaux in N-leg spin ladders

D. C. Cabra
Departamento de Física, Universidad Nacional de la Plata, C.C. 67, (1900) La Plata, Argentina and Facultad de Ingeniería, Universidad Nacional de Lomas de Zamora, Cno. de Cintura y Juan XXIII, (1832), Lomas de Zamora, Argentina

A. Honecker and P. Pujol
International School for Advanced Studies, Via Beirut 2-4, 34014 Trieste, Italy
(Received 6 February 1998; revised manuscript received 8 April 1998)

In this paper we continue and extend a systematic study of plateaux in magnetization curves of antiferromagnetic Heisenberg spin-1/2 ladders. We first review a bosonic field-theoretical formulation of a single XXZ chain in the presence of a magnetic field, which is then used for an Abelian bosonization analysis of N weakly coupled chains. Predictions for the universality classes of the phase transitions at the plateaux boundaries are obtained in addition to a quantization condition for the value of the magnetization on a plateau. These results are complemented by and checked against strong-coupling expansions. Finally, we analyze the strong-coupling effective Hamiltonian for an odd number N of cylindrically coupled chains numerically. For $N=3$ we explicitly observe a spin gap with a massive spinon-type fundamental excitation and obtain indications that this gap probably survives the limit $N\to\infty$. [S0163-1829(98)07633-4]

I. INTRODUCTION

So-called ''spin ladders'' have recently attracted a considerable amount of attention (for reviews see, e.g., Ref. 1). They consist of coupled one-dimensional chains and may be regarded as interpolating truly one- and two-dimensional systems. Such an intermediate situation may be useful (among others) for the understanding of high-T_c superconductors. In fact, modifications of the high-T_c materials (see, e.g., Ref. 2) give rise to experimental realizations of spin ladders. However, the field was motivated by an observation that mainly concerns the magnetic spin degrees of freedom, namely the appearance of a spin gap in $N=2$ coupled gapless chains (see, e.g., Ref. 3).

One-dimensional quantum magnets have been studied in great detail over the past decades. One remarkable observation in this area is the so-called ''Haldane conjecture''[4] which states that isotropic half-integer spin Heisenberg chains are gapless while those with integer spin are gapped. Although this statement has not been proven rigorously yet, a wealth of evidence supporting this conjecture has accumulated in the meantime[5] (see also[6] for a recent field-theoretical treatment).

Spin ladders are more general quasi-one-dimensional quantum magnets. Again, one of the attractions is a natural generalization of Haldane's conjecture[4] to such N coupled spin-S chains: If SN is an integer, one expects a gap in zero field, otherwise not. This conjecture is suggested among others by the large-S limit (see Ref. 7 for a recent review and references therein), strong-coupling considerations,[3,8] numerical computations,[9–11] and even experiments (see, e.g., Ref. 2).[12] If one includes a strong magnetic field, these Haldane gaps become just a special case of plateaux in magnetization curves. In the presence of a magnetic field, one of the central issues is the quantization condition on the magnetization $\langle M\rangle$ for the appearance of such plateaux, which for the purposes of the present paper will be some special form of

$$lSN(1-\langle M\rangle)\in\mathbf{Z}. \tag{1.1}$$

Here $\langle M\rangle$ is normalized to a saturation value $\langle M\rangle=\pm 1$ and l is the number of lattice sites to which translational symmetry is either spontaneously or explicitly broken. Haldane's original conjecture[4] is related to $l=N=1$, $\langle M\rangle=0$. More general cases for $N=1$ were treated in Refs. 13–15. In an earlier paper,[16] we have studied realizations of the condition (1.1) for $N>1$ but with the specializations $l=1$ and $S=1/2$.

So far, spin ladders in strong magnetic fields have attracted surprisingly little attention: To our knowledge, only the case of an $N=2$-leg ladder had been investigated prior to Ref. 16. The experimental measurement of the magnetization curve of the organic two-leg ladder material $Cu_2(C_5H_{12}N_2)_2Cl_4$ (Ref. 17) gave rise to theoretical studies using numerical diagonalization,[18] series expansions,[19] and a bosonic field-theory approach.[20] In this case (i.e., $N=2$ and $S=1/2$), there is a spin gap which gives rise to an $\langle M\rangle=0$ plateau in the magnetization curve. The transition between this zero magnetization plateau and saturation is smooth and no nontrivial effects (in particular no symmetry breaking) were observed.

For $N>2$ one can expect plateaux at nontrivial N-dependent fractions of the saturation magnetization.[16] Though this was a new observation for spin ladders, the phenomenon itself is not completely new. For example, the possibility of magnetization plateaux for the case of single spin-S Heisenberg chains has been discussed systematically in Ref. 13 which also motivated some of our work. The attraction of this phenomenon in spin ladders is that they provide clear and natural realizations of such plateaux. For example a numerical analysis of the case $N=3$ explicitly exhibits a

robust plateau with $\langle M\rangle = 1/3$ (Ref. 16) which should also be observable experimentally, e.g., in a suitable organic spin-ladder material.

It is the purpose of the present paper to continue a systematic study of Eq. (1.1) for generic $N \geqslant 1$ by using different complementary techniques, such as Abelian bosonization, strong-coupling expansions, and numerical computations (the reader may find, e.g., Ref. 16 helpful in the understanding of the present work). Here, we will among others provide evidence that for $S = 1/2$ spontaneous breaking of the translational symmetry to $l = 2$ can be induced by strong frustration or an Ising-like anisotropy, while $l \geqslant 3$ presumably needs explicit symmetry breaking. (In Ref. 15 a slightly different example of spontaneous symmetry breaking with $l = 2$ was studied.)

The prefactor lSN in Eq. (1.1) may seem quite cumbersome, but it just counts the possible S^z values in a unit cell of a one-dimensional translationally invariant ground state. It should also be noted that Eq. (1.1) is just a necessary condition; whether a plateau actually appears or not depends on the parameters and the details of the model under consideration. For example, plateaux with nonzero $\langle M\rangle \neq 0$ have not been observed in the SU(2) symmetric higher spin-S Heisenberg chains (see, e.g., Ref. 21), unless translational invariance is explicitly broken (cf. Ref. 14 for $S = 1$).

Conditions of the type (1.1) occur also in generalizations of the Lieb-Schultz-Mattis theorem.[22–24,13] This theorem constructs a *nonmagnetic* excitation which in the thermodynamic limit is degenerate with the ground state for a given magnetization $\langle M\rangle$ and orthogonal to it unless $\langle M\rangle$ satisfies Eq. (1.1). In this manner one proves the existence of either gapless excitations or spontaneous breaking of translational symmetry. Unfortunately it is at present not clear that this theorem applies to plateaux in magnetization curves since they require a gap to *magnetic* excitations.

Here we concentrate mainly on the case $S = 1/2$ and all couplings in the antiferromagnetic regimes, but try to keep N as general as possible. Other situations can be analyzed as well, but may lead to somewhat different physics (compare, e.g., Ref. 25 for the example of $N = 3$ antiferromagnetically coupled ferromagnetic chains).

This paper is organized as follows: In Sec. II we first review some aspects of the formulation of a single XXZ chain as a bosonic $c = 1$ conformal field theory. This serves as a basis of later investigations and illustrates some generic features also present in N-leg spin ladders. In Sec. III we first introduce the precise lattice model and its field-theoretic counterpart which we then analyze in the weak-coupling regime. Section IV starts from the other extreme—the strong-coupling limit—and proceeds with series expansions around this limit. In Sec. V we discuss an effective Hamiltonian for the strong-coupling limit of an odd number N of cylindrically coupled chains which we then analyze numerically in Sec. VI. We summarize our results by presenting ''magnetic phase diagrams'' in Sec. VII before we conclude with some comments and open problems (Sec. VIII).

II. A SINGLE XXZ CHAIN

First, we recall some results for the XXZ chain on a ring of L sites in the presence of a magnetic field h applied along the z axis:

$$H_{XXZ} = J\sum_{x=1}^{L}\left\{\Delta S_x^z S_{x+1}^z + \frac{1}{2}(S_x^+ S_{x+1}^- + S_x^- S_{x+1}^+)\right\} - h\sum_{x=1}^{L} S_x^z. \tag{2.1}$$

Apart from being the basis for the investigation in later sections, this also serves as an illustration of some general features. It should be noted that in Eq. (2.1) the magnetic field is coupled to a conserved quantity which is related to the magnetization $\langle M\rangle$ via $\langle M\rangle = \langle (2/L)\Sigma_{x=1}^{L} S_x^z\rangle$. For this reason, properties of Eq. (2.1) in the presence of a magnetic field $h \neq 0$ can be related to those at $h = 0$ and the magnetic field h can be considered as a chemical potential.

The Hamiltonian (2.1) is exactly solvable by Bethe ansatz also for $h \neq 0$. In this way it can be rigorously shown that its low-energy properties are described by a $c = 1$ conformal field theory of a free bosonic field compactified at radius R in the thermodynamic limit for $\Delta > -1$ and any given magnetization $\langle M\rangle$ (see, e.g., Ref. 26 and compare also Ref. 27 for a detailed discussion of the case $|\Delta| < 1$). More precisely, upon insertion of the bosonized representation of the spin operators into the Hamiltonian (2.1) (see, e.g., Ref. 28) one obtains the following low-energy effective Hamiltonian for the XXZ chain:

$$\overline{H}_{XXZ} = \int dx \frac{\pi}{2}\{\Pi^2(x) + R^2(\langle M\rangle, \Delta)(\partial_x \phi(x))^2\} \tag{2.2}$$

with $\Pi = (1/\pi)\partial_x \tilde{\phi}$, and $\phi = \phi_L + \phi_R$, $\tilde{\phi} = \phi_L - \phi_R$. In Eq. (2.2) we have suppressed a (for our purposes) irrelevant proportionality constant that includes the velocity of sound. In this formulation, the effect of both the magnetic field h and XXZ anisotropy Δ turns up only via the radius of compactification $R(\langle M\rangle, \Delta)$. This radius governs the conformal dimensions, in particular the conformal dimension of a vertex operator $e^{i\beta\phi}$ is given by $(\beta/4\pi R)^2$. We now describe how R can be computed.

We parametrize the XXZ anisotropy by $\Delta = \cos\theta$ with $0 < \theta < \pi$ for $-1 < \Delta < 1$ and by $\Delta = \cosh\gamma$ with $\gamma > 0$ for $\Delta > 1$. Now for given magnetization $\langle M\rangle \geqslant 0$ and XXZ anisotropy Δ, the associated radius of compactification R and magnetic field h/J can be obtained by solving integral equations (see, e.g., Refs. 27,29–31) in the following way: First, introduce a function $\sigma(\eta)$ for the density of particles satisfying the integral equation

$$\sigma(\eta) = \frac{1}{2\pi}\left\{g(\eta) - \int_{-\Lambda}^{\Lambda} K(\eta - \eta')\sigma(\eta')d\eta'\right\}, \tag{2.3}$$

where the kernel $K(\eta)$ and the right-hand side $g(\eta)$ are presented in Table I.

The real parameter $\Lambda \geqslant 0$ in Eq. (2.3) describes the spectral parameter value at the Fermi surface and is determined by the magnetization $\langle M\rangle$ via the filling condition

$$\int_{-\Lambda}^{\Lambda} \sigma(\eta)d\eta = \frac{1}{2}(1 - \langle M\rangle). \tag{2.4}$$

In general, one has to adjust Λ iteratively by first numerically solving Eq. (2.3) and then checking for Eq. (2.4). Only some

TABLE I. Functions appearing in the integral equations.

Δ	$K(\eta)$	$g(\eta)$	$\epsilon_0(\eta)$
$\cos\theta=\Delta<1$	$\dfrac{\tan\theta}{\tan^2\theta\,\cosh^2(\eta/2)+\sinh^2(\eta/2)}$	$\dfrac{\cot(\theta/2)}{\cosh^2(\eta/2)+\cot^2(\theta/2)\sinh^2(\eta/2)}$	$\dfrac{h}{J}-\dfrac{\sin^2\theta}{\cosh\eta-\cos\theta}$
$\Delta=1$	$\dfrac{4}{\eta^2+4}$	$\dfrac{2}{\eta^2+1}$	$\dfrac{h}{J}-\dfrac{2}{\eta^2+1}$
$\cosh\gamma=\Delta>1$	$\dfrac{\tanh\gamma}{\tanh^2\gamma\cos^2(\eta/2)+\sin^2(\eta/2)}$	$\dfrac{\coth(\gamma/2)}{\cos^2(\eta/2)+\coth^2(\gamma/2)\sin^2(\eta/2)}$	$\dfrac{h}{J}-\dfrac{\sinh^2\gamma}{\cos\eta-\cosh\gamma}$

special cases can be solved explicitly. This includes the case $\langle M\rangle=0$ and $\Delta\leqslant 1$ where $\Lambda=\infty$ is the correct choice. Once the desired value of Λ is determined, one introduces a dressed charge function $\xi(\eta)$ (see, e.g., Refs. 29,30) as a solution of the integral equation

$$\xi(\eta)=1-\frac{1}{2\pi}\int_{-\Lambda}^{\Lambda}K(\eta-\eta')\xi(\eta')d\eta' \tag{2.5}$$

giving directly rise to the radius of compactification

$$R(\langle M\rangle,\Delta)=\frac{1}{\sqrt{4\pi}\xi(\Lambda)}. \tag{2.6}$$

If one further wants to determine the associated magnetic field h, one has to introduce another function $\epsilon_d(\eta)$, the dressed energy, satisfying the integral equation

$$\epsilon_d(\eta)=\epsilon_0(\eta)-\frac{1}{2\pi}\int_{-\Lambda}^{\Lambda}K(\eta-\eta')\epsilon_d(\eta')d\eta' \tag{2.7}$$

with the bare energy $\epsilon_0(\eta)$ listed in Table I. Then the magnetic field h/J is determined by the condition that the energy of the dressed excitations vanishes at the Fermi surface

$$\epsilon_d(\Lambda)=0. \tag{2.8}$$

Using Eq. (2.5) one can see that $\epsilon(\eta)=\epsilon(\eta)|_{h=0}+(h/J)\xi(\eta)$ solves Eq. (2.7) if $\epsilon(\eta)|_{h=0}$ solves Eq. (2.7) with formally $h=0$ (but for the given $\langle M\rangle$). From this and Eq. (2.8) one can easily obtain h once Λ is known via $h/J=-\epsilon(\Lambda)|_{h=0}/\xi(\Lambda)$.

In general, these integral equations have to be solved numerically and Λ has to be determined by some iterative method. Although this is readily done by standard methods, a generally accessible implementation seems to be still unavailable. We have therefore decided to tentatively provide access to such solutions on the World Wide Web.[32] This implementation works in the way described above. Typically, it gives results with an absolute accuracy of 10^{-6} or better. Of course, one can change the order of the procedure: For example, one could also prescribe h/J, then determine Λ from Eqs. (2.7) and (2.8), next the radius of compactification R from Eqs. (2.5) and (2.6) and finally (optionally) the magnetization $\langle M\rangle$ from Eqs. (2.3) and (2.4).

Some remarks are in order concerning the case $\Delta>1$: In this region the identification with a $c=1$ conformal field theory has been established directly only by a numerical analysis of the Bethe-ansatz equations (for a summary see, e.g., Sec. II of Ref. 33). However, the six-vertex model in external fields has been shown[34] to yield a $c=1$ conformal field theory, and since the XXZ chain arises as the Hamiltonian limit of the six-vertex model, this indirectly establishes the identification. Still, explicit formulas, e.g., for R are not available in the literature and therefore we have obtained the integral equations presented for the case $\Delta>1$ above by an analytical continuation of those for $\Delta<1$, as is suggested, e.g., by Ref. 35 (see, also, Ref. 36—apparently such a continuation was also used in the recent work[14]). We have performed some checks that this yields indeed correct results. For example, some radii R associated to certain magnetic fields h and anisotropies Δ obtained numerically for chains of length up to $L=234$ (Ref. 37) are reproduced in this way.

As a further check, one can compare the critical magnetic field for the boundary of the $\langle M\rangle=0$ plateau at $\Delta>1$ obtained by numerical solution of the above integral equations with the exact solution of the Bethe-ansatz equations[38]

$$\frac{h_c}{J}=\frac{2\pi\,\sinh\gamma}{\gamma}\sum_{n=0}^{\infty}\frac{1}{\cosh[(2n+1)\pi^2/2\gamma]}, \tag{2.9}$$

where as before $\Delta=\cosh\gamma$. In this case (i.e., for $\langle M\rangle=0$) one has $\Lambda=\pi$ and the above integral equations can be solved using Fourier series.[35,36,38] If one solves the above integral equations numerically, the deviation from the exact result (2.9) is of the order of the numerical accuracy (in our implementation[32] always less than 10^{-6}).

In passing we make a comment which will turn out to be useful later. The result (2.9) is the gap to $S^z=1$ excitations. However, the fundamental excitation of the XXZ chain is known to be a so-called ''spinon'' which carries $S^z=1/2$.[39–41] This spinon can be regarded as a domain wall between the two antiferromagnetic ground states for $\Delta>1$. Since a single spin-flip creates two domain walls, the lowest $S^z=1$ excitation is a scattering state of two spinons. This picture can be useful, e.g., in numerical computations. For example, a single spinon can be observed for odd L with periodic boundary conditions.

After this digression let us now return to the above integral equations. The results obtained from them are summarized in the magnetic phase diagram for the XXZ chain Fig. 1 (see, also, Refs. 42,33 for similar pictures). There are two gapped phases: A ferromagnetic one at sufficiently strong fields (which is actually the only one for $\Delta<-1$) and an antiferromagnetic phase for $\Delta>1$ at small fields. In between is the massless phase where the bosonized form (2.2) is valid. An elementary computation of the spin-wave dispersion above the ferromagnetic ground state shows that the transition between the ferromagnetic phase and the massless phase is located at $h/J=1+\Delta$. This transition is a very clear

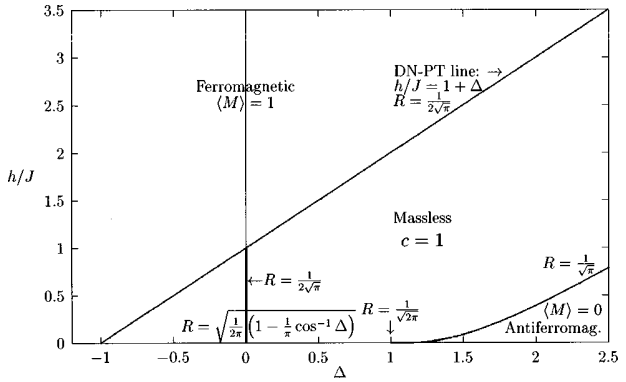

FIG. 1. Magnetic phase diagram of the XXZ chain (2.1). For explanations compare the text.

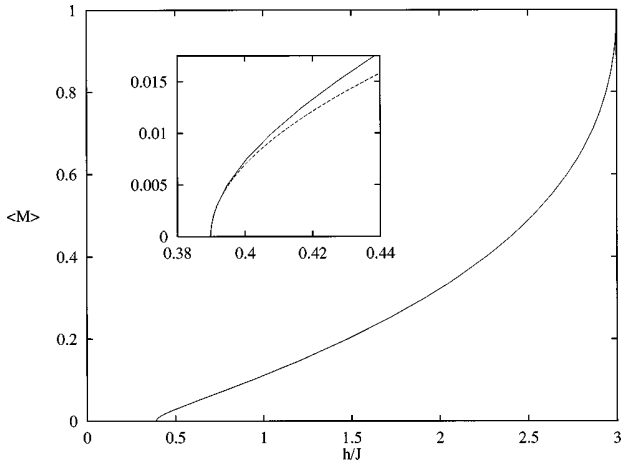

FIG. 2. Magnetization curve of the XXZ chain at $\Delta=2$ obtained from the integral equations (2.3), (2.4), (2.7), and (2.8). The inset shows the region of small magnetization and illustrates that also the transition $\langle M\rangle\to 0$ is compatible with the DN–PT universality class for $\Delta>1$ [the dashed line is a fit to the universal form (2.10)].

example of the Dzhaparidze-Nersesyan–Pokrovsky-Talapov (DN–PT) universality class,[43–45] i.e., for $\langle M\rangle\to 1$ the magnetization behaves as (compare also Ref. 46)

$$(\langle M\rangle - M_c)^2 \sim h^2 - h_c^2, \tag{2.10}$$

here $M_c=1$ and $h_c/J=1+\Delta$. At this transition the radius takes the universal value $R(1,\Delta)=1/(2\sqrt{\pi})$.

The other transition line starts at the SU(2) symmetric point $\langle M\rangle=0$, $\Delta=1$ with a radius $R(0,1)=1/\sqrt{2\pi}$. Actually, at $\langle M\rangle=0$ the additional operator

$$\cos(4\sqrt{\pi}\phi) \tag{2.11}$$

appears in the continuum limit, which we have suppressed in Eq. (2.2) since it is irrelevant inside the massless phase. At $\Delta=1$ it is marginal and becomes relevant for $\Delta>1$, opening the gap that gives the boundary of the antiferromagnetic phase in Fig. 1. The associated phase transition is a Kosterlitz-Thouless (K-T) transition[47] (see, e.g., Refs. 48–50). The almost marginal nature of the operator responsible for the gap leads to a stretched exponential decay for Δ slightly bigger than one which is characteristic for a K-T transition.[51] The exact asymptotic form for the gap (or critical magnetic field) of the XXZ chain is easily obtained from the Bethe-ansatz solution (2.9) upon noting that $\gamma \approx \sqrt{2(\Delta-1)}$ and that in the limit $\Delta\to 1$ only the term $n=0$ contributes to the sum. One then finds[38]

$$\frac{h_c}{J} \sim 4\pi e^{-\pi^2/(2\sqrt{2(\Delta-1)})} \quad (\text{for } \Delta \text{ slightly bigger than } 1). \tag{2.12}$$

For this reason the phase boundary is indistinguishable from the $h=0$ line for XXZ anisotropies up to $\Delta\approx 1.2$ on the scale of Fig. 1. In this region, the numerical determination of the radius R is difficult for $\langle M\rangle\to 0$. Nevertheless, using that $\Lambda=\pi$ for $\langle M\rangle=0$ and $\Delta>1$, one can readily check that the constant function $\xi(\eta)=\frac{1}{2}$ solves the integral equation (2.5). Then one obtains from Eq. (2.6) that $R(0,\Delta>1)=1/\sqrt{\pi}$.

For $\langle M\rangle=0$ and $|\Delta|\leqslant 1$ one has $\Lambda=\infty$ (see above) and one can use the Wiener-Hopf method to solve the above integral equations in closed form. This yields in particular $R(0,\Delta)=\sqrt{1/2\pi[1-(1/\pi)\cos^{-1}\Delta]}$.[28] In general, the radius R increases with increasing Δ. For $\Delta>0$, it decreases with increasing magnetization $\langle M\rangle$, while for $\Delta<0$ this is reversed to an increase in R with increasing $\langle M\rangle$. Clearly, the radius must be constant on the XY line which separates these two regions: $R(\langle M\rangle,0)=1/2\sqrt{\pi}$ (though the magnetic field associated to a given $\langle M\rangle$ is still a nontrivial function which should be computed from the above integral equations).

Including the operator (2.11) in the bosonized language (2.2), one recovers a Hamiltonian treated in Ref. 52 as a model for commensurate-incommensurate transitions. This means that the transition $\langle M\rangle\to 0$ for $\Delta>1$ is predicted to be in the DN–PT universality class,[43,44] too. The same bosonization argument also leads to the already mentioned result $R(0,\Delta>1)=1/\sqrt{\pi}$ (see, also, Ref. 26). The inset in Fig. 2 illustrates for $\Delta=2$ that for sufficiently small magnetizations one can indeed observe a behavior that is compatible with the universal square root (2.10). It should be noted though that the window for the universal DN–PT behavior is too small to permit verification within our numerical accuracy for smaller values of Δ (e.g., $\Delta\leqslant 1.2$) where neither a reliable numerical check of the result $R=1/\sqrt{\pi}$ is possible. An analytic check of the asymptotic behavior of the magnetization from the Bethe-ansatz solution would be interesting, but is beyond the scope of the present paper.

It should be noted that the height of the entire inset in Fig. 2 corresponds to the first step in the magnetization curve of a chain of the finite size $L=112$. Therefore, the exact solution is crucial in verifying the exponent (2.10)—a numerical or experimental verification of this behavior restricted to such a small region would be extremely difficult. Similar difficulties will be faced in an experimental or numerical verification of $R(0,\Delta)=1/\sqrt{\pi}$ or the equivalent statement for the correlation function exponents in the region of Δ slightly larger than 1.

III. LADDERS: WEAK COUPLING AND ABELIAN BOSONIZATION

In this section we apply Abelian bosonization to the weak-coupling region $J'\ll J$ of N-leg spin ladders. In particular, we will show how the necessary condition (1.1)

arises in this formulation and discuss under which circumstances an allowed plateau does indeed open as a function of the parameters J' and Δ. The lattice Hamiltonian for this system is given by

$$H^{(N)}=J'\sum_{i,j}\sum_{x=1}^{L}\vec{S}_{i,x}\vec{S}_{j,x}+J\sum_{i=1}^{N}\sum_{x=1}^{L}\left\{\Delta S^z_{i,x}S^z_{i,x+1}+\frac{1}{2}(S^+_{i,x}S^-_{i,x+1}+S^-_{i,x}S^+_{i,x+1})\right\}-h\sum_{i,x}S^z_{i,x}, \quad (3.1)$$

where J' and J are, respectively, the interchain and intrachain couplings, h is the external magnetic field and the indices i and j label the different chains (legs) in the ladder. The sum in the first term is over all possible couplings between chains. The case of periodic boundary conditions (PBC) and open boundary conditions (OBC) will be discussed later. Here we have explicitly included an XXZ anisotropy Δ in the intrachain coupling. We have kept the interchain coupling J' SU(2) symmetric for simplicity in later sections although this is not substantial in the weak-coupling region which we will discuss in the remainder of this section.

The corresponding effective field-theoretic Hamiltonian is obtained using standard methods[53,28] (see, also, Refs. 13–15 for the case of nonzero magnetization). One essentially uses Eq. (2.2) as the effective Hamiltonian for each chain and the bosonized expressions for the spin operators which read

$$S^z_{i,x}\approx\frac{1}{\sqrt{2\pi}}\frac{\partial\phi_i}{\partial x}+\text{const}:\cos(2k^i_F x+\sqrt{4\pi}\phi_i):+\frac{\langle M_i\rangle}{2}, \quad (3.2)$$

and

$$S^{\pm}_{i,x}\approx:e^{\pm i\sqrt{\pi}\tilde{\phi}_i}[1+\text{const}\,\cos(2k^i_F x+\sqrt{4\pi}\phi_i)]:. \quad (3.3)$$

Here we have set a lattice constant to unity which appears in passing to the continuum limit. The colons denote normal ordering which we take with respect to the ground state of a given mean magnetization $\langle M_i\rangle$ in the ith chain which is a natural choice. This leads to the constant term in Eq. (3.2) which will play an important role in the discussion of the terms that can be generated radiatively. The prefactor 1/2 arises from our normalization of the magnetization to saturation values $\langle M\rangle=\pm 1$. The Fermi momenta k^i_F are given by $k^i_F=\pi(1-\langle M_i\rangle)/2$.

In the weak-coupling limit along the rungs, $J'\ll J$, we obtain the following bosonized low-energy effective Hamiltonian for the N-leg ladder keeping only the most relevant perturbation terms:

$$\overline{H}^{(N)}=\int dx\left[\frac{\pi}{2}\sum_{i=1}^{N}\{\Pi_i^2(x)+R^2(\langle M\rangle,\Delta)(\partial_x\phi_i(x))^2\}+\frac{\lambda_1}{2\pi}\sum_{i,j}(\partial_x\phi_i(x))(\partial_x\phi_j(x))+\sum_{i,j}\{\lambda_2:\cos[2x(k^i_F+k^j_F)+\sqrt{4\pi}(\phi_i+\phi_j)]:+\lambda_3:\cos[2x(k^i_F-k^j_F)+\sqrt{4\pi}(\phi_i-\phi_j)]:+\lambda_4:\cos[\sqrt{\pi}(\tilde{\phi}_i-\tilde{\phi}_j)]:\}\right]. \quad (3.4)$$

The four coupling constants λ_i essentially correspond to the coupling J' between the chains: $\lambda_i\sim J'/J$. In arriving at the Hamiltonian (3.4) we have discarded a constant term and absorbed a term linear in the derivatives of the free bosons into a redefinition of the applied magnetic field.

The Hamiltonian (3.4) has been also used to represent spin-N/2 chains (see, e.g., Refs. 53,54), since they can be obtained in the limit of N strongly ferromagnetically coupled chains ($J'\to-\infty$). However, here we will analyze Eq. (3.4) mainly in the case of small antiferromagnetic J' and discuss various boundary conditions.

Note that the λ_2 and λ_3 perturbation terms contain an explicit dependence on the position (in the latter case this x dependence disappears for symmetric configurations with equal k^i_F). Such operators survive in passing from the lattice to the continuum model, assuming that the fields vary slowly, only when they are commensurate. In particular, the λ_2 term appears in the continuum limit only if the oscillating factor $\exp(i2x(k^i_F+k^j_F))$ equals unity. If the configuration is symmetric, this in turn happens only for zero magnetization (apart from the trivial case of saturation).

For simplicity let us first analyze the case with $N=3$ and PBC. We first have to diagonalize the Gaussian (derivative) part of the Hamiltonian. This is achieved by the following change of variables in the fields:

$$\psi_1=\frac{1}{\sqrt{2}}(\phi_1-\phi_3),\quad \psi_2=\frac{1}{\sqrt{6}}(\phi_1+\phi_3-2\phi_2),\quad \psi_D=\frac{1}{\sqrt{3}}(\phi_1+\phi_2+\phi_3). \quad (3.5)$$

In terms of these fields the derivative part of the Hamiltonian can be written as

$$\overline{H}_{\text{der}}=\int dx\,\frac{\pi}{2}\{R^2(\langle M\rangle,\Delta)[(1+a)(\partial_x\psi_D(x))^2+(1-b)\times[(\partial_x\psi_1(x))^2+(\partial_x\psi_2(x))^2]]\}, \quad (3.6)$$

where $a=2J'/(J\pi^2R^2)=2b$. We can now study the large-scale behavior of the effective Hamiltonian (3.4) where we assume all k^i_F equal due to the symmetry of the chosen configuration of couplings. Let us first consider the case when

the magnetization $\langle M\rangle$ is nonzero. In this case only the λ_3 and λ_4 terms are present. The one-loop renormalization group (RG) equations are

$$\frac{db}{d\ \ln L}=4\pi\left(-\frac{3\lambda_3^2}{2R^2}+12\pi^2R^2\lambda_4^2\right),$$

$$\frac{d\lambda_3}{d\ \ln L}=\left(2-\frac{1}{2\pi R^2(1-b)}\right)\lambda_3-\pi\lambda_3^2, \tag{3.7}$$

$$\frac{d\lambda_4}{d\ \ln L}=[2-2\pi R^2(1-b)]\lambda_4-\pi\lambda_4^2.$$

It is important to notice that only the fields ψ_1 and ψ_2 enter in these RG equations, since the perturbing operators do not contain the field ψ_D. The behavior of these RG equations depends on the value of R. The main point is that always one of the two λ perturbation terms will dominate and the corresponding cosine operator tends to order the associated fields. This gives a finite correlation length in correlation functions containing the fields ψ_1 and ψ_2 (or their duals). For example, for $\Delta\leqslant 1$ we have that $R^2<(2\pi)^{-1}$ since $\langle M\rangle\neq 0$. Then, from Eq. (3.7) one can easily see that the dominant term will be the λ_4 one. This term orders the dual fields associated with ψ_1 and ψ_2. Then, the correlation functions involving these last fields decay exponentially to zero. In either case, the field ψ_D remains massless. A more careful analysis of the original Hamiltonian shows that this diagonal field will be coupled to the massive ones only through very irrelevant operators giving rise to a renormalization of its compactification radius. However, due to the strong irrelevance of such coupling terms these corrections to the radius are expected to be small, implying that the value of the large-scale effective radius keeps close to the zero-loop result $R\sqrt{1-a}$. It is straightforward to generalize this to N chains when all possible coupling are present and have the same value J'. One can find a change of variables on the fields to

$$\psi_D;\quad \psi_i\quad i=1,\ldots,N-1,$$

where $\psi_D=1/\sqrt{N}\Sigma_{i=1}^N\phi_i$. Again, for nonzero magnetization, all but the diagonal field ψ_D will be present in the perturbing terms λ_3 and λ_4. The RG equations are essentially the same as Eq. (3.7) and the result is that only the field ψ_D will be massless.

We are then left in principle with a free Gaussian action for the diagonal field. However some operators can be radiatively generated. We see from Eqs. (3.2),(3.3) that when we turn on the interchain coupling, the ''N-Umklapp'' term

$$J'^N\cos\left(2x\sum_{i=1}^N k_F^i+\sqrt{4\pi}\sum_{i=1}^N\phi_i\right)$$
$$=J'^N\cos\left(2x\sum_{i=1}^N k_F^i+\sqrt{4\pi N}\psi_D\right) \tag{3.8}$$

appears in the operator product expansion (OPE).

Again, this operator survives in passing from the lattice to the continuum model, assuming that the fields vary slowly, only when the oscillating factor $\exp(i2x\Sigma_{j=1}^N k_F^j)$ equals one. This in turn will happen when the following specialized version of the condition (1.1)

$$\frac{N}{2}(1-\langle M\rangle)\in\mathbf{Z} \tag{3.9}$$

is satisfied. At such values of the magnetization, the field ψ_D can then undergo a K-T transition to a massive phase, indicating the presence of a plateau in the magnetization curve. An estimate of the value of J' at which this operator becomes relevant can be obtained from its scaling dimension which in zero-loop approximation is given by

$$\dim(\cos(\sqrt{4\pi N}\psi_D))=\frac{N}{4[\pi R^2+(N-1)/\pi(J'/J)]}. \tag{3.10}$$

At $\Delta=1$ one then obtains $J_c'\approx 0.09J$ for the $\langle M\rangle=1/3$ plateau at $N=3$ and $J_c'\approx 0.7J$ for $\langle M\rangle=1/2$ at $N=4$ and also for $\langle M\rangle=1/5$ at $N=5$. At the opening of such plateaux, the effective radius of compactification is fixed to be

$$R_{\rm eff}^2=\frac{N}{8\pi} \tag{3.11}$$

and the large-scale effective spin operators are (cf. Ref. 53):

$$S_{\rm eff}^z(x)\approx\sqrt{\frac{N}{2\pi}}\frac{\partial\psi_D}{\partial x}$$
$$+\text{const}:\cos(2k_Fx+\sqrt{4\pi N}\psi_D):+\frac{\langle M\rangle}{2}, \tag{3.12}$$

and

$$S_{\rm eff}^{\pm}(x)\approx :e^{\pm i\sqrt{\pi/N}\tilde{\psi}_D}[1+\text{const}\cos(2k_Fx+\sqrt{4\pi N}\psi_D)]:. \tag{3.13}$$

Then, Eq. (3.11) fixes the values of the correlation exponents at this point to be

$$\eta_z=4;\quad \eta_{xy}=\frac{1}{4}. \tag{3.14}$$

On the other hand, commensurate-incommensurate transition results[52,20,14] imply that the values of these exponents should be

$$\eta_z=2;\quad \eta_{xy}=\frac{1}{2} \tag{3.15}$$

along the upper and lower boundary of a plateau. This situation is similar to the XXZ chain at $\Delta=1$ and $\Delta>1$ for the boundary of the $\langle M\rangle=0$ plateau. However, the values of the exponents are different since the perturbing operators are different.

Note that the ''N-Umklapp'' process which allows the appearance of Eq. (3.8) produces a complete family of operators given by

$$\cos\left(2xl\sum_{i=1}^{N}k_F^i+l\sqrt{4\pi}\sum_{i=1}^{N}\phi_i\right)$$

$$=\cos\left(2xl\sum_{i=1}^{N}k_F^i+l\sqrt{4\pi N}\psi_D\right) \qquad (3.16)$$

with l an arbitrary integer. The values of the magnetization for which one of these operators is allowed are subject to a generalization of Eq. (3.9), namely Eq. (1.1) in the Introduction (with $S=1/2$). However, the dimensions of these operators increase with l^2. So, these operators cannot be relevant unless we consider regimes with an anisotropy parameter Δ bigger than one or very big values of the interchain coupling J' far from the perturbative regime of the present analysis. Therefore, higher values of l are realized only under special conditions. While $l=2$ can be obtained by either strong Ising-like anisotropy Δ or frustration at strong coupling (see Sec. VI below), it is possible that $l\geqslant 3$ can be realized only if suitable symmetry-breaking terms are explicitly introduced into the Hamiltonian (3.1).

Note that formally, the preceding analysis can also be carried out using the fermionic Jordan-Wigner formulation. For example, in this formulation the N-Umklapp operator (3.8) is given by

$$\left(\prod_{a=1}^{N}R_a^{\dagger}(x)L_a(x)\exp(2ik_F^a x)\right)$$

$$+\left(\prod_{a=1}^{N}L_a^{\dagger}(x)R_a(x)\exp(-2ik_F^a x)\right),$$

where R_a and L_a are the right- and left-moving components of the fermions. We have chosen to use the bosonized language because it is more appropriate for general values of the anisotropy Δ.

The analysis above was for the case where all the chains were coupled together with the same coupling value. More precisely, the estimates for the appearance of plateaux were for positive (frustrating) interchain coupling. To generalize this to PBC (which is different from the preceding case for $N\geqslant 4$), we first notice, using the bosonized expression of the effective Hamiltonian, that this configuration of couplings is not stable under RG transformation. E.g., the OPE between terms like $\cos(\phi_1-\phi_2)$ and $\cos(\phi_2-\phi_3)$ generates an effective coupling between the fields ϕ_1 and ϕ_3, etc. The underlying intuitive picture is that antiferromagnetic couplings between the chain 2 with the chains 1 and 3 generates an effective ferromagnetic coupling between the chains 1 and 3. For example, for $N=4$ and PBC, ferromagnetic couplings are generated along the diagonals between originally uncoupled chains. This case is part of the family of configurations with antiferromagnetic nearest-neighbor and ferromagnetic next-nearest-neighbor couplings. For this general situation at $N=4$, the coupling matrix in the derivative part is given by

$$\begin{pmatrix} 1 & a & -b & a \\ a & 1 & a & -b \\ -b & a & 1 & a \\ a & -b & a & 1 \end{pmatrix}, \qquad (3.17)$$

where a and b are positive. As in the preceding analysis, one can change variables to

$$\psi_D=\frac{1}{\sqrt{4}}(\phi_1+\phi_2+\phi_3+\phi_4);$$

$$\psi_1=\frac{1}{\sqrt{4}}(\phi_1-\phi_2+\phi_3-\phi_4);$$

$$\psi_2=\frac{1}{\sqrt{2}}(\phi_1-\phi_3); \quad \psi_3=\frac{1}{\sqrt{2}}(\phi_2-\phi_4). \qquad (3.18)$$

For generic values of the magnetization, it is easy to see that the diagonal field ψ_D is again the only field that does not acquire a mass under the perturbation. Then, the analysis of the appearance of the N-Umklapp term for particular values of the magnetization is identical to the one performed before. The generalization to generic N with PBC is straightforward, one first builds the radiatively generated couplings by keeping only the lowest order in J'. Once this step is performed, the only difference with respect to the case of equal interchain couplings is the zero-loop value of the dimension of the N-Umklapp operator (which enters via the initial conditions for the RG flow). This has the effect of changing the value of the coupling J' at which a plateau opens with a given value of the magnetization, but the qualitative behavior of the system is similar. This conclusion is not so straightforward for $\langle M\rangle=0$, where as we will see, the difference between frustrating and nonfrustrating configurations can become crucial.

Concerning finally the case of OBC, let us first consider again the case $N=3$ with antiferromagnetic coupling between the first and second chain and the second and the third chain. Again, this coupling is not stable under RG transformation. Under RG transformations the OBC configuration will flow towards a nonfrustrating cyclically coupled configuration. The main point is that for weak coupling and nonzero magnetization, the most relevant perturbing term will be again the one containing differences of fields or their duals. Then they will produce a mass gap for all the relative degrees of freedom and one recovers a scenario similar to the symmetric case, where only one massless field is left. On the other hand, the appearance of N-Umklapp operators and their commensurability is unchanged, since these criteria depend on the value of the magnetization and not on the particular couplings between the chains.

Let us study now the more complicated case of zero magnetization. For $\langle M\rangle=0$ the λ_2 term in Eq. (3.4) is commensurate and must be included in the perturbation terms. The situation is now much more complicated because this relevant operator couples the diagonal field ψ_D with the massive ones. For equal coupling between $N=3$ chains, the RG equations are now

$$\frac{da}{d\ \ln L}=\frac{16\pi\lambda_2^2}{R^2},$$

$$\frac{db}{d\ \ln L}=4\pi\left(-\frac{\lambda_2^2}{2R^2}-\frac{3\lambda_3^2}{2R^2}+12\pi^2R^2\lambda_4^2\right),$$

TABLE II. Values of h at which the magnetization jumps for Eq. (2.1) with coupling constant J', $\Delta=1$, N sites and different boundary conditions.

	h/J'	
N	OBC	PBC
2	± 1	
3	$\pm\frac{3}{2}$, 0	$\pm\frac{3}{2}$, 0
4	$\pm\left(1+\frac{1}{\sqrt{2}}\right)$, $\pm\frac{1+\sqrt{3}-\sqrt{2}}{2}$	± 2, ± 1
5	$\pm\frac{5+\sqrt{5}}{4}=\pm 1.80902$, ± 1.11887, 0	$\pm\frac{5+\sqrt{5}}{4}$, $\pm\frac{3+\sqrt{5}}{4}$, 0
6	± 1.86603, ± 1.38597, ± 0.49158	± 2, $\pm\frac{1+\sqrt{5}}{2}$, $\pm\frac{\sqrt{13}-\sqrt{5}}{2}$

$$\frac{d\lambda_2}{d\ \ln L}=\left[2-\frac{2}{3}\frac{1}{4\pi R^2}\left(\frac{2}{1+a}+\frac{1}{1-b}\right)\right]\lambda_2-\pi\lambda_2\lambda_3,$$

$$\frac{d\lambda_3}{d\ \ln L}=\left(2-\frac{1}{2\pi R^2(1-b)}\right)\lambda_3-\pi\lambda_3^2-\pi\lambda_2^2,$$

$$\frac{d\lambda_4}{d\ \ln L}=[2-2\pi R^2(1-b)]\lambda_4-\pi\lambda_4^2 \tag{3.19}$$

with the RG initial conditions

$$a(0)=2b(0)=\frac{2J'}{J\pi^2R^2}, \tag{3.20}$$

and

$$\lambda_2(0)=\lambda_3(0)=1/2(\text{const})^2J'/J;\quad \lambda_4(0)=J'/J, \tag{3.21}$$

where we kept the notation of Eqs. (3.4),(3.6). We see that the radius of compactification of the diagonal field is now strongly affected by the presence of the λ_2 term. Note also that the N-Umklapp process generates the operator

$$J'^N\cos(\sqrt{4\pi N}\psi_D) \tag{3.22}$$

for N even, and

$$J'^N\cos(2\sqrt{4\pi N}\psi_D) \tag{3.23}$$

for N odd. For nonfrustrating interchain coupling (a negative J' coupling between all the chains for example), all relative fields are massive according to Ref. 54. We can then integrate out these massive degrees of freedom. The crucial point is that now the radius of the diagonal field gets a nontrivial correction due to the strong interaction with the massive fields. Since this field is the only one expected to describe the large-scale behavior of the system, for $\Delta=1$ and $\langle M\rangle=0$, the SU(2) symmetry of the model would fix the radius of this field to be[54]

$$R_{\text{eff}}=\sqrt{\frac{N}{2\pi}}. \tag{3.24}$$

For such a value of the renormalized radius, the N-Umklapp term becomes strongly relevant for N even, and marginally irrelevant for N odd. These arguments are based on the assumption that the (uncontrolled) RG flow will drive our system to the [SU(2) symmetric] strong-coupling regime. The situation is even more subtle for positive J' (or λ_i), because in this case, from Eq. (3.19) one sees that the quadratic terms could now prevent the RG flow to reach the same strong-coupling regime as for $J'<0$. A numerical analysis of the RG flow for a frustrated three-leg Hubbard ladder at half filling provides evidence for the opening of a gap.[55] On the other hand, a non-Abelian bosonization analysis[56] leads to the conclusion that the weak-coupling region is gapless. This case deserves further investigation and series expansions are one way to approach this issue.

IV. STRONG-COUPLING EXPANSIONS FOR N-LEG LADDERS

In this section we diagonalize the interaction along the rungs exactly for $J=0$ and then expand quantities of interest in powers of J/J' around this limit. In order to be able to cover a variety of cases, we used a quite general method to perform the series expansions which is summarized, e.g., in Sec. III of Ref. 57 (actually, the program used in the present paper is a modified version of the one used *loc.cit.*).

As was already pointed out in Ref. 16, one can simply count the number of chains N in the limit $J/J'\to 0$ in order to determine the allowed values of the magnetization $\langle M\rangle$. This is presumably the simplest way to obtain the quantization condition (3.9). A less trivial fact is that all these values of the magnetization are in fact realized. For example, for ferromagnetic coupling $J'<0$, the magnetization jumps immediately from one saturated value $\langle M\rangle=-1$ to the other one ($\langle M\rangle=+1$) as the magnetic field h passes through zero. Nevertheless, for not too large N one can readily compute the magnetization curve of Eq. (2.1) and check for antiferromagnetic coupling $J'>0$ that all possible values of the magnetization are indeed successively realized as the field is increased. The critical magnetic fields h at which one value of the magnetization jumps to the next largest one are given in Table II.

As a next step, one can take the intrachain coupling J

perturbatively into account. First, we look at a two-leg ladder ($N=2$). The rung Hamiltonian $H_r=J'\vec{S}_1\vec{S}_2$ has two eigenvalues whose difference corresponds to the critical fields presented in Table II. The lower eigenvalue equals $-3J'/4$ and belongs to the spin $S=0$ eigenstate, while the other threefold degenerate one equals $J'/4$ and corresponds to the spin triplet ($S=1$). For convenience, we concentrate on an isotropic interaction for the rungs, but it is straightforward to include an XXZ anisotropy Δ in the interaction along the chains. One motivation for doing so is that this permits further comparison with the weak-coupling analysis ($J'\ll J$) of the previous section. At $J=0$ the ground state is obtained by putting singlets on each rung. A basic excitation at $J=0$ is given by one triplet in a sea of singlets. Since the SU(2) symmetry is broken down to U(1) by the perturbation, different series are obtained for the $S^z=\pm 1$ and $S^z=0$ components of the triplet.

Here we concentrate just on the series for the gap, but also previous results for the ground-state energy and the dispersion relations are readily extended to higher orders,[8] or to analytical expressions in Δ for longer series[58] at $\Delta=1$ with numerical coefficients.

The gap is obtained by the value of the excitation energy of a single flipped spin at momentum $k=\pi$ with $S^z=\pm 1$. We find

$$\frac{\mathsf{E}_2}{J'}=1-\left(\frac{J}{J'}\right)+\frac{1+\Delta^2}{4}\left(\frac{J}{J'}\right)^2+\frac{(1+\Delta)^2}{16}\left(\frac{J}{J'}\right)^3+\frac{-2+6\Delta-9\Delta^2+\Delta^4}{32}\left(\frac{J}{J'}\right)^4+\frac{21-84\Delta+39\Delta^2-48\Delta^3+2\Delta^4}{256}\left(\frac{J}{J'}\right)^5$$
$$-\frac{82-98\Delta+155\Delta^2-50\Delta^3+80\Delta^4-12\Delta^6}{1024}\left(\frac{J}{J'}\right)^6+\mathcal{O}\left(\left(\frac{J}{J'}\right)^7\right). \tag{4.1}$$

At the isotropic point $\Delta=1$ we recover well-known results: For this special case, the first three orders can be found in Ref. 8, a fourth order was given in Ref. 16 and numerical values of the coefficients until 13th order are contained in Ref. 58.

The series (4.1) contains a singularity at $J'=0$ which has no physical meaning but is simply due to the choice of expansion parameter. We therefore analyze it by removing this singularity via the substitutions

$$x=\frac{J'}{J+J'};\quad \tilde{x}=\tan^{-1}\left(\frac{J}{J'}\right). \tag{4.2}$$

From the raw transformed series one can then find some indication of an extended massless phase at small J' if $\Delta<\Delta_c$ with $\Delta_c\approx 0.25$–0.5. The opening of this massless phase is predicted by the zero-loop analysis of the previous section to take place at $\Delta_c=0$. Since the information obtained in the weak-coupling regime from a strong-coupling series is not extremely accurate, this agreement can be considered reasonable.

Now we turn to $N=3$ and OBC. In a way similar to the previously discussed series one finds the following fourth-order series for the lower and upper boundary of the $\langle M\rangle=1/3$ plateau:

$$\frac{h_{c_1}}{J'}=(\Delta+1)\frac{J}{J'}-\frac{(\Delta+1)(8\Delta-5)}{27}\left(\frac{J}{J'}\right)^2+\frac{(\Delta+1)(142\Delta^2-307\Delta-23)}{972}\left(\frac{J}{J'}\right)^3$$
$$+\frac{(\Delta+1)(40\,572\Delta^3-83\,025\Delta^2+76\,961\Delta-73\,295)}{367\,416}\left(\frac{J}{J'}\right)^4+\mathcal{O}\left(\left(\frac{J}{J'}\right)^5\right), \tag{4.3}$$

$$\frac{h_{c_2}}{J'}=\frac{3}{2}-\frac{J}{J'}+\frac{10+17\Delta^2}{36}\left(\frac{J}{J'}\right)^2+\frac{2196\Delta+252-554\Delta^3+171\Delta^2}{3888}\left(\frac{J}{J'}\right)^3$$
$$+\frac{30\,172+38\,988\Delta-28\,387\Delta^2+7028\Delta^3-8886\Delta^4}{326\,592}\left(\frac{J}{J'}\right)^4+\mathcal{O}\left(\left(\frac{J}{J'}\right)^5\right). \tag{4.4}$$

A third-order version of these series was already presented in Ref. 16 for the special case $\Delta=1$. We employ again the transformations (4.2) to analyze these series. The raw transformed series indicate for $\Delta=1$ that the $\langle M\rangle=1/3$ plateau does not extend down until $J'=0$ but ends at a critical value J_c'. The numerical value is found to be $J_c'\approx 1.0$–$1.4J$ at $\Delta=1$. This number should however not be taken too seriously as is also indicated by the large uncertainty of the critical anisotropy Δ_c above which this plateau extends over all nonzero J': $\Delta_c\approx 1.0$–1.6. At least, this rough estimate for Δ_c is compatible with $\Delta_c\approx 1.19$ as obtained from the zero-loop weak-coupling analysis.

The next case we consider is $N=4$ and PBC. In the strong-coupling limit we find plateaux at $\langle M\rangle=0$ and at $\langle M\rangle=1/2$. Series can be computed readily for the gap (which determines the boundary of the $\langle M\rangle=0$ plateau) and the lower and upper boundary of the $\langle M\rangle=1/2$ plateau. In this order, they read

$$\frac{\mathsf{E}_4^{(p)}}{J'}=1-\frac{4}{3}\left(\frac{J}{J'}\right)+\frac{33\Delta^2-12\Delta+20}{108}\left(\frac{J}{J'}\right)^2+\frac{24+194\Delta^2+131\Delta}{1296}\left(\frac{J}{J'}\right)^3$$
$$+\frac{3\,524\,213-17\,599\,776\Delta^2+9\,014\,208\Delta+1\,923\,768\Delta^3+7\,733\,988\Delta^4}{39\,191\,040}\left(\frac{J}{J'}\right)^4+\mathcal{O}\left(\left(\frac{J}{J'}\right)^5\right), \tag{4.5}$$

$$\frac{h_{c_1}^{(p)}}{J'}=1+\frac{3\Delta+8}{6}\left(\frac{J}{J'}\right)+\frac{9\Delta^2+96\Delta-308}{864}\left(\frac{J}{J'}\right)^2+\frac{369\Delta+972\Delta^3-1314\Delta^2-9464}{31\,104}\left(\frac{J}{J'}\right)^3$$
$$-\frac{885\,195\Delta^4-69\,076\,728\Delta^2-61\,318\,885-545\,832\Delta^3+117\,897\,360\Delta}{156\,764\,160}\left(\frac{J}{J'}\right)^4+\mathcal{O}\left(\left(\frac{J}{J'}\right)^5\right), \tag{4.6}$$

$$\frac{h_{c_2}^{(p)}}{J'}=2+\frac{\Delta-2}{2}\left(\frac{J}{J'}\right)+\frac{5\Delta^2+22}{32}\left(\frac{J}{J'}\right)^2-\frac{8\Delta^3-42\Delta-9\Delta^2-51}{256}\left(\frac{J}{J'}\right)^3+\frac{38\Delta^4-1981\Delta^2-56\Delta^3+1634\Delta-403}{4096}\left(\frac{J}{J'}\right)^4$$
$$+\mathcal{O}\left(\left(\frac{J}{J'}\right)^5\right). \tag{4.7}$$

The superscript (p) means that these series are for PBC.

Again, we analyze these series using the transformations (4.2). We apply this first to the gap (4.5) and find that the gap closes for some $J'>0$ if $\Delta<\Delta_c$ where the estimates for the critical value span an interval $\Delta_c\approx 0.8$–1.2. This interval is centered around the value $\Delta_c=1$ predicted by power counting in the context of Abelian bosonization.

Concerning the opening of the $\langle M\rangle=1/2$ plateau, we can first locate its ending point in the same way as before as $J_c'\approx 0.8$–$1.6J$ at $\Delta=1$. What is more interesting is the conclusion that this ending point cannot be pushed down to $J_c'=0$ by increasing Δ. This is in agreement with the zero-loop weak-coupling analysis which implies that an $\langle M\rangle=1/2$ plateau does not exist for $J'\ll J$ and $N=4$ regardless of the choice of Δ.

Finally we present second-order versions of analogous series for $N=4$ and OBC (denoted by a superscript o):

$$\frac{\mathsf{E}_4^{(o)}}{J'}=\frac{1}{2}(1+\sqrt{3}-\sqrt{2})-\left(\frac{1}{\sqrt{6}}+\frac{2}{3}\right)\frac{J}{J'}-\left\{\frac{\sqrt{6}}{1104}(764\Delta^2-1288\Delta+947)-\frac{\sqrt{3}}{1656}(1682\Delta^2-2760\Delta+1847)\right.$$
$$\left.+\frac{\sqrt{2}}{3312}(4176\Delta^2-7176\Delta+4063)-\frac{1}{414}(862\Delta^2-1242\Delta+869)\right\}\left(\frac{J}{J'}\right)^2+\mathcal{O}\left(\left(\frac{J}{J'}\right)^3\right), \tag{4.8}$$

$$\frac{h_{c_1}^{(o)}}{J'}=\frac{1}{2}(1+\sqrt{3}-\sqrt{2})+\frac{2\sqrt{6}+9\Delta+8}{12}\left(\frac{J}{J'}\right)+\left\{\frac{\sqrt{6}}{1656}(1146\Delta^2-1932\Delta-155)+\frac{\sqrt{3}}{1656}(-1406\Delta^2+2691\Delta+637)\right.$$
$$\left.+\frac{\sqrt{2}}{26\,496}(27\,819\Delta^2-57\,408\Delta-97\,216)+\frac{1}{828}(-1425\Delta^2+2553\Delta+3920)\right\}\left(\frac{J}{J'}\right)^2+\mathcal{O}\left(\left(\frac{J}{J'}\right)^3\right), \tag{4.9}$$

$$\frac{h_{c_2}^{(o)}}{J'}=1+\frac{1}{\sqrt{2}}+\frac{\Delta-4}{4}\left(\frac{J}{J'}\right)+\frac{27\sqrt{2}\Delta^2+416\sqrt{2}-528}{128}\left(\frac{J}{J'}\right)^2+\mathcal{O}\left(\left(\frac{J}{J'}\right)^3\right). \tag{4.10}$$

A second-order expansion of the dispersion relation at $\Delta=1$ has already been presented before,[8] though with floating-point coefficients. Equation (4.8) agrees with the result of Ref. 8 for the gap $\omega^-(k=\pi)$ up to first order, but there is a minor difference in the second order: We believe that the coefficient of $\cos 2k$ in Eq. (23) of Ref. 8 should read $-0.527\,81\ldots$ (not -0.469). We have also checked Eq. (24) *loc.cit.* and in this case found perfect agreement.

Given the low order of the series (4.8)–(4.10) we do not try to draw conclusions for the weak-coupling region from them. We have restricted to only second order since a symbolic computation of higher orders is very difficult. This is due to the many square roots encountered, as is already indicated by the results presented here.

V. THE STRONG-COUPLING EFFECTIVE HAMILTONIAN OF A FRUSTRATED LADDER

Here we look at strong coupling ($J'\gg J$) for PBC and odd N. In this case additional degeneracies preclude a simple analysis as in the preceding section. From a first-order consideration in J one infers that the low-energy effective Hamiltonian for Eq. (3.1) with $\Delta=1$ and $h=0$ is then given by (see Refs. 56,54 for $N=3$ and Ref. 59 for larger N):

$$H_{\rm eff}^{(N,p)}=\frac{J}{N}\sum_{x=1}^{L}\left[\mathbb{1}+\alpha_N(\sigma_x^+\sigma_{x+1}^-+\sigma_x^-\sigma_{x+1}^+)\right]\vec{S}_x\vec{S}_{x+1}, \tag{5.1}$$

where the $\vec{S}_x$ are su(2) operators acting in the spin space and $\sigma_x^{\pm}$ act on another two-dimensional space which comes from a degeneracy due to the permutational symmetry of the chains.

We have checked the validity of Eq. (5.1) for $N=3$, 5, 7, and 9 in the following way: First one has to determine the ground-state space at each rung for $J=0$ which is nothing but the ground-state space of an N-site Heisenberg chain. For N odd, the lowest energy states have $S^z=\pm 1/2$. In the case of OBC, this would be the only degeneracy. SU(2) symmetry is then sufficient to conclude that the effective Hamiltonian is a simple Heisenberg chain which is gapless in accordance with the generalized Haldane conjecture.

For PBC there is another twofold degeneracy in addition to this twofold degeneracy in spin space: For N odd and PBC the ground states of a Heisenberg chain carry momenta $k=\pm 2\pi\lfloor(N+1)/4\rfloor/N$ where parity symmetry is reflected in the freedom of choice of sign. So, the ground-state space at each rung x is four dimensional: The operators $\vec{S}_x$ act in the two-dimensional spin space and the $\sigma_x^{\pm}$ act in the two-dimensional space spanned by the ground-state momenta.

This degeneracy makes perturbation expansions in J highly nontrivial: At first order in J one has to diagonalize the matrix (5.1) which is determined by the matrix elements of the interaction along the legs in Eq. (3.1). That the only nonzero matrix elements are those given in Eq. (5.1) can be inferred just from the following symmetries of the full Hamiltonian: Global SU(2) symmetry [actually one needs only the U(1) Cartan subalgebra of su(2)] and invariance under simultaneous translations or reflections along all the rungs. These symmetries also imply some identities between the nonzero matrix elements, but at the end one still has to explicitly compute some matrix elements—at least in order to determine the constants α_N. We have performed such direct computations of matrix elements for $N=3$, 5, 7, and 9 and found the associated values of α_N to be

$$\alpha_3=1,\quad \alpha_5=\frac{16}{9},\quad \alpha_7=2.620\,685\,9\ldots,$$

$$\alpha_9=3.501\,208\,3\ldots. \tag{5.2}$$

In contrast, e.g., to the XXZ chain (2.1), already for $N=3$ the Hamiltonian (5.1) does not satisfy the Reshetikhin criterion [Eq. (3.20) on p. 101 of Ref. 60]. Therefore, it is in general not integrable (in the sense that it would be the Hamiltonian of a one-parameter family of transfer matrices which commute among themselves and with this Hamiltonian). So, one has to treat it by other approximate or numerical methods; e.g., a density matrix renormalization-group study was carried out for $N=3$ in Ref. 59 providing evidence for a gap to $S=1$ excitations.

In the present paper we are interested in generic XXZ anisotropies $\Delta\neq 1$ in the interaction along the chains in Eq. (3.1) and thus we should generalize Eq. (5.1). This generalization is obvious from the way the XXZ anisotropy appears in Eq. (3.1) and our derivation of Eq. (5.1): Δ just multiplies the matrix elements of the S^z-S^z interaction. Therefore, the effective Hamiltonian for generic Δ is given by

$$H_{\Delta}^{(N,p)}=\frac{J}{N}\sum_{x=1}^{L}\left[\mathbb{1}+\alpha_N(\sigma_x^+\sigma_{x+1}^-+\sigma_x^-\sigma_{x+1}^+)\right]\times\left(\Delta S_x^zS_{x+1}^z+\frac{1}{2}(S_x^+S_{x+1}^-+S_x^-S_{x+1}^+)\right), \tag{5.3}$$

where the parameters α_N remain those given in Eq. (5.2). The generalization (5.3) includes in particular the case $\Delta=0$, corresponding to two coupled XY models. Then (i.e., for $\Delta=0$) one can apply a Jordan-Wigner transformation to Eq. (5.3). However, even in this case one obtains a four-fermion interaction with the effect that the problem does not simplify (in contrast to the familiar case of fermion bilinears). In particular, the determination of the ground state of Eq. (5.3) for $\Delta=0$ is far from being straightforward.

As was pointed out in Ref. 16, the effective Hamiltonian (5.3) describes the response of Eq. (3.1) to a magnetic field for $|\langle M\rangle|\leqslant 1/N$ at strong coupling. For $N=3$ (i.e., $\alpha_3=1$) and $\Delta=1$ we find by exact diagonalization of Eq. (5.1) that the transition to $\langle M\rangle=1/3$ (full magnetization for the effective Hamiltonian) takes place at $3h/J=4.3146$, 4.3121, 4.3108, 4.3100, 4.3096 for $L=8$, 10, 12, 14, 16, respectively. This is in reasonable agreement with numerical values for the lower boundary of the $\langle M\rangle=1/3$ plateau of (3.1) at $J'\gg J$ (compare Fig. 4 of Ref. 16).

VI. NUMERICAL ANALYSIS OF THE STRONG-COUPLING EFFECTIVE HAMILTONIAN

To learn more about the spectrum of Eq. (5.3), we have performed numerical diagonalizations mainly for $N=3$ on finite systems, as was already done in Ref. 59 for $\Delta=1$. The Hamiltonian has two conserved quantities: S^z (for $\Delta=1$ actually the total spin S) and a second similar quantity related to the first factor in Eq. (5.3) which we denote by Σ^z. The lowest eigenvalues are located in the $\Sigma^z=0$ sector. First we look at the gap to the excitations in the $S^z=1$ sector. It turns out that one can fit the system-size dependence of this gap nicely by[61]

$$\mathsf{E}_{\Sigma^z=0,S^z=1}(L)=\mathsf{E}_{\Sigma^z=0,S^z=1}(\infty)+\frac{a}{L}. \tag{6.1}$$

Estimates for these parameters based on data for lengths up to $L=14$ are presented in Table III for some values of Δ and $N=3$. The numbers in brackets indicate the 1σ-confidence interval of the fit for the last given digit. Since this ignores possible other error sources, the true error may be a little larger. Our result for $\Delta=1$ [$\mathsf{E}_{\Sigma^z=0,S^z=1}(\infty)=0.208(1)J$] agrees within error bounds with that of Ref. 59 [$\mathsf{E}_{\Sigma^z=0,S^z=1}(\infty)=0.27(7)J$]. From Table III we conclude that the $S^z=1$ excitation of Eq. (5.3) is gapped for all $\Delta\geqslant 0$ and that there is nothing special about the case $\Delta=1$ from this point of view.

One comment is in place regarding the form (6.1) since in a gapped situation the convergence should ultimately be exponential (or at least of order L^{-2}—see, e.g., Ref. 57, and references therein). Here we seem to observe a typical cross-

TABLE III. Parameters for the fit Eq. (6.1) to the $S^z=1$ gap of Eq. (5.3). The first six columns are for $N=3$, but various values of Δ. The rightmost column is for ''$N=\infty$'' with $\alpha_N/N\to 1$.

Δ	0	0.2	0.4	0.8	1.0	1.2	1.0
$\mathsf{E}_{\Sigma^z=0,S^z=1}(\infty)/J$	0.139(5)	0.134(8)	0.166(5)	0.200(1)	0.208(1)	0.214(2)	0.390(6)
a/J	2.78(4)	3.35(6)	3.19(4)	3.079(7)	3.088(7)	3.13(2)	5.72(4)

over phenomenon, i.e., the small values of the gap imply a large correlation length such that our system sizes may be well below the correlation length. In such a range of system sizes one would indeed expect to observe finite-size corrections which are typical for massless situations. Since the corrections should ultimately become smaller, this would lead to obtaining systematically too small values of the gap. With the fit (6.1) we thus obtain a lower bound for the gap which is presumably not far from the true value. In particular, we can safely infer the presence of a gap.

Concerning the case of $N>3$, one observes from Eq. (5.2) and a further value for α_{11} (Ref. 59) that α_N is roughly proportional to N, i.e., $\alpha_N\approx 0.44N$ for large N. Using this information, we have extrapolated Eq. (5.1) to infinite N setting $\lim_{N\to\infty}\alpha_N/N=1$ in order to avoid the uncertainty in the true proportionality constant. This limit eliminates the term $\mathbb{1}\times\vec{S}_x\vec{S}_{x+1}$ in Eq. (5.1). The rightmost column in Table III shows the value for the $S=1$ gap that we obtain in this case. It should be noted that the properly rescaled value for $N\to\infty$ is slightly lower than that for $N=3$ at $\Delta=1$ (the former is about 80% of the latter). However, even for $N=\infty$ our estimate for the gap is still remarkably distinct from zero. This suggests a gap in the strong-coupling limit (5.1) for all N which slightly decreases as $N\to\infty$, but does not close even in this limit.

Now we turn to the ''gap'' in the $S^z=0$ sector for $N=3$. The data in Table IV can be interpreted as evidence that it asymptotically decreases roughly as

$$\mathsf{E}_{\Sigma^z=0,S^z=0}\sim\frac{1}{L^2};\tag{6.2}$$

at least this ''gap'' clearly tends to zero in the thermodynamic limit [in particular close to $\Delta=0$ the finite-size exponent could be different from that given in Eq. (6.2)]. This energy level corresponds to the state constructed in the generalized Lieb-Schultz-Mattis theorem.[22–24,13] According to Ref. 59 this energy level should be interpreted as a degenerate ground state arising due to spontaneous dimerization in the thermodynamic limit. The fact that the energy levels in Table IV have momentum π relative to the ground state is compatible with this interpretation and yields $l=2$ for the condition (1.1).

TABLE IV. Rescaled $S^z=0$ ''gaps'' of Eq. (5.3) with $N=3$ for various values of Δ.

Δ	0	0.2	0.4	0.8	1.0	1.2
L	$L^2\mathsf{E}_{\Sigma^z=0,S^z=0}/J$					
4	11.04294	12.16715	13.29556	15.54226	16.65656	17.76262
6	14.71647	15.34371	16.29211	18.64172	19.94276	21.29515
8	17.68885	17.48479	18.05673	20.22660	21.6	23.0955
10	20.18126	18.90011	19.00079	20.85874	22.23517	23.80763
12	22.28842	19.75430	19.34576	20.83216	22.17023	23.76822
14	24.06309	20.15994	19.24047	20.33604	21.60791	23.19367

Next, we investigate the momentum dependence of the gaps to the lowest excited states of Eq. (5.1) with $N=3$. The data for $\Sigma^z=0$ and total spin $S=0$ is shown in Fig. 3 and that for total spin $S=1$ (also $\Sigma^z=0$) in Fig. 4 (compare also Fig. 4 of Ref. 59). Here, we measure the momentum of the excitations relative to the ground state. It should be noted that due to parity conservation only half of the spectrum is shown (the parts for $k>\pi$ or $k<0$ are mirror-symmetric extensions of this figure). The two figures look quite similar. Both can be interpreted as the lower boundary of a (two-particle) scattering continuum. In particular, we do not observe one-particle states.

To extrapolate the lower boundaries of these two-particle scattering states, we have Fourier transformed E^2.[62] Then we have extrapolated each coefficient of the Fourier series separately using a Shanks transform (which is the $\alpha=0$ special case of the vanden Broeck-Schwartz algorithm—see, e.g., Ref. 63). This leads to

$$\begin{aligned}\mathsf{E}^2_{\Sigma^z=0,S=0}(k)/J=&\,0.654(478)-0.014(191)\cos k\\&-0.411(108)\cos 2k+0.040(136)\cos 3k\\&-0.044\cos 4k,\end{aligned}\tag{6.3}$$

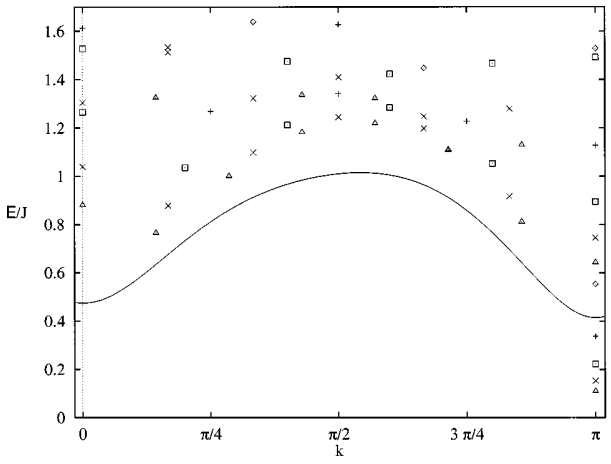

FIG. 3. Lowest gaps of Eq. (5.1) with $N=3$ in the sector with $\Sigma^z=0$ and total spin $S=0$ as a function of momentum k relative to the ground state. The symbols are for $L=6$ (rhombi), $L=8$ (+), $L=10$ (squares), $L=12$ (×), and $L=14$ (triangles), respectively. The line is the extrapolation (6.3) of the lower boundary $L\to\infty$.

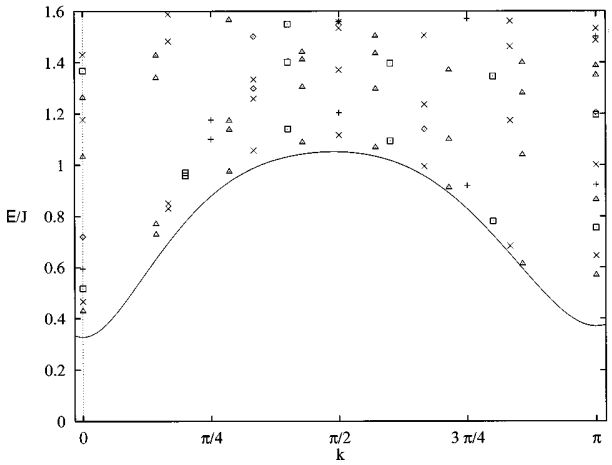

FIG. 4. Same as Fig. 3, but for total spin $S=1$. The line shows the extrapolation (6.4).

$$\mathsf{E}^2_{\Sigma^z=0,S=1}(k)/J = 0.671(43) + 0.023(24)\cos k - 0.492\cos 2k - 0.025\cos 3k - 0.058(11)\cos 4k - 0.013(50)\cos 5k. \quad (6.4)$$

The numbers in brackets indicate estimates for the error of the last given digits. Here we have suppressed the highest harmonics, since they cannot be reasonably extrapolated but are expected to be small anyway.

In this way we obtain a rather inaccurate estimate for the gap $\mathsf{E}\approx 0.3J$ with a large uncertainty which is due to the large errors in particular in Eq. (6.3) and the uncertainty in the higher harmonics. Nevertheless, this estimate is still quite close to the one in Table III. A more interesting observation is that Eqs. (6.3) and (6.4) are equal within error bounds. This suggests that these two thresholds can be interpreted in terms of two-particle scattering states of a single fundamental particle. Such a fundamental excitation would have to be similar to the spinon in the XXZ chain; in particular it would have to carry $S=1/2$ (and $\Sigma^z=\pm 1/2$).

Let us now try to exhibit this fundamental excitation explicitly. For even L and periodic boundary conditions we have only found two-particle scattering states in the low-lying excitation spectrum. Therefore, it is natural to look for a spinon-type excitation at odd L (still periodic boundary conditions) in the same way as one can exhibit the spinon for the XXZ chain.[39–41] We have computed the spectrum of Eq. (5.1) for $N=3$ and odd L from 5 to 13 in the sector with $\Sigma^z=1/2$ and total spin $S=1/2$. The main difference between the present situation and the XXZ chain is that here we expect a charge conjugate pair of spinons ($\Sigma^z=\pm 1/2$), while for the XXZ chain there was only one.

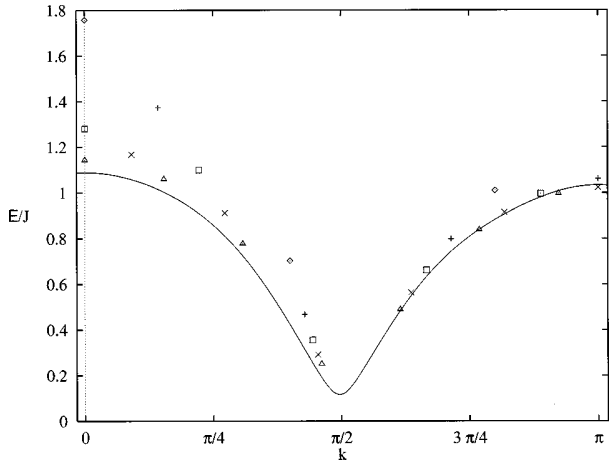

FIG. 5. The spinon of Eq. (5.1) with $N=3$, i.e., lowest gaps in the sector with $\Sigma^z=1/2$ and total spin $S=1/2$. The symbols are for $L=5$ (rhombi), $L=7$ (+), $L=9$ (squares), $L=11$ (×), and $L=13$ (triangles), respectively. The line is the extrapolation (6.6) of the dispersion curve to the thermodynamic limit.

Making single-particle states visible is traded for the absence of a ground state at odd L. In order to permit interpretation of the results as gaps we have therefore interpolated the ground-state energy using the values at $L\pm 1$. The resulting dispersion relation for the spinon is shown in Fig. 5. As was already the case for the spectra at even L, it turns out that k should be defined such that translationally invariant states on the lattice appear alternately at $k=0$ and $k=\pi$—the actual convention can be read off from Fig. 5 noting that only either $k=0$ or $k=\pi$ can be realized for odd L.

To interpret the data, we have again Fourier transformed E^2. First, this gives an interpolation of $\mathsf{E}_{\Sigma^z=1/2,S=1/2}$ at $k=\pi/2$. Analogously to Eq. (6.1) we fit the data for $L=5,9,13$ to the form (the values for $L=7$ and 11 should be omitted to obtain a monotonic sequence)

$$\mathsf{E}_{\Sigma^z=1/2,S=1/2}(L) = \mathsf{E}_{\Sigma^z=1/2,S=1/2}(\infty) + \frac{\bar{a}}{L}, \quad (6.5)$$

and obtain an estimate for the gap of the spinon $\mathsf{E}_{\Sigma^z=1/2,S=1/2}(\infty)=0.131(8)J$ with $\bar{a}=0.51(6)J$. This is roughly consistent with half the value in Table III or that given in Ref. 59, as it should be if our interpretation as single-, respectively, two-spinon scattering states is correct.

An alternate way to analyze the data is to extrapolate each coefficient of the Fourier series separately using a Shanks transform. Using now all available L, we find

$$\mathsf{E}^2_{\Sigma^z=1/2,S=1/2}(k)/J = 0.6331(155) + 0.0592(184)\cos k + 0.5387(122)\cos 2k + 0.0121(63)\cos 3k - 0.0633(160)\cos 4k - 0.0127\cos 5k + 0.0177\cos 6k. \quad (6.6)$$

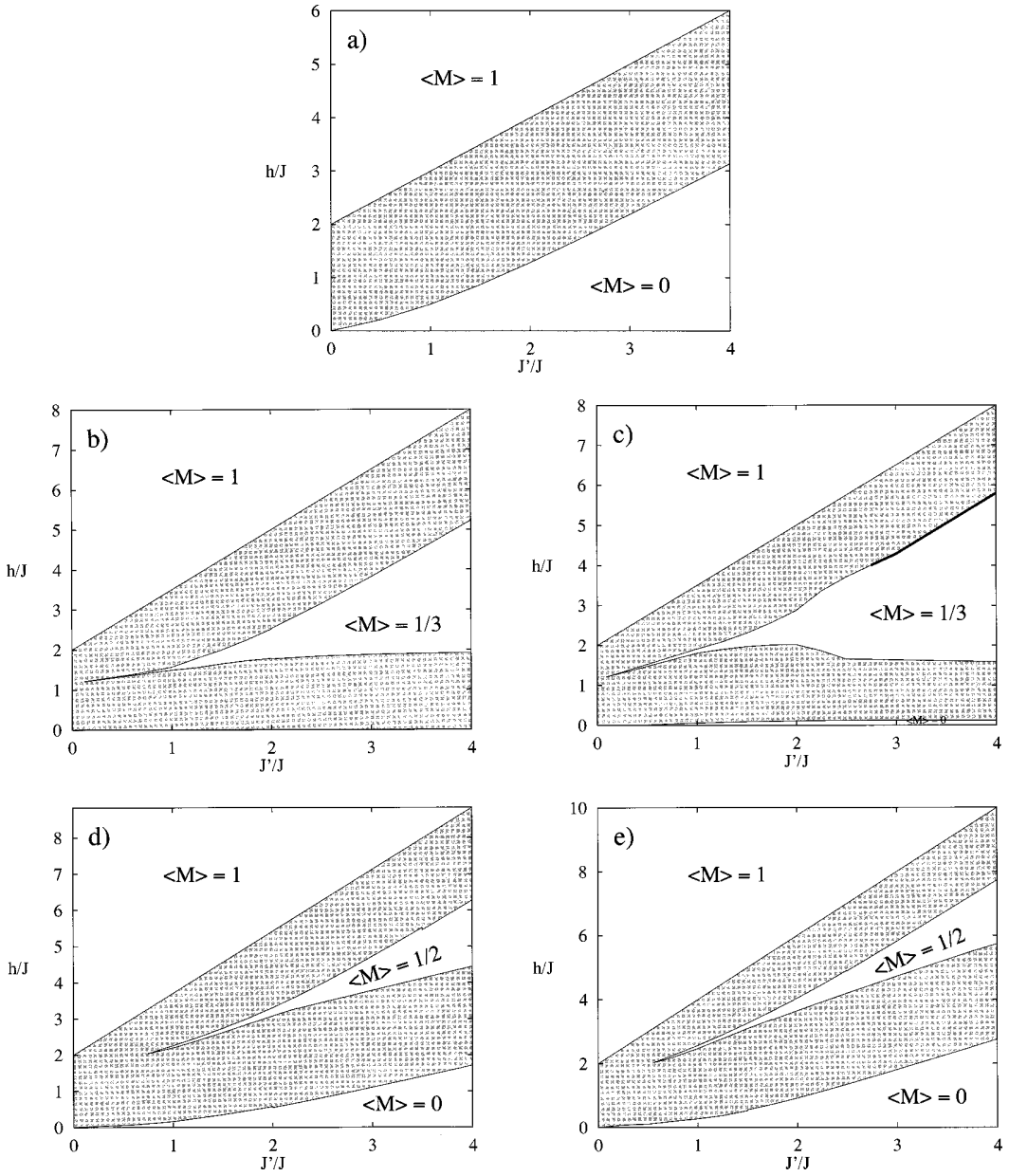

FIG. 6. Schematic magnetic phase diagram at $\Delta=1$ for (a) $N=2$, (b) $N=3$ and OBC, (c) $N=3$ and PBC, (d) $N=4$ and OBC, (e) $N=4$ and PBC. White regions in the h-J'/J plane indicate gapped regions with a plateau in the magnetization curve, while the shaded areas are massless and the magnetization $\langle M\rangle$ changes continuously if the applied field h is varied.

As before, the numbers in brackets indicate estimates for the error of the last given digits. For the two highest harmonics there is not sufficient data for an extrapolation, so we just take the $L=13$ estimate without being able to estimate an error. The extrapolation (6.6) is shown by the line in Fig. 5. Obviously, finite-size effects are more important for $k<\pi/2$ than for $k>\pi/2$. Equation (6.6) yields another estimate for the gap of the spinon $\mathsf{E}_{\Sigma^z=1/2,S=1/2}(\infty)\approx 0.116J$. The error estimate obtained from Eq. (6.6) is not sensible, but the value for the gap itself is very close to our previous extrapolation or half the value given in Table III.

Finally, we have checked that within error bounds the dispersion relation (6.4) can be written in terms of Eq. (6.6) as $\mathsf{E}_{\Sigma^z=0,S=1}(k)=\mathsf{E}_{\Sigma^z=1/2,S=1/2}(k-k')+\mathsf{E}_{\Sigma^z=1/2,S=1/2}(k')$ with some k'. Such a decomposition must be possible if our particle interpretation is correct.

Methods similar to the ones used in the present section may be useful also in other cases beyond the present one and the study of Ref. 41. One natural such candidate is a direct observation of a spinon-type excitation in $N=3$ cylindrically coupled chains at intermediate or small couplings J'.

VII. SUMMARY OF RESULTS

Our results are best summarized in (schematic) magnetic phase diagrams. For definiteness we consider the SU(2) symmetric situation $\Delta=1$, though similar pictures can be drawn for other values of Δ as well.

For completeness, let us start with the case $N=2$, where the corresponding picture is given by Fig. 6(a). The boundary of the $\langle M\rangle=0$ plateau is determined by the spin gap in

zero field which for an $N=2$-leg ladder has been studied in great detail. For $J'/J \leqslant 1.5$ we use the quantum Monte Carlo results of Ref. 11 in Fig. 6(a); for $J'/J \geqslant 1.5$ the raw 13th order strong-coupling series of Ref. 58 is used instead (note the excellent matching at $J'/J=1.5$).

Both the numerical data[11] and the series expansions[58] support a linear opening of the gap for small J', as was predicted by a dimensional analysis of the perturbing operator in the field-theoretic formulation.[64–66]

Figure 6(b) shows a more interesting case, i.e., $N=3$ with OBC. The boundaries of the $\langle M\rangle=1/3$ plateau have been determined from the fourth-order strong-coupling series (4.3) and (4.4) for $J'/J \geqslant 2$. For $1 \leqslant J'/J \leqslant 2$ we obtained them from a Shanks extrapolation of the finite-size data in our earlier paper.[16] The remaining weak-coupling region is the most speculative part of the figure. We located the ending point of the $\langle M\rangle=1/3$ plateau in the vicinity of the corresponding point on the magnetization curves of decoupled Heisenberg chains, as is suggested by the Abelian bosonization analysis if one assumes a similar behavior for OBC and PBC (the bosonization analysis predicts for PBC that the $\langle M\rangle=1/3$ plateau disappears for small but nonzero J'/J).

The analogous case with changed boundary conditions (i.e., $N=3$ and PBC) is shown in Fig. 6(c). Here, no series expansions are possible due to extra degeneracies at strong coupling. The boundaries of the plateaux have therefore been determined in this case mainly on the basis of older numerical data.[16] We have used a Shanks extrapolation for $L=4$, 6, and 8 for $J'/J \geqslant 2.75$ at the lower boundary of the $\langle M\rangle=1/3$ plateau and for $J'/J=2.5$ at its upper boundary to estimate their location. For smaller couplings, the finite-size data is nonmonotonic. The best we can do in the range $1 \leqslant J'/J \leqslant 2.5$ is to fit the $L=4$ and 8 data to a form with $1/L$ corrections like Eqs. (6.1),(6.5). The ending point of the plateau is again placed on the basis of the weak-coupling analysis. It should be noted that the nature of the transition at the upper boundary of the $\langle M\rangle=1/3$ plateau changes qualitatively for $J'/J \gtrsim 2.75$.[16] This strongly frustrated region is indicated by the bold line in Fig. 6(c). It is possible that the transition becomes first order along this line. Note that the region in question is far outside the weak-coupling region, where we expect all transitions to be continuous.

Another interesting difference between Figs. 6(b) and 6(c) is that in the latter a tiny $\langle M\rangle=0$ plateau (i.e., a gap) opens. Its boundary has been estimated at intermediate couplings by fitting the $L=4$, 6, and 8 data[16] to the form (6.1). This yields slightly smaller values than those given in Ref. 59 in the cases where we overlap. However, we agree with Ref. 59 in the most important point, namely the existence of such a plateau. A numerical determination of its ending point is difficult, and the field-theoretical weak-coupling analysis is not yet conclusive either[55,56]—the ending point may well be anywhere in the weak-coupling region $0 \leqslant J' \leqslant J$.

Finally, the magnetic phase diagrams for $N=4$ are given by Figs. 6(d) and 6(e) for OBC and PBC, respectively. To obtain them, we have performed further numerical computations. For the upper boundary of the $\langle M\rangle=1/2$ plateau we have numerical data for $L=4$, 6, and 8 such that we can apply a Shanks transform to it. For its lower boundary we have only $L=4$ and 6 data and therefore we have to make an assumption on the finite-size corrections to extrapolate it (we assumed $1/L$ corrections, though this is not entirely satisfactory). In the strong-coupling region we used our series instead of numerical data. The series and numerical data are matched at $J'/J=3.5$ or $J'/J=2.5$ for the series corresponding to the upper boundary for OBC Eq. (4.10) or PBC Eq. (4.7), respectively. At the lower boundary of the $\langle M\rangle=1/2$ plateau we matched the series (4.9) and (4.6) to the numerical data at $J'/J=2.25$ and $J'/J=1.75$, respectively. Neither of the methods accessible to us is very accurate in the region where this plateau closes, but all three methods (numerical, series and Abelian bosonization) point to a location of the ending point in the region where J' and J are of the same order.

The gaps for $N=4$ are taken from our series (4.8) for $J'/J \geqslant 2$ for OBC and Eq. (4.5) for $J'/J \geqslant 1.5$ for PBC. For OBC the accurate numerical data for the gap of Ref. 11 is used in the weak-coupling region. The corresponding line in Fig. 6(e) is in comparison rather an educated guess which is inspired though by $L=4$ and $L=6$ numerical data. Regarding the series both for the gap and the boundaries of the $\langle M\rangle=1/2$ plateau, we observe a trend that those for PBC can be used for somewhat smaller values of J'/J than those for OBC. This is expected since the former are fourth order but the latter only second order.

Although Fig. 6 is for the particular choice $\Delta=1$ there is nothing particular about this case (at least for nonzero magnetizations), and one would obtain similar figures for other values of Δ as well. Further plateaux may open for $\Delta>1$. In particular, there should always be an $\langle M\rangle=0$ plateau in N coupled XXZ chains with $\Delta>1$, since each such chain is massive and this should be preserved at least for sufficiently weak coupling. In the Ising limit $\Delta\to\infty$ and for nonfrustrating boundary conditions it is easy to see that this is accompanied by breaking of translational symmetry to a period $l=2$ in the ground state. In the general case $\Delta>1$, such a period $l=2$ reconciles the appearance of a gap for both even and odd N with Eq. (1.1).

The Abelian bosonization analysis predicts all the massless shaded regions in Fig. 6 to be $c=1$ theories (with the exception $J'=0$ where one trivially has a $c=N$ theory). In these regions the exponents governing the asymptotics of the correlation functions depend continuously on the parameters. Predictions can be made, however, for the transitions at the boundaries between such massless phases and plateau regions. The opening of a plateau when varying J' is a transition of the K-T type.[47] Like in the case of the transition at $\Delta=1$ in the XXZ chain, this implies a very narrow plateau after the transition [cf. Eq. (2.12)] which makes it difficult to observe numerically.[16] At the transition point the asymptotics of the correlation functions is governed by the exponents (3.14), while along the boundaries of the plateaux one has the universal exponents (3.15). It should be noted that an attempt to verify the latter exponents numerically or experimentally is likely to rather lead to the exponents characteristic for the transition point if one is sufficiently close to it.

The field-theoretical analysis also predicts the asymptotic behavior of the magnetization in a massless phase but close to a plateau boundary to be given by the universal DN–PT behavior[43,44] Eq. (2.10). We have in fact numerically verified such a square-root behavior close to saturation ($\langle M\rangle\to 1$) at some values of J'/J for $N=2$, 3, and 4 with both OBC and

PBC. However, the example of the XXZ chain shows (cf. Fig. 2) that close to other plateau boundaries this universal behavior may be restricted to a tiny region and its observation could be very difficult. In experimental situations, it will be further obscured by thermal fluctuations and other effects such as disorder (see, e.g., Ref. 18). This explains why rather accurate experiments on $N=2$-leg spin-ladder materials[17,67] show no evidence of a square-root behavior for $\langle M\rangle \to 0$.

Quite surprisingly, massless excitations (though nonmagnetic ones) also arise in plateau regions. This can be seen from Eq. (5.3) which for $\langle M\rangle = 1/N$ is just an XY chain and therefore massless. This yields massless excitations in the limit $J' \to \infty$ in Fig. 6(c), or more generally in the strong-coupling limit on the $\langle M\rangle = 1/N$ plateau for N odd and PBC. Whether $J/J'=0$ is just a critical point or if massless nonmagnetic excitations also arise at finite J' remains to be investigated.

VIII. DISCUSSION AND CONCLUSION

In this paper we have investigated the conditions under which plateaux appear in N-leg spin ladders as well as the universality classes of the transitions at the boundaries of such plateaux. Certain small plateaux may have slipped our attention. For example, there could be a narrow $\langle M\rangle = 2/3$ plateau for $N=3$ and PBC at intermediate or strong coupling J' which would be accompanied by spontaneous breaking of translational symmetry to a period $l=2$. If this should turn out to be the case, it would have to be added to Fig. 6(c). However, our main point is the presence of such plateaux, not the absence of particular ones.

We also confirmed the conclusion of Ref. 59 that in the case $N=3$ frustration induces a zero-field gap at least for sufficiently strong coupling. It may be even more intriguing that, according to our strong-coupling data, this gap seems to survive the $N \to \infty$ limit for an odd number N of cylindrically coupled chains. This shows that it is necessary to specify at least boundary conditions along the rungs in the generalization of the Haldane conjecture to spin ladders. The peculiar behavior of a cylindrical configuration may be interpreted as follows: Strongly frustrating boundary conditions force a one-dimensional domain wall into the two-dimensional system corresponding to $N=\infty$. The $N \to \infty$ limit of the one-dimensional Hamiltonian (5.3) is just the effective Hamiltonian for the low-energy excitations of this domain wall. As a consequence, there cannot be any long-range order which is typical for the two-dimensional Heisenberg model, and there is no reason why the low-energy spectrum should not be gapped as it apparently is.

Similar surprises cannot be completely ruled out in the weak-coupling region for N even and $\langle M\rangle = 0$. The zero-field case is difficult to control since there is an additional relevant interaction between the massive degrees of freedom and the possibly massless ones [the coefficient of λ_2 in Eq. (3.4)]. In general, this gives rise to nonperturbative renormalization. In the isotropic case $\Delta=1$ one can use the SU(2) symmetry[54] to infer the renormalized radius of compactification of the remaining massless field. This then leads to the generalized Haldane conjecture in the framework of Abelian bosonization. For $\Delta>1$ a gap is always expected in the weak-coupling regime since already the decoupled chains are massive. The situation is far less clear for anisotropies $\Delta<1$ since then it is not known how to control the renormalization-group flow. An investigation of this region by other nonperturbative methods would be interesting. It may also be desirable to perform further checks of the absence of an extended massless phase in the SU(2) symmetric situation for even $N \geqslant 6$.

Beyond a more detailed understanding of the N-leg spin-ladder model (3.1) treated here, a similar investigation of other models could be interesting. One natural step would be to include charge degrees of freedom, and see if interesting effects arise from the interplay of a magnetic field with transport properties.

Last but not least, it would be desirable to have an experimental verification of our predictions. We are confident that this is possible, in principle, and hope that it will in fact be carried out.

ACKNOWLEDGMENTS

We would like to thank G. Albertini, F. C. Alcaraz, F. H. L. Essler, T. Giamarchi, M. Oshikawa, K. Totsuka, and B. Wehefritz for helpful discussions concerning in particular a single XXZ chain. A.H. is supported under TMR Grant No. FMRX-CT96-0012 and D.C.C. by CONICET and Fundación Antorchas. We are indebted to the Max-Planck-Institut für Mathematik Bonn-Beuel where the more complicated numerical computations have been performed.

[1] E. Dagotto and T. M. Rice, Science **271**, 618 (1996); T. M. Rice, Z. Phys. B **103**, 165 (1997).

[2] M. Azuma, Z. Hiroi, M. Takano, K. Ishida, and Y. Kitaoka, Phys. Rev. Lett. **73**, 3463 (1994).

[3] E. Dagotto, J. Riera, and D. J. Scalapino, Phys. Rev. B **45**, 5744 (1992); T. Barnes, E. Dagotto, J. Riera, and E. S. Swanson, *ibid.* **47**, 3196 (1993).

[4] F. D. M. Haldane, Phys. Rev. Lett. **50**, 1153 (1983).

[5] T. Ziman and H. J. Schulz, Phys. Rev. Lett. **59**, 140 (1987); M. Takahashi, *ibid.* **62**, 2313 (1989); O. Golinelli, T. Jolicoeur, and R. Lacaze, Phys. Rev. B **50**, 3037 (1994); K. Hallberg, X. Q. G. Wang, P. Horsch, and A. Moreo, Phys. Rev. Lett. **76**, 4955 (1996).

[6] D. C. Cabra, P. Pujol, and C. von Reichenbach, Phys. Rev. B **58**, 65 (1998).

[7] G. Sierra, in *Strongly Correlated Magnetic and Superconducting Systems*, edited by G. Sierra and M. A. Martín-Delgado, Lecture Notes in Physics Vol. 478 (Springer, Berlin, 1997), p. 136.

[8] M. Reigrotzki, H. Tsunetsugu, and T. M. Rice, J. Phys.: Condens. Matter **6**, 9235 (1994).

[9] S. R. White, R. M. Noack, and D. J. Scalapino, Phys. Rev. Lett. **73**, 886 (1994).

[10] B. Frischmuth, B. Ammon, and M. Troyer, Phys. Rev. B **54**, R3714 (1996).
[11] M. Greven, R. J. Birgeneau, and U.-J. Wiese, Phys. Rev. Lett. **77**, 1865 (1996).
[12] This result was obtained for planar configurations and often even an equal strength of coupling constants is assumed. Such properties may be crucial as we will show below.
[13] M. Oshikawa, M. Yamanaka, and I. Affleck, Phys. Rev. Lett. **78**, 1984 (1997).
[14] K. Totsuka, Phys. Lett. A **228**, 103 (1997).
[15] K. Totsuka, Phys. Rev. B **57**, 3454 (1998).
[16] D. C. Cabra, A. Honecker, and P. Pujol, Phys. Rev. Lett. **79**, 5126 (1997).
[17] G. Chaboussant, P. A. Crowell, L. P. Lévy, O. Piovesana, A. Madouri, and D. Mailly, Phys. Rev. B **55**, 3046 (1997).
[18] C. A. Hayward, D. Poilblanc, and L. P. Lévy, Phys. Rev. B **54**, R12 649 (1996).
[19] Z. Weihong, R. R. P. Singh, and J. Oitmaa, Phys. Rev. B **55**, 8052 (1997).
[20] R. Chitra and T. Giamarchi, Phys. Rev. B **55**, 5816 (1997).
[21] J. B. Parkinson and J. C. Bonner, Phys. Rev. B **32**, 4703 (1985).
[22] E. Lieb, T. Schultz, and D. Mattis, Ann. Phys. (N.Y.) **16**, 407 (1961).
[23] I. Affleck, Phys. Rev. B **37**, 5186 (1988).
[24] A. G. Rojo, Phys. Rev. B **53**, 9172 (1996).
[25] A. Honecker, M. Kaulke, and K. D. Schotte (unpublished).
[26] F. D. M. Haldane, Phys. Rev. Lett. **45**, 1358 (1980).
[27] F. Woynarovich, H.-P. Eckle, and T. T. Truong, J. Phys. A **22**, 4027 (1989).
[28] I. Affleck, in *Fields, Strings and Critical Phenomena, Les Houches, Session XLIX*, edited by E. Brézin and J. Zinn-Justin (North-Holland, Amsterdam, 1988), p. 563.
[29] N. M. Bogoliubov, A. G. Izergin, and V. E. Korepin, Nucl. Phys. B **275**, 687 (1986).
[30] V. E. Korepin, N. M. Bogoliubov, and A. G. Izergin, *Quantum Inverse Scattering Method and Correlation Functions* (Cambridge University Press, Cambridge, 1993).
[31] S. Qin, M. Fabrizio, L. Yu, M. Oshikawa, and I. Affleck, Phys. Rev. B **56**, 9766 (1997).
[32] URL http://www.he.sissa.it/~honecker/roc.html (backup under URL http://thew02.physik.uni-bonn.de/~honecker/roc.html).
[33] F. C. Alcaraz and A. L. Malvezzi, J. Phys. A **28**, 1521 (1995).
[34] J. D. Noh and D. Kim, Phys. Rev. E **53**, 3225 (1996).
[35] O. Babelon, H. J. de Vega, and C. M. Viallet, Nucl. Phys. B **220**, 13 (1983).
[36] Y. A. Izyumov and Y. N. Skryabin, *Statistical Mechanics of Magnetically Ordered Systems* (Consultants Bureau, New York, 1988), Sec. 17.
[37] F. C. Alcaraz (private communication).
[38] J. des Cloizeaux and M. Gaudin, J. Math. Phys. **7**, 1384 (1966).
[39] L. D. Faddeev and L. A. Takhtajan, Phys. Lett. **85A**, 375 (1981).
[40] G. Gómez-Santos, Phys. Rev. B **41**, 6788 (1990).
[41] T. M. Rice, S. Haas, M. Sigrist, and F.-C. Zhang, Phys. Rev. B **56**, 14 655 (1997).
[42] J. D. Johnson and B. M. McCoy, Phys. Rev. A **6**, 1613 (1972).
[43] G. I. Dzhaparidze and A. A. Nersesyan, JETP Lett. **27**, 334 (1978).
[44] V. L. Pokrovsky and A. L. Talapov, Phys. Rev. Lett. **42**, 65 (1979).
[45] This terminology is motivated as follows: This type of transition is usually known under the name ''Pokrovsky-Talapov'' (Ref. 44), but in the context of magnetization processes was actually discovered by Dzhaparidze and Nersesyan (Ref. 43).
[46] R. P. Hodgson and J. B. Parkinson, J. Phys. C **18**, 6385 (1985).
[47] J. M. Kosterlitz and D. J. Thouless, J. Phys. C **6**, 1181 (1973).
[48] A. Luther, Phys. Rev. B **14**, 2153 (1976).
[49] D. J. Amit, Y. Y. Goldschmidt, and G. Grinstein, J. Phys. A **13**, 585 (1980).
[50] M. P. M. den Nijs, Phys. Rev. B **23**, 6111 (1981).
[51] J. M. Kosterlitz, J. Phys. C **7**, 1046 (1974).
[52] H. J. Schulz, Phys. Rev. B **22**, 5274 (1980).
[53] H. J. Schulz, Phys. Rev. B **34**, 6372 (1986).
[54] H. J. Schulz, in *Correlated Fermions and Transport in Mesoscopic Systems*, edited by T. Martin, G. Montambaux, and J. Tran Thanh Van (Editions Frontières, Gif-sur-Yvette, 1996), p. 81.
[55] E. Arrigoni, Phys. Lett. A **215**, 91 (1996).
[56] M. Suzuki and K. Totsuka, J. Phys. A **29**, 3559 (1996).
[57] A. Honecker, J. Stat. Phys. **82**, 687 (1996).
[58] Z. Weihong, V. Kotov, and J. Oitmaa, Phys. Rev. B **57**, 11 439 (1998).
[59] K. Kawano and M. Takahashi, J. Phys. Soc. Jpn. **66**, 4001 (1997).
[60] P. P. Kulish and E. K. Sklyanin, in *Integrable Quantum Field Theories*, edited by J. Hietarinta and C. Montonen, Lecture Notes in Physics Vol. 151 (Springer, Berlin, 1982), p. 61.
[61] This appears to be also a good fit to the data presented in Fig. 1 of Ref. 59 at least for intermediate system sizes and would lead to results compatible with the exponential fit used there. Note also that convergence is typically faster and clearer for the periodic boundary conditions used here than for open boundary conditions (used in Ref. 59).
[62] We Fourier transform E^2 rather than E, since then higher harmonics are better suppressed, as must be the case for the scaling limit of a lattice model close to a second-order critical point.
[63] M. Henkel and G. M. Schütz, J. Phys. A **21**, 2617 (1988).
[64] S. P. Strong and A. J. Millis, Phys. Rev. B **50**, 9911 (1994).
[65] K. Totsuka and M. Suzuki, J. Phys.: Condens. Matter **7**, 6079 (1995).
[66] D. G. Shelton, A. A. Nersesyan, and A. M. Tsvelik, Phys. Rev. B **53**, 8521 (1996).
[67] W. Shiramura, K. Takatsu, H. Tanaka, K. Kamishima, M. Takahashi, H. Mitamura, and T. Goto, J. Phys. Soc. Jpn. **66**, 1900 (1997).

2.1.2 Degrés de liberté de charge et de spin

Dans cette section nous étudions une généralisation des résultats obtenus sur les chaînes et les échelles de spins de la section précédente. Les spins 1/2 traités auparavant proviennent d'électrons dont les propriétés de transport jouent dans certains cas un rôle très important. Nous allons mettre en évidence les deux aspects fondamentaux des systèmes fortement corrélés en une dimension en étudiant d'une part la relative indépendance des degrés de libertés de spin et de charge et de l'autre l'intrication persistante entre les phénomènes magnétiques et de transport dans ces systèmes.

La relation entre magnétisme et transport peut être mise mise en évidence en une dimension avec le modèle de Hubbard. La version bi-dimensionnelle de ce modèle est en effet la pierre d'angle pour étudier le phénomène de supraconductivité à hautes températures dans les oxydes de cuivre.

Le Hamiltonien du modèle de Hubbard pour des électrons de spins 1/2 en une dimension est :

$$H = \sum_i \sum_{\sigma=\uparrow,\downarrow} \left(-t \ (\psi^\dagger_{i,\sigma}\psi_{i+1,\sigma} + h.\ c.) + U \ \psi^\dagger_{i,\uparrow}\psi_{i,\uparrow}\psi^\dagger_{i,\downarrow}\psi_{i,\downarrow} \right) \tag{11}$$

Le premier terme correspond à un Hamiltonien de "saut" entre sites voisins sur une chaîne et le deuxième à un terme d'interaction (que l'on considérera généralement répulsif) entre électrons au même site. Bien qu'on puisse facilement imaginer des généralisations de ce modèle, (11) peut être résolu de façon exacte et nous donnera déjà un comportement très riche qui nous permettra de comprendre plusieurs des phénomènes caractéristiques des systèmes fortement corrélés en basses dimensions.

Commençons par considérer un nombre d'électrons général, qui ne correspond pas au "demi-remplissage" (un électron par site) $< n_i >=< \psi^\dagger_{i,\uparrow}\psi_{i,\uparrow} + \psi^\dagger_{i,\downarrow}\psi_{i,\downarrow} >= 1$. Dans ce cas, la théorie de champs correspondant au comportement à grandes échelles du système sera donnée par l'action [1] [2] :

$$S_{Hubbard} = S^s_{WZNW_{SU(2)_1}} + S^c_{U(1)} \tag{12}$$

où le premier terme correspond aux degrés de liberté de spins, avec l'action du modèle de WZNW comme nous l'avons vu plus haut pour les chaînes de spins 1/2, et le deuxième terme est donné par l'action (9) mais sans opérateur de perturbation. Cette écriture est révélatrice du phénomène de séparation spin-charge que nous avons mentionné. En effet, on voit clairement que l'on peut créer des excitations de spin ou de charge indépendamment. Ce fait se retrouve aussi dans la forme des fonctions de corrélations, qui dans la théorie euclidienne sont données par des fonctions algébriques de $x \pm v_s t$ pour le secteur de spin et $x \pm v_c t$ pour le secteur de charge : les vitesses v_s et v_c coïncident uniquement pour $U = 0$. Cette différence est encore plus marquée dans le cas du demi-remplissage ($< n_i >= 1$).

Dans ce cas, du fait de la valeur de l'impulsion de Fermi $k_F = \pi/a$ (a étant la distance entre sites du réseau), un opérateur correspondant à un processus de rétro-diffusion devient conmensuré avec le réseau. Le fait que cet opérateur (ainsi que d'autres) soit présent dans la théorie discrète, mais avec un terme oscillant de site en site, fait que dans la théorie continue à grandes distances on aura des compensations site par site, et seul une dérivée de cet opérateur, correspondant typiquement à un opérateur non-pertinent sera présente. En revanche, pour le demi-remplissage, le terme osicilant disparaît et on obtient pour l'action effective du secteur de charge l'action (9) avec $n = 2$. Pour $U > 0$, l'opérateur de perturbation est pertinent dans le sens du groupe de renormalisation et produit un gap. Les fonctions de corrélation du secteur de charge sont donc exponentiellement décroissantes avec la distance et, à grandes échelles, on retrouve uniquement les degrés de libertés de spin comme pour la chaîne de spins 1/2 discutée plus haut. Sans entrer dans les détails techniques qui sont explicités dans l'article qui suit, nous illustrons ce comportement en mentionnant deux opérateurs définits dans le continu, correspondant à la densité de charge et de spin et qui sont définit respectivement par :

$$\rho(x) = \psi_\uparrow^\dagger \psi_\uparrow(x) + \psi_\downarrow^\dagger \psi_\downarrow(x) \tag{13}$$

et

$$S^z(x) = \psi_\uparrow^\dagger \psi_\uparrow(x) - \psi_\downarrow^\dagger \psi_\downarrow(x) \tag{14}$$

Bien que le comportement à grandes distances du premier possède une décroissance exponentielle, les fonctions de corrélation du deuxième sont données, à grandes distances, par celles de l'opérateur de spins S^z de la chaîne de Heisenberg de spins 1/2. On peut donc considérer la chaîne de spins 1/2 comme un système effectif construit au niveau microscopique par un modèle de Hubbard à demi remplissage, avec U très grand, où les degrés de libertés de charge sont "gelés" ; ce résultat peut en fait être obtenu directement par une simple analyse au deuxième ordre en théorie de perturbation pour U grand en toutes dimensions.

Comme les modèles de Hubbard sur divers réseaux semblent contenir dans une certaine limite les chaînes et échelles de pins que nous discutions plus haut, il est intéressant de voir si l'on peut retrouver et généraliser les résultats sur les plateaux d'aimantation dans le contexte du modèle de Hubbard. Pour cela, nous introduisons un terme de champ magnétique dans (11)

$$-\frac{h}{2} \sum_i \psi_{i,\uparrow}^\dagger \psi_{i,\uparrow} - \psi_{i,\downarrow}^\dagger \psi_{i,\downarrow} \tag{15}$$

Le modèle sur réseau est toujours intégrable par Ansatz de Bethe [2] et la solution peut ensuite être utilisée pour construire une théorie de champs effective. Il y a toujours une séparation entre deux degrés de liberté, comme pour le cas $h = 0$, mais cette fois-ci ces degrés de liberté n'ont pas une interprétation directe en termes de charge et de spin. Ils correspondent en fait à un "mélange" de ces

degrés de liberté. Dans le langage de la bosonisation, si $\phi_\uparrow$ et $\phi_\downarrow$ correspondent aux champs bosoniques pour spin "up" et "down" respectivement, alors les degrés de libertés pertinent pour décrire le théorie (que l'on continue d'indexer avec les lettres "c" et "s" par commodité) seront donnés par :

$$\begin{pmatrix} \phi_c \\ \phi_s \end{pmatrix} = \frac{1}{\det\ Z} \begin{pmatrix} Z_{ss} & Z_{ss} - Z_{cs} \\ Z_{sc} & Z_{sc} - Z_{cc} \end{pmatrix} \begin{pmatrix} \phi_\uparrow \\ \phi_\downarrow \end{pmatrix} \tag{16}$$

La matrice Z dépend des valeur de U et h et nous donne le résultat déjà connu dans le cas $h = 0$. La façon la plus simple de favoriser la présence de plateaux dans la courbe d'aimantation est d'introduire une périodicité non-triviale dans le réseau, avec un terme de la forme :

$$-\delta \sum_{i'=mp,\alpha} (\psi^\dagger_{i'+1,\alpha}\psi_{i',\alpha} + H.c.) \tag{17}$$

qui introduit une différence dans l'amplitude de saut avec une périodicité p. Nous avons montré que dans ce cas, si le nombre total d'électrons est maintenu fixe -ce qui est typiquement le cas des matériaux dopés- la courbe d'aimantation a des plateaux chaque fois que :

$$\frac{p}{2}(N_c \pm M) \in \mathbb{Z} \tag{18}$$

où N_c est le nombre moyen d'électrons par site et M est l'aimantation par site normalisée à $M_{max} = 1$. Pour $N_c = 1$ ce résultat correspond à la généralisation de la condition de plateau pour les chaînes p mérisées et peut aussi s'étendre à des échelles de spins. En effet, ce travail à été complété par l'étude d'une échelle formée par N chaînes [3], où l'on montre que, toujours pour un nombre total d'électrons fixés, la condition de plateau est donnée par :

$$\frac{N}{2}(N_c \pm M) \in \mathbb{Z} \tag{19}$$

Ce résultat nous donne non seulement la généralisation de celui des chaînes de spins mentionnées plus haut, mais il nous indique aussi que la position en aimantation de tels plateaux peut être réglée avec du dopage, et rendue ainsi plus accessible pour les oxydes de cuivre où les champs magnétiques nécessaires pour avoir des valeur de l'aimantation non négligeables sont généralement très grands.

Références

[1] E. Lieb and F. Y. Wu, Phys. Rev. Lett. **20**, 1445 (1968).

[2] H. Frahm and V. E. Korepin, Phys. Rev. **B 42**, 10553 (1990), Phys. Rev. **B 43**, 5653 (1991).

[3] D.C. Cabra, A. De Martino, P. Pujol and P. Simon, Europhys. Lett. **57** (3), 402 (2002).

Emergence of irrationality: Magnetization plateaus in modulated Hubbard chains

D. C. Cabra,[1] A. De Martino,[2,*] A. Honecker,[3] P. Pujol,[2] and P. Simon[4,†]
[1]*Departamento de Física, Universidad Nacional de la Plata, C.C. 67, 1900 La Plata, Argentina and Facultad de Ingeniería, Universidad Nacional de Lomas de Zamora, Cno. de Cintura y Juan XXIII, 1832 Lomas de Zamora, Argentina*
[2]*Laboratoire de Physique,‡ Groupe de Physique Théorique, ENS Lyon, 46 Allée d'Italie, 69364 Lyon Cédex 07, France*
[3]*Institut für Theoretische Physik, TU Braunschweig, Mendelssohnstraße 3, D-38106 Braunschweig, Germany*
[4]*International School for Advanced Studies, Via Beirut 2-4, 34014 Trieste, Italy*
(Received 24 August 2000; revised manuscript received 19 October 2000; published 30 January 2001)

Hubbard chains with periodically modulated coupling constants in a magnetic field exhibit gaps at zero temperature in their magnetic and charge excitations in a variety of situations. In addition to fully gapped situations (plateau in the magnetization curve *and* charge gap), we have shown [Phys. Lett. A **268**, 418 (2000)] that plateaus also appear in the presence of massless modes, leading to a plateau with a magnetization m whose value depends continuously on the filling n. Here we detail and extend the arguments leading to such doping-dependent magnetization plateaus. First we analyze the low-lying excitations using Abelian bosonization. We compute the susceptibility and show that due to the constraint of fixed n, it vanishes at low temperatures (thus leading to a magnetization plateau) even in the presence of one massless mode. Next we study correlation functions and show that one component of the superconducting order parameter develops quasi-long-range order on a doping-dependent magnetization plateau. We then use perturbation theory in the on-site repulsion U to compute the width of these plateaus up to first order in U. Finally, we compute ground state phase diagrams and correlation functions by Lanczos diagonalization of finite clusters, confirming the presence of doping-dependent plateaus and their special properties.
DOI: 10.1103/PhysRevB.63.094406 PACS number(s): 71.10.Fd, 71.10.Pm, 75.60.Ej

I. INTRODUCTION

Strongly correlated electron systems in low dimensions are presently a subject of intense research. In particular, the magnetism of such systems has revealed very interesting properties and it is by now well established that spin chains and spin ladders present plateaus in their magnetization curves. It has been shown theoretically that plateaus occur in general at *rational* fractions of the saturation magnetization. The position of these plateaus is subject to a quantization condition that involves the volume of a translationally invariant unit cell (see, e.g., Refs. 1–7). From the experimental side, different materials have been found which exhibit plateaus. One example is a dimerized spin-1 chain,[8] which exhibits a plateau at half the saturation magnetization as predicted in Ref. 3. A good candidate for a plateau at one third of the saturation magnetization is $Cu_3Cl_6(H_2O)_2 \cdot 2H_8C_4SO_2$,[9] though it is not yet fully clear whether the proposed frustrated trimer chain model is really appropriate or which parameters should be used.[10]

The most striking examples of plateaus have so far been observed experimentally in the materials $SrCu_2(BO_3)_2$ (Ref. 11) and NH_4CuCl_3 (Ref. 12) and again both constitute challenges for theory. There is general agreement that $SrCu_2(BO_3)_2$ is a predominately two-dimensional material and how it should be modeled theoretically. Though some progress has been made in understanding the origin of some of the observed plateaus,[13] it remains a difficult problem to compute the complete magnetization process within this model. On the other hand, the high-temperature crystal structure of NH_4CuCl_3 suggests a one-dimensional model, but nevertheless it remains unclear which model is appropriate theoretically for this compound.

Materials with a ladder structure (see, e.g. Ref. 14) are also good candidates for exhibiting magnetization plateaus. However, since the copper-oxide related materials are strongly coupled, plateaus with nonzero magnetization are predicted in a magnetic field range, which causes difficulties with the present experimental tools. A mechanism yielding plateaus at lower values of magnetic fields would therefore be very attractive. As we have shown in the case of modulated Hubbard chains,[15] doping may actually provide such a mechanism since it allows a continuous variation of the plateau magnetization m with the filling n—extending in this particular case also into the low-field region. Doping-dependent magnetization plateaus have also recently been theoretically studied in a different system, namely an integrable spin-S generalization of the t-J chain doped with $(S-1/2)$ carriers,[16] where, however, the appearance of plateaus is restricted to large magnetization values. Another example of such a situation occurs in the one-dimensional Kondo lattice model,[17] where unpaired spins behave ferromagnetically, giving rise to a spontaneous magnetization of a value controlled by doping.

Here we detail and extend our previous study[15] of the effect of a magnetic field and a periodic modulation (p-merization) of the hopping amplitude or the on-site energy on a *doped* one-band Hubbard chain whose Hamiltonian is given by

$$H = -\sum_{x,\alpha} t(x)(c^{\dagger}_{x+1,\alpha}c_{x,\alpha} + \text{H.c.}) + U\sum_{x=1}^{L} c^{\dagger}_{x,\uparrow}c_{x,\uparrow}c^{\dagger}_{x,\downarrow}c_{x,\downarrow} + \sum_{x,\alpha} \mu(x)c^{\dagger}_{x,\alpha}c_{x,\alpha} - \frac{h}{2}\sum_{x=1}^{L}(c^{\dagger}_{x,\uparrow}c_{x,\uparrow} - c^{\dagger}_{x,\downarrow}c_{x,\downarrow}). \tag{1.1}$$

Here $c^{\dagger}_{x,\alpha}$ and $c_{x,\alpha}$ are electron creation and annihilation operators at site x, $\alpha=\uparrow,\downarrow$ the two spin orientations, and h the external magnetic field. The hopping amplitude $t(x)$ and the chemical potential $\mu(x)$ are taken as periodic in the variable x with period p.

The one-dimensional Hubbard model with dimerized coupling constants ($p=2$) is realized in a number of real compounds like the organic (super)conductors[18] and the ferroelectric perovskites.[19] While some materials in the former class come at quarter filling, one frequently also finds realizations of the half-filled Hubbard model. In this case, the model, Eq. (1.1), is in the same universality class as a modulated spin-1/2 Heisenberg chain. Realizations of the latter exist also at periods $p>2$: Some examples of trimerized chains ($p=3$) have been studied in Refs. 20,21, and 9.

A technical motivation for resorting to the one-dimensional Hubbard model is that the uniform chain is exactly solvable by Bethe Ansatz (BA) for arbitrary values of the on-site repulsion U, filling, and magnetic field.[22] The exact solution can then be used to construct a low energy bosonized effective field theory,[23–25] which can in turn be used to study perturbations of this model (see, e.g. Ref. 26). Here we first review some aspects of the bosonization description of the Hubbard chain[27,28] and extend it for the case of a finite magnetic field $h\neq 0$.

Focusing on the case of constant chemical potential $\mu(x)=\mu$, we have shown in Ref. 15 that magnetization plateaus can appear for the model, Eq. (1.1), if the density of particles n and magnetization m[29] satisfy

$$\frac{p}{2}(n\pm m)\in\mathbb{Z}. \tag{1.2}$$

These conditions are commensurability conditions for the up electrons $n_{\uparrow}=(n+m)/2$ and down electrons $n_{\downarrow}=(n-m)/2$, respectively. More precisely, if both conditions are simultaneously satisfied, the system has both charge and spin gaps. On the other hand, if only one of these conditions is fulfilled, the filling has to be kept fixed in order to have a magnetization plateau. A simple explanation of the conditions, Eq. (1.2), can be given[15] in the noninteracting limit ($U=0$). Then, the Hamiltonian Eq. (1.1) can be easily diagonalized and is found to have p bands $\varepsilon^{\lambda}(k)$ (see Sec. III for more details). The magnetic field breaks the symmetry between up- and down-spin electrons by shifting their chemical potentials by opposite amounts. It is then possible that one chemical potential (say for the up electrons) lies in one of the $p-1$ band gaps while the other (for the down electrons) is in the middle of a band. This situation leads to a doping-dependent plateau, if one imposes the constraint of fixed filling n (and only in this case). Then the magnetization can be increased only by moving an electron from the down-spin band into the up-spin band, which requires a finite energy or equivalently a finite change of magnetic field, leading to a plateau. However, since the filling of the down-spin electrons remains adjustable, one obtains a doping-dependent value of the magnetization at the plateau.

Finally, we have also shown[15] that a charge gap opens if the combination $pn\in\mathbb{Z}$ of the two conditions Eq. (1.2) is satisfied. The latter case generalizes the well known charge gap at half filling ($n=1$) as well as the charge gap at quarter filling in the dimerized Hubbard chain ($n=1/2$, $p=2$).[30–33]

The plan of this paper is as follows: In Sec. II A we briefly review the bosonization approach for the Hubbard chain for arbitrary filling and on-site Coulomb repulsion U in the presence of an external magnetic field (our conventions are summarized in Appendix A and details on the bosonization approach in Appendix B).[23,25] In Sec. II B we then use this bosonization scheme to study the effect of a modulation of the hopping amplitudes and the on-site energy $\mu(x)$ and find the conditions under which a plateau is present. The appearance of plateaus for irrational values of the magnetization and superconducting correlations are analyzed in Secs. II C and II D, respectively. In Sec. III we study the limit of small U perturbatively and show that the doping-dependent plateaus are also present there. Then we study the ground state phase diagram (Sec. IV A) and correlation functions (Sec. IV B) numerically on finite size systems by means of Lanczos diagonalization. Finally, we summarize our results in Sec. V, discuss some experimental settings where the features presented in this paper could be observed, and point out open routes for further research.

II. BOSONIZATION APPROACH

A. Field theory description of the Hubbard chain in a magnetic field

In this section, we summarize the analysis of the Hubbard model in a magnetic field using Abelian bosonization. For further details see Ref. 25. The lattice Hamiltonian is the standard one, i.e., Eq. (1.1), with constant $t(x)=t$, $\mu(x)=\mu$:

$$H=-t\sum_{x,\alpha}\left(c^{\dagger}_{x+1,\alpha}c_{x,\alpha}+\text{H.c.}\right)+U\sum_{x}c^{\dagger}_{x,\uparrow}c_{x,\uparrow}c^{\dagger}_{x,\downarrow}c_{x,\downarrow}$$
$$+\mu\sum_{x}\left(c^{\dagger}_{x,\uparrow}c_{x,\uparrow}+c^{\dagger}_{x,\downarrow}c_{x,\downarrow}\right)-\frac{h}{2}\sum_{x}\left(c^{\dagger}_{x,\uparrow}c_{x,\uparrow}-c^{\dagger}_{x,\downarrow}c_{x,\downarrow}\right). \tag{2.1}$$

This model was already solved exactly by BA in 1968,[22] but it took until 1990 for the correlation functions to be computed by combining BA results with conformal field theory (CFT) techniques.[23] Spin-charge separation is a well known feature of the Hubbard chain at zero magnetic field. Interestingly, it is no longer spin and charge degrees of freedom that are separated if an external magnetic field is switched on.[23] Nevertheless it has been shown that in the presence of a magnetic field, the spectrum of low energy excitations can be described by a semidirect product of two CFT's with central charges $c=1$.[23] This in turn implies that the model is still in the universality class of the Tomonaga-Luttinger (TL) liquid and therefore allows for a bosonization treatment.

In order to proceed, we write the fermion operator as

$$c_{x,\alpha}\rightarrow\psi_{\alpha}(x)\sim e^{ik_{F,\alpha}x}\psi_{L,\alpha}(x)+e^{-ik_{F,\alpha}x}\psi_{R,\alpha}(x)+\ldots \tag{2.2}$$

$$= e^{ik_{F,\alpha}x} e^{-i\sqrt{4\pi}\phi_{L,\alpha}(x)} + e^{-ik_{F,\alpha}x} e^{i\sqrt{4\pi}\phi_{R,\alpha}(x)} + \ldots, \tag{2.3}$$

where $k_{F,\alpha}$ are the Fermi momenta for up- and down-spin electrons and $\phi_{R,L,\alpha}$ are the chiral components of two bosonic fields, introduced as usual in order to bosonize the spin-up and -down chiral fermion operators $\psi_{R,L,\alpha}$. (Our conventions are settled in Appendix A.) The dots stand for higher order terms, some of which are written explicitly in Appendix B. They take into account the corrections arising from the curvature of the dispersion relation due to the Coulomb interaction. For nonzero Hubbard repulsion U and magnetic field h, the low energy effective Hamiltonian corresponding to Eq. (2.1), written in terms of the bosonic fields $\phi_\uparrow$ and $\phi_\downarrow$, has a complicated form mixing up and down degrees of freedom. The crucial step to obtain a simpler bosonized Hamiltonian is to consider the Hamiltonian of a generalized (two component) TL model and identify the excitations of the latter with the exact BA ones for the model Eq. (2.1), providing in this way a *nonperturbative* bosonic representation of the low energy sector of the full Hamiltonian Eq. (2.1). This program has been carried out in Ref. 25 and we just quote here the final result. The fixed point (i.e., neglecting all irrelevant terms) bosonized Hamiltonian reads

$$H = \int dx \left[\frac{u_c}{2} \partial_x \vec{\Phi}^t \mathcal{A}_c \partial_x \vec{\Phi} + \frac{u_s}{2} \partial_x \vec{\Phi}^t \mathcal{A}_s \partial_x \vec{\Phi} \right], \tag{2.4}$$

where $\vec{\Phi}^t = (\phi_{R,\uparrow}, \phi_{L,\uparrow}, \phi_{R,\downarrow}, \phi_{L,\downarrow})$. The matrices $\mathcal{A}_{c,s}$ have the following form:

$$\mathcal{A}_{c,s} = \begin{pmatrix} a_{c,s}+b_{c,s} & a_{c,s}-b_{c,s} & c_{c,s}+d_{c,s} & c_{c,s}-d_{c,s} \\ a_{c,s}-b_{c,s} & a_{c,s}+b_{c,s} & c_{c,s}-d_{c,s} & c_{c,s}+d_{c,s} \\ c_{c,s}+d_{c,s} & c_{c,s}-d_{c,s} & e_{c,s}+f_{c,s} & e_{c,s}-f_{c,s} \\ c_{c,s}-d_{c,s} & c_{c,s}+d_{c,s} & e_{c,s}-f_{c,s} & e_{c,s}+f_{c,s} \end{pmatrix}, \tag{2.5}$$

where

$$\begin{cases} a_c = (Z_{cc}^{-1})^2 & b_c = (Z_{cc} - Z_{sc})^2 & c_c = Z_{cc}^{-1}(Z_{cc}^{-1} + Z_{cs}^{-1}) \\ d_c = Z_{sc}(Z_{cc} - Z_{sc}) & e_c = (Z_{cc}^{-1} + Z_{cs}^{-1})^2 & f_c = Z_{cs}^2 \end{cases} \tag{2.6}$$

$$\begin{cases} a_s = (Z_{sc}^{-1})^2 & b_s = (Z_{cs} - Z_{ss})^2 & c_s = Z_{sc}^{-1}(Z_{ss}^{-1} + Z_{sc}^{-1}) \\ d_s = Z_{ss}(Z_{cs} - Z_{ss}) & e_s = (Z_{ss}^{-1} + Z_{sc}^{-1})^2 & f_s = Z_{ss}^2 \, . \end{cases} \tag{2.7}$$

In these expressions Z_{ij} (respectively, Z_{ij}^{-1}), $i,j = c,s$, are the entries of the dressed charge matrix Z (respectively, its inverse Z^{-1}) taken at the Fermi points

$$Z = \begin{pmatrix} Z_{cc} & Z_{cs} \\ Z_{sc} & Z_{ss} \end{pmatrix}. \tag{2.8}$$

These matrix elements are solutions of a set of coupled integral equations obtained from the BA[23] and depend on the coupling U, the chemical potential μ, and the magnetic field h. In turn they can be related to physical thermodynamic quantities.[23]

Substituting for the bosonic fields

$$\begin{pmatrix} \phi_c \\ \phi_s \end{pmatrix} = \frac{1}{\det Z} \begin{pmatrix} Z_{ss} & Z_{ss} - Z_{cs} \\ Z_{sc} & Z_{sc} - Z_{cc} \end{pmatrix} \begin{pmatrix} \phi_\uparrow \\ \phi_\downarrow \end{pmatrix}, \tag{2.9}$$

and for their dual fields

$$\begin{pmatrix} \theta_c \\ \theta_s \end{pmatrix} = \begin{pmatrix} Z_{cc} - Z_{sc} & Z_{sc} \\ Z_{ss} - Z_{cs} & -Z_{ss} \end{pmatrix} \begin{pmatrix} \theta_\uparrow \\ \theta_\downarrow \end{pmatrix}, \tag{2.10}$$

the Hamiltonian takes the form

$$\sum_{i=c,s} \frac{u_i}{2} \int dx [(\partial_x \phi_i)^2 + (\partial_x \theta_i)^2], \tag{2.11}$$

where $\phi = \phi_R + \phi_L$ and $\theta = \phi_R - \phi_L$.

At zero magnetic field, the matrix Z reduces to

$$Z(h=0) = \begin{pmatrix} \xi & 0 \\ \xi/2 & 1/\sqrt{2} \end{pmatrix}, \tag{2.12}$$

with $\xi = \xi(\mu, U)$. In this case we recover the well known expressions for the charge and spin fields

$$\phi_c = \frac{1}{\xi}(\phi_\uparrow + \phi_\downarrow), \quad \phi_s = \frac{1}{\sqrt{2}}(\phi_\uparrow - \phi_\downarrow), \tag{2.13}$$

where the compactification radius of the spin field (i.e., the parameter which indicates the period of ϕ_s, $\phi_s = \phi_s + 2\pi R_s$, $R_s = 1/\sqrt{2\pi}$)[34] is fixed by the SU(2) symmetry of the spin sector. The radius for the charge field, on the other hand, depends on the chemical potential μ and the Coulomb coupling U. Furthermore, for $h=0$ the charge and spin degrees of freedom are completely decoupled.

It should be noted that for $m \neq 0$, the fields arising in the diagonalized form of the bosonic Hamiltonian Eq. (2.11) are no longer the charge and spin fields even though they have

been labeled c and s. For example, the charge field is in general given by $\phi_\uparrow+\phi_\downarrow=Z_{cc}\phi_c-Z_{cs}\phi_s$.

For generic values of the parameters of the model Eq. (2.1), we can now write down for example the bosonized expression for the charge density operator

$$\begin{aligned}\rho(x)&=\psi_\uparrow^\dagger\psi_\uparrow(x)+\psi_\downarrow^\dagger\psi_\downarrow(x)\\&=\frac{1}{\sqrt{\pi}}\partial_x(Z_{cc}\phi_c-Z_{cs}\phi_s)\\&\quad+a_\rho\sin[k_+x-\sqrt{\pi}(Z_{cc}\phi_c-Z_{cs}\phi_s)]\\&\quad\times\cos[k_-x-\sqrt{\pi}((Z_{cc}-2Z_{sc})\phi_c-(Z_{cs}-2Z_{ss})\phi_s)]\\&\quad+b_\rho\sin(2k_+x-\sqrt{4\pi}(Z_{cc}\phi_c-Z_{cs}\phi_s)),\end{aligned}\tag{2.14}$$

where a_ρ, b_ρ are nonuniversal constants, whose numerical values are known only in special cases. Details on how such expressions are obtained are given in Appendix B. Formulas of the type Eq. (2.14) are our fundamental bosonization rules.

B. Space dependent modulations

In the present subsection we study two different perturbations of the Hubbard chain Eq. (2.1), which consist of space dependent modulations of certain parameters. In particular we shall consider a space dependent modulation of the hopping amplitude $t(x)$ and of the on-site energy $\mu(x)$.

1. Modulated hopping amplitude

In this case, the Hamiltonian reads as in Eq. (1.1) with $\mu(x)=\text{const}$ and $t(x)=t$ if $x\neq lp$ and $t(lp)=t'=t+\delta$, with p,l integers and p fixed. This is equivalent to the uniform Hubbard Hamiltonian Eq. (2.1) perturbed by the term

$$H_{\text{pert}}=-\delta\sum_{x'=lp,\alpha}(c^\dagger_{x',\alpha}c_{x'+1,\alpha}+\text{H.c.}).\tag{2.15}$$

At half filling and for large U, a standard second order perturbative computation in $1/U$ shows that the effective Hamiltonian is given by

$$\tilde{H}=\sum_x\frac{4t^2(x)}{U}\vec{S}_x\cdot\vec{S}_{x+1},\tag{2.16}$$

thus leading to the p-merized Heisenberg chain studied in Ref. 6. It was predicted there that magnetization plateaus occur when the condition $p/2(1-m)\in\mathbb{Z}$ is satisfied.[29] We now use Abelian bosonization techniques to analyze the more general case of the model Eq. (1.1) in the small δ (weak p-merization) limit.

Using the bosonization dictionary given in Appendix B, we find the expression for the continuum limit of the lattice perturbation Eq. (2.15)

$$\begin{aligned}O_{\text{pert}}&=\lambda_1\sin[k_+/2+pk_+x-\sqrt{\pi}(Z_{cc}\phi_c-Z_{cs}\phi_s)]\\&\quad\times\cos[k_-/2+pk_-x-\sqrt{\pi}((Z_{cc}-2Z_{sc})\phi_c\\&\quad-(Z_{cs}-2Z_{ss})\phi_s)]+\lambda_2\sin[k_++2pk_+x\\&\quad-\sqrt{4\pi}(Z_{cc}\phi_c-Z_{cs}\phi_s)],\end{aligned}\tag{2.17}$$

where $\lambda_1,\lambda_2\propto\delta$ and the Fermi momenta are $k_+=k_{F,\uparrow}+k_{F,\downarrow}=\pi n$, $k_-=k_{F,\uparrow}-k_{F,\downarrow}=\pi m$, where n is the filling and m is the magnetization. The presence of a factor p in the oscillating part will play an important role in the following.

The operator

$$\begin{aligned}&\lambda_3\cos[k_-+2pk_-x-2\sqrt{\pi}((Z_{cc}-2Z_{sc})\phi_c\\&\quad-(Z_{cs}-2Z_{ss})\phi_s)],\end{aligned}\tag{2.18}$$

with $\lambda_3\propto\delta^2$ is radiatively generated from the first term in Eq. (2.17) and must therefore be included as well.

In the case of zero magnetic field the dressed charge matrix is given by Eq. (2.12) and we have then a neat separation between charge and spin fields. The most relevant perturbation takes the form

$$\begin{aligned}O_{\text{pert}}&=\lambda_1\sin\left[\frac{\pi n}{2}+pn\pi x-\sqrt{\pi}\xi\phi_c\right]\cos[\sqrt{2\pi}\phi_s]\\&\quad+\lambda_2\sin[\pi n+2pn\pi x-\sqrt{4\pi}\xi\phi_c].\end{aligned}\tag{2.19}$$

The marginal operator associated with λ_3 contains only the spin field, its dimension (fixed by the SU(2) symmetry) is 2, and it is marginally irrelevant. A term like this is already present in the original model and is also marginally irrelevant. Hence, for δ small enough, this term can be absorbed in the original marginally irrelevant perturbation term without changing its relevance character.

The λ_2 term affects only the charge degrees of freedom and its dimension runs from 1, for $U\to\infty$ to 2, for $U=0$, being then always relevant for the cases of interest. We can therefore conclude that the charge field is massive whenever this operator is commensurate, which in turn happens if the condition $pn\in\mathbb{Z}$ is satisfied.

If this happens, we can integrate out the massive charge degrees of freedom which leaves us with an effective theory for the spin degrees of freedom. This effective theory is massless except when the operator associated with λ_1 becomes also commensurate, i.e., if the condition $pn/2\in\mathbb{Z}$ is satisfied. In that case, we have also a spin gap in the system.

These considerations are easily generalized to the case of nonzero magnetization as long as the condition $pn\in\mathbb{Z}$ is satisfied. In this case, the λ_2 term in Eq. (2.17) is always commensurate. Since it contains only the proper charge field $\phi_\uparrow+\phi_\downarrow$, a charge gap opens for all values of m at these commensurate values of the filling. The condition $pn\in\mathbb{Z}$ is also satisfied when the two conditions Eq. (1.2) are simultaneously satisfied. In this case, also the λ_1 term in Eq. (2.19) becomes commensurate, thus leading also to a spin gap.

In particular for $p=2,3$, we predict the following fully gapped situations:

$p=2$: Half filling ($n=1$): gap for the charge, and plateau for $m=0$. Quarter filling ($n=1/2$) (and also $n=3/2$): gap for the charge,[30–33] and plateau for $m=\pm 1/2$.

$p=3$: $n=1$, $n=1/3$, and $n=5/3$: gap for the charge, and plateau for $m=\pm 1/3$. $n=2/3$ and $n=4/3$: gap for the charge, and plateau for $m=\pm 2/3,\ 0$.

The final case where only one of the conditions Eq. (1.2) holds is more complicated since then the charge and spin degrees of freedom can no longer be separated. We therefore postpone discussion of this case.

2. Modulated on-site energy

Now we consider the Hubbard chain Eq. (1.1) with a uniform hopping amplitude $t(x)=t$ but a periodic modulation of the chemical potential $\mu(x)=\mu$ if $x\neq lp$ and $\mu(lp)=\mu+\delta\mu$, with p,l integers, p fixed. This is equivalent to the uniform chain Eq. (2.1) plus an on-site energy term that reads

$$H'_{\text{pert}}=\delta\mu\sum_{x'=lp,\alpha}c^{\dagger}_{x,\alpha}c_{x,\alpha}. \tag{2.20}$$

The case $p=2$, $h=0$ has been studied in detail in Ref. 35.

In the continuum limit the perturbing operator Eq. (2.20) becomes

$$\begin{aligned}O'_{\text{pert}}=&\lambda_1\sin[pk_+x-\sqrt{\pi}(Z_{cc}\phi_c-Z_{cs}\phi_s)]\\&\times\cos[pk_-x-\sqrt{\pi}((Z_{cc}-2Z_{sc})\phi_c-(Z_{cs}-2Z_{ss})\phi_s)]\\&+\lambda_2\sin(2pk_+x-\sqrt{4\pi}(Z_{cc}\phi_c-Z_{cs}\phi_s)),\end{aligned} \tag{2.21}$$

which radiatively generates a term of the form

$$\lambda_3\cos[2pk_-x-2\sqrt{\pi}((Z_{cc}-2Z_{sc})\phi_c-(Z_{cs}-2Z_{ss})\phi_s)]. \tag{2.22}$$

The only difference with respect to the previous case, Eqs. (2.17) and (2.18), is a phase in each of the sines or cosines, which however plays a role only at half filling and zero magnetic field (see also Ref. 35). Apart from this particular case, the conclusions remain the same as in the previous case.

C. Partial gap: irrational plateaus

We have shown in the previous subsection that, when both commensurability conditions Eq. (1.2) are satisfied, the spectrum of the model Eq. (1.1) is fully gapped. It is not yet understood what happens if only one of these conditions is satisfied. In this case, apparently one degree of freedom remains massless. We will show that the system nevertheless exhibits a gap for magnetic excitations (i.e., excitations changing the value of the magnetization), provided the total charge (i.e., the filling n) remains fixed.

For the sake of simplicity we will restrict ourselves to the dimerized chain ($p=2$) in this subsection although the argument can be generalized easily to $p>2$. Suppose that

$$\frac{p}{2}(n-m)=n-m=2n_{\downarrow}\in\mathbb{Z}, \tag{2.23}$$

but that $n+m$ is not an integer, i.e., the commensurability condition is fulfilled only for down electrons. Assume first that there is no interaction between up and down electrons ($U=0$). Then we are led to analyze the excitation spectrum of the following Hamiltonian in a system of length L:

$$\begin{aligned}H=&\int_0^L dx\,\frac{v_{\uparrow}}{2}[(\partial_x\phi_{\uparrow})^2+(\partial_x\theta_{\uparrow})^2]+\frac{v_{\downarrow}}{2}[(\partial_x\phi_{\downarrow})^2+(\partial_x\theta_{\downarrow})^2]\\&+\lambda\cos(2\sqrt{\pi}\phi_{\downarrow}),\end{aligned} \tag{2.24}$$

with total magnetization

$$M=\int_0^L dx\,\frac{1}{\sqrt{\pi}}\partial_x(\phi_{\uparrow}-\phi_{\downarrow})=\frac{1}{\sqrt{\pi}}(\phi_{\uparrow}-\phi_{\downarrow})|_0^L. \tag{2.25}$$

Motivated by experimental realizations of Hubbard systems, where typically doping is fixed, we also impose the constraint that the total particle number is fixed:

$$N=\int dx\,\frac{1}{\sqrt{\pi}}\partial_x(\phi_{\uparrow}+\phi_{\downarrow})=\frac{1}{\sqrt{\pi}}(\phi_{\uparrow}+\phi_{\downarrow})|_0^L. \tag{2.26}$$

From Eqs. (2.25) and (2.26) we see that the fields $\phi_{\uparrow,\downarrow}$ satisfy the following boundary conditions:

$$2\phi_{\uparrow}|_0^L=\sqrt{\pi}(N+M), \tag{2.27}$$

$$2\phi_{\downarrow}|_0^L=\sqrt{\pi}(N-M). \tag{2.28}$$

Notice, furthermore, that the fields $\phi_{\uparrow,\downarrow}$ are compactified, i.e., they satisfy the periodicity condition

$$\phi_{\uparrow,\downarrow}\rightarrow\phi_{\uparrow,\downarrow}+\sqrt{\pi}\mathbb{Z}. \tag{2.29}$$

Therefore, in a semiclassical picture, the vacuum configuration for $\phi_{\uparrow}$ is

$$\phi_{\uparrow}(x)=\frac{\sqrt{\pi}}{2L}(N+M)x+\text{const.} \tag{2.30}$$

On the other hand, for $\phi_{\downarrow}$ the vacuum configuration is a kink

$$\phi_{\downarrow}(x)=k(x), \tag{2.31}$$

where $k(x)$ is a configuration interpolating between two minima of the cosine potential in the Hamiltonian Eq. (2.24) and satisfying the boundary condition Eq. (2.28). Now we change the total magnetization, keeping the total number of particles fixed. The lowest energy excitation of this type consists of reversing the spin of a particle, which corresponds to the change $M\rightarrow M+2$. The new boundary conditions then become

$$2\phi_{\uparrow}|_0^L=\sqrt{\pi}(N+M+2), \tag{2.32}$$

$$2\phi_{\downarrow}|_0^L=\sqrt{\pi}(N-M-2). \tag{2.33}$$

The new vacuum configuration for $\phi_{\uparrow}$ is therefore

$$\phi_\uparrow(x)=\frac{\sqrt{\pi}}{2L}(N+M+2)x+\text{const}, \tag{2.34}$$

and it is straightforward to show that the difference in energy with respect to the original one is linear in $1/L$. On the contrary, changing the configuration of the kink requires a finite amount of energy (proportional to λ) because the new configuration is in a different topological sector. This corresponds to the presence of a gap in the spectrum of magnetic excitations, and therefore of a plateau in the magnetization curve.

To support the previous conclusion further, we analyze the magnetic susceptibility for a chain of finite size L. It is given by the integral of the correlation function of the spin density operator $(1/\sqrt{\pi})\partial_x(\phi_\uparrow-\phi_\downarrow)$. Since the down sector is gapped it does not contribute to the zero temperature limit of the susceptibility. Let us therefore focus on the up sector, which is apparently massless but constrained to be in a particular topological sector. One can easily see that determination of the susceptibility amounts to

$$\left\langle\left(\int_0^L dx\,\partial_x\phi_\uparrow\right)^2\right\rangle-\left\langle\left(\int_0^L dx\,\partial_x\phi_\uparrow\right)\right\rangle^2. \tag{2.35}$$

For the free massless sector, the Hamiltonian in a finite size L can be written in Fourier space for each topological sector as (see for example Ref. 36):

$$H_L=\frac{v}{2}\sum_{q\neq 0}\left[\frac{1}{K}q^2\phi_{-q}\phi_q+Kq^2\theta_{-q}\theta_q\right]+\frac{\pi v}{2L}\left(\frac{1}{K}Q^2+KJ^2\right), \tag{2.36}$$

where Q and J stand for the particle number and current zero modes:

$$Q=\frac{1}{\sqrt{\pi}}\phi_\uparrow\Big|_0^L,\quad J=\frac{1}{\sqrt{\pi}}\theta_\uparrow\Big|_0^L,$$

and the summation over q is for oscillatory modes. If the global constraint is not present, one has to sum over all possible values of Q, i.e., one has to compute

$$\chi=\frac{1}{\beta L}\left(\frac{1}{Z}\text{Tr}(\exp(-\beta H_L)Q^2)-\left(\frac{1}{Z}\text{Tr}(\exp(-\beta H_L)Q)\right)^2\right). \tag{2.37}$$

The local part (the oscillator modes) decouples, and if the constraint is not imposed we obtain the standard result

$$\begin{aligned}\chi&=\frac{1}{\beta L}\left(\frac{1}{Z}\sum_Q\left(\exp\left(-\beta\frac{\pi v Q^2}{2LK}\right)Q^2\right)\right.\\&\quad\left.-\left(\frac{1}{Z}\sum_Q\left(\exp\left(-\beta\frac{\pi v Q^2}{2LK}\right)Q\right)\right)^2\right)\\&=\frac{K}{2\pi v}.\end{aligned} \tag{2.38}$$

If we now impose the global constraint on N, due to the gap in the down sector as discussed above, all the sectors will be exponentially suppressed, except the sector $Q=(N+M)/2$. Therefore, for small enough temperature, the distribution $\exp[-\beta(\pi v Q^2/2LK)]$ has to be replaced by a delta function in $Q=(N+M)/2$, giving

$$\chi=\frac{1}{\beta L}(\langle Q^2\rangle-\langle Q\rangle^2)=0. \tag{2.39}$$

We find then an exotic situation in which we have simultaneously algebraic decay of correlation functions, since the local dynamics is massless, but zero magnetic susceptibility, due to the global constraint imposed on the system. The only somewhat similar situations we are aware of include plateau states of strongly frustrated spin ladders with gapless nonmagnetic excitations,[4,37,38] as well as the large number of singlets inside the gap of the Heisenberg antiferromagnet on a Kagomé lattice.[39]

D. Superconducting fluctuations

Having found a situation with a gap that can be attributed to magnetic excitations and another massless degree of freedom, one may wonder whether superconducting fluctuations develop. Therefore we now briefly analyze the correlators of the superconducting order parameter. In the presence of a magnetic field, the superconducting order parameter has four components which read on the lattice:

$$\Delta_{\alpha,\beta}=c_{x+1,\alpha}c_{x,\beta}. \tag{2.40}$$

For $h=0$, these components can be grouped in a triplet t and a singlet s. On the lattice, the corresponding $S^z=0$ components can be chosen as

$$\Delta_{t,s}^{\text{latt}}=c_{x,\uparrow}c_{x+1,\downarrow}\pm c_{x,\downarrow}c_{x+1,\uparrow}. \tag{2.41}$$

In the continuum, using Eq. (A1) this leads to the following expression:

$$\begin{aligned}\Delta_{t,s}&=e^{-ik_-x}\psi_{R,\uparrow}\psi_{L,\downarrow}(e^{ik_{F\downarrow}}\mp e^{-ik_{F\uparrow}})+e^{ik_-x}\psi_{L,\uparrow}\psi_{R,\downarrow}\\&\quad\times(e^{-ik_{F\downarrow}}\mp e^{ik_{F\uparrow}})+e^{-ik_+x}\psi_{R,\uparrow}\psi_{R,\downarrow}(e^{-ik_{F\downarrow}}\mp e^{-ik_{F\uparrow}})\\&\quad+e^{ik_+x}\psi_{L,\uparrow}\psi_{L,\downarrow}(e^{ik_{F\downarrow}}\mp e^{ik_{F\uparrow}}).\end{aligned} \tag{2.42}$$

In particular, for zero magnetic field $k_{F\uparrow}=k_{F\downarrow}=k_F$ and neglecting ''$2k_F$'' terms, Eqs. (2.42) reduce to the standard ones (see for example Ref. 26):

$$\begin{aligned}\Delta_t&=2i\sin k_F(\psi_{R,\uparrow}\psi_{L,\downarrow}+\psi_{R,\downarrow}\psi_{L,\uparrow}),\\\Delta_s&=2\cos k_F[\psi_{R,\uparrow}\psi_{L,\downarrow}-\psi_{R,\downarrow}\psi_{L,\uparrow}(x)].\end{aligned} \tag{2.43}$$

For general m, one finds instead

$$\begin{aligned}\Delta_t&\sim\frac{1}{\pi a}e^{i\sqrt{\pi}(\theta_\uparrow+\theta_\downarrow)}\cos(\sqrt{\pi}(\phi_\uparrow-\phi_\downarrow)-k_-x),\\\Delta_s&\sim\frac{i}{\pi a}e^{i\sqrt{\pi}(\theta_\uparrow+\theta_\downarrow)}\sin(\sqrt{\pi}(\phi_\uparrow-\phi_\downarrow)-k_-x).\end{aligned} \tag{2.44}$$

These expressions show that the correlators associated to the order parameters Δ_t and Δ_s decay exponentially, even in the partially massless plateau phases. Indeed, since the $S^z=0$ components of $\Delta_{\alpha,\beta}$ are products of up and down degrees of

freedom, it is sufficient that one of them is gapped in order to lead to an exponential decay of the composite object.

On the other hand, the diagonal components are bosonized as

$$\Delta_{\alpha,\alpha}\sim 2\cos(k_{F,\alpha})e^{i\sqrt{4\pi}\theta_\alpha}+e^{-ik_{F,\alpha}(1+2x)}e^{i\sqrt{4\pi}(\phi_\alpha+\theta_\alpha)} + e^{ik_{F,\alpha}(1+2x)}e^{i\sqrt{4\pi}(-\phi_\alpha+\theta_\alpha)}+\ldots, \tag{2.45}$$

where the dots include terms which mix $\phi_\uparrow$ with $\phi_\downarrow$. It is then clear that on a doping-dependent plateau, where only one of the fields is gapful, only one of the correlators $\langle\Delta^\dagger_{\alpha,\alpha}\Delta_{\alpha,\alpha}\rangle$ decays exponentially, but the other exhibits *algebraic* behavior. In fact, all fields involving only the gapless spin component decay algebraically. In particular, the two-point correlator of $c_{x,\alpha}$ also decays algebraically if $\Delta_{\alpha,\alpha}$ exhibits quasi-long-range order. The algebraic decay of the latter should therefore not be taken as a sign of superconductivity, but is interesting nevertheless.

III. SMALL-U LIMIT

The previous section was dedicated to the bosonization approach to the p-merized Hubbard chain in the small p-merization limit. In the present section, we give a further argument for doping dependent plateaus, valid in the low U limit but at arbitrary p-merization strength. For the sake of simplicity, we will concentrate on the case of modulated hopping amplitude $t(x)=t'$ for x a multiple of p, otherwise $t(x)=t$ and constant $\mu(x)=\mu$, but the arguments can be generalized easily.

First we diagonalize the Hamiltonian Eq. (1.1) at $U=0$ by a unitary transformation

$$d^\lambda_{k,\sigma}=\frac{1}{\sqrt{L}}\sum_{x=1}^{L/p}\mathrm{e}^{ikx}\sum_{j=1}^{p}a^\lambda_{k,j}c_{xp+j,\sigma}. \tag{3.1}$$

In order for the kinetic part of the Hamiltonian Eq. (1.1) to take the form

$$H_0=\sum_{\lambda=1}^{p}\sum_{\sigma}\epsilon^\lambda(k)d^{\dagger\lambda}_{k,\sigma}d^\lambda_{k,\sigma}, \tag{3.2}$$

the coefficients $a^\lambda_{k,j}$ have to satisfy the following eigenvalue equation:

$$-\begin{pmatrix} 0 & t & 0 & \cdots & 0 & t'\mathrm{e}^{-ik}\\ t & 0 & t & \ddots & & 0\\ 0 & t & \ddots & \ddots & \ddots & \vdots\\ \vdots & \ddots & \ddots & \ddots & t & 0\\ 0 & & \ddots & t & 0 & t\\ t'\mathrm{e}^{ik} & 0 & \cdots & 0 & t & 0 \end{pmatrix}\begin{pmatrix} a^\lambda_{k,1}\\ a^\lambda_{k,2}\\ \vdots\\ a^\lambda_{k,p}\end{pmatrix} = \epsilon^\lambda(k)\begin{pmatrix} a^\lambda_{k,1}\\ a^\lambda_{k,2}\\ \vdots\\ a^\lambda_{k,p}\end{pmatrix}. \tag{3.3}$$

The resulting p energy bands $\epsilon^\lambda(k)$ are illustrated in Fig. 2 of Ref. 30 for $p=2$ and in Fig. 2 of Ref. 15 for $p=3$ (note that in the latter case, the energy ϵ was plotted with the wrong sign which can be absorbed by shifting $k\to k+\pi$).

In the sequel we first work out the simpler case $p=2$ and then generalize to $p\geqslant 3$.

A. Case $p=2$

In the dimerized case, the eigenvalue equation (3.3) reduces to

$$-\begin{pmatrix} 0 & t+t'\mathrm{e}^{-ik}\\ t+t'\mathrm{e}^{ik} & 0\end{pmatrix}\begin{pmatrix} a^\lambda_{k,1}\\ a^\lambda_{k,2}\end{pmatrix}=\epsilon^\lambda(k)\begin{pmatrix} a^\lambda_{k,1}\\ a^\lambda_{k,2}\end{pmatrix}. \tag{3.4}$$

The eigenvalue problem Eq. (3.4) is solved readily, yielding

$$\epsilon^\pm(k)=\pm\sqrt{t^2+t'^2+2tt'\cos k},$$
$$a^\pm_1=\mp\sqrt[4]{\frac{t+t'e^{-ik}}{t+t'e^{ik}}}, \tag{3.5}$$
$$a^\pm_2=\sqrt[4]{\frac{t+t'e^{ik}}{t+t'e^{-ik}}}.$$

The inverse of the transformation Eq. (3.1) is

$$c_{2x+2,\sigma}=\frac{1}{\sqrt{L}}\sum_k e^{-ikx}\sqrt[4]{\frac{t+t'e^{-ik}}{t+t'e^{ik}}}\,(d^-_{k,\sigma}+d^+_{k,\sigma}),$$
$$c_{2x+1,\sigma}=\frac{1}{\sqrt{L}}\sum_k e^{-ikx}\sqrt[4]{\frac{t+t'e^{ik}}{t+t'e^{-ik}}}\,(d^-_{k,\sigma}-d^+_{k,\sigma}). \tag{3.6}$$

Eigenstates $|\{k^\lambda_{j,\sigma}\}\rangle$ of the free Hamiltonian H_0 are now written down by simply specifying the momenta $k^\lambda_{j,\sigma}$ occupied in the various bands. Now we treat the Coulomb repulsion

$$H_I=U\sum_{x=1}^{L}n_{x,\uparrow}n_{x,\downarrow} \tag{3.7}$$

in first order perturbation theory.

To proceed further, we assume that none of the bands are half filled. Then H_I has only diagonal terms (i.e., Umklapp scattering is absent) which are readily evaluated as (denoting $n^\lambda_{k,\sigma}=d^{\dagger\lambda}_{k,\sigma}d^\lambda_{k,\sigma}$)

$$\langle\{k^\lambda_{j,\sigma}\}|H_I|\{k^\lambda_{j,\sigma}\}\rangle = \frac{U}{L}\langle\{k^\lambda_{j,\sigma}\}|\sum_{k,k'}(n^-_{k,\uparrow}+n^+_{k,\uparrow})(n^-_{k',\downarrow}+n^+_{k',\downarrow})|\{k^\lambda_{j,\sigma}\}\rangle$$
$$=\frac{U}{L}(N^-_\uparrow+N^+_\uparrow)(N^-_\downarrow+N^+_\downarrow)=\frac{U}{4}L(n^-_\uparrow+n^+_\uparrow)(n^-_\downarrow+n^+_\downarrow). \tag{3.8}$$

In the second line, we have defined the number of particles with spin σ in band λ by $N_\sigma^\lambda = n_\sigma^\lambda L/2$.[40] The densities have been normalized such that $n_\sigma^\lambda = 1$ for a completely filled band.

Similarly, expectation values of the number operators $\Sigma_{x=1}^{L} n_{x,\sigma}$ give $L(n_\sigma^- + n_\sigma^+)/2$. Putting everything together, we find the energy of the Hamiltonian Eq. (1.1) to first order in U as

$$E = \sum_\lambda \sum_{k_{j,\sigma}^\lambda} \epsilon^\lambda(k_{j,\sigma}^\lambda) + \frac{U}{4} L(n_\uparrow^- + n_\uparrow^+)(n_\downarrow^- + n_\downarrow^+) + \frac{\mu}{2} L(n_\uparrow^- + n_\uparrow^+ + n_\downarrow^- + n_\downarrow^+) - \frac{h}{4} L(n_\uparrow^- + n_\uparrow^+ - n_\downarrow^- - n_\downarrow^+). \tag{3.9}$$

Assume now that the ''$-$'' bands are both partially filled. Then Eq. (3.9) specializes to

$$E/L = \frac{1}{4\pi} \sum_\sigma \int_{-n_\sigma \pi}^{n_\sigma \pi} dk \epsilon^-(k) + \frac{U}{4} n_\uparrow n_\downarrow + \frac{\mu}{2}(n_\uparrow + n_\downarrow) - \frac{h}{4}(n_\uparrow - n_\downarrow), \tag{3.10}$$

where $n_\sigma = n_\sigma^-$.[41] Setting $n = n_\uparrow + n_\downarrow$ and fixing $n_\uparrow \approx 1$, we find from the condition that it does not require energy to flip $\uparrow$ to $\downarrow$ spins

$$h_{c_1} = \epsilon^-(\pi) - \epsilon^-((n-1)\pi) + U\left(\frac{n}{2} - 1\right). \tag{3.11}$$

On the other hand, if we consider the case of a completely filled ''$-,\uparrow$'' band and partially filled ''$+,\uparrow$'' and ''$-,\downarrow$'' bands, Eq. (3.9) specializes as follows:

$$E/L = \frac{1}{2\pi} \int_{(1-n_\uparrow^+)\pi}^{n_\uparrow^+ \pi} dk \epsilon^+(k) + \frac{1}{2\pi} \int_0^\pi dk \epsilon^-(k) + \frac{1}{2\pi} \int_0^{n_\downarrow \pi} dk \epsilon^-(k) + \frac{U}{4}(1 + n_\uparrow^+) n_\downarrow + \frac{\mu}{2}(1 + n_\uparrow^+ + n_\downarrow) - \frac{h}{4}(1 + n_\uparrow^+ - n_\downarrow). \tag{3.12}$$

Setting $n = 1 + n_\uparrow^+ + n_\downarrow$ and fixing $n_\uparrow^+ \approx 0$, we find in the same way as before that

$$h_{c_2} = \epsilon^+(\pi) - \epsilon^-((n-1)\pi) + U\left(\frac{n}{2} - 1\right). \tag{3.13}$$

Using Eqs. (3.13) and (3.11) we find that the width of the plateau at fixed N is not affected by the on-site Coulomb repulsion to first order in U:

$$h_{c_2} - h_{c_1} = 2|t - t'| + \mathcal{O}(U^2). \tag{3.14}$$

This ensures the presence of a doping-dependent plateau with $m = 1 - n$ in the low U limit. The absence of a first-order correction in U to the width in Eq. (3.14) can be traced to the mean-field form Eq. (3.8) of the matrix elements of the on-site repulsion H_I. This in turn is due to the fact that $|a_i^\pm| = 1$ for all k as can be seen from Eq. (3.5) and is a manifestation of the symmetry between the lower and upper band. Both the mean-field form of the interaction as well as the absence of a first-order correction to the plateau width are special properties of the case $p = 2$, as will become clear in the following discussion of the case $p \geqslant 3$.

B. Case $p \geqslant 3$

For general p, the diagonalization Eq. (3.3) is more complicated leading to the absence of explicit expressions such as Eq. (3.6). Nevertheless, we can still use unitarity of the transformation Eq. (3.1) to formally invert it

$$c_{xp+j,\sigma} = \frac{1}{\sqrt{L}} \sum_k \sum_\lambda \mathrm{e}^{-ikx} a_{k,j}^{*\lambda} d_{k,\sigma}^\lambda. \tag{3.15}$$

First, we look at the transformation of number operators $n_{x,\sigma} = c_{x,\sigma}^\dagger c_{x,\sigma} \to n_{k,\sigma}^\lambda = d_{k,\sigma}^{\dagger\lambda} d_{k,\sigma}^\lambda$:

$$\sum_x n_{x,\sigma} = \frac{1}{p} \sum_{k,\lambda} \sum_{j=1}^{p} |a_{k,j}^\lambda|^2 n_{k,\sigma}^\lambda = \sum_{k,\lambda} n_{k,\sigma}^\lambda. \tag{3.16}$$

Here, we note that $\Sigma_{j=1}^p |a_{k,j}^\lambda|^2 = p$.

The diagonal terms of the interaction Eq. (3.7) can now be treated similarly as for $p = 2$. Instead of Eq. (3.8) one finds for general p

$$\langle \{k_{j,\sigma}^\lambda\} | H_I | \{k_{j,\sigma}^\lambda\} \rangle = \frac{U}{pL} \langle \{k_{j,\sigma}^\lambda\} | \sum_{j=1}^{p} \sum_{k,\lambda} |a_{k,j}^\lambda|^2 n_{k,\uparrow}^\lambda \sum_{k',\lambda'} |a_{k',j}^{\lambda'}|^2 n_{k',\downarrow}^{\lambda'} | \{k_{j,\sigma}^\lambda\} \rangle = \frac{U}{pL} \sum_{j=1}^{p} \sum_{k_{j,\uparrow}^\lambda \text{ occupied}} |a_{k,j}^\lambda|^2 \sum_{k'_{j,\downarrow}{}^{\lambda'} \text{ occupied}} |a_{k',j}^{\lambda'}|^2. \tag{3.17}$$

Next we pass to the thermodynamic limit which leads to replacing sums by integrals. Due to Eq. (3.16), integrals and differentials over densities can be replaced by integrals in k space. We work at a fixed particle number n, which implies

$$0=dn=dn_{\uparrow}+dn_{\downarrow}\Rightarrow dn_{\downarrow}=-dn_{\uparrow}. \tag{3.18}$$

Now we concentrate on the situation where all bands $\lambda \leqslant \lambda_0$ are completely occupied with up spins and those with $\lambda>\lambda_0$ do not contain any up spins, thus generalizing the reasoning of the previous section. The band λ_0' is partially occupied with down spins, those with $\lambda'<\lambda_0'$ are completely filled with down spins, while those with $\lambda'>\lambda_0'$ do not contain any down spins. For a partially filled band ν, let us denote the range of occupied states by $[k_l^{\nu},k_u^{\nu}]$.

Then we can generalize Eq. (3.10) to first order in U as follows:[41]

$$E/L=u+v+\frac{\mu}{p}(n_{\uparrow}+n_{\downarrow})-\frac{h}{2p}(n_{\uparrow}-n_{\downarrow}) \tag{3.19}$$

with

$$u=\frac{1}{2\pi p}\left\{\sum_{\lambda\leqslant\lambda_0}\int_{-\pi}^{\pi}dk\,\epsilon^{\lambda}(k)+\int_{k_l^{\lambda_0'}}^{k_u^{\lambda_0'}}dk'\,\epsilon^{\lambda_0'}(k')+\sum_{\lambda'<\lambda_0'}\int_{-\pi}^{\pi}dk'\,\epsilon^{\lambda'}(k')\right\} \tag{3.20}$$

and

$$v=\frac{U}{4\pi^2p^3}\left\{\sum_{j=1}^{p}\sum_{\lambda\leqslant\lambda_0}\int_{-\pi}^{\pi}dk|a_{k,j}^{\lambda}|^2\left(\int_{k_l^{\lambda_0'}}^{k_u^{\lambda_0'}}dk'|a_{k',j}^{\lambda_0'}|^2+\sum_{\lambda'<\lambda_0'}\int_{-\pi}^{\pi}dk'|a_{k',j}^{\lambda'}|^2\right)\right\}. \tag{3.21}$$

This yields for the lower boundary of the associated plateau

$$h_{c_1}=\epsilon^{\lambda_0}(k_u^{\lambda_0})-\epsilon^{\lambda_0'}(k_u^{\lambda_0'})+\mathcal{U}(\lambda_0)+\mathcal{O}(U^2) \tag{3.22}$$

with

$$\mathcal{U}(\nu)=\frac{U}{2\pi p^2}\left\{\sum_{j=1}^{p}|a_{k_u^{\nu},j}^{\nu}|^2\left(\int_{k_l^{\lambda_0'}}^{k_u^{\lambda_0'}}dk'|a_{k',j}^{\lambda_0'}|^2+\sum_{\lambda'<\lambda_0'}\int_{-\pi}^{\pi}dk'|a_{k',j}^{\lambda'}|^2\right)-\sum_{j=1}^{p}\sum_{\lambda\leqslant\lambda_0}\int_{-\pi}^{\pi}dk|a_{k,j}^{\lambda}|^2|a_{k_u^{\lambda_0'},j}^{\lambda_0'}|^2\right\}. \tag{3.23}$$

For the corresponding upper boundary one finds

$$h_{c_2}=\epsilon^{\lambda_0+1}(k_u^{\lambda_0+1})-\epsilon^{\lambda_0'}(k_u^{\lambda_0'})+\mathcal{U}(\lambda_0+1)+\mathcal{O}(U^2). \tag{3.24}$$

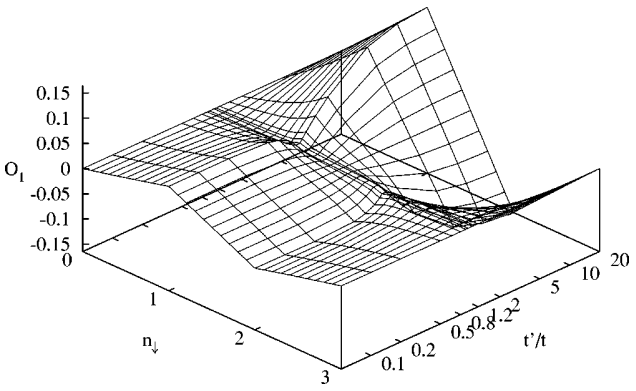

FIG. 1. Value of the first-order correction O_1 to the plateau width as given by Eq. (3.26) for $p=3$ and $n_{\uparrow}=2$.

Equations (3.22) and (3.24) imply that

$$h_{c_2}-h_{c_1}=\epsilon^{\lambda_0+1}(k_u^{\lambda_0+1})-\epsilon^{\lambda_0}(k_u^{\lambda_0})+UO_1+\mathcal{O}(U^2) \tag{3.25}$$

with

$$O_1=\frac{1}{2\pi p^2}\sum_{j=1}^{p}(|a_{k_u^{\lambda_0+1},j}^{\lambda_0+1}|^2-|a_{k_u^{\lambda_0},j}^{\lambda_0}|^2)\times\left(\int_{k_l^{\lambda_0'}}^{k_u^{\lambda_0'}}dk'|a_{k',j}^{\lambda_0'}|^2+\sum_{\lambda'<\lambda_0'}\int_{-\pi}^{\pi}dk'|a_{k',j}^{\lambda'}|^2\right). \tag{3.26}$$

Generally, the first-order contribution does not vanish (for $p>2$). It can be estimated as

$$|O_1|\leqslant\frac{1}{2\pi p^2}\sum_{j=1}^{p}p\left(\int_{k_l^{\lambda_0'}}^{k_u^{\lambda_0'}}dk'|a_{k',j}^{\lambda_0'}|^2+\sum_{\lambda'<\lambda_0'}\int_{-\pi}^{\pi}dk'|a_{k',j}^{\lambda'}|^2\right)=\frac{n_{\downarrow}}{p}, \tag{3.27}$$

which shows that in principle it can be of order one.

In general, it is not difficult to evaluate the first-order contribution Eq. (3.26) to the plateau width numerically. We will illustrate this now for $p=3$. First notice that, for the case $p=3$, the contribution from the kinetic energy can be readily evaluated as

$$\epsilon^3(0)-\epsilon^2(0)=\epsilon^2(\pi)-\epsilon^1(\pi)=\left|\frac{\sqrt{8t^2+t'^2}-3t'}{2}\right|. \tag{3.28}$$

Now we fix $n_{\uparrow}=2$, i.e., the lowest two bands of up electrons are completely filled. Then one has that $k_u^3=k_u^2=0$ in Eq. (3.26). Numerical diagonalization of Eq. (3.3) and evaluation of the remaining integrals in Eq. (3.26) then leads to Fig. 1. Note that in the conventions of the other sections (where $0\leqslant n\leqslant 2$) this corresponds to the plateau with $m=4/3-n$. The numerical data satisfy $O_1\rightarrow -O_1$ as $n_{\downarrow}\rightarrow 3-n_{\downarrow}$. This implies in particular that the values of O_1 can be both posi-

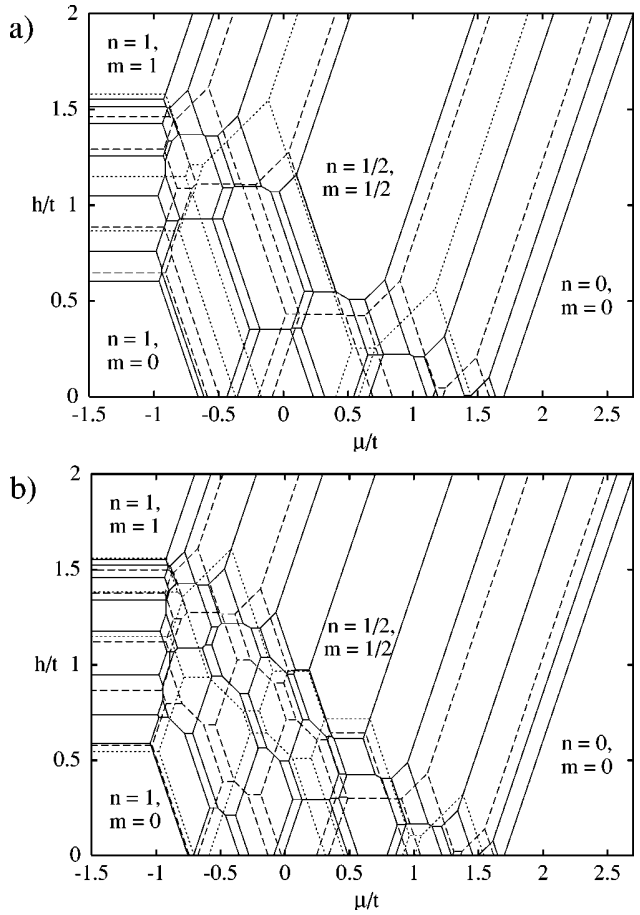

FIG. 2. Ground state phase diagram of the dimerized chain ($p=2$) with $U=3t$, $t'=0.7t$. In (a) the lines are for $L=6$ (dotted), $L=10$ (dashed), and $L=14$ (full) while in (b) they are for $L=8$ (dotted), $L=12$ (dashed), and $L=16$ (full).

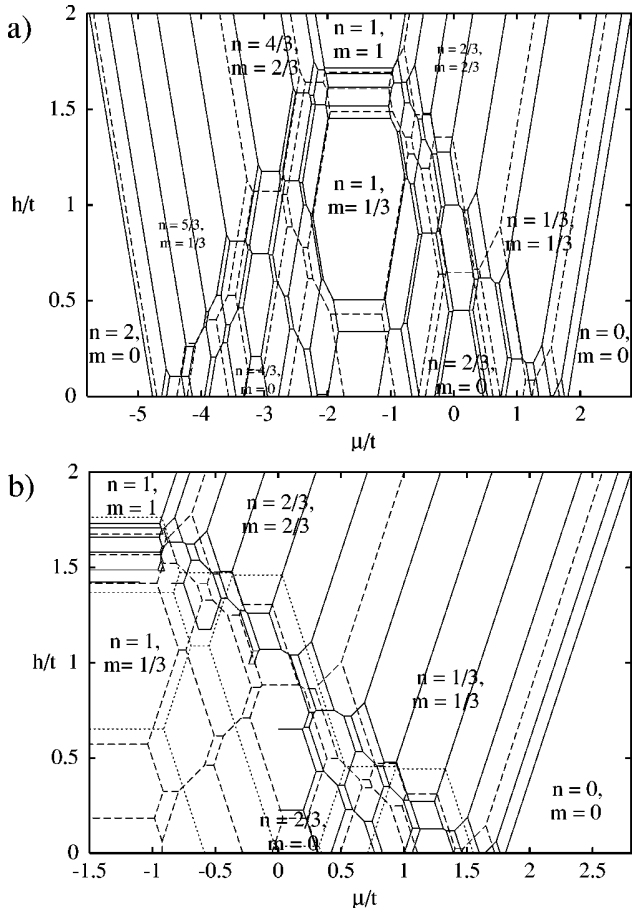

FIG. 3. Ground state phase diagram of the trimerized chain ($p=3$) with $U=3t$, $t'=0.7t$. In (a) the lines are for $L=9$ (dashed) and $L=15$ (full) while in (b) they are for $L=6$ (dotted), $L=12$ (dashed), and $L=18$ (full). Note that the $L=18$ data in (b) are incomplete for $n>2/3$ (e.g., only $m\geqslant 1/3$ for $n=1$).

tive and negative, corresponding to an enhancement or reduction of the plateau width, respectively. Furthermore, for $t\to 0$ and $n_\downarrow<1$, the linear behavior of Eq. (3.27) is reproduced, although with a coefficient which is 1/6, i.e., by a factor of 2 smaller than in the estimate. The maximal values attained are $\pm 1/6$ for $n_\downarrow\to 1$ or 2, respectively, and $t\to 0$. This shows that the doping-dependent plateaus should be stable features for $p=3$ as well.

We conclude this section by noting that the calculations are also valid for the on-site p-merized energy. The free Hamiltonian H_0 to be diagonalized is modified, but the conclusions remain qualitatively unchanged.

IV. LANCZOS DIAGONALIZATION

Finally, we have performed Lanczos diagonalizations of the Hamiltonian Eq. (1.1) for $p=2$ and $p=3$ with constant $\mu(x)=\mu$ and periodic boundary conditions on finite lattices in order to further support the previous results. The particle numbers $n_\uparrow$ and $n_\downarrow$ have been used as quantum numbers and translational symmetry was exploited. Furthermore, reflection symmetry was exploited for $k=0,\pi$ and spin inversion for $n_\uparrow=n_\downarrow$.

A. Ground state phase diagrams

Computations have been performed mainly for one choice of parameters due to the large number of sectors for which the ground state energy had to be found (for $p=2$ and $L=16$ of the order of 10^3 sectors). Keeping Eq. (2.16) in mind, we have chosen the parameters $U=3t$ and $t'=0.7t$ in order to look at a situation sufficiently different from the limiting cases discussed before, i.e., both intermediate (to strong, as compared to the bandwidth) on-site repulsion U and intermediate t'/t.

For the interpretation of our Lanczos results to be presented below, it is useful to remember the following consequences of particle-hole symmetry on a finite size lattice (see Refs. 22 and 42 and references therein): For L even, the ground state phase diagram of the Hubbard chain with periodic boundary conditions is symmetric under $\mu \square -U-\mu$ (with our conventions), while for L odd the particle-hole transformation interchanges periodic and antiperiodic boundary conditions.

Our numerical results for the ground state phase diagram are shown in Figs. 2 and 3 for $p=2$ and $p=3$, respectively. The polygons in the figures denote regions in the (μ,h)

plane where the ground state has a fixed filling n and magnetization m at the given system size L (those values of m and n which are common to all investigated system sizes are indicated in the figures). The ground state phase diagrams are symmetric under spin inversion ($m \to -m$ when $h \to -h$) and as mentioned before, for even L also under a particle-hole transformation ($n \to 2-n$ when $\mu \to -U-\mu$). Therefore, for even L we show only the quadrant with $\mu \geqslant -U/2$, $h \geqslant 0$, and for odd L only the region with $h \geqslant 0$.

The schematic ground state phase diagrams in Ref. 15 were in fact based on parts of these results and the reader may wish to use them as a guide to the diagrams at finite size.

We note that for the saturated case $n_\downarrow = 0$ (and by particle-hole symmetry also for $n_\uparrow = 1$), the Coulomb repulsion is not effective and the noninteracting result [$\epsilon^{\pm}(k)$ given by Eq. (3.5) for $p=2$] can be used to determine the transitions between different particle numbers. Complete agreement between this analytical computation and the corresponding numerical results in Figs. 2 and 3 is found. This also guides the interpretation of the finite-size data since it follows in particular that the completely gapped situations at saturation are those with $pn \in \mathbb{Z}$ in the thermodynamic limit. Such a guide is useful since the fermions behave differently for even and odd particle numbers, thus yielding nonmonotonic finite-size effects which can be still strong for the small systems sizes considered here. In the particular case of the gapped states with $pn \in \mathbb{Z}$ at $m=n$ (or $m=2-n$), the corresponding ground state always has an even number of fermions when L/p is even while cases with an odd number occur when L/p is odd. This leads to vanishing finite-size effects for the transition lines in the former case, but not always in the latter. Since even and odd L/p behave differently, we show separate figures for the two cases.

For $p=2$, one can quite clearly recognize the fully gapped situations at $(n,m)=(1,0)$, $(1,1)$, $(1/2,1/2)$ and $(0,0)$ from the finite-L data shown in Fig. 2. Also the charge gap at half filling ($n=1$) is obvious. The most interesting region is the doping-dependent plateau with $m=1-n$ which is a stable feature in Fig. 2(a), but less clear in Fig. 2(b). Still, in the latter case the region of stability of states with $m=1-n$ can be seen to increase with increasing system size, thus supporting the presence of a gap. Just the charge gap at quarter filling ($n=1/2$) is not distinct in this numerical data, however it is known to be small for these parameters.[30]

The case $p=3$ is shown in Fig. 3. There is clear evidence for the expected fully gapped situations (the labeled regions in the figure) as well as the charge gap at half filling. There is also evidence for the charge gap at $n=2/3$ and the equivalent case $n=4/3$, just the charge gap at $n=1/3,5/3$ is again difficult to see. Also the expected doping-dependent magnetization plateau with $m=|n-2/3|$ can be recognized in Fig. 3(a). By particle-hole symmetry, the plateau with $m=|4/3-n|$ must be present as well though it is more difficult to recognize. The finite-size behavior of its stability region in Fig. 3(a) [and of both plateaus in the case of Fig. 3(b)] can again be taken as an indication that it will indeed be present in the thermodynamic limit.

B. Correlation functions

Having also provided numerical evidence for the existence of doping-dependent magnetization plateaus, we now present a few numerical results for correlation functions at $p=2$.

Is technically useful to consider only objects which respect the decomposition of the Hilbert space according to symmetries of the Hamiltonian. We therefore define averages of an operator A_x as

$$\langle A_x \rangle = \begin{cases} \dfrac{1}{L} \left\langle \psi_0(k) \left| \displaystyle\sum_{x_0=1}^{L} A_{x_0} \right| \psi_0(k) \right\rangle & \text{for } k \neq 0,\pi, \\ \dfrac{1}{2L} \left\langle \psi_0(k) \left| \displaystyle\sum_{x_0=1}^{L} (A_{x_0} + A_{-x_0}) \right| \psi_0(k) \right\rangle & \text{for } k = 0,\pi, \end{cases} \tag{4.1}$$

where $|\psi_0(k)\rangle$ is the ground state with momentum k. An additional advantage of this definition is that oscillations originating from the modulation of $t(x)$ are smoothed by taking averages of the up to $p=2$ correlation functions at a given distance.

The connected correlation function of two quantities A and B is defined as

$$C_{A,B}(x) = \langle A^{\dagger}_{x_0+x} B_{x_0} \rangle - \langle A^{\dagger}_{x_0} \rangle \langle B_{x_0} \rangle. \tag{4.2}$$

Of particular interest are the diagonal components of the superconducting order parameter Eq. (2.40) since quasi-long-range order is expected for one of them.

Numerical results for correlation functions on an $L=18$ system at the plateau with $m=1-n$ are shown in Fig. 4. Characteristic oscillations are observed in the density-density and electron-electron correlation functions. This and the finite system size make a detailed analysis of the asymptotics difficult. Nevertheless, one observes that correlation functions containing up electrons decay faster than the corresponding ones containing only down electrons (the latter may still be smaller in absolute value due to a smaller overall prefactor). In fact, all correlation functions shown in Fig. 4 are very similar to those obtained in the noninteracting situation ($U=0$) at the same L. We therefore interpret our results as support for exponential decay of all correlation func-

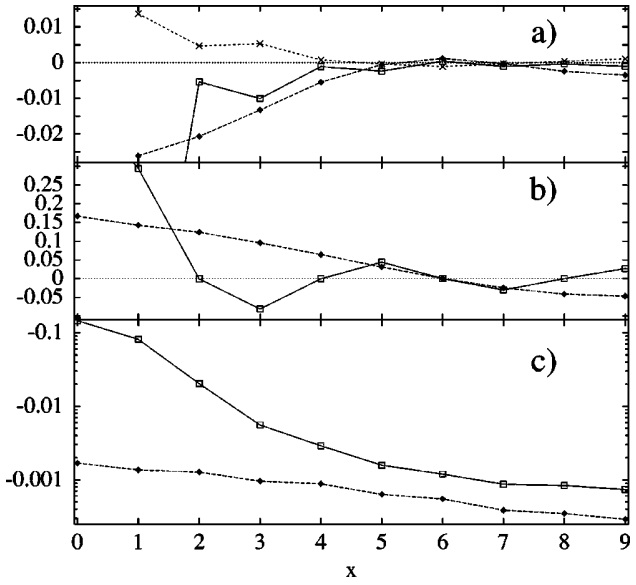

FIG. 4. Correlation functions for the dimerized chain ($p=2$) with $U=3t$, $t'=0.7t$ at $L=18$, $n=2/3$, and $m=1/3$. Panel (a) shows density-density correlations $C_{n_\alpha,n_\beta}(x)$, panel (b) electron-electron correlations $C_{c_\alpha,c_\beta}(x)$, and panel c) superconducting correlations $C_{\Delta_{\alpha,\alpha},\Delta_{\beta,\beta}}(x)$. The symbols are for $\alpha=\beta=\uparrow$ (boxes), $\alpha=\beta=\downarrow$ (filled diamonds), and $\alpha=\uparrow$, $\beta=\downarrow$ ($\times$); the lines are guides to the eye.

tions containing $\uparrow$ operators and power-law decay for those containing only $\downarrow$ operators, as is expected according to the analysis of Sec. II. In particular, these numerical results are compatible with quasi-long-range order in $\Delta_{\downarrow,\downarrow}$ on the $m=1-n$ plateau.

V. DISCUSSION AND CONCLUSIONS

We have shown that Hubbard chains with periodic hopping or on-site energy present a rich structure of magnetization plateaus. More precisely, for a periodicity p, we obtain the conditions Eq. (1.2) for the appearance of the plateaus. If both conditions are simultaneously satisfied, both spin and charge degrees of freedom are massive. When the combination $pn\in\mathbb{Z}$ of these two conditions is satisfied, a charge gap opens irrespective of the value of m. Finally, if just one of the conditions Eq. (1.2) is satisfied, a magnetization plateau appears *if* the total filling n remains fixed. This result has been shown first by means of bosonization techniques, valid in the regime where the differences in the modulation amplitudes δ in Eq. (2.15) and $\delta\mu$ in Eq. (2.20) are small and for arbitrary values of U. We have then shown that these results are confirmed by standard quantum mechanical arguments valid for small U and arbitrary p-merization strength and provided an expression for the width of the plateau to first order in U. We finally showed explicitly such plateaus in finite size systems by means of Lanczos diagonalization.

The combination of a gap, which can be attributed to the spin degrees of freedom and gapless (charge) modes, prompted us to look for superconducting correlations. Indeed, we found quasi-long-range order in one component of the superconducting order parameter in those cases where only one of the conditions Eq. (1.2) is satisfied.

In Ref. 15 it has been pointed out that the fully gapped situations can be most easily understood in the limit $t'=0$ (the same argument applies also for $\delta\mu=\infty$). Then the chain effectively decomposes into clusters of p sites, whose magnetization curves are obviously staircase-like. The charge gap at $pn\in\mathbb{Z}$ can also be understood in the limit of $t'\ll t$ ($\delta\mu\gg\mu$), one just needs to generalize the mapping of a quarter-filled dimerized chain to an effective half-filled homogeneous chain[30] to $m\neq 0$ and commensurate filling at general p. Finally, this mapping can also be adapted to provide a further complementary argument for the existence of the doping-dependent magnetization plateaus. Again, to first order in t', an effective Hamiltonian can be found in the regime of strong p-merization, i.e., in the limit $t'\ll t,U$ (respectively, $\delta\mu\gg t,U$) for the case of modulation of the hopping amplitude (respectively, of the on-site energy). When only one of the conditions Eq. (1.2) is satisfied, which amounts to a condition on the filling of spin-up or spin-down bands, this effective Hamiltonian acquires a gap in the spin sector, thus leading to a doping-dependent magnetization plateau.

We would like to emphasize that such irrational plateaus are not present in systems where the doping is not fixed. Moreover, due to the remaining massless mode on such a plateau, the thermodynamical behavior of the system retains some particularities of a gapless system, such as a specific heat vanishing linearly as $T\to 0$. An important feature is that the value of the magnetization m on the plateaus at fixed n depends continuously on doping n. Analogous situations[16,17] encourage us to believe that this scenario is generic in doped systems. Doping could therefore be used as a tool to study experimentally irrational plateaus in systems whose half-filled parent compounds exhibit plateaus only at prohibitively high magnetic fields. A natural candidate are ladders systems,[14] where doping can indeed be controlled. Theoretical results on doping-dependent magnetization plateaus in Hubbard ladders will be reported elsewhere.[43]

There are also natural problems for further study in the case of modulated chains. For example, the large-U limit of the Hubbard model leads to the t-J model. As a check of the generality of our results, one could therefore investigate the t-J model, which at half filling would then be exactly the situation studied in Ref. 6. Due to the reduced Hilbert space, the t-J model would be particularly well suited for further numerical checks. Another problem to be addressed is the universality class of the transitions associated to the corners of a plateau. In the case of the BA solvable model[16], it was found that the presence of a massless mode on a doping-dependent plateau may modify the universality class of part of these transitions—a fact that would also be interesting to investigate in the present model.

ACKNOWLEDGMENTS

We acknowledge useful discussions with P. Degiovanni, B. Douçot, M. Fabrizio, E. Fradkin, H. Frahm, A. Izergin, F. Mila, T. M. Rice, and C. Sobiella. This work has been done

under partial support of the EC TMR Program *Integrability, nonperturbative effects and symmetry in Quantum Field Theories*. A.H. is grateful to the Institut für Theoretische Physik of the ETH Zürich for hospitality and to the Alexander von Humboldt Foundation for financial support during the initial stages of this project, as well as to the C4 cluster of the ETH for allocation of CPU time. The research of D.C.C. is partially supported by CONICET, ANPCyT (Grant No. 03-02249) and Fundación Antorchas, Argentina (Grant No. A-13622/1-106).

APPENDIX A: CONVENTIONS

In this short Appendix, we define our conventions and notations. The continuum fermion operators read

$$\psi_\alpha(x)=e^{-ik_{F,\alpha}x}\psi_{R,\alpha}(x)+e^{ik_{F,\alpha}x}\psi_{L,\alpha}(x), \tag{A1}$$

$$\psi^\dagger_\alpha(x)=e^{ik_{F,\alpha}x}\psi^\dagger_{R,\alpha}(x)+e^{-ik_{F,\alpha}x}\psi^\dagger_{L,\alpha}(x). \tag{A2}$$

Using standard bosonization rules we have

$$\psi_{R,\alpha}(x)=\frac{1}{\sqrt{2\pi a}}e^{i\sqrt{4\pi}\phi_{R,\alpha}(x)}+\ldots, \tag{A3}$$

$$\psi_{L,\alpha}(x)=\frac{1}{\sqrt{2\pi a}}e^{-i\sqrt{4\pi}\phi_{L,\alpha}(x)}+\ldots, \tag{A4}$$

where a is the lattice constant and $\phi_{R,L,\alpha}$ are the chiral components of two real bosonic fields

$$\phi_\alpha(x)=\phi_{R,\alpha}(x)+\phi_{L,\alpha}(x), \tag{A5}$$

whose dual fields are defined by

$$\theta_\alpha(x)=\phi_{R,\alpha}(x)-\phi_{L,\alpha}(x). \tag{A6}$$

The dots in Eqs. (A3) and (A4) stand for higher order terms, due to the curvature of the dispersion relation, which are discussed in Appendix B. The up and down Fermi momenta are related to filling and magnetization:

$$k_+=k_{F,\uparrow}+k_{F,\downarrow}=\pi n; \quad k_-=k_{F,\uparrow}-k_{F,\downarrow}=\pi m, \tag{A7}$$

where

$$n=\frac{1}{L}\left\langle\sum_{x,\alpha} n_{x,\alpha}\right\rangle, \quad m=\frac{2}{L}\left\langle\sum_x S^z_x\right\rangle=\frac{1}{L}\left\langle\sum_{x,\alpha} n_{x,\uparrow}-n_{x,\downarrow}\right\rangle, \tag{A8}$$

$n_{x,\alpha}=c^\dagger_{x,\alpha}c_{x,\alpha}$ and L is the number of sites. Note that our definition of m (which is the one used for the XXZ chains in Ref. 4) differs by a factor of 2 from the one of Frahm and Korepin.[23]

APPENDIX B: FERMION FIELD OPERATOR

In this Appendix we discuss the bosonization of the fermion operator in the Hubbard model in a magnetic field starting from the exact BA solution. According to Frahm and Korepin[23], the long-distance asymptotics of zero-temperature correlation functions of physical fields is in general a sum of terms of the form

$$\frac{\exp(-i2D_ck_{F\uparrow}x)\exp[-i(D_c+D_s)k_{F\downarrow}x]}{(x-iv_c\tau)^{2\Delta_c^+}(x+iv_c\tau)^{2\Delta_c^-}(x-iv_s\tau)^{2\Delta_s^+}(x+iv_s\tau)^{2\Delta_s^-}}, \tag{B1}$$

where the scaling dimensions $\Delta^\pm_{c,s}$ are given by

$$2\Delta^\pm_c=\left(Z_{cc}D_c+Z_{sc}D_s\pm\frac{Z_{ss}\Delta N_c-Z_{cs}\Delta N_s}{2\det Z}\right)^2+N^\pm_c, \tag{B2}$$

$$2\Delta^\pm_s=\left(Z_{cs}D_c+Z_{ss}D_s\pm\frac{Z_{cc}\Delta N_s-Z_{sc}\Delta N_c}{2\det Z}\right)^2+N^\pm_s. \tag{B3}$$

$\Delta N_{c,s}, D_{c,s}, N^\pm_{c,s}$ are the quantum numbers characterizing the low energy excitations. ΔN_c and ΔN_s are integers denoting the number of electrons and down spins with respect to the ground state and are fixed by the correlator under consideration. The summation runs over all integers or half integers $D_{c,s}$ (depending on the parity of $\Delta N_c, \Delta N_s$) and on positive integers $N^\pm_c, N^\pm_s$.

By analyzing the leading contributions to the fermion two-point correlator, one can write down, after some algebra, the bosonized fermion operator

$$\begin{aligned}\psi_\downarrow=&e^{-ik_{F\downarrow}x}e^{i\sqrt{4\pi}\phi_{R\downarrow}(x)}(r_1+r_2e^{-i2k_{F\uparrow}x}e^{i\sqrt{4\pi}\phi_\uparrow}\\&+r_3e^{i2k_{F\uparrow}x}e^{-i\sqrt{4\pi}\phi_\uparrow}+r_4e^{-i2k_{F\downarrow}x}e^{i\sqrt{4\pi}\phi_\downarrow}\\&+r_5e^{-i2k_+x}e^{i\sqrt{4\pi}(\phi_\uparrow+\phi_\downarrow)}+\ldots)\\&+e^{ik_{F\downarrow}x}e^{-i\sqrt{4\pi}\phi_{L\downarrow}(x)}(l_1+l_2e^{i2k_{F\uparrow}x}e^{-i\sqrt{4\pi}\phi_\uparrow}\\&+l_3e^{-i2k_{F\uparrow}x}e^{i\sqrt{4\pi}\phi_\uparrow}+l_4e^{i2k_{F\downarrow}x}e^{-i\sqrt{4\pi}\phi_\downarrow}\\&+l_5e^{i2k_+x}e^{-i\sqrt{4\pi}(\phi_\uparrow+\phi_\downarrow)}+\ldots),\end{aligned} \tag{B4}$$

where r_i, l_i are unknown numerical constants. Notice that at $U=0$, $h=0$ all these constants vanish except $r_1=l_1=1/\sqrt{2\pi a}$. At $h=0$, the scaling dimensions of the different contributions in Eq. (B4) are known from BA for arbitrary repulsion U and density $n\neq 1$. It follows that it is sufficient to retain only the following terms:

$$\begin{aligned}\psi_\downarrow=&e^{-ik_{F\downarrow}x}e^{i\sqrt{4\pi}\phi_{R\downarrow}(x)}(r_1+r_2e^{-i2k_{F\uparrow}x}e^{i\sqrt{4\pi}\phi_\uparrow}\\&+r_3e^{i2k_{F\uparrow}x}e^{-i\sqrt{4\pi}\phi_\uparrow}+\ldots)\\&+e^{ik_{F\downarrow}x}e^{-i\sqrt{4\pi}\phi_{L\downarrow}(x)}(l_1+l_2e^{i2k_{F\uparrow}x}e^{-i\sqrt{4\pi}\phi_\uparrow}\\&+l_3e^{-i2k_{F\uparrow}x}e^{i\sqrt{4\pi}\phi_\uparrow}+\ldots).\end{aligned} \tag{B5}$$

The expression for $\psi_\uparrow$ can be easily obtained by exchanging $\downarrow$ and $\uparrow$, with the numerical constants generically different.

Using this expression for $\psi_\downarrow$ and $\psi_\uparrow$, one obtains

$$\psi_\downarrow^\dagger \psi_\downarrow = \text{const}\partial_x \phi_{R\downarrow} + \text{const}\partial_x \phi_{L\downarrow} + 2r_1 l_1 \sin(2k_{F\downarrow}x - \sqrt{4\pi}\phi_\downarrow) + 2(r_1 l_2 + r_2 l_1)\sin[2k_+ x - \sqrt{4\pi}(\phi_\uparrow + \phi_\downarrow)] - 2(r_1 l_3 + r_3 l_1)\sin[2k_- x - \sqrt{4\pi}(\phi_\uparrow - \phi_\downarrow)] + \ldots \tag{B6}$$

and

$$\psi_\uparrow^\dagger \psi_\uparrow = \text{const}\partial_x \phi_{R\uparrow} + \text{const}\partial_x \phi_{L\uparrow} + 2r_1' l_1' \sin(2k_{F\uparrow}x - \sqrt{4\pi}\phi_\uparrow) + 2(r_1' l_2' + r_2' l_1')\sin[2k_+ x - \sqrt{4\pi}(\phi_\uparrow + \phi_\downarrow)] + 2(r_1' l_3' + r_3' l_1')\sin[2k_- x - \sqrt{4\pi}(\phi_\uparrow - \phi_\downarrow)] + \ldots, \tag{B7}$$

where we assumed the constants r, l to be real. Otherwise, the only modification would consist in shifts of the arguments of the sines or cosines by unknown constant phases.

Now, assuming the constants to be equal for up and down fields, and adding Eqs. (B6) and (B7) we obtain for the bosonized density operator

$$\rho = \psi_\uparrow^\dagger \psi_\uparrow + \psi_\downarrow^\dagger \psi_\downarrow = \text{const}\partial_x(\phi_\uparrow + \phi_\downarrow) + 4r_1 l_1 \sin[k_+ x - \sqrt{\pi}(\phi_\uparrow + \phi_\downarrow)] \times \cos[k_- x - \sqrt{\pi}(\phi_\uparrow - \phi_\downarrow)] + 4(r_1 l_2 + r_2 l_1)\sin[2k_+ x - \sqrt{4\pi}(\phi_\uparrow + \phi_\downarrow)] + \ldots. \tag{B8}$$

Substituting finally Eq. (2.9), one obtains Eq. (2.14).

Similarly, the difference of Eqs. (B6) and (B7) yields the S^z operator:

$$2S^z = \psi_\uparrow^\dagger \psi_\uparrow - \psi_\downarrow^\dagger \psi_\downarrow = \text{const}\partial_x(\phi_\uparrow - \phi_\downarrow) + 4r_1 l_1 \times \cos[k_+ x - \sqrt{\pi}(\phi_\uparrow + \phi_\downarrow)]\sin[k_- x - \sqrt{\pi}(\phi_\uparrow - \phi_\downarrow)] - 4(r_1 l_3 + r_3 l_1)\sin[2k_- x - \sqrt{4\pi}(\phi_\uparrow - \phi_\downarrow)] + \ldots. \tag{B9}$$

Notice the last term in the S^z operator. In the usual treatments (see for example Ref. 26), this term does not appear. As it is obvious from Eq. (B9), this term would be absent if we retain only the first two terms in Eq. (B5) or if $r_1 = l_1$ and $r_3 = -l_3$.

The assumptions on the constants r_i, l_i, r_i', l_i' to be real and equal for up and down fields are supported by operator product expansion computations of the original free fermion operator with the perturbing Umklapp operator of the Hubbard Hamiltonian

$$\cos[2k_+ x - \sqrt{4\pi}(\phi_\uparrow + \phi_\downarrow)]. \tag{B10}$$

These computations also show that, at lowest order, the constants r_2, r_3, l_2, l_3 are linear in U.

*Present address: Fakultät für Physik, Albert-Ludwigs-Universität, 79104 Freiburg, Germany.

†Present address: Department of Physics and Astronomy, University of British Columbia, Vancouver, B.C., Canada V6T 1Z1.

‡URA 1325 du CNRS associée à l'Ecole Normale Supérieure de Lyon.

[1] K. Hida, J. Phys. Soc. Jpn. **63**, 2359 (1994); K. Okamoto, Solid State Commun. **98**, 245 (1996).

[2] M. Oshikawa, M. Yamanaka, and I. Affleck, Phys. Rev. Lett. **78**, 1984 (1997).

[3] K. Totsuka, Phys. Lett. A **228**, 103 (1997); Phys. Rev. B **57**, 3454 (1998); Eur. Phys. J. B **5**, 705 (1998).

[4] D. C. Cabra, A. Honecker, and P. Pujol, Phys. Rev. Lett. **79**, 5126 (1997); Phys. Rev. B **58**, 6241 (1998); Eur. Phys. J. B **13**, 55 (2000).

[5] A. Fledderjohann, C. Gerhardt, M. Karbach, K.-H. Mütter, and R. Wiesser, Phys. Rev. B **59**, 991 (1999).

[6] D. C. Cabra and M. D. Grynberg, Phys. Rev. B **59**, 119 (1999); A. Honecker, *ibid.* **59**, 6790 (1999).

[7] S. Yamamoto and T. Sakai, Phys. Rev. B **62**, 3795 (2000).

[8] Y. Narumi, M. Hagiwara, R. Sato, K. Kindo, H. Nakano, and M. Takahashi, Physica B **246–247**, 509 (1998).

[9] M. Ishii, H. Tanaka, M. Hori, H. Uekusa, Y. Ohashi, K. Tatani, Y. Narumi, and K. Kindo, J. Phys. Soc. Jpn. **69**, 340 (2000).

[10] K. Okamoto, T. Tonegawa, Y. Takahashi, and M. Kaburagi, J. Phys.: Condens. Matter **11**, 10 485 (1999); T. Tonegawa, K. Okamoto, T. Hikihara, Y. Takahashi, and M. Kaburagi, J. Phys. Soc. Jpn. **69**, 332 (2000); K. Sano and K. Takano, *ibid.* **69**, 2710 (2000); A. Honecker and A. Läuchli, cond-mat/0005398 (unpublished).

[11] H. Kageyama, K. Yoshimura, R. Stern, N. V. Mushnikov, K. Onizuka, M. Kato, K. Kosuge, C. P. Slichter, T. Goto, and Y. Ueda, Phys. Rev. Lett. **82**, 3168 (1999); K. Onizuka, H. Kageyama, Y. Narumi, K. Kindo, Y. Ueda, and T. Goto, J. Phys. Soc. Jpn. **69**, 1016 (2000).

[12] W. Shiramura, K. Takatsu, B. Kurniawan, H. Tanaka, H. Uekusa, Y. Ohashi, K. Takizawa, H. Mitamura, and T. Goto, J. Phys. Soc. Jpn. **67**, 1548 (1998).

[13] S. Miyahara and K. Ueda, Phys. Rev. Lett. **82**, 3701 (1999); T. Momoi and K. Totsuka, Phys. Rev. B **61**, 3231 (2000); E. Müller-Hartmann, R. R. P. Singh, C. Knetter, and G. S. Uhrig, Phys. Rev. Lett. **84**, 1808 (2000); T. Momoi and K. Totsuka, Phys. Rev. B **62**, 15 067 (2000).

[14] E. Dagotto and T. M. Rice, Science **271**, 618 (1996); T. M. Rice, Z. Phys. B: Condens. Matter **103**, 165 (1997).

[15] D. C. Cabra, A. De Martino, A. Honecker, P. Pujol, and P. Simon, Phys. Lett. A **268**, 418 (2000).

[16] H. Frahm and C. Sobiella, Phys. Rev. Lett. **83**, 5579 (1999).

[17] H. Tsunetsugu, M. Sigrist, and K. Ueda, Rev. Mod. Phys. **69**, 809 (1997).

[18] *Highly Conducting One-Dimensional Solids*, edited by J. T. Devreese, R. P. Evrard, and V. E. van Doren (Plenum, New York, 1979); T. Ishiguro and K. Yamaji, *Organic Superconductors*, Springer Series in Solid-State Sciences Vol. 88 (Springer, Berlin, 1990).

[19] T. Egami, S. Ishihara, and M. Tachiki, Science **261**, 1307 (1993).
[20] M. R. Bond, R.D. Willett, R. S. Rubins, P. Zhou, C. E. Zaspel, S. L. Hutton, and J. E. Drumheller, Phys. Rev. B **42**, 10 280 (1990).
[21] Y. Ajiro, T. Asano, T. Inami, H. Aruga-Katori, and T. Goto, J. Phys. Soc. Jpn. **63**, 859 (1994).
[22] E. Lieb and F. Y. Wu, Phys. Rev. Lett. **20**, 1445 (1968).
[23] H. Frahm and V. E. Korepin, Phys. Rev. B **42**, 10 553 (1990); **43**, 5653 (1991).
[24] F. H. L. Essler and H. Frahm, Phys. Rev. B **60**, 8540 (1999).
[25] K. Penc and J. Sólyom, Phys. Rev. B **47**, 6273 (1993).
[26] A. O. Gogolin, A. A. Nersesyan, and A. M. Tsvelik, *Bosonization and Strongly Correlated Electron Systems* (Cambridge University Press, Cambridge, 1998).
[27] H. J. Schulz, Int. J. Mod. Phys. B **5**, 57 (1991); *Proceedings of Les Houches Summer School LXI*, edited by E. Akkermans, G. Montambaux, J. Pichard, and J. Zinn-Justin (Elsevier, Amsterdam, 1995), p. 533.
[28] J. Voit, Rep. Prog. Phys. **58**, 977 (1995).
[29] m is normalized to its saturation value. For our conventions on filling and magnetization see Appendix A.
[30] K. Penc and F. Mila, Phys. Rev. B **50**, 11 429 (1994).
[31] S. Nishimoto and Y. Ohta, Phys. Rev. B **59**, 4738 (1999).
[32] M. L. Doublet and M. B. Lepetit, J. Chem. Phys. **110**, 1767 (1999).
[33] S. Nishimoto, M. Takahashi, and Y. Ohta, J. Phys. Soc. Jpn. **69**, 1594 (2000).
[34] The compactification radius R and the parameter ξ in Eq. (2.13) are related to the standard Luttinger parameter K, respectively, as $1/(2\pi R^2)=K$ and $\xi^2=2K$.
[35] M. Fabrizio, A. O. Gogolin, and A. A. Nersesyan, Phys. Rev. Lett. **83**, 2014 (1999).
[36] P. Degiovanni, Ch. Chaubet, and R. Melin, Theor. Math. Phys. **117**, 5 (1998).
[37] K. Tandon, S. Lal, S. K. Pati, S. Ramasesha, and D. Sen, Phys. Rev. B **59**, 396 (1999).
[38] D. Green and C. Chamon, Phys. Rev. Lett. **85**, 4128 (2000).
[39] P. Lecheminant, B. Bernu, C. Lhuillier, L. Pierre, and P. Sindzingre, Phys. Rev. B **56**, 2521 (1997); C. Waldtmann, H.-U. Everts, B. Bernu, C. Lhuillier, P. Sindzingre, P. Lecheminant, and L. Pierre, Eur. Phys. J. B **2**, 501 (1998).
[40] The total number of particles denoted by N is given by $N=\Sigma_{\lambda,\sigma}N_\sigma^\lambda$.
[41] In this section we use the notation $n_\sigma=\Sigma_\lambda n_\sigma^\lambda$, i.e., the normalization is such that $0\leqslant n_\sigma\leqslant p$.
[42] N. Andrei, in *Summer Course on Low-Dimensional Quantum Field Theories for Condensed Matter Physicists*, Trieste 1992, edited by S. Lundqvist, G. Morandi, and Yu Lu (World Scientific, Singapore, 1995).
[43] D. C. Cabra, A. De Martino, P. Pujol, and P. Simon, cond-mat/0012235 (unpublished).

2.1.3 Le rôle des impuretés dans la courbe d'aimantation

Comme nous l'avons évoqué dans les sections précédentes, on dispose à l'heure actuelle d'une quantité considérable de résultats pour les systèmes fortement corrélés en une dimension. La raison clé de cette richesse repose sur le fait que beaucoup de ces systèmes sont intégrables. Par ailleurs, les méthodes d'ansatz de Bethe sont ensuite relayées par des théories de champs que l'on contrôle très bien et qui nous permettent de faire de nombreuses prédictions que l'on peut confronter aux résultats expérimentaux. Cela dit, pour cette confrontation avec la réalité expérimentale, nous devons nous poser la question de la "robustesse" de tels résultats vis-à-vis de la présence d'impuretés. Cette question est d'autant plus pertinente que les systèmes que nous considérons sont uni-dimensionnels. Or, on connaît bien des exemples où le désordre provoque des changements considérables dans des systèmes quantiques en basses dimensions. L'exemple qui vient tout de suite à l'esprit est la théorie de la localisation d'Anderson. Considérons des particules sans interaction en une dimension. La moindre présence de désordre, pour plus faible qu'elle soit, aura comme effet une localisation de tous [2] les états du système. En 1-D, la présence d'interactions entre particules ne change pas en général ce résultat. Il est donc important de voir ce que deviennent tous les résultats que nous avons énoncés jusqu'à présent quand on considère la présence d'impuretés.

Pour les chaînes de spins 1/2 en champ magnétique nul, le résultat le plus remarquable a été obtenu par D. Fisher [1]. En utilisant une procédure de renormalisation en espace réel -proposée auparavant par Dasgupta et Ma-, Fisher a obtenu des résultats assymptotiquement exacts dans la limite de taille infinie et très basse température. Considérons une chaîne XXZ de spins 1/2 avec des couplages entre premiers voisins aléatoires :

$$H = \sum_i J_i \left(S_i^x S_{i+1}^x + S_i^y S_{i+1}^y + \Delta S_i^z S_{i+1}^z \right) \tag{20}$$

où $\Delta > -1/2$ et $J_i > 0$ est une variable aléatoire dont la distribution de probabilité est supposée assez large. Cette dernière supposition est faite pour garantir que la procédure de décimation qui est appliquée soit une bonne approximation. Nous ne donnons pas les détails techniques qui peuvent être trouvés dans l'article de Fisher et nous bornons à commenter les résultats obtenus. Le comportement à grandes échelles de ce système est donné par une phase de 'singulets aléatoires', où l'on peut considérer que chaque spin est couplé avec un autre spin pour former un singulet. Cet autre spin se trouve cependant à une distance qui peut être très grande, et entre ces deux spins formant un singulet nous pouvons avoir plusieurs paires de spins, plus rapprochés spatialement, formant eux aussi des

[2] On connaît des cas particuliers de désordre en une dimension où certains états sont non localisés, mais ceux-ci correspondent à un nombre fini de points dans le continu de l'espace des états.

singulets. Ces singulets de 'longue portée' sont cependant très rares, et la plupart des spins vont être corrélés avec un spin qui leur est très proche. La majorité des spins a donc des corrélations à courte portée, ce qui se traduit par le fait que si on considère la fonction de corrélation spin-spin **typique** on a une décroissance assez rapide avec la distance :

$$< S_i^z S_j^z >_{typique} \sim e^{-\sqrt{|i-j|}} \tag{21}$$

Si on veut maintenant étudier la moyenne d'une fonction de corrélation, qui sont celles auquelles on aura accès par une mesure de diffusion de neutrons, les singulets formés à très grandes distances -certes rares mais toujours possibles- vont dominer la moyenne pour les grandes distances et nous aurons donc un comportement tout à fait différent pour la fonction de corrélation moyenne :

$$\overline{< S_i^z S_j^z >} \sim |i-j|^{-2} \tag{22}$$

Cette différence notable entre valeurs typiques et moyennes nous montre que la loi de distribution pour les fonctions de corrélations est non-triviale et reflète la richesse de cette phase de singulets aléatoires de ces systèmes de spins avec désordre.

Ces résultats se traduisent aussi par un comportement particulier dans les propriétés d'aimantation. Du fait qu'une proportion non-négligeable de spins se trouvent liés à leur environnement avec un couplage très faible, la susceptibilité magnétique en fonction du champ H appliqué diverge pour $H \to 0$ (alors qu'elle tend vers une constante dans le cas pur) :

$$\chi(H) \sim \frac{1}{H\left(ln(H^2)\right)^3} \tag{23}$$

Ce résultat implique bien sur que la courbe d'aimantation est de pente infinie pour $H \to 0$.

A la lumière de ces résultats, il est intéressant de voir l'effet des impuretés sur les plateaux dans les courbes d'aimantation que nous avons discutées antérieurement. Nous allons pour cela considérer le cas le plus simple de plateau : celui présent à $M = 0$ dans la chaîne XXZ dimérisée. La méthode utilisée par Fisher a été appliquée aussi à la chaîne dimérisée et nous montre que le gap (et donc le plateau à $M = 0$) disparaît et donne lieu à un comportement de la susceptibilité magnétique [2] :

$$\chi(H) \sim H^{\alpha-1} \tag{24}$$

α est un exposant non-universel qui dépend du détail de la quantité de dimérisation et de désordre (typiquement la largeur de la distribution de probabilité des liens), et peut avoir des valeurs aussi bien supérieures que inférieures à 1. Ce résultat peut aussi être obtenu pour la chaîne XY dans la cadre d'une description en termes de particules sans interactions localisées dont le comportement

universel de la densité d'états peut être obtenu de façon simple, comme nous le montrons dans le premier article que nous présentons dans cette section. Il nous montre que la susceptibilité magnétique peut diverger ou tendre vers 0 pour $H \to 0$, mais dans tous les cas le plateau a disparu : le gap est peuplé par des états créés par le désordre. Cet effet n'est pas spécifique du plateau à $M = 0$ de la chaîne dimérisée : de façon générale, si l'on considère une distribution de probabilité continue pour les liens formant une chaîne ou échelle, tous les plateaux qui étaient présents dans le cas pur, y compris ceux à $M \neq 0$, disparaissent.

Il existe cependant un certain type de distribution de probabilité qui produit un comportement intéressant dans la courbe d'aimantation. Ce type de désordre peut modéliser l'effet du dopage dans divers oxydes de cuivre et correspond à une loi de distribution discrète pour les liens. Imaginons en effet que nous écrivions le Hamiltonien d'une chaîne avec des liens aléatoires dont la distribution a une périodicité de q sites :

$$P(J_i) = p\delta(J_i - J') + (1-p)\delta(J_i - J_0 - \gamma_i J) \tag{25}$$

où $\gamma_i = -\gamma$ (γ) si $i = qn$ ($\neq qn$). Comme nous le montrons dans les articles qui suivent, les résultats pour $H \to 0$ ont leur transcription pour les divers cas, avec un comportement du type (23) pour q impair et (24) pour q pair. Le résultat le plus remarquable est cependant obtenu en applicant la procédure de décimation en champ H non nul, qui nous dit que des 'pseudo-plateaux' vont apparaître pour certaines valeurs de l'aimantation. En effet, pour (voir figure (2)) :

$$M = 1 - \frac{2(1-p)}{q} \tag{26}$$

la courbe d'aimantation présente un plateau principal suivit de plateaux plus petits à des valeurs précises que l'on peut retrouver dans le premier article.

Le deuxième article généralise ce résultat au cas où le désordre ne correspond pas à des impuretés de liens mais de sites. Nous avons fait une classification extensive des divers cas possibles, en fonction des paramètres microscopiques et du type d'impuretés présentes. Nous pouvons citer comme exemple le cas du dopage par du Si dans du $CuGeO_3$, pour lequel nous pouvons espérer un plateau pour :

$$M = 1 - p^2 \tag{27}$$

p étant la densité de dopants, mais le tableau I du deuxième article ainsi que les divers résultats présentés dans le texte constituent une classification qui nous donne une grand pouvoir prédictif face à une situation expérimentale précise une fois comprise la nature du dopage, ou des impuretés présentes dans le matériau. Il est remarquable que grâce à la courbe d'aimantation nous puissions identifier de façon systématique la présence d'impuretés, et leur concentration. On remarque en plus que celles-ci jouent un rôle similaire à celui des degrés de liberté de charge, en déplaçant les plateaux et en les rendant éventuellement plus accessibles dans

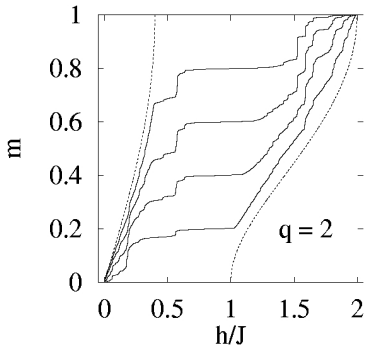

FIG. 2 – Courbe d'aimantation pour une chaîne dimérisée avec un désordre binaire pour différentes concentrations d'impuretés. Ce désordre sert à interpoler entre le cas pur dimérisé et le cas pur non dimérisé, dont les courbes sont représentées en pointillé.

le cas des oxydes de cuivre où les champs magnétiques requis pour obtenir des valeurs d'aimantation non-négligeables sont d'une grandeur considérable.

Références

[1] D. S. Fisher, Phys. Rev. **B 50**, 3799 (1994).

[2] R. A. Hyman, K. Yang, R. N. Bhatt and S. M. Girvin, Phys. Rev. Lett. **76**, 839 (1996).

Random Bond XXZ Chains with Modulated Couplings

D. C. Cabra,[1,2] A. De Martino,[3] M. D. Grynberg,[1] S. Peysson,[3] and P. Pujol[3]

[1]*Departamento de Física, Universidad Nacional de la Plata, C.C. 67, (1900) La Plata, Argentina*

[2]*Facultad de Ingeniería, Universidad Nacional de Lomas de Zamora, Cno. de Cintura y Juan XXIII, (1832) Lomas de Zamora, Argentina*

[3]*Laboratoire de Physique, Groupe de Physique Théorique ENS Lyon, 46 Allée d'Italie, 69364 Lyon Cédex 07, France*

(Received 12 July 2000)

The magnetization behavior of q-periodic antiferromagnetic spin-1/2 Heisenberg chains under uniform magnetic fields is investigated in a background of disorder exchange distributions. By means of both real space decimation procedures and numerical diagonalizations in XX chains, it is found that for binary disorder the magnetization exhibits wide plateaus at values of $1 + 2(p - 1)/q$, where p is the disorder strength. In contrast, no spin gaps are observed in the presence of continuous exchange distributions. We also study the magnetic susceptibility at low magnetic fields.

PACS numbers: 75.10.Jm, 75.10.Nr, 75.60.Ej

The study of low dimensional antiferromagnets has received much renewed attention largely owing to the synthesis of ladder materials [1]. One particular issue that captured both experimental and theoretical efforts in the past few years is the appearance of magnetization plateaus, i.e., massive spin excitations in the magnetization curve. In general, the latter are quite robust and for pure spin systems appear at rational magnetization values [2–4]. More recently, some experiments have indeed confirmed these theoretical predictions in a few particular cases [5] but some issues yet remain unresolved [6].

In order to make closer contact with experiments, one has to take into account the disorder that is almost inevitably present due to lattice imperfections and magnetic doping. A relevant question related to the appearance of magnetization plateaus is whether they are robust in the presence of quenched disorder. As a first step in this direction, in this paper we analyze the effect of a disordered distribution of exchange couplings with a periodically modulated mean on the magnetic behavior of an XXZ antiferromagnetic chain. Both even [7] and odd [8] modulations are known to exist and are ultimately responsible for the structure of the magnetization curve [2,3,9]. q-merized XX chains have also been studied in [10] using a Jordan-Wigner transformation.

By means of a decimation procedure similar to that used in [11,12] we argue that plateaus in the magnetization curve appear at specific magnetization values m which depend both on the couplings periodicity q and the strength of the disorder p. Hence disorder, instead of removing completely the plateau structure, shifts the position of certain plateaus in a precise way which depends on the disorder strength. Surprisingly, as we shall see from our numerical evidence, the plateaus predicted via this simple argument are indeed present. Moreover, they are rather wide and therefore could be eventually observable in low temperature experiments which in turn would allow for a precise determination of the disorder degree.

By extending the methods of [13], we also investigate the characteristics of the magnetic susceptibility at low fields. Its behavior shows an interesting even-odd effect, similar to that found in the study of disordered XX N-leg ladders [14]. In fact, for q odd we find the same kind of divergence as for the homogeneously disordered case ($q = 1$) [13], namely,

$$\chi_z \propto \frac{1}{H[\ln(H^2)]^3}, \tag{1}$$

whereas the even q modulations yield a generic nonuniversal power law behavior as in [15,16] for $q = 2$,

$$\chi_z \propto H^{\alpha-1}, \tag{2}$$

where we give an analytic expression for α for arbitrary q. In principle, these results should emerge from experimental susceptibility measurements in disordered low dimensional compounds.

In what follows we focus attention on the occurrence conditions of zero temperature plateaus in a random q-merized XXZ spin-1/2 chain whose Hamiltonian is

$$H = \sum_i J_i (S_i^x S_{i+1}^x + S_i^y S_{i+1}^y + \Delta S_i^z S_{i+1}^z), \tag{3}$$

where J_i are randomly distributed bonds. Specifically, let us consider a binary distribution of strength p ($p = 0$ corresponds to the pure q-merized case, while $p = 1$ corresponds to the uniform chain),

$$P(J_i) = p\,\delta(J_i - J') + (1 - p)\delta(J_i - J_0 - \gamma_i J), \tag{4}$$

where $\gamma_i \equiv \gamma$ $(-\gamma)$ if $i = qn$ $(i \neq qn)$, along with a Gaussian disorder $P(J_i) \propto \exp(-\frac{(J_i - \bar{J}_i)^2}{2\sigma_i^2})$ and a log-normal distribution given in terms of $W_i = \ln(J_i)$ and $P(W_i) \propto \exp(-\frac{(W_i - \bar{W}_i)^2}{2\lambda_i^2})$. All of these distributions, taken with same mean and variance, are built to enforce

q-merization, whose value is measured on average by γJ. In what follows we assume that J' is the smallest coupling and consider $0 < \gamma < J_0/J$.

(a) *Decimation procedure.*—Here we follow the arguments used by Fisher in [12]. The procedure is roughly to decimate the strongest bonds up to an energy scale given by the temperature. The remaining spins can be considered as free, and each of them will then give rise to a Curie behavior in the magnetic susceptibility.

In our problem (which is at $T = 0$) the energy scale is provided by the magnetic field, and, in order to compute the magnetization, decimation has to be stopped at an energy scale of the order of the magnetic field. We assume that all spins coupled by bonds stronger than the magnetic field form singlets and do not contribute to the magnetization, whereas spins coupled by weaker bonds are completely polarized. The magnetization is thus proportional to the fraction of remaining spins at the step where we stop decimation. Our argument happens to apply well to the binary distribution, provided the energy scales of the involved exchanges are well separated.

(b) *Plateaus in q-merized chains.*—Let us first consider the case $q = 2$ and assume we start at high enough magnetic field, such that all spins are polarized (saturation, $m = 1$) and begin decreasing the magnetic field. The magnetization stays constant for a while, then decreases abruptly at $h \sim J_0 + \gamma J$ and after that a plateau occurs at $m = p$. This can be easily understood: at $h \sim J_0 + \gamma J$ we can decimate all of the strongest bonds $J_0 + \gamma J$ (the corresponding spin pairs form singlets and do not contribute), and the number of remaining (completely polarized) spins is $N - 2 \times (1 - p)N/2 = pN$. Here, the factor of 2 comes from the removal of two spins each time we decimate a bond. Hence, the first plateau occurs at $m = p$. The appearance of this spin gap is due to the fact that the remaining strongest bonds have values $J_0 - \gamma J$ [17], and all spins left from the first step of decimation remain polarized (and the magnetization constant) until the magnetic field decreases to $h \sim J_0 - \gamma J$. At this point the magnetization again decreases abruptly and a second plateau occurs. The abrupt change corresponds to the decimation of bonds $J_0 - \gamma J$ which leaves us with $N - 2 \times (1 - p)\frac{N}{2} - 2 \times (1 - p)\frac{N}{2}p^2$ completely polarized bonds. The plateau occurs then at magnetization $m = p - p^2 + p^3$. The term $(1 - p)\frac{N}{2}p^2$ comes from the bonds $J_0 - \gamma J$ which, having a J' bond at each side, were not decimated in the first step and thus is the number of bonds actually decimated at the second step. Evidently, for $q > 2$ we can follow the same reasoning. Thus, the number of spins which yield finite contributions to the total magnetization at $h \sim J_0 + \gamma J$ is simply $N - 2 \times (1 - p)N/q$. Hence, we find the first plateau at

$$m = 1 + \frac{2}{q}(p - 1). \tag{5}$$

Notice that this result locates correctly the spin gaps appearing in a pure q-merized chain ($p = 0$). In this sense, Eq. (5) provides an extension of this latter case [9] in the presence of binary disorder. Since the decimation procedure applies for generic XXZ chains [12], we conclude that the emergence of the plateaus predicted in (5) is a generic feature, at least with the anisotropy parameter $|\Delta| < 1$. It is straightforward to generalize this analysis to the case of an arbitrary but *discrete* probability distribution. Given a finite difference between the highest values of the couplings in the nonequivalent sites, one can predict the presence and position of the plateaus.

To enable an independent check of these assertions, we turn to a numerical diagonalization of the Hamiltonian (3), contenting ourselves with the analysis of the subcase $\Delta = 0$. This allows us to explore rather long chains, using a fair number of disorder realizations. In Figs. 1(a)–1(c) we show, respectively, the whole magnetization curves obtained for $q = 2$, 3, and 4 after averaging over 100 samples of $L = 5 \times 10^4$ sites under the exchange disorder (4).

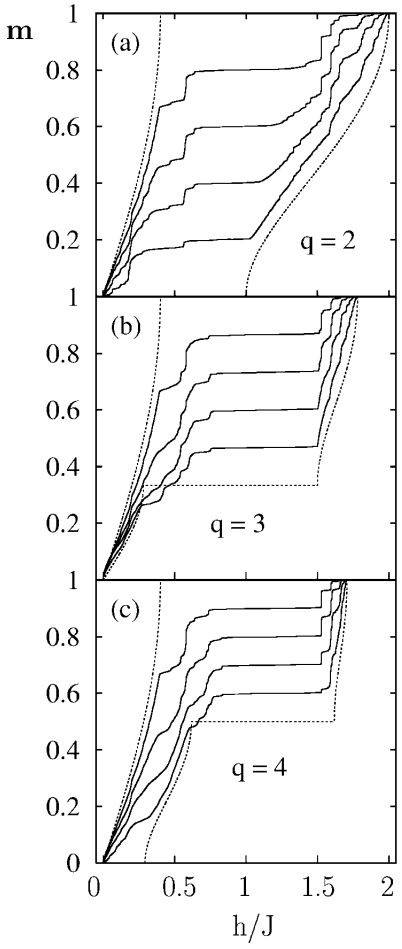

FIG. 1. Magnetization curves of modulated XX spin chains with $q = 2$ (a), 3 (b), and 4 (c), immersed in disordered binary backgrounds of strength p. The solid lines represent averages over 100 samples with 5×10^4 sites, $J'/J_0 = 0.2, \gamma J = 0.5$, and $p = 0.2$, 0.4, 0.6, and 0.8 in ascending order. The leftmost and rightmost dotted lines denote, respectively, the pure uniform and pure modulated cases $p = 1$ and $p = 0$.

It can be readily verified that this set of robust plateaus emerges quite precisely at the critical magnetizations given by Eq. (5). The secondary plateaus, though narrower, are still visible in Fig. 1.

It is important to stress that the derivation of our results for the quantization conditions derived above relies strongly on the discreteness of the probability distribution and would not be applicable to an arbitrary continuous exchange disorder. In fact, for the Gaussian case referred to above it turns out that no traces of plateaus can be observed. Furthermore, the magnetic susceptibility in the Gaussian case vanishes asymptotically only when approaching the saturation regime, as can be seen in Fig. 2, for a variety of coupling periodicities. Here, the sampling was improved up to 5×10^4 realizations though the length of the chain was reduced to $L = 1500$ sites, as the CPU time per spectrum grows as L^2.

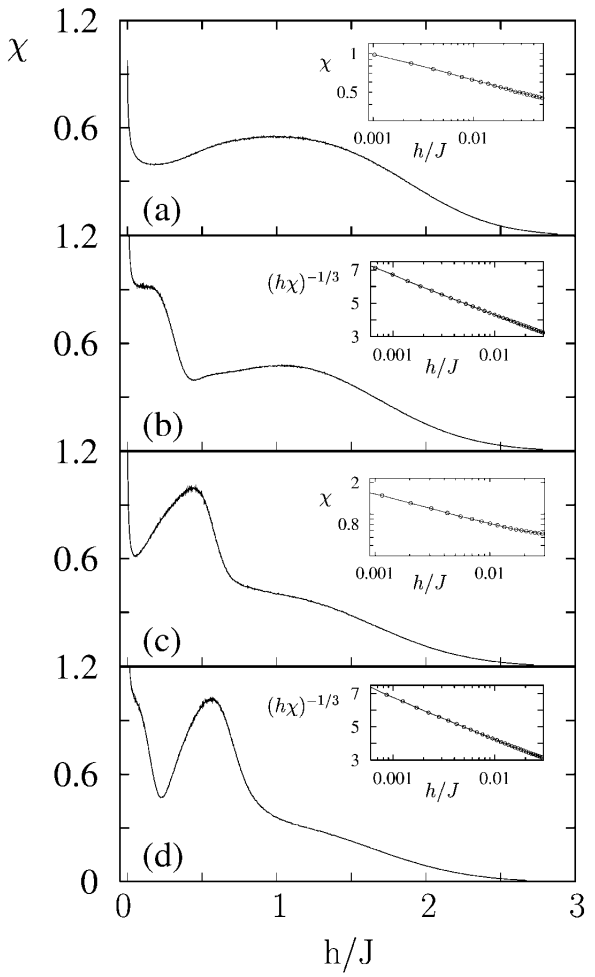

FIG. 2. Magnetic susceptibility of q-merized XX chains after averaging over 5×10^4 samples with 1500 sites, using q-periodic Gaussian exchange distributions for $q = 2$ (a), 3 (b), 4 (c), 5 (d), and strength $p = 0.4$. The insets show the susceptibility behavior at low magnetic fields which follows closely the regimes predicted by Eqs. (1) (q odd), and (2) (q even) in the text.

From the numerical curves, it appears that the usual Dzhaparidze Nersesyan–Pokrovsky Talapov (DN-PT) [18] transition is smoothed in the presence of disorder, both in the cases of binary and Gaussian distributions. By using the exact results of [19] for a family of Poissonian distributions, one sees that the behavior of the magnetization close to saturation has a nonuniversal exponential decrease. On the other hand, this nonuniversality is reflected for the binary case, in the fact that saturation occurs with an upper bound given by $2J_{\max}$. Since the universal DN-PT transition is destroyed near saturation, we expect that the same will occur in the vicinity of a nontrivial plateau. In fact, this is noticeable in the numerical data.

(c) *Susceptibility at low magnetic fields.*—For homogeneously disordered chains (i.e., $q = 1$), one can use the decimation procedure of [12], along with the universality of the fixed point, to show that either for discrete or continuous distributions the low field magnetic susceptibility behaves according to Eq. (1). Following a simple argument based on random walk motion used in [13], it can be readily shown that, for $\Delta = 0$ (or XX chains), these arguments can be extended to the case of q *odd* giving the same singularities. In fact, these expectations can be compared to the numerical results obtained for q odd with both Gaussian and binary disorders, as shown in Figs. 2 and 3, respectively. In particular, we direct the reader to the semilog insets of Figs. 2(b), 2(d), 3(b), and 3(d) which evidently follow the universal singularity referred to in Eq. (1). The numerical results for the log-normal distribution lead to the same qualitative behavior obtained for the Gaussian case.

For q *even*, for which there is a plateau at $m = 0$ in the pure case, the situation is more subtle. By using the notation of [13], for XX chains we can again define a random walk of the variable $u_i = \ln(\Delta_i)$ between the boundaries $\ln(\tilde{V}^2/E)$ and $\ln(E)$, now with a driving force F and diffusion coefficient D given by

$$F = \frac{2}{q}\langle \ln J^2_{i=qn} - \ln J^2_{i\neq qn}\rangle, \tag{6}$$

$$D = \frac{1}{q}[\mathrm{var}^2(\ln J^2_{i=qn}) + (q-1)\mathrm{var}^2(\ln J^2_{i\neq qn})]. \tag{7}$$

By means of the method given in [13] for the undriven random walk, one can approximate the problem to a discrete time diffusion problem with an absorbing and reflecting wall. One can then show that the average number of bonds for a cycle to be completed now goes like $\bar{n} \sim e^{\alpha \Delta u/2}$, which gives the asymptotic behavior for the magnetic susceptibility as in (2). The non-universal exponent α turns out to depend on the distribution parameters (6) and (7), namely, $\alpha = 2F/D$. Also, this exponent coincides with the results obtained in [16], using decimation and other methods for the $q = 2$, XXZ chain.

Once more, our numerical results for the binary and Gaussian coupling distributions considered above lend further support to this nonuniversal picture of even modulations. Specifically, there are in fact situations for which

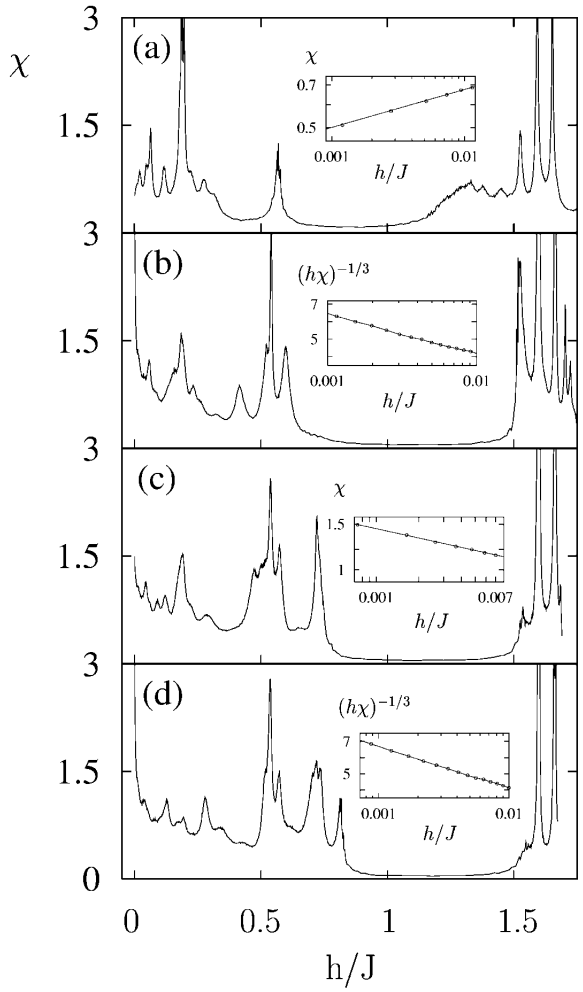

FIG. 3. Same as Fig. 2, but averaging over a binary exchange disorder of strength $p = 0.4$. The small field susceptibility behavior displayed in the insets reflects the typical singularity of odd periodicities [$q = 3$ (b) and 5 (d)], whereas even modulated distributions [$q = 2$ (a) and 4 (c)] are nonuniversal in this regime.

the low field susceptibility can either diverge ($\alpha < 1$) as displayed in Figs. 2(a), 2(c), and 3(c) or collapse ($\alpha > 1$) as shown in Fig. 3(a). Moreover, we checked that our α exponents can fit reasonably the numerical behavior obtained in this regime, as indicated by the log-log insets of Figs. 2(a) and 2(c).

To summarize, we have studied the effect of disorder on the plateaus structure in q-merized XXZ chains. By means of a simple real space decimation procedure we could account for a nontrivial phenomenon, namely, the shift in the magnetization values for which certain plateaus emerge, as compared to the pure system. This was tested by numerical diagonalizations of large XX chains finding a remarkable agreement with Eq. (5). We have also analyzed the behavior of the low magnetic field susceptibility which exhibits a clear q-odd (-even) logarithmic (power law) behavior. Our theoretical predictions could be experimentally checked on dimerized compounds such as $CuGeO_3$ doped with Si [20] under magnetic fields. Also trimerized compounds exist in nature [8] and it would be interesting to see if they can be doped. We trust this work will convey an interesting motivation for further experimental studies.

We acknowledge useful discussions with P. Degiovanni, F. Delduc, A. Honecker, R. Mélin, and C. Mudry. This work was done under partial support of EC TMR Contract No. FMRX-CT96-0012. The research of D. C. C. and M. D. G. is partially supported by CONICET, ANPCYT (Grant No. 03-02249) and Fundación Antorchas, Argentina (Grant No. A-13622/1-106).

[1] For reviews, consult E. Dagotto and T. M. Rice, Science **271**, 618 (1996); T. M. Rice, Z. Phys. B **103**, 165 (1997).
[2] M. Oshikawa, M. Yamanaka, and I. Affleck, Phys. Rev. Lett. **78**, 1984 (1997).
[3] D. C. Cabra, A. Honecker, and P. Pujol, Phys. Rev. Lett. **79**, 5126 (1997); Phys. Rev. B **58**, 6241 (1998).
[4] K. Totsuka, Phys. Rev. B **57**, 3454 (1998).
[5] Y. Narumi *et al.,* Physica (Amsterdam) **246B–247B**, 509 (1998).
[6] H. Tanaka *et al.,* Physica (Amsterdam) **246B**, 230 (1998); W. Shiramura *et al.,* J. Phys. Soc. Jpn. **67**, 1548 (1998); P. Lemmens *et al.,* Adv. Solid State Phys. **39**, 281 (1999).
[7] J. P. Boucher and L. P. Regnault, J. Phys. I (France) **6**, 1939 (1996).
[8] See K. Hida, J. Phys. Soc. Jpn. **63**, 2359 (1994); K. Okamoto, Solid State Commun. **98**, 245 (1995).
[9] D. C. Cabra and M. D. Grynberg, Phys. Rev. B **59**, 119 (1999); A. Honecker, Phys. Rev. B **59**, 6790 (1999).
[10] A. A. Zvyagin, Phys. Lett. A **158**, 333 (1991); Sov. J. Low Temp. Phys. **18**, 558 (1992).
[11] S. K. Ma, C. Dasgupta, and C.-K. Hu, Phys. Rev. Lett. **43**, 1434 (1979); C. Dasgupta and S. K. Ma, Phys. Rev. B **22**, 1305 (1980).
[12] D. S. Fisher, Phys. Rev. B **50**, 3799 (1994).
[13] T. P. Eggarter and R. Riedinger, Phys. Rev. B **18**, 569 (1978).
[14] P. W. Brouwer, C. Mudry, and A. Furusaki, Phys. Rev. Lett. **84**, 2913 (2000).
[15] A. A. Ovchinnikov and N. S. Érikhman, Sov. Phys. JETP **46**, 340 (1977).
[16] R. A. Hyman, K. Yang, R. N. Bhatt, and S. M. Girvin, Phys. Rev. Lett. **76**, 839 (1996); P. Henelius and S. M. Girvin, Phys. Rev. B **57**, 11 457 (1998); F. Iglói, R. Juhász, and H. Rieger, Phys. Rev. B **61**, 11 552 (2000).
[17] In fact, this depends on the values of $J', J_0, \gamma J$. This is generically true for $J_0 + \gamma J > J_0 - \gamma J > J'$ which is satisfied by the values used in the numerical diagonalizations.
[18] G. I. Dzhaparidze and A. A. Nersesyan, JETP Lett. **27**, 334 (1978); V. L. Pokrovsky and A. L. Talapov, Phys. Rev. Lett. **42**, 65 (1979).
[19] F. J. Dyson, Phys. Rev. **92**, 1331 (1953).
[20] J.-P. Renard *et al.,* Europhys. Lett. **30**, 475 (1995); L. P. Regnault *et al., ibid.* **32**, 579 (1995); M. Fabrizio, R. Mélin, and J. Souletie, Eur. Phys. J. B **10**, 607 (1999).

Site-centered impurities in quantum spin chains

P. Pujol and J. Rech
Laboratoire de Physique, Groupe de Physique Théorique, ENS Lyon, 46 Allée d'Italie, 69364 Lyon Cédex 07, France
(Received 26 November 2001; revised manuscript received 28 May 2002; published 4 September 2002)

The magnetic behavior of antiferromagnetic spin 1/2 chains with site-centered impurities in a magnetic field is investigated. The effect of impurities is implemented by considering different situations of both diagonal and off-diagonal disorder. The resulting magnetization curves present a wide variety of plateaus, whose position strongly depends on the kind of disorder considered. The relevance of these results to experimental situations is also discussed.

DOI: 10.1103/PhysRevB.66.104401 PACS number(s): 75.10.Jm, 75.10.Nr, 75.60.Ej

I. INTRODUCTION

The study of the magnetic properties of low dimensional antiferromagnets has received much renewed attention during the last years. One particular issue that captured both experimental and theoretical efforts is the appearance of magnetization plateaus in spin chains and ladders systems. In general, those plateaus appear for pure spin systems at rational magnetization values.[1–4] Some experiments have indeed confirmed these theoretical predictions in a few particular cases.[5]

More recently, the effect of the presence of impurities on such magnetic behavior was also investigated. From the theoretical point of view, the properties at zero magnetic field have largely been elucidated,[6,7] and recent analysis explored also the robustness of the rational plateaus for small amplitude of the disorder.[8] A very interesting phenomenon recently discovered was also that, for bond-disorder with discrete probability distributions, plateaus at nonrational values of the magnetization are present.[9] Moreover, the position of such plateaus in the curve is related in a simple way to the concentration of impure bonds in the system. Since this kind of disorder is a good candidate for modeling concrete experimental situations, this result opens new perspectives in the interpretation of experimental curves. In order to make closer contact with experiments, one has to take into account all the effects that can be produced by nonmagnetic impurities, and provide a wide range of possibilities for implementing the presence of such impurities in realistic models.

In this paper we analyze a simple model where different kinds of diagonal and off-diagonal disorder are present. The techniques used are based on a decimation procedure,[10] as well as standard quantum mechanics tools and numerical calculations for XX chains of sizes ranging from 50 000 to 100 000 sites. Despite the simplicity of our model, we find that a huge number of families of cases is present, each of them presenting its own hierarchy of magnetization plateaus. Moreover, we show how a simple tuning of the microscopic parameters can drive our system from one family to another. We also argue that this simple example serves as a good laboratory for understanding and classifying the wide variety of cases one can encounter in experimental curves of antiferromagnetic systems with impurities.

II. THE MODEL

The model we are going to study is a spin-1/2 chain whose Hamiltonian is given by

$$H=\sum_i \left[J_i(S_i^x S_{i+1}^x+S_i^y S_{i+1}^y+\Delta S_i^z S_{i+1}^z)+h_i S_i^z\right]. \quad (1)$$

The randomness is implemented by considering J_i and h_i as random variables. Specifically, bond randomness will be obtained by assigning to all the variables h_i the same value fixed at h, and by giving a probability distribution to the set of variables $\{J_i\}$. The probability distribution can, of course, be chosen in such a way to give, on average, a periodicity of q to the bond variables. It is important to say that realistic distributions relevant for many possible experimental situations are discrete. In this sense, a binary distribution captures the essential characteristics of the phenomena we want to describe here, the generalization to more complicated discrete distributions being straightforward. In Ref. 9, a distribution of the form;

$$P(J_i)=p\ \delta(J_i-J')+(1-p)\,\delta(J_i-J-\gamma_i J), \quad (2)$$

was considered, where $\gamma_i \equiv \gamma$, $(-\gamma)$ if $i=qn$, $(i\neq qn)$. In order to match the behavior of a disorder originating from a site impurity, a most appropriate distribution can be given by the following algorithm: distribute first regular values for the bonds J_i with the desired periodicity q, and parameter γ, then, to each site of the chain assign a probability $1-p$ to be an ''original'' site, and p to be an ''impure'' site. Finally, for each site i which turned out to be impure, change the values of the surrounding bonds J_i and J_{i-1} to J'. We are, as in Ref. 9, concerned with three different values for the bond strength, $J\pm\gamma J$ and J', but now with a correlated probability distribution.

For site-centered disorder, we are going to consider two different cases. The first is just obtained by writing h_i as $h+h_i'$, where h_i' is a random variable taking values of 0 with probability p and h' with probability $1-p$. This case can be considered as academic, since it violates the symmetry $h\rightarrow -h$, but it will nevertheless provide useful insight for more realistic disorders. The second and more realistic case is the $h\rightarrow -h$ symmetry preserving case where $h_i=h(1+\alpha_i)$, with values for α_i being binary distributed among 0 and α

with probability p and $1-p$, and $\alpha \geqslant -1$ (the limiting case of $\alpha=-1$ corresponding to an impurity which does not couple to the magnetic field).

In the case of $\Delta=0$, the model can be mapped, via the well known Jordan-Wigner transformation, to a problem of free fermions, whose first quantized Schrödinger-type equation is

$$J_{i-1}\, c_{i-1} + J_i\, c_{i+1} = h_i\, c_i\,. \tag{3}$$

The magnetization is simply related to the number of states occupied and the z component of the susceptibility is just proportional to the density of states. For a given energy, the number of states can be simply obtained by the node counting method,[11] related to the number of positive ''self-energy'' variables,

$$\Delta_i = c_{i-1}\, J_{i-1}/c_i\,. \tag{4}$$

The recursive formula for these variables is

$$\Delta_{i+1} = J_i^2/(h_i - \Delta_i), \tag{5}$$

which, for the case of bond and $h \rightarrow -h$ symmetry preserving site disorder can be written as

$$D_{i+1} = W_i^2/(h - D_i), \tag{6}$$

where $D_i = \Delta_i/1+\alpha_i$ and $W_i^2 = J_i^2/[(1+\alpha_i)(1+\alpha_{i+1})]$. Note that D_i has the same sign as Δ_i, then the node counting can be done in the D variables. This remark will be very useful when discussing the presence of plateaus and the behavior of the magnetization curve close to $h=0$.

III. OFF-DIAGONAL DISORDER

As mentioned above, this case corresponds to a generalization for bond-disorder considered in Ref. 9. In this case each time a site is considered as an impurity, it must be surrounded by bonds with lower values. The decimation procedure used in Ref. 9 is again well adapted for identifying the location of magnetization plateaus. However, some care has to be taken in counting the number of bonds for each decimation step, particularly in the case of two impurities sitting in neighboring sites. We refer to the reference mentioned above for the details of this reasoning and present here the result for a dimerized chain which is the most relevant case for experimental situations, the generalization to generic periodicity of the lattice being straightforward. The principal plateau is located at

$$M = 2p - p^2 \tag{7}$$

coming from the decimation of the bonds with the highest value. The second step of the decimation gives a secondary plateau at

$$M = 2p - 2p^2 + 2p^3 - p^4. \tag{8}$$

These plateaus are well observed in the numerical curves of Fig. 1, where we show the result for an XX chain.

The behavior of the magnetization for small magnetic fields can also be obtained as a generalization of the normal

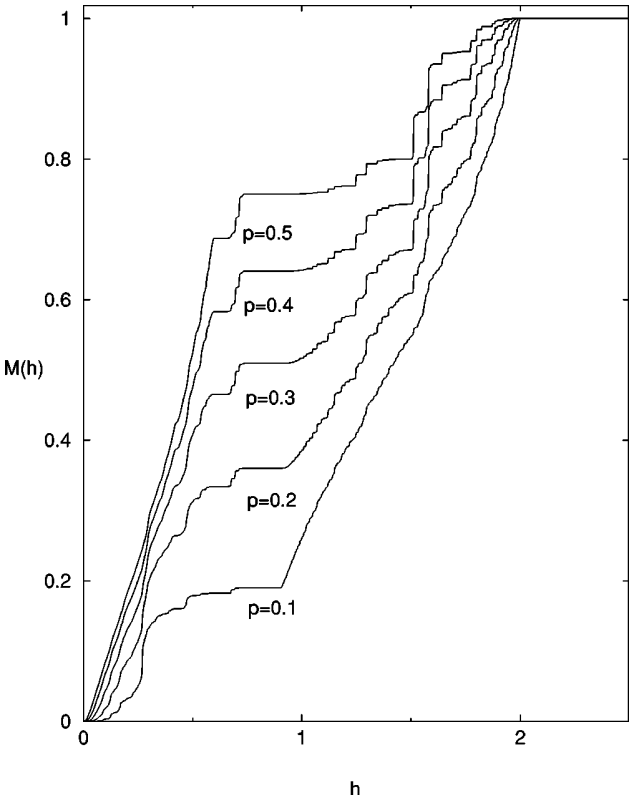

FIG. 1. Magnetization curves of XX chains with off-diagonal disorder for the parameters values of $J=2$, $J'=0.6$, $\gamma=0.45$.

off-diagonal disorder. For example, for the XX case, a mapping to a random walk in the self-energy variables shows, as for a standard dimerized chain with random bonds,[12,7] a power law behavior for the magnetic susceptibility for even periodicity of the lattice,

$$\chi_z \propto H^{\lambda-1}, \tag{9}$$

where the exponent can be easily obtained from the mean and variance of $\ln(J)$ (see, for example Ref. 9). Using the same method, a logarithmic behavior for the susceptibility is obtained for odd periodicity of the lattice,

$$\chi_z \propto \frac{1}{H[\ln(H^2)]^3}. \tag{10}$$

IV. DIAGONAL DISORDER

We first concentrate on the naive diagonal disorder one can introduce in a dimerized chain, by supposing that a supplementary magnetic field h' at each impurity is present. While for low h' no noticeable changes at the curve occur, for strong enough values of h', we see in Fig. 2 the appearance of new plateaus. A simple way to understand such plateaus is by considering the strong coupling case $\gamma \sim 1$. The order zero in powers of $(1-\gamma)$ is just given by a combination of dimers which can contain two, one or zero impurities with probability $(1-p)^2/2$, $p(1-p)$ and $p^2/2$, respectively. It is then easy to draw the magnetization curve for each case

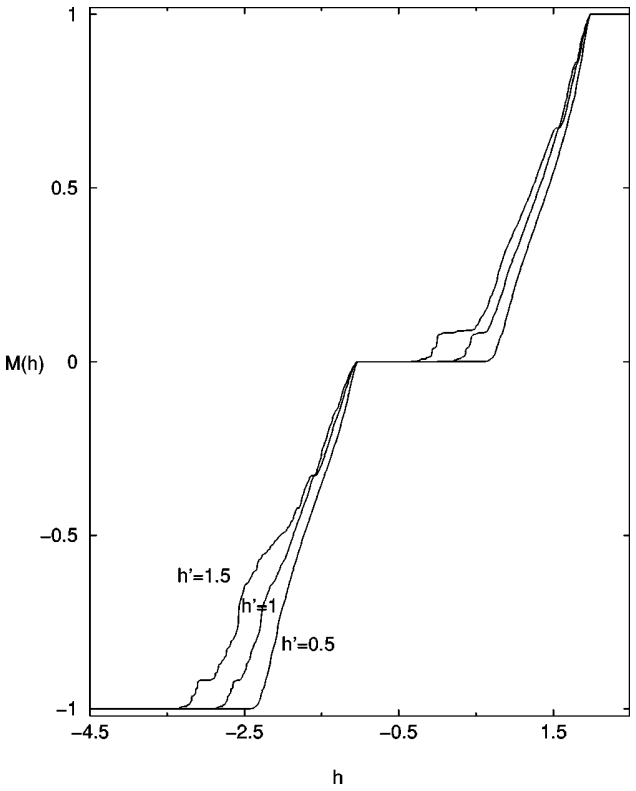

FIG. 2. Magnetization curves for the first kind of diagonal disorder mentioned in the text [see Eq. (11)] taken with $p=0.3$, $\gamma=0.5$, $J=2$.

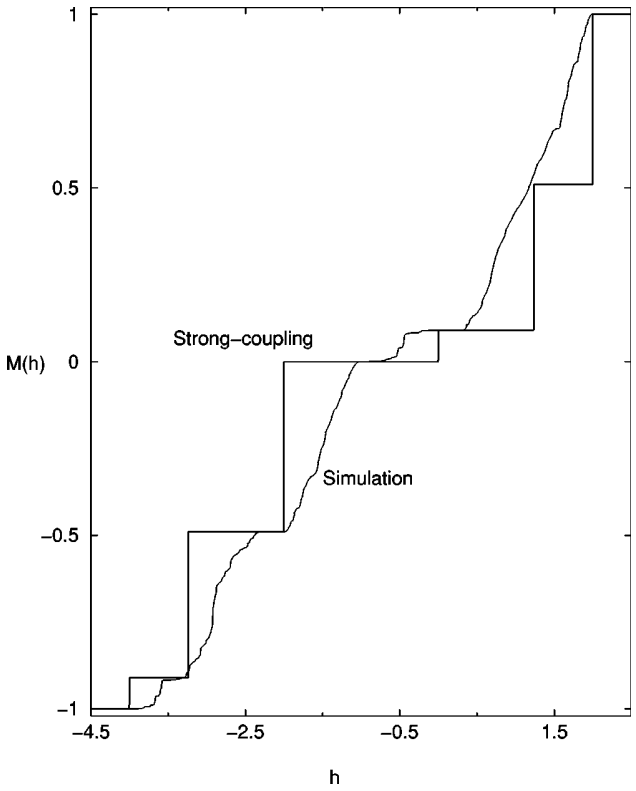

FIG. 3. Same as in Fig. 2 with $J=2$, $\gamma=0.45$, $h'=2$, $p=0.3$.

(a three step stair like curve obtained by trivially diagonalizing the dimer Hamiltonian) and then superpose the curves with the appropriate weight. The result is compared to the numerical data in Fig. 3. The positions of the plateaus predicted at this order are located at

$$M=-1+p^2,\ -(1-p)^2,\ 0,\ p^2,\ 2p-p^2. \qquad (11)$$

Note in passing the lack of $M\leftrightarrow -M$ symmetry in the magnetization curve due to the very nature of the disorder. Comparing with the numerical result, one sees that some plateaus are softened due to the presence of nonzero coupling which was neglected in our procedure. The next step is as usual to turn on a nonzero value for γ and use standard quantum mechanics perturbation theory (see, for example Ref. 13 for a similar treatment). The result is a smoothing of the jumps between the plateaus and a correction to their width which can be calculated in powers of $(1-\gamma)$. Since we are concerned with more realistic kinds of disorder these computations are beyond the scope of this work. We point out to the reader that this zeroth order in strong coupling leaves the $M=0$ plateau present, a result which seems to be confirmed for the XX case by the numerical argument.

The second case is obtained by assuming that each impurity couples to the magnetic field with a factor of $(1+\alpha)$. It gives a symmetric magnetization curve by the change $h\rightarrow -h$. It is sufficient to study only the case $\alpha<0$. Indeed, the case of positive α is obtained by a simple rescaling of the magnetic field and the change $p\leftrightarrow 1-p$ (impurities become pure sites and vice versa). In the case of XX chains, we can make use of the change of variables defined in (6). We have then the equivalence between the model we are considering and a system with constant magnetic field, but with a wide hierarchy of values for the bonds; there are now six values of W_i instead of the two allowed for J_i (J' is forbidden in the diagonal disorder case). The decimation procedure can then be used on this special off-diagonal disorder to predict the presence of plateaus. We have however to identify different cases corresponding to each hierarchic structure of the bonds, and these are given by the values of α and γ we are considering. As already stated before, the decimation procedure is implemented by eliminating the strongest bonds, and their relative weight in the system gives the position of the corresponding plateau in magnetization. We omit the details of the combinatorics and present the results for the position of the principal plateaus for each case in Table I. Figure 4 shows also the magnetization curve obtained for one of these cases, showing a fair agreement with the decimation predictions.

Let us now analyze the behavior of the system at low magnetic fields. We will use here the mapping process explained in Ref. 11 on our D variables. At low magnetic fields, we can write (6) as

$$D_{i+1}=-W_i^2/D_i\,. \qquad (12)$$

TABLE I. Magnetization at the principal plateaus for the ($h \leftrightarrow -h$) symmetric diagonal disorder (see text).

Range of α parameter	Magnetization plateaus
$\left(\frac{1-\gamma}{1+\gamma}\right)^2 - 1 < \alpha < 0$	$1-p^2$ $(1-p)^2$ 0
$\left(\frac{1-\gamma}{1+\gamma}\right)^2 - 1 < \alpha < \left(\frac{1-\gamma}{1+\gamma}\right)^4 - 1$	$1-p^2$ $1-p^2-p^2(1-p)^2$ $(1-p)^2(1+p^2)$ $(1-p)^2$ 0
$\alpha < \left(\frac{1-\gamma}{1+\gamma}\right)^4 - 1$	$1-p^2$ $1-p^2-p^2(1-p)^2$ $1-p^2-p^2(1-p)^2(1+p^2)$ $(1+p^2+p^4)(1-p)^2$ $(1+p^2)(1-p)^2$ $(1-p)^2$ 0

Doing the recursion one step further, we obtain for even sites,

$$D_{2i} = \left(\frac{1-\gamma}{1+\gamma}\right)^2 \frac{1+\alpha_{2i-2}}{1+\alpha_{2i}} D_{2i-2}. \tag{13}$$

Thus, defining $x_{2i} = \ln(D_{2i})$, this leads to a random walk problem where the $\ln((1+\alpha_{2i-2})/(1+\alpha_{2i}))$ term plays the role of the noise. By inspecting the form of this last term, one can easily see that the noise is cancelled step by step, giving rise to a regular and non-random walk at large times (large m),

$$\sum_{i=1}^{m} x_{2i+2} - x_{2i} = 2m \ln\left(\frac{1-\gamma}{1+\gamma}\right) + \ln\left(\frac{1+\alpha_2}{1+\alpha_{2m+2}}\right). \tag{14}$$

Then, at low magnetic fields, the behavior of our systems is asymptotically equivalent to the one of a pure chain, and for an even periodicity of the bonds shares in particular the presence of a plateau at zero magnetization. Strictly speaking, these results are valid for XX chains only, since we have used the change of variables (6). We conjecture however that the qualitative behavior for the curve, and in particular, the position of the magnetization plateaus remains valid for generic XXZ chains.

V. MIXED DISORDER

This last case can be considered as the combination of both kinds of disorder studied before. It is important to notice that the equivalence between positive and negative α is not valid anymore due to the extra presence of bond disorder. For the XX case, it is however easy to see by means of (6) and the subsequent decimation procedure, that the case $\alpha > 0$ has the same plateaus as for the off-diagonal disorder discussed above. This is still the case for negative but small values of α, since the hierarchy of coupling in the effective system is unchanged. The situation is however radically changed when α goes below the critical value,

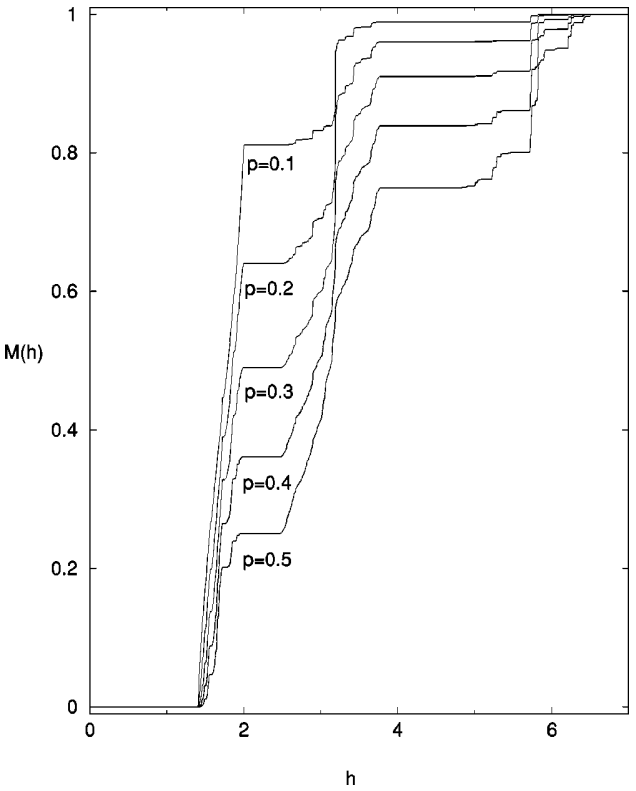

FIG. 4. Magnetization curves for the ($h \leftrightarrow -h$) symmetric disorder with $J=2$, $\alpha=-0.7$, $\gamma=0.7$.

$$\alpha_c = \frac{J'}{J+\gamma J} - 1, \tag{15}$$

where the hierarchy of values for the bonds is completely changed. Figure 5 shows that crossing the critical value of α indeed changes completely the nature of the magnetization curve and the position of the plateaus in the curve. In that case, the strongest bonds have the values $J'/(1+\alpha)$ and can be found in arbitrary long chains of impurities. This fact invalidates the standard decimation procedure for locating the position of the plateaus. However, one can proceed by noticing that, for values of α close enough to -1, the inter-impurities bonds in the effective model are much larger than the others. One can then use a kind of strong-coupling treatment in which the zeroth order system is obtained by equating the value of the remaining bonds to zero. We are then left with a collection of decoupled spin chains with arbitrary length. Each spin of the chain is only coupled to his two neighbors (with a coupling value J_{eff}) so that the Hamiltonian matrix is tridiagonal. The characteristic polynomial of such a matrix is obtained by a recursive way. In our case, the recursion formula leads, after a change of variables, to a Chebyshev polynomial. Thus, for an array containing n spins, the eigenvalues of the Hamiltonian are simply given by the roots of second order Chebyshev polynomials,

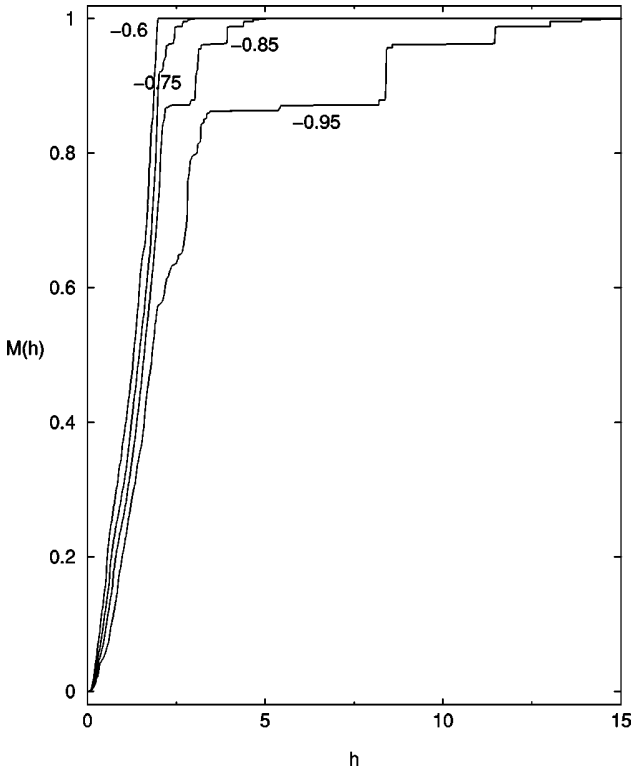

FIG. 5. Magnetization curves for the case of mixed disorder with $J=2$, $J'=0.8$, $\gamma=0.5$, $p=0.4$ and different values of α. In this case $\alpha_c=-0.73$ (see text).

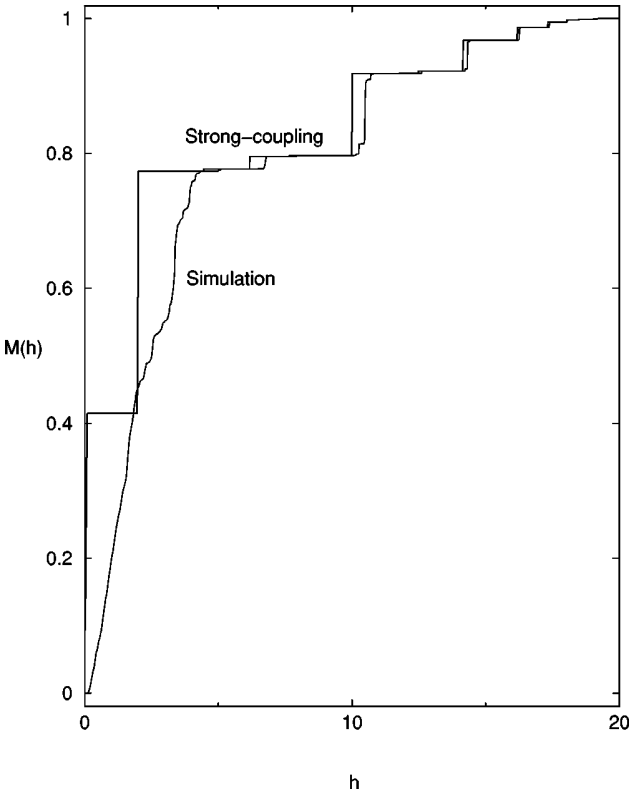

FIG. 6. Strong-coupling and numerical result for the mixed disorder case with $J=2$, $J'=0.8$, $\alpha=-0.95$, $\gamma=0.5$, $p=0.3$.

$$E_p=J_{\text{eff}}\cos\left(\frac{p\pi}{n+1}\right);\quad p=1\cdots n, \tag{16}$$

and J_{eff} is the value of the coupling between the spins. The magnetization curve for such a finite chain can also be easily obtained. To draw the magnetization curve for the total system one just has to superpose the curves for all possible values of n with the corresponding probability of appearance $(1-p)^2p^n$. The result is shown in Fig. 6, where we compare the numerical result with the strong coupling computation performed up to 11th order in p. The appearance of a hierarchy of plateaus close to saturation predicted by the theory is clearly observable in the numerical data.

The plateau at low values of the magnetization and the jump in the magnetization at zero field is an artifact of the zeroth order approximation. This can be cured now by turning on the remaining coupling to nonzero values and treating them in perturbation theory. On what concerns the jump at $M=0$, there is however a much simpler way of studying the shape of the curve close to $M=0$. This is achieved again by the mapping to the random walk problem used in Sec. IV. The difference here is that the coupling term is not a constant anymore because J_i can be either $J\pm\gamma J$ or J',

$$D_{2i}=\left(\frac{J_{2i-1}}{J_{2i-2}}\right)^2\frac{1+\alpha_{2i-2}}{1+\alpha_{2i}}D_{2i-2}. \tag{17}$$

As in Sec. IV, the term containing α is canceled step by step and we are left with a random walk problem strictly identical to that of a pure off-diagonal disorder. One recovers in this way the power law or logarithmic behavior as in (9)–(10) depending on the periodicity of the bonds.

VI. CONCLUSION

To summarize, we have shown that the magnetization curve of spin chains with different kinds of impurities exhibits a rich variety of plateaus. While the phenomenon of nonrational plateaus was already observed in a disordered case,[9] we have shown in this paper with simple examples that the position of such plateaus strongly depend on the particular values of the microscopic parameters. While one can speak of a sort of universality for the position of the plateaus, depending only on the concentration of impurities and periodicity of the averaged bonds, we have clearly seen that different families of disorder produce qualitatively different magnetization curves. Moreover, within the same kind of disorder (the mixed disorder case in particular) a simple tuning of the microscopic parameters can switch the system from one ''universality class'' to another. This scenario teaches us that the characterization of spin chains with impurities is better understood in terms of families of disorder, at least to understand the behavior of the magnetization curve. While some results in this paper have been obtained for the XX case only, it is reasonable to think that such a characterization in terms of families of disordered chains re-

mains valid for generic XXZ chains. Of particular interest is the mixed case, for which we believe the case $\alpha \to -1$ should represent the magnetization curve for materials such as $CuGeO_3$ doped with Si.[14] Some attempt to explain realistic materials magnetization curves has already been pruchased using other techniques.[15] We trust this work provides the necessary tools for predicting the shape of the magnetization curve in future experimental situations, where higher periodicities than 2 are also conceivable.[4]

ACKNOWLEDGMENTS

We acknowledge B. Dujardin for fruitful discussions and D. C. Cabra and A. Honecker for constructive comments and a careful reading of the manuscript.

[1] M. Oshikawa, M. Yamanaka, and I. Affleck, Phys. Rev. Lett. **78**, 1984 (1997).
[2] D.C. Cabra, A. Honecker, and P. Pujol, Phys. Rev. Lett. **79**, 5126 (1997); Phys. Rev. B **58**, 6241 (1998).
[3] K. Totsuka, Phys. Lett. A **228**, 103 (1997); Phys. Rev. B **57**, 3454 (1998).
[4] K. Hida, J. Phys. Soc. Jpn. **63**, 2359 (1994); K. Okamoto, Solid State Commun. **98**, 245 (1995).
[5] Y. Narumi *et al.*, Physica B **246-247**, 509 (1998).
[6] D.S. Fisher, Phys. Rev. B **50**, 3799 (1994).
[7] R.A. Hyman, K. Yang, R.N. Bhatt and S.M. Girvin, Phys. Rev. Lett. **76**, 839 (1996); P. Henelius and S.M. Girvin, Phys. Rev. B **57**, 11457 (1998); F. Iglói, R. Juhász, H. Rieger, *ibid.* **61**, 11 552 (2000).
[8] K. Totsuka, Physica B **284-288**, 1559 (2000); K. Totsuka, Phys. Rev. B **64**, 134420 (2001).
[9] D.C. Cabra, A. De Martino, M.D. Grynberg, S. Peysson, and P. Pujol, Phys. Rev. Lett. **85**, 4791 (2000).
[10] S.K. Ma, C. Dasgupta, and C.-K. Hu, Phys. Rev. Lett. **43**, 1434 (1979); C. Dasgupta and S.K. Ma, Phys. Rev. B **22**, 1305 (1979).
[11] T.P. Eggarter and R. Riedinger, Phys. Rev. B **18**, 569 (1978).
[12] A.A. Ovchinnikov and N.S. Erikhman, Sov. Phys. JETP **46**, 340 (1977).
[13] D.C. Cabra, A. De Martino, A. Honecker, P. Pujol, and P. Simon, Phys. Rev. B **63**, 094406 (2001).
[14] J.-P. Renard *et al.*, Europhys. Lett. **30**, 475 (1995); L.P. Regnault, *et al.*, *ibid.* **32**, 579 (1995); M. Fabrizio, R. Mélin, and J. Souletie, Eur. Phys. J. B **10**, 607 (1999).
[15] K. Hida, cond-mat/0111521 (unpublished).

2.1.4 Fluctuations quantiques dans les systèmes frustrés

Nous connaissons un très grand nombre d'exemples en physique statistique où les fluctuations thermiques pour un système classique jouent un rôle similaire, sinon équivalent, à celui des fluctuations quantiques. Cette analogie est, par exemple, souvent exploitée dans les études d'ondes de spins des systèmes magnétiques. Dans cette section nous discutons le rôle des fluctuations dans un système frustré. Nous commençons par analyser les fluctuations thermiques dans la version classique du système pour ensuite aborder les fluctuations quantiques et constatons les similitudes et différences entre les effets produits dans les deux cas. Nous avons pour cela choisi de faire la discution sur un seul modèle, celui d'un système de spins sur le réseau de kagomé, qui, grâce à sa richesse, servira à illustrer tous les phénomènes intéressants qui peuvent avoir lieu dans la physique des systèmes frustrés en général.

Considérons le modèle de Heisenberg pour des spins classiques dans le réseau de kagomé, avec interactions entre plus proches voisins :

$$H = J \sum_{<i,j>} \vec{S}_i . \vec{S}_j \ ; \ J > 0, \ \vec{S}_i^2 = 1. \tag{28}$$

Ce Hamiltonien peut se réécrire comme une somme sur tous les triangles du réseau :

$$H = \frac{J}{2} \sum_{\triangle} \left(\vec{S}_{\triangle}^2 - 3 \right) \tag{29}$$

où $\vec{S}_{\triangle} = \sum_{i \in \triangle} \vec{S}_i$. Il est clair que l'état de plus basse énergie sera donné par les conditions sur chaque triangle $\vec{S}_{\triangle} = 0$. Or, pour le réseau de kagomé, Il existe une infinité de configurations qui satisfont à ces équations. Cet ensemble forme en fait une sous-variété dont certains des éléments auront une importance capitale. Nous pouvons maintenant nous placer à une température basse mais non-nulle, et étudier les fluctuations thermiques sur chacune des configurations de basse énergie. Nous renvoyons le lecteur aux références originelles pour les détails techniques [1] et mentionnons ici que les configurations où tous les spins sont contenus dans un même plan sont favorisées par rapport aux autres configurations. Cette sélection d'un certain type de configuration à basses températures est connue sous le nom de "ordre par désordre" où sous les initiales de l'expression en anglais "OBD". L'origine de ce phénomène se base sur le fait que les fluctuations "d'ondes de spins" au dessus d'une configuration de basse énergie ont des modes "mous", ou des modes dont l'énergie est quartique et non pas quadratique en termes des petites déviations par rapport à la position de basse énergie. Imaginons qu'une configuration particulière contient N_2 modes quadratiques et N_4 modes quartiques, si nous voulons estimer la contribution à l'énergie libre des fluctuations sur cette configuration nous pouvons obtenir le terme dominant avec la méthode

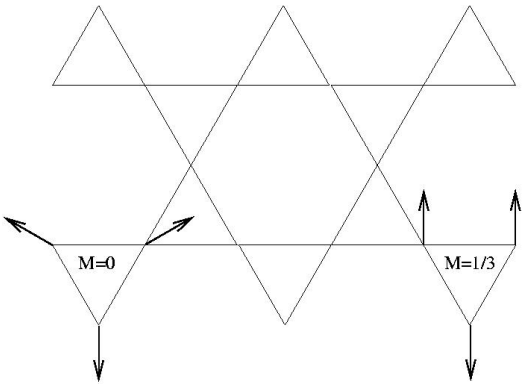

FIG. 3 – Le réseau de kagomé et la configuration des spins avec $M = 0$ et $M = 1/3$

du col :

$$f(T) \sim E_0 - T\left(\frac{N_4}{4} + \frac{N_2}{2}\right) ln(T/J) \tag{30}$$

nous voyons donc que plus une configuration aura des modes quartiques (au détriment du nombre de modes quadratiques), plus son énergie libre sera basse. Les configurations planaires ayant le plus grand nombre de modes "mous", elles seront sélectionnés par rapport aux autres configurations et dominerons donc le comportement à basse température du système. Le calcul détaillé nous montre aussi que l'ordre quadratique sur les ondes de spins est identique pour toutes les configurations planaires (*i. e.* aussi bien le nombre de modes mous N_4 que la loi de dispersion des modes quadratiques seront les mêmes pour toutes les configurations planaires). Ce dernier résultat a des conséquences importantes pour le cas quantique, comme nous le verrons plus bas.

Imaginons maintenant que l'on introduit un champ magnétique h dans la direction $\hat{z}$, le Hamiltonien devient :

$$\begin{aligned} H &= J\sum_{<i,j>} \vec{S}_i.\vec{S}_j - h\sum_i S_i^z \\ &= \frac{J}{2}\sum_{\triangle}\left(\vec{S}_{\triangle}^2 - 3\right) - \frac{h}{2}\sum_{\triangle} S_{\triangle}^z \end{aligned} \tag{31}$$

et la configuration d'énergie minimale sera donc donnée par une aimantation par triangle

$$\vec{M} \equiv \frac{1}{3}\sum_{i\in\triangle}\vec{S}_i = \frac{h}{6J}\hat{z}.$$

L'analyse des fluctuations du modèle classique à basse température a été faite dans [2]. Un point particulièrement intéressant correspond au cas $M = 1/3$. Ceci

d'abord du fait que, en présence d'un terme d'anisotropie, XXZ avec $\Delta > 1$, la courbe d'aimantation classique présente un plateau [3]. En plus, dans le cas isotrope, les configurations 'UUD' où, par triangle, deux spins sont parallèles au champ magnétique et le troisième est antiparallèle (voir figure (3)) aura le même type de comportement que les configurations planaires pour le cas $M = 0$ [2]. De ce fait, ces configurations dites coplanaires seront sélectionnées à basse température dans le système classique. Une observation importante est que, comme pour le cas des configurations planaires pour $M = 0$, il existe, dans la limite thermodynamique, une infinité de 'pavages' inéquivalents de configurations 'UUD'. Cependant, les fluctuations thermiques considérées à l'ordre le plus bas donneront le même résultat pour toutes les configurations collinéaires. En effet, Nous pouvons écrire les petites déviations par rapport à la position d'équilibre de chaque spin $\vec{S}_l$ comme :

$$\vec{S}_l = (\epsilon_l^x, \epsilon_l^y, 1 - \alpha_l) \tag{32}$$

avec $\alpha_l = ((\epsilon_l^x)^2 + (\epsilon_l^y)^2)/2$. Nous obtenons alors le Hamiltonien au premier ordre :

$$H = E_0 + J \sum_{i \to j} \left[\mathbf{C}_{i,j}^x \epsilon_i^x \epsilon_j^x + \mathbf{C}_{i,j}^y \epsilon_i^y \epsilon_j^y \right] \ , \tag{33}$$

où E_0 est l'énergie de la configuration classique non déformée. Pour le cas $M = 0$, il est possible de choisir un repère des axes pour chaque spin pour que les matrices $\mathbf{C}_{i,j}^x$ et $\mathbf{C}_{i,j}^y$ soient les mêmes pour tous les pavages. Dans le cas $M = 1/3$, bien qu'on puisse toujours choisir les repères pour chaque spin pour que les matrices $\mathbf{C}_{i,j}^x$ soient identiques, les matrices $\mathbf{C}_{i,j}^y$ dépendent du pavage UUD que nous avons choisi. L'observation clé est que, sous le changement de variable : $\epsilon_i^y \to -\epsilon_i^y$ sur chaque site i où le spin non déformé est 'D' (down), nous obtenons des matrices $\mathbf{C}_{i,j}^y$ qui sont aussi indépendantes du pavage choisi. Il est donc évident que toutes les configurations planaires pour $M = 0$ ou UUD pour $M = 1/3$ sont, au premier ordre, équivalentes vis à vis des fluctuations thermiques.

Imaginons maintenant que notre système dans le réseau de kagomé est composé de spins quantiques, de grandeur $\vec{S}^2 = \hbar^2 S(S+1)$. Si nous nous plaçons à température nulle, il est légitime de se demander si les fluctuations quantiques vont avoir un rôle similaire à celui des fluctuations thermiques pour le modèle classique. Un premier pas pour répondre à cette question est d'étudier les fluctuations de point zéro au premier ordre en $1/S$ en utilisant la représentation de Holstein-Primakoff. Pour cela, nous écrivons chaque spin comme :

$$\vec{S}_l = S\left(\frac{1}{\sqrt{2S}}(a_l^\dagger + a_l), i\frac{1}{\sqrt{2S}}(a_l^\dagger - a_l), 1 - \frac{a_l^\dagger a_l}{S}\right) \ , \tag{34}$$

et nous obtenons le Hamiltonien :

$$H = H_0 + \frac{S}{2}(H_2 + O(1/\sqrt{S})) \tag{35}$$

où H_2 est quadratique en termes des opérateurs de création et annihilation. La partie en $O(1/\sqrt{S})$ contient des termes d'ordre supérieur. Considérons par exemple des pavages avec une certaine périodicité de façon à pouvoir utiliser la transformée de Fourier. Par transformation de Fourier, on obtient alors :

$$H_2 = \frac{J}{2} \sum_{\vec{q}} \left(a^{\dagger i}_{-\vec{q}}, a^i_{\vec{q}} \right) \cdot \begin{pmatrix} \tilde{C}^+ & \tilde{C}^- \\ \tilde{C}^- & \tilde{C}^+ \end{pmatrix}_{ij} \cdot \begin{pmatrix} a^j_{-\vec{q}} \\ a^{\dagger j}_{\vec{q}} \end{pmatrix} , \tag{36}$$

où $\tilde{C}^{\pm}$ sont les transformées de Fourier de $C^x \pm C^y$. Nous pouvons donc en conclure que, pour $M = 0$, les fluctuations quantiques au premier ordre joueront un rôle similaire à celui des fluctuations thermiques en ne favorisant aucune configuration classique planaire particulière. Il faut donc une technique d'analyse des effets quantiques plus poussée pour pouvoir se prononcer sur le spectre du système quantique, notamment pour des spins 1/2. A ce jour les résultats les plus solides [4] proposent un scénario où le modèle de spins 1/2, à $M = 0$, a un gap de spin [3] et une bande d'excitations de spin 0, au dessous du gap, qui rejoint l'état fondamental qui est désordonné. Le nombre d'états dans cette bande de singulets au dessous du gap de spin semble croître exponentiellement avec la taille du système. Ce scénario exotique est la trace au niveau quantique de cette grande dégénérescence thermique au niveau classique. On peut remarquer la rigidité du système vis à vis des excitations magnétiques qui coexiste avec la 'molesse' de celui-ci par rapport à des excitations non magnétiques.

Pour $M = 1/3$ la situation est très différente : la remarque la plus importante est que le changement de variable $\epsilon^y_i \to -\epsilon^y_i$ fait dans le cas classique ne peut plus être fait maintenant car ϵ^x_i et ϵ^y_i sont des variables canoniques qui doivent satisfaire à des lois de commutation bien précises (reliées à l'algèbre de $su(2)$ des spins). Il n'y a donc plus de raison pour que le tout premier ordre des fluctuations quantiques donne le même résultat pour tous les pavages. On peut en fait faire explicitement le calcul des corrections de point zéro pour deux pavages bien connus, la configuration $q = 0$ (avec une périodicité de 3 sous-réseaux) et celle nommée $\sqrt{3} \times \sqrt{3}$ (avec une périodicité de 9 sous-réseaux) et constater que les fluctuations de point zéro de l'état $q = 0$ sont en effet plus basses.

Bien que ce résultat nous permette d'anticiper que la situation va être différente de celle du cas $M = 0$ il nous faut des techniques plus poussées pour donner un résultat définitif sur la nature de l'état fondamental et des excitations de plus basse énergie. De ce fait, nous considérons le modèle XXZ avec paramètre d'anisotropie Δ et considérons le cas $\Delta >> 1$ (le cas Δ infini correspondant au modèle d'Ising anti-ferromagnétique sur le réseau de kagomé). Le premier ordre non-nul en puissances de $1/\Delta$ nous donne un Hamiltonien effectif composé d'opérateurs

[3] qui se traduit, comme nous le savons, par un plateau dans la courbe d'aimantation.

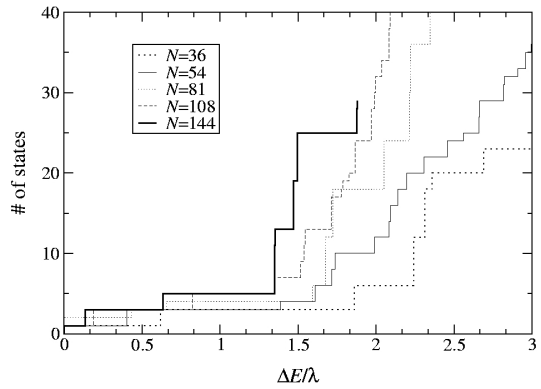

FIG. 4 – Nombre d'états singulets sous le gap de spin. On remarquera la dégénérescence trois de l'état fondamental et le gap des singulets, beaucoup plus petit que le gap de spin.

agissant sur les hexagones :

$$H_{\text{eff.}} = \lambda \sum_{\text{hexagone } i} \left(s^+_{i,1} s^-_{i,2} s^+_{i,3} s^-_{i,4} s^+_{i,5} s^-_{i,6} + s^-_{i,1} s^+_{i,2} s^-_{i,3} s^+_{i,4} s^-_{i,5} s^+_{i,6} \right) , \tag{37}$$

L'état fondamental de ce hamiltonien est trois fois dégénéré et correspond à un solide de plaquettes $\uparrow\downarrow\uparrow\downarrow\uparrow\downarrow$ résonantes. Au dessus de ce fondamental dégénéré on trouve un gap pour les excitations de singulets beaucoup plus petit que le gap de spin, mais non nul. Dans l'article que nous présentons à la suite nous donnons les détails techniques qui nous permettent d'arriver à ce résultat ainsi que des arguments qui nous permettent de dire que ce scénario reste valable dans le cas isotrope $\Delta = 1$. La figure (4) correspond à l'obtention par diagonalisation numérique du Hamiltonien effectif du nombre d'états singulets en fonction de l'énergie. Nous pouvons voir la présence du gap ainsi que de la bande d'états singulets, qui, comme dans le cas $M = 0$, est exponentiellement croissante avec la taille du système. Nous avons donc dans ce système deux ordres de grandeur pour des gaps différent, correspondant à la rigidité magnétique, beaucoup plus forte que la rigidité des excitations non magnétiques.

Références

[1] J. T. Chalker, P. C. W. Holdsworth, and E. F. Shender, Phys. Rev. Lett. **68**, 855 (1992) ; E. F. Shender and P. C. W. Holdsworth, *Order by Disorder and Topology in Frustrated Magnetic Systems*, in *Fluctuations and Order*, M. Millonas Ed., Springer.

[2] M.E. Zhitomirsky, Phys. Rev. Lett. **88**, 057204 (2002).

[3] D.C. Cabra, M. D. Grynberg, P.C.W. Holdsworth and P. Pujol, Phys. Rev. **B 65**, 094418 (2002).

[4] C. Waldtmann H. -U. Everts, B. Bernu, P. Sindzingre, C. Lhuillier, P. Lecheminant, L. Pierre, Eur. Phys. J. B **2**, 501 (1998) ; F. Mila, Phys. Rev. Lett. **81**, 2356 (1998).

Quantum kagomé antiferromagnet in a magnetic field: Low-lying non-magnetic excitations versus valence-bond crystal order

D.C. Cabra,[1] M.D. Grynberg,[2] P.C.W. Holdsworth,[3] A. Honecker,[4,5]
P. Pujol,[3] J. Richter,[6] D. Schmalfuß,[6] and J. Schulenburg[7]

[1] *Université Louis Pasteur, Laboratoire de Physique Théorique, 67084 Strasbourg Cédex, France*
[2] *Departamento de Física, Universidad Nacional de La Plata, C.C. 67, (1900) La Plata, Argentina*
[3] *Laboratoire de Physique, ENS Lyon, 46 Allée d'Italie, 69364 Lyon Cédex 07, France*
[4] *TU Braunschweig, Institut für Theoretische Physik, 38106 Braunschweig, Germany*
[5] *Universität Hannover, Institut für Theoretische Physik, Appelstrasse 2, 30167 Hannover, Germany*
[6] *Institut für Theoretische Physik, Otto-von-Guericke Universität Magdeburg, 39016 Magdeburg, Germany*
[7] *Universitätsrechenzentrum, Otto-von-Guericke-Universität Magdeburg, 39016 Magdeburg, Germany*

(Dated: April 13, 2004)

We study the ground state properties of a quantum antiferromagnet on the kagomé lattice in the presence of a magnetic field, paying particular attention to the stability of the plateau at magnetization 1/3 of saturation and the nature of its ground state. We discuss fluctuations around classical ground states and argue that quantum and classical calculations at the harmonic level do not lead to the same result in contrast to the zero-field case. For spin $S = 1/2$ we find a magnetic gap below which an exponential number of non-magnetic excitations are present. Moreover, such non-magnetic excitations also have a (much smaller) gap above the three-fold degenerate ground state. We provide evidence that the ground state has long-range order of valence-bond crystal type with nine spins in the unit cell.

The appearance of exotic quantum phases in systems described by two-dimensional frustrated antiferromagnets is presently the subject of intense research (see e.g. [1, 2] for recent reviews). The Heisenberg antiferromagnet on highly frustrated lattices such as the pyrochlore and kagomé lattice has a huge degeneracy of the classical ground state such that no magnetic order arises at any temperature (see e.g. [3] for a recent review). At the quantum level one may then obtain different exotic phases without magnetic (Néel) order. One such phase is the so-called 'valence-bond crystal' which is characterized by formation of local singlets in a long-range ordered pattern. An even more exotic phase, namely one without any kind of long-range order, is suspected to arise in the $S = 1/2$ Heisenberg model on the kagomé lattice [1, 4, 5, 6, 7]. In the latter case, there is a small spin gap and, although this is still under discussion [8, 9], the ground state is suspected to be disordered. In particular, a huge number of singlets (exponentially growing with the system size) is found inside the spin gap which are reminiscent of the classical degeneracy.

The spin $S = 1/2$ kagomé Heisenberg antiferromagnet (KHAFM) is realized e.g. in volborthite [10], although presumably in some distorted form. Another possible realization is given by atomic quantum gases in optical lattices [11]. In the latter case, magnetization corresponds to particle number and a magnetic field to chemical potential, opening the possibility to perform experiments for the behavior of the spin model in a magnetic field.

The magnetization process of the KHAFM has been studied theoretically both for classical [12, 13, 14] as well as quantum spins [14, 15, 16, 17]. Numerical results for the magnetization curve of the $S = 1/2$ Heisenberg model exhibit among others a clear plateau at 1/3 of the saturation magnetization [14, 15, 16, 17] (see also Fig. 1). For the classical KHAFM at one third of the saturation field thermal fluctuations select collinear states, but there appears to be no real order [12]. For the $S = 1/2$ KHAFM we will argue in this Letter that the state with magnetization $\langle M \rangle = 1/3$ exhibits order of the valence-bond crystal type although it shares some similarities with the case $\langle M \rangle = 0$.

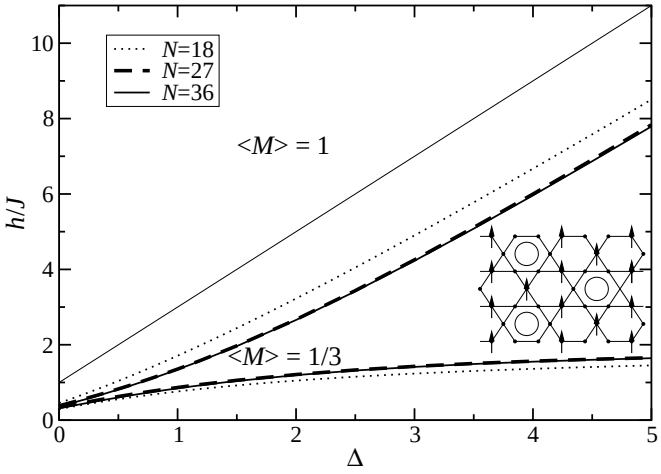

FIG. 1: Boundaries of the $\langle M \rangle = 1/3$ plateau as a function of the anisotropy Δ for different lattice sizes (see legend) and the transition to saturation $\langle M \rangle = 1$ for the thermodynamic limit (thin full line). Inset: kagomé lattice with an ordered state of the valence-bond crystal type at $\langle M \rangle = 1/3$: circles in certain hexagons indicate local resonances between different Néel configurations on the hexagons, arrows indicate spins which are aligned with the field.

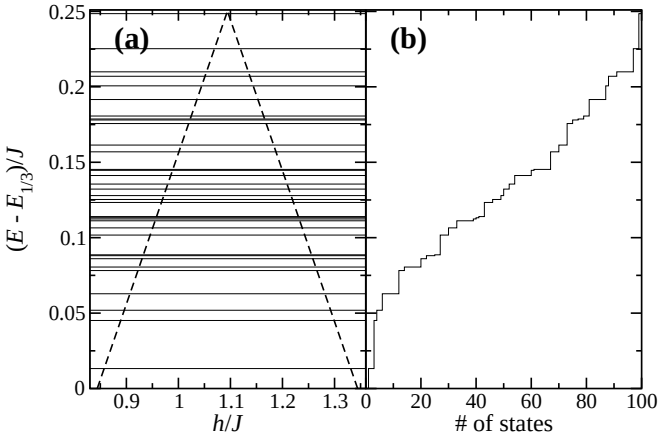

FIG. 2: Low-lying excitations above the $\langle M\rangle = 1/3$ plateau for the $S = 1/2$ Heisenberg antiferromagnet on the $N = 36$ kagomé lattice. (a) Full lines show all excitations with $S^z = 6$ in the given energy range, bold dashed lines the lowest excitations with $S^z = 5$ and $S^z = 7$ as a function of magnetic field h. (b) Excitation energy versus number of states with $S^z = 6$ below that energy. One observes a total of 100 states below the magnetic gap in the middle of the $\langle M\rangle = 1/3$ plateau (corresponding to the largest gap to magnetic excitations).

In the present Letter we study the XXZ model in a magnetic field h

$$H = J\sum_{\langle i,j\rangle}\left(s_i^x s_j^x + s_i^y s_j^y + \Delta s_i^z s_j^z\right) - h\sum_i s_i^z\,, \qquad (1)$$

where $\langle i,j\rangle$ indicates nearest neighbors on the kagomé lattice (see inset of Fig. 1), s_i^α are spin-half operators acting at site i and Δ is the XXZ-anisotropy.

The main panel of Fig. 1 shows the boundaries of the fully polarized state (which we normalize to $\langle M\rangle = 1$) and a state with $\langle M\rangle = 1/3$ in the XXZ model (1). Fig. 2(a) shows the low-lying excitations above the $\langle M\rangle = 1/3$ ground state computed by exact diagonalization for $N = 36$ and $\Delta = 1$. The dashed lines show the gap to states with $S^z = 5$ and 7 which vanishes at the boundaries of the plateau. The maximum magnetic gap occurs in the middle of the plateau where these two lines intersect and we will use this as a definition of the magnetic gap. Horizontal straight lines denote states with $S^z = 6$ (*i.e.* $\langle M\rangle = 1/3$) and correspond to non-magnetic excitations. The large number of non-magnetic excitations below the magnetic gap is reminiscent of the classical degeneracy. The shape of the integrated density of non-magnetic excitations (see Fig. 2(b)) is very similar to the corresponding integrated density of singlets at $\langle M\rangle = 0$ (see Fig. 2 of [5]). In combination with the disordered classical ground state [12], one might be tempted to take this as evidence that also the ground state of the $S = 1/2$ KHAFM at $\langle M\rangle = 1/3$ is disordered. However, we will argue next that here classical and quantum fluctuations are in fact not equivalent at the harmonic level and then present evidence in favor of an *ordered* state for $S = 1/2$.

Classical (thermal) fluctuations were studied in [12, 14, 18] such that we make only a few comments valid for non-zero magnetization and arbitrary anisotropy Δ. As was shown explicitly for $\Delta = 1$ in [12], thermal fluctuations select collinear 'up-up-down' (UUD) configurations at $\langle M\rangle = 1/3$ against the other non-collinear configurations that also minimize the classical energy, but all UUD configurations have the same spectra of harmonic fluctuations. Indeed, a local change of variables shows that the covering-dependent Hamiltonians of classical Gaussian fluctuations [14] are equivalent.

The role of quantum fluctuations is however radically different. Now quantum commutation relations to be preserved and the change of variables used for the classical case is no longer possible. To analyze this in more detail, we compute the zero-point contribution to the ground state energy at $\langle M\rangle = 1/3$ for two different coverings with a $q = 0$ and the $\sqrt{3}\times\sqrt{3}$ structure shown in Fig. 1 of [12], respectively. By writing the spin operators on each site in terms of bosonic creation and annihilation operators:

$$\vec{s}_l = S\left(\frac{1}{\sqrt{2S}}(a_l^\dagger + a_l), i\frac{1}{\sqrt{2S}}(a_l^\dagger - a_l), 1 - \frac{a_l^\dagger a_l}{S}\right)\,, \qquad (2)$$

we obtain the Hamiltonian:

$$H = H_0 + \frac{S}{2}(H_2 + O(1/\sqrt{S}))\,, \qquad (3)$$

where H_2 is quadratic in creation and annihilation operators and the $O(1/\sqrt{S})$ part contains higher orders. By Fourier transforming, we obtain:

$$H_2 = \frac{J}{2}\sum_{\vec{k}}\left(a_{-\vec{k}}^{\dagger i},\, a_{\vec{k}}^{i}\right)\cdot\begin{pmatrix}\tilde{M}^+ & \tilde{M}^-\\ \tilde{M}^- & \tilde{M}^+\end{pmatrix}_{ij}\cdot\begin{pmatrix}a_{-\vec{k}}^{j}\\ a_{\vec{k}}^{\dagger j}\end{pmatrix}\,, \qquad (4)$$

where $\tilde{M}^\pm$ are 3×3 and 9×9 matrices for the $q = 0$ and the $\sqrt{3}\times\sqrt{3}$ states since these coverings have 3 and 9 sublattices, respectively. No further change of variables is possible here since the commutation relations of the $su(2)$ algebra of the spins have to be preserved. At $\Delta = 1$ one finds for the zero-point fluctuations $\frac{1}{2}\sum_{\vec{k}}\omega_{\vec{k}} = JS/3$ and $\approx 0.5643\,JS$ for the $q = 0$ and the $\sqrt{3}\times\sqrt{3}$ state, respectively, demonstrating the inequivalence of the different coverings at the quantum level.

Let us now turn to the extreme quantum case $S = 1/2$ and, following [19, 20], study the anisotropic XXZ limit. In the Ising limit $\Delta = \infty$, the ground states are those states where around each triangle two spins point up and one down. This ground-state space of the Ising model can then be taken as configuration space for a perturbative treatment of the XY-part of the XXZ Hamiltonian,

For sufficiently large lattices, the lowest non-trivial order is third order, flipping simultaneously pairwise antiparallel spins around a hexagon. This is described by

an effective Hamiltonian [19, 20]

$$H_{\rm eff.} = \lambda \sum_{\rm hexagon\ } _{i} \left(s^+_{i,1} s^-_{i,2} s^+_{i,3} s^-_{i,4} s^+_{i,5} s^-_{i,6} + s^-_{i,1} s^+_{i,2} s^-_{i,3} s^+_{i,4} s^-_{i,5} s^+_{i,6} \right) , \qquad (5)$$

where the spin operator $s^\alpha_{i,j}$ operates at the jth site around hexagon i and $\lambda = 3J/(2\Delta^2)$. Note that in the Ising-basis the effective Hamiltonian (5) has only off-diagonal matrix elements of size λ.

The configurations of the Ising model can be mapped to dimer coverings of the dual lattice which in the case of the kagomé lattice is the hexagonal lattice. Now one can use known results for dimer coverings [21, 22] to write down the asymptotic growth law for the number of Ising configurations $\mathcal{N}_{\rm conf.}$ on an N-site kagomé lattice:

$$\mathcal{N}_{\rm conf.} \sim (1.11372781\ldots)^N . \qquad (6)$$

Exploiting results for the related quantum dimer model on the hexagonal lattice [23], Moessner and Sondhi concluded [20] that the ground state of the effective Hamiltonian (5) is of the valence-bond crystal type. To be more precise, the case studied in [20, 23] corresponds to $\lambda < 0$ whereas we have $\lambda > 0$, but there exist unitary transformations which change the sign of λ [24]. Hence the spectra of the effective Hamiltonian (5) are invariant under $\lambda \to -\lambda$. The three-fold degenerate ground-state wave functions are sketched in the inset of Fig. 1. Circles in one third of the hexagons denote resonances between the two different Néel states on the surrounding hexagon; a background of the remaining third of all spins points in the direction of the field. Note that these wave functions were argued in [20, 23] to yield a qualitatively correct description, but they should not be used for a quantitative analysis. Furthermore, we emphasize that due to the resonances, these wave functions are of a purely quantum nature and have no counterparts as unique states of the classical Heisenberg model.

According to the above, at large Δ the $\langle M \rangle = 1/3$ state of the XXZ model on the kagomé lattice should be *three*-fold degenerate with a *gap* to the next non-magnetic excitations. To check this conclusion and compare it to Fig. 2, let us look at the spectrum of the effective Hamiltonian (5). This effective model has a substantially reduced Hilbert space (e.g. for $N = 36$ there are only 120 states). We can therefore go to larger lattice sizes than in the full model. Results for kagomé lattices with up to $N = 144$ sites are shown in Fig. 3. Additional short cycles wrap around the boundaries of the lattice for $N \leq 27$ and lead to non-generic ground states of $H_{\rm eff.}$. Accordingly, systems with $N < 36$ should not be considered and are not included in Fig. 3.

Two features are apparent in Fig. 3 at least for the two biggest system sizes ($N = 108$ and 144). Firstly, there are two further levels above the ground state which appear

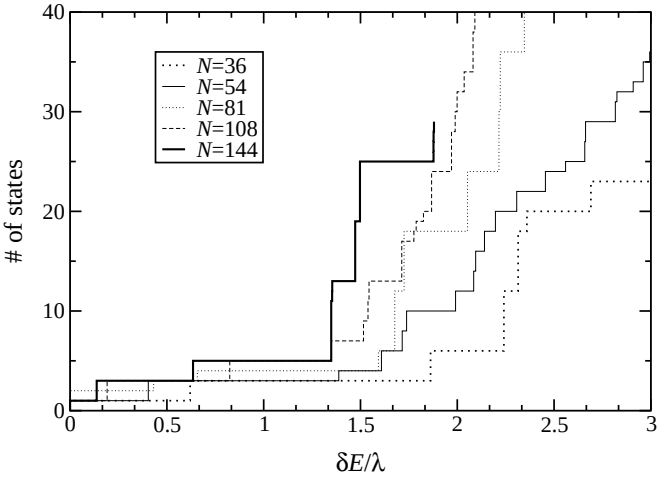

FIG. 3: Spectra of effective Hamiltonian (5) for $\Delta \to \infty$ with $N = 36$, 54, 81, 108 and 144.

to be converging to $\delta E \to 0$ which is consistent with the expected three-fold degeneracy of the ground state in the thermodynamic limit. Secondly, there is a huge density of states emerging for $\delta E \geq 1.3\lambda$ which is consistent with a gap of the order $\sim 1.3\lambda$. For $N = 108$ and 144 there are two further levels in between. Inspection of the wave-functions indicates that these additional low-lying levels may arise from the three classical $\sqrt{3}\times\sqrt{3}$ configurations.

Although the effective Hamiltonian leads to higher degeneracies of some excited states, the $N = 36$ curves in Figs. 2 and 3 have a very similar shape which can be taken as a first indication that the same scenario as for $\Delta \gg 1$ also applies to $\Delta = 1$. Comparison of the overall scales leads to an estimate for the gap in the $\langle M \rangle = 1/3$ sector at $\Delta = 1$ of about $0.04\,J$. Furthermore, the total number of Ising configurations is very close to the number of non-magnetic excitations below the magnetic gap for $\Delta = 1$ at a given system size. Hence, the growth law (6) yields a good approximation also to the number of non-magnetic excitations in the Heisenberg model ($\Delta = 1$).

It is instructive to compute the overlap of the wave function of the full XXZ model, $|\text{full } XXZ\rangle$, with the ground state wave function, $|\text{effective}\rangle$, of the effective Hamiltonian with the same number of spins N. The analysis of the effective Hamiltonian implies that one should study only sizes which are multiples of 9 and that $N = 36$ is the smallest which is representative of the general case. However, $N = 36$ is the biggest system we have been able to study the full XXZ model and hence the only case we can discuss. Results for the overlap $|\langle\text{effective}|\text{full } XXZ\rangle|$ are shown by the full line in Fig. 4. We observe that this overlap tends to 1 for large values of Δ, as expected. Furthermore, the overlap remains appreciable even close to the Heisenberg model ($|\langle\text{effective}|\text{full } XXZ\rangle| \approx 0.22$ for $\Delta = 1$), in particu-

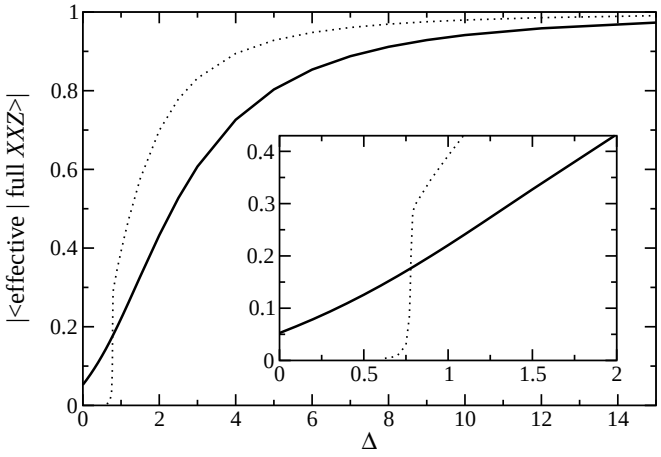

FIG. 4: Overlap between the ground state of the full XXZ model and the effective Hamiltonian with $N = 36$ for different values of the anisotropy parameter Δ (full line). For comparison we include the corresponding result for the $N = 36$ triangular lattice [17] (dotted line) which exhibits a sharp drop around $\Delta = 0.77$.

lar if one considers that the dimension of the symmetry subspace under consideration is of the order 10^7. Note further that the corresponding computation for the triangular lattice at $\langle M\rangle = 1/3$ leads to a sharp drop at $\Delta \approx 0.76$ in the overlap at a fixed N (see dotted curve in Fig. 4 for $N = 36$), signaling an instability of the plateau state [17]. No such sharp drop is observed on the kagomé lattice (full line in Fig. 4) which we take as a sign of absence of phase transitions between $\Delta = \infty$ and ≈ 0 in the XXZ model on the kagomé lattice at $\langle M\rangle = 1/3$. In particular, $\Delta = 1$ and ∞ should belong to the same phase.

To conclude, we have analyzed the low-energy spectrum of the kagomé XXZ $S = 1/2$ model at magnetization $\langle M\rangle = 1/3$. While the existence of a magnetization plateau is clear, the nature of the non-magnetic excitations over the ground state is more difficult to clarify. We have argued by different techniques that the ground state has an order of the valence-bond crystal type, *i.e.* the ground state is three-fold degenerate and there is a small gap to all higher excitations. While in the case $\Delta \gg 1$ this scenario is derived from a mapping to an effective Hamiltonian [19, 20, 23], our numerical data indicates that it persists down to the isotropic limit $\Delta = 1$.

One of the key differences between the present case and $\langle M\rangle = 0$ lies in the unrenormalized classical thermal and quantum fluctuations. In the absence of a magnetic field, they are equivalent regarding the lifting of degeneracy of configurations with soft modes (planar configurations). However, for $\langle M\rangle = 1/3$, classical thermal fluctuations select the collinear UUD configurations and the weight in the free energy of any UUD covering is equivalent at the harmonic level. Because of commutation relations that have to be preserved at the quantum level, the zero-point corrections over the UUD configurations are not any more equal. This is the first indication that a spin liquid phase is less likely to appear than for the $\langle M\rangle = 0$ case.

For $S = 1/2$ and $\Delta = 1$ we find, for $\langle M\rangle = 1/3$, an exponential number of non-magnetic excitations below the magnetic gap which are reminiscent of the classical degeneracy; just as for $\langle M\rangle = 0$ [1, 5, 6]. In the latter case the macroscopic number of non-magnetic excitations has been taken as evidence for a completely disordered ground state. Here, however, we find evidence for a further small gap, separating the continuum of states from a ground state, which has long-range order of valence-bond crystal type. We remark that the $N = 36$ spectrum [5] suggests that candidates for valence-bond ordered states for $\langle M\rangle = 0$ would have a larger unit cell than the state above. Hence, we believe that the issue of order at very low energies in the $S = 1/2$ KHAFM at $\langle M\rangle = 0$ remains a challenging problem.

Acknowledgments: We would like to thank the Rechenzentrum, TU Braunschweig for allocation of CPU time on the compute-server `cfgauss` and J. Schüle for technical support. We are grateful to H.-U. Everts, C. Lhuillier, F. Mila and R. Moessner for useful discussions. This work was financially supported by ECOS-Sud and Procope-Egide exchange programs. The research of D.C.C. and M.D.G. was partially supported by CONICET and Fundación Antorchas, Argentina (grant No. A-13622/1-106).

[1] G. Misguich, C. Lhuillier, cond-mat/0310405.
[2] J. Richter, J. Schulenburg, A. Honecker, *Quantum magnetism in two dimensions: From semi-classical Néel order to magnetic disorder* [`http://www.tu-bs.de/~honecker/papers/2dqm.ps.gz`].
[3] R. Moessner, Can. J. Phys. **79**, 1283 (2001).
[4] P. Lecheminant, B. Bernu, C. Lhuillier, L. Pierre, P. Sindzingre, Phys. Rev. B **56**, 2521 (1997).
[5] Ch. Waldtmann, H.-U. Everts, B. Bernu, C. Lhuillier, P. Sindzingre, P. Lecheminant, L. Pierre, Eur. Phys. J. B **2**, 501 (1998).
[6] F. Mila, Phys. Rev. Lett. **81**, 2356 (1998).
[7] C. Lhuillier, P. Sindzingre, J.-B. Fouet, Can. J. Phys. **79**, 1525 (2001).
[8] A.V. Syromyatnikov, S.V. Maleyev, Phys. Rev. B **66**, 132408 (2002).
[9] P. Nikolic, T. Senthil, Phys. Rev. B **68**, 214415 (2003).
[10] Z. Hiroi, M. Hanawa, N. Kobayashi, M. Nohara, H. Takagi, Y. Kato, M. Takigawa, J. Phys. Soc. Jpn **70**, 3377 (2001).
[11] L. Santos, M.A. Baranov, J.I. Cirac, H.-U. Everts, H. Fehrmann, M. Lewenstein, preprint cond-mat/0401502.
[12] M.E. Zhitomirsky, Phys. Rev. Lett. **88**, 057204 (2002).
[13] A. Honecker, O.A. Petrenko, M.E. Zhitomirsky, Physica B **312-313**, 609 (2002).
[14] D.C. Cabra, M.D. Grynberg, P.C.W. Holdsworth, P. Pujol, Phys. Rev. B **65**, 094418 (2002).

[15] K. Hida, J. Phys. Soc. Jpn **70**, 3673 (2001).
[16] J. Schulenburg, A. Honecker, J. Schnack, J. Richter, H.-J. Schmidt, Phys. Rev. Lett. **88**, 167207 (2002).
[17] A. Honecker, J. Schulenburg, J. Richter, J. Phys.: Condens. Matter **16**, S749 (2004).
[18] J.T. Chalker, P.C.W. Holdsworth, E.F. Shender, Phys. Rev. Lett. **68**, 855 (1992); E.F. Shender, P.C.W. Holdsworth, In *Fluctuations and Order: a new synthesis*, M.M. Millonas ed. Springer-Verlag, 1996.
[19] R. Moessner, S.L. Sondhi, P. Chandra, Phys. Rev. Lett. **84**, 4457 (2000).
[20] R. Moessner, S.L. Sondhi, Phys. Rev. B **63**, 224401 (2001).
[21] G.H. Wannier, Phys. Rev. **79**, 357 (1950).
[22] F.Y. Wu, preprint cond-mat/0303251.
[23] R. Moessner, S.L. Sondhi, P. Chandra, Phys. Rev. B **64**, 144416 (2001).
[24] One of these maps sends $s^{\pm}_{i,j} \to -s^{\pm}_{i,j}$ with a suitable choice of *one* j for each possible hexagon i; R. Moessner, private communication.

2.2 Systèmes classiques en deux dimensions

Dans ce chapitre nous allons aborder certaines propriétés statiques et dynamiques de systèmes classiques en deux dimensions. De façon plus précise, dans un premier temps nous allons étudier dans un exemple concret le rôle joué par les impuretés dans un système qui a une transition de phase continue. Cette question est en effet fondamentale si l'on pense à tous les efforts qui ont été fournis pendant les années 60, 70 et 80 pour comprendre les phénomènes de transitions de phases continues, avec en particulier des notions comme celles de groupe de renormalisation et d'universalité ou les théories conformes. Cela dit, si l'on veut confronter les prédictions théoriques aux résultats expérimentaux, il ne faut pas oublier que dans pratiquement la totalité des cas, des impuretés seront présentes dans les échantillons où les mesures seront faites. Le type de questions qui viennent tout d'abord à l'esprit est de comprendre si la présence du désordre préserve ou pas la nature de la transition de phase, et si oui, la classe d'universalité va-t-elle être la même ? Ces questions ont bien sûr déjà été étudiées dans divers cas et nous ne prétendons pas donner ici une liste exhaustive. Dans [1] on étudie cette questions pour certains modèles bidimensionnels, dont le modèle d'Ising et de Potts, et l'on peut trouver une discussion générale sur ce sujet. Le résultat qui est peut-être le plus important, et qui en tous cas répond partiellement à ces questions est le critère de Harris [2]. Celui-ci nous dit que, si α est l'exposant avec lequel diverge la chaleur spécifique en fonction de la température au voisinage du point de transition, c'est à dire :

$$C(T) \sim |T - T_c|^{-\alpha}$$

alors, si $\alpha < 0$ la présence d'un désordre faible ne change ni la nature ni la classe d'universalité de la transition. En revanche, pour $\alpha > 0$, la présence, même en faible concentration, d'impuretés affecte la classe d'universalité de la transition. Bien que ce critère nous dise si la classe d'universalité change, il ne nous renseigne pas sur la nature des nouveaux points fixes qui peuvent apparaître en présence d'impuretés. Il existe des cas, comme le modèle de Potts à trois états [1], où l'on a des points fixes dit perturbatifs, correspondant à des concentrations relativement faibles d'impuretés et dont les exposants critiques associés peuvent être obtenus avec une bonne précision en combinant des techniques du groupe de renormalisation et la théorie des perturbations à partir du modèle pur (sans impuretés), que l'on contrôle bien. Il existe cependant d'autres points fixes, non-perturbatifs, qui eux ne peuvent pas être atteints à partir du comportement du modèle pur.

Le deuxième volet de cette section se base sur l'étude d'un système classique, en deux dimensions et sans désordre. La particularité de ce modèle consiste à imposer des contraintes locales qui donnent lieu à un comportement particulièrement intéressant. La statique du système est déjà intéressante car, comme nous les verrons, le système est critique à température infinie. Cette criticalité persiste à mesure que l'on diminue la température jusqu'à obtenir une transition de phase

du premier ordre très particulière. En effet, le paramètre d'ordre passe de la valeur 0 pour $T > T_c$ à la valeur de saturation directement. En d'autre termes, pour toute température non-nulle mais inférieure à T_c, seule la configuration de plus basse énergie a un poids statistique non nul dans la limite thermodynamique, et n'admet pas d'excitations microscopiques, comme c'est le cas dans la presque totalité des systèmes statistiques que l'on connaît. La raison de ce comportement est entièrement due aux contraintes imposées, qui limitent l'espace de phases et marginalise l'état de plus basse énergie dans celui-ci.

On peut aussi anticiper que cette restriction dans l'espace des phases a des conséquences importantes dans la dynamique du système, et en particulier dans sa relaxation vers l'équilibre. Les contraintes locales imposent déjà une dynamique (par exemple de Monte Carlo) non locale, où la mise à jour microscopique se fait en modifiant plusieurs spins élémentaires du système à la fois de façon à satisfaire à toutes les contraintes à chaque étape. Nous verrons que, malgré cette dynamique non-locale, qui peut-être considérée comme accélérée, le système n'arrive pas à atteindre l'équilibre pour $T < T_c$ et présente alors un comportement en plusieurs points similaire à celui des verres structurels ou de spins. Il est important de constater que cette dynamique hors d'équilibre, très lente, est obtenue sans la présence de désordre.

Les deux exemples traités dans cette section illustrent les sujet de recherche actuels dans le domaine des systèmes classiques en deux dimensions et la richesse des résultats nouveaux que l'on peut observer malgré le fait que la physique classique bidimensionelle soit peut-être un des domaines les plus étudiés en physique théorique pendant les dernières décennies.

Références

[1] P. Pujol : *Théories Conformes et Systèmes Désordonnés*, thèse de doctorat, Université de Paris VI, Octobre 4 1996. disponible sur le site : http ://tel.ccsd.cnrs.fr/documents/archives0/00/00/11/67/index_fr.html

[2] A. B. Harris : J. Phys. **C 7**, 1671, (1974).

2.2.1 Effet des impuretés dans la criticalité

Les techniques de théorie des champs que l'on peut désormais considérer comme traditionnelles ont permis d'aller au delà du critère de Harris pour répondre à la question d'universalité dans une transition de phase en faible désordre. En effet, en combinant les méthodes de théories conformes avec la théorie de perturbations et le groupe de renormalisation on peut décrire les changements qui peuvent intervenir dans des modèles tels que le modèle d'Ising ou de Potts en 2-D avec une faible concentration d'impuretés. Pour le modèle d'Ising, où le critère de Harris ne donne pas de réponse concrète, on sait qu'un désordre faible ne

modifie pas la classe d'universalité [1] et donne lieu tout juste à des corrections logarithmiques à certaines fonctions de corrélations. Pour le modèle de Potts à trois états, où le désordre est pertinent, un nouveau point fixe, toujours à faible désordre apparaît. Bien que nous ne disposions pas de la solution exacte du modèle, les exposants critiques associés à ce nouveau point fixe peuvent être calculés perturbativement.

Ces techniques perturbatives ne nous permettent pas cependant d'obtenir des résultats pour les cas où le désordre est fort, ou la concentrations d'impuretés est grande. Non seulement ce scénario nous éloigne considérablement du voisinage du modèle pur, mais des comportements nouveaux, liés par exemple à la frustration peuvent apparaître. La question est donc de savoir, dans le cas où la transition Para-Ferro existe encore, quelle sera la classe d'universalité de celle-ci. Pour des raisons de simplicité nous allons centrer notre discussion sur le modèle d'Ising en 2-D, qui est assez représentatif du scénario général que l'on retrouve dans plusieurs modèles et dont les résultats qualitatifs que nous allons présenter sont souvent directement transposables à ceux-ci.

Dans le contexte de la théorie des champs, une première tentative consiste à examiner l'action effective du modèle d'Ising avec désordre traité dans le cadre de la méthode des répliques [1]. L'action effective correspond dans ce cas au modèle de Gross-Neveu à symétrie $O(n)$, où selon la prescription de la méthode des répliques nous devrons prendre la limite $n \to 0$ une fois les quantités physiques calculées. Or, le modèle de Gross-Neveu est intégrable, et l'on connaît la matrice S. Pour $n > 2$ entier, le modèle présente une génération dynamique de masse (due à la liberté asymptotique dans l'UV). Le prolongement analytique en n de la fonction β nous montre cependant que le modèle devient asymptotiquement libre à l'IR et donc non-massif. Ce même prolongement analytique peut être fait dans la matrice S du modèle pour obtenir une matrice qui correspond maintenant à celle d'un flot non-massif entre deux points fixes. Ce flot correspond en fait à celui que l'on attend entre un point fixe non-trivial de désordre fort et celui du modèle pur. Avec cette matrice S nous pouvons aussi [2] calculer des facteurs de forme et des fonctions de corrélations qui nous donnerons de façon non-perturbative le "cross-over" entre les points fixes IR et UV, qui correspondent respectivement aux points fixes de désordre fort et du modèle pur. Ce travail à été fait dans [2] où nous avons trouvé effectivement un flot hautement non trivial. Malheureusement, l'identification de ce nouveau point fixe avec un modèle sur réseau n'est pas immédiate. En effet, nous pouvons imaginer différentes façons d'introduire des impuretés dans le système au niveau microscopique. Écrivons notre Hamiltonien d'Ising comme :

$$E(\{S_i\}) = \sum_{\langle i,j \rangle} J_{i,j} S_i \; S_j \, , \tag{38}$$

où le désordre est ici introduit par les couplages $J_{i,j}$. Si nous prenons un modèle de dilution, où certains des couplages $J_{i,j}$, choisis de façon aléatoire sont nuls, on

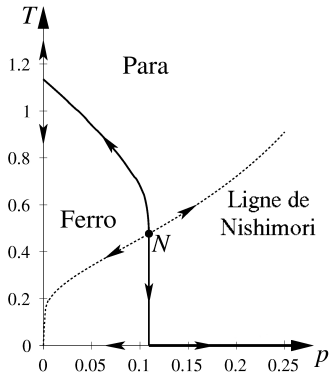

FIG. 5 – le diagramme de phases T *vs.* p du modèle d'Ising avec une distribution aléatoire binaire pour les liens (de concentration p). Le point N, d'intersection de la ligne de transition Para-Ferro et la ligne de Nishimori est le point de Nishimori.

peut montrer que la ligne critique qui sépare les phases Para et Ferro ne contient que deux points fixes : celui du modèle pur et un point à température nulle, dont la classe d'universalité correspond à celle de la percolation. En revanche, comme nous allons le voir plus bas, il existe des cas où les couplages sont aléatoires mais non-nuls et où on aura un point fixe à température non-nulle hautement non-trivial. Or, ces deux types de désordre donnent tous les deux, dans la limite d'une concentration de liens 'impurs' faible, la même action effective donnée par le modèle de Gross-Neveu. On voit donc que, en remontant le flot en direction du point fixe de désordre fort, nous ne pouvons pas avoir l'information du modèle microscopique pourtant si importante pour savoir quel point fixe sera atteint.

Étudions plus en détail maintenant le Hamiltonien (38) avec une distribution de probabilité pour les liens donnée par :

$$P(J_{i,j}) = p\delta(J_{i,j} - 1) + (1 - p)\delta(J_{i,j} + 1)\,. \tag{39}$$

L'observation fondamentale de Nishimori [3] consiste à dire que dans le diagramme de phases T *vs* p, il existe une ligne, donnée par :

$$\mathrm{e}^{\beta} = \frac{1-p}{p}\,, \tag{40}$$

et représentée dans la figure (5), où l'on peut obtenir des résultats exacts sur le système.

La relation (40) est le cas particulier pour la distribution binaire d'une relation plus générale qui s'écrit comme :

$$P(-J_{i,j}) = \mathrm{e}^{-2\beta J_{i,j}} P(J_{i,j}) \tag{41}$$

ou encore comme :

$$P(J_{i,j}) = \mathrm{e}^{-\beta J_{i,j}} Q(|J_{i,j}|) \tag{42}$$

où $Q(|J_{i,j}|)$ est une distribution paire pour les valeurs de $J_{i,j}$. Il existe clairement d'autre types de distributions de probabilité qui ont une ligne de Nishimori, telles que la distribution gaussienne. En revanche, les distributions qui n'ont des valeurs non-nulles que pour des valeurs des $J_{i,j}$ positives ou négatives uniquement ne peuvent en aucun point, à température finie et non-nulle, satisfaire à cette relation. On voit donc que la présence de liens de signes différent, ce qui impliquera la présence de frustration, est indispensable pour les résultats que nous allons énoncer. Nous n'entrons pas ici dans les détails techniques qui peuvent être trouvés dans [3] et énonçons les résultats essentiels uniquement. L'idée fondamentale est d'utiliser les propriétés de transformation du système et des observables sous la transformation de jauge :

$$\begin{aligned} S_i \rightarrow \epsilon_i S_i \ ; \ J_{i,j} \rightarrow \epsilon_i \epsilon_j J_{i,j} \ ; \ \epsilon_i = \pm \\ P(J_{i,j}) = \mathrm{e}^{-\beta J_{i,j}} Q(|J_{i,j}|) \rightarrow \mathrm{e}^{-\beta \epsilon_i \epsilon_j J_{i,j}} Q(|J_{i,j}|) \end{aligned} \tag{43}$$

et de sommer sur toutes les transformations de jauge possibles $\{\epsilon_i\}$, qui nous donnera une somme similaire à celle de la fonction de partition. On obtient avec de simples calculs des résultats assez étonnants valables tout au long de la ligne de Nishimori : l'énergie interne du système peut être calculée exactement

$$\overline{< E >} = -N_{liens} \overline{J} = -N_{liens} \int dJ \ J \ P(J) \tag{44}$$

où $\overline{A}$ correspond à la moyenne sur le désordre de la quantité A et $< A >$ à sa moyenne thermique. En plus, on peut donner une borne supérieure pour la chaleur spécifique du système

$$kT^2 \overline{< C >} \leq N_{liens} \left(\overline{J^2} - \overline{J}^2 \right) \tag{45}$$

Par ailleurs, pour les fonctions de corrélations à N spins on a :

$$\overline{< S_i S_j \cdots >^{2n+1}} = \overline{< S_i S_j \cdots >^{2n+2}} \ ; \ \forall n \in \mathbb{N} \tag{46}$$

et que, dans le diagramme T *vs* p, à p fixé, l'aimantation pour toute température T est bornée supérieurement par sa valeur à cette température au point de Nishimori. Ce dernier résultat implique entre autres que la ligne de transition para-ferro en dessous du point de Nishimori (voir figure (5)) est soit réentrante soit au plus verticale. Les conséquences que l'on peut tirer des résultats de Nishimori sont très nombreuses et d'une très grande richesse. Malheureusement nous ne pouvons ici les mentionner toutes en détails et précisons notre discours sur un point particulièrement important.

Nous pouvons considérer des Hamiltoniens plus généraux avec des interactions à plusieurs spins dans lesquels il est possible d'étendre la condition de Nishimori. Imaginons ensuite que nous faisons des transformations du groupe de renormalisation sur un de ces Hamiltoniens. Un fait remarquable est que la condition de Nishimori est invariante sous les transformations du groupe de renormalisation, et donc la ligne de Nishimori est une variété invariante sous le groupe de renormalisation, au même titre que la ligne de transition Para-Ferro [4]. Le point de Nishimori correspond à l'intersection entre ces deux lignes, et correspond donc à un point fixe du groupe de renormalisation. Il regroupe à la fois les propriétés de la ligne de Nishimori et celles de la criticalité de la ligne de transition Para-Ferro. Les résultats jusqu'ici énoncés sont valables en toutes dimensions et pour tout type de réseau. Nous allons désormais nous spécialiser dans le cas bi-dimensionnel où les travaux que nous présentons ici ont été faits.

Comme la chaleur spécifique est bornée dans la ligne de Nishimori, il est clair qu'elle ne peut donc pas diverger au point de Nishimori. Cet argument seul suffit pour garantir que la classe d'universalité de ce point fixe est différente de celle du modèle pur. Ce point correspond en fait à un point fixe non-perturbatif dont nous parlions plus haut, et dont les caractéristiques sont un problème ouvert. Sous des hypothèses raisonnables de localité de la théorie à grande échelle qui le décrit, on peut donc parler d'une théorie conforme qui décrit la classe d'universalité, très probablement non-unitaire et dont les caractéristiques ne peuvent pas être obtenues à partir de raisonnement perturbatifs simples en partant du système pur. Il existe des propositions faites à partir d'arguments de symétrie du modèle sur réseau [5], mais nous n'avons à ce jour toujours pas une classification des exposants critiques. Les premières simulations numériques faites pour les exposants critiques sur ce point donnaient des résultats très proches de ceux de la percolation. Ces résultats avait en plus l'avantage de suggérer un scénario unificateur où la classe d'universalité de la percolation était celle de tous ces points fixes de désordre fort[4]. Cependant, comme nous le montrons dans l'article annexé à cette section, des mesures numériques plus précises montrent que le point de Nishimori n'est pas dans la même classe d'universalité que la percolation. Les détails techniques peuvent être trouvés dans l'article et nous mentionnons seulement ici que la technique qui s'est avérée la plus efficace est celle du calcul de matrices de transfert dans des bandes très longues, de largeurs 6 à 14 spins, et avec des conditions aux bords périodiques. Les fonctions de corrélation au point critique peuvent être obtenues de façon exacte dans une géométrie cylindrique et comparées aux résultats numériques pour localiser le point de Nishimori et en extraire certains exposant critiques. Les relations (46) sont aussi vérifiées. Le long de la ligne de Nishimori, on constate que, bien que les moments des fonctions de corrélations soient égaux deux à deux, ils ne sont pour autant pas tous égaux, ce

[4]Rappelons que dans le cas où les liens distribués de façon aléatoire sont soit positifs, soit nuls, le seul point fixe non trivial se situe à $T = 0$ et correspond bien à la percolation

qui est le cas en percolation du fait du caratère purement géométrique de celle-ci.

Au delà de la valeur précise des exposants critiques de cette nouvelle théorie conforme encore inconnue, se pose la question de classifier les différents points fixes de désordre fort que l'on peut avoir dans un système. Bien que la percolation semble être la seule issue pour le désordre non frustrant, nous pouvons nous demander si un seul point fixe gouverne le comportement de désordre fort des systèmes où la frustration joue un rôle important. Ces résultats sont directement transposables, par exemple, au modèle de Potts à trois états, où le même scénario se produit. Il existe donc une famille de théories conformes qui décrivent les points fixes de désordre fort et dont les propriétés peuvent nous apprendre beaucoup sur la physique des systèmes désordonnés en général. Un exemple auquel on pense tout de suite et celui de la transition localisé-délocalisé des fermions en deux dimensions dont le comportement décrit, entre autres, la transition de plateau dans l'effet Hall quantique [5].

Références

[1] Vik. S. Dotsenko and Vl. S. Dotsenko, Sov. Phys. JETP lett. **33**, 37 (1981) ; Adv. Phys. **32**, 129 (1983).

[2] D.C. Cabra, A. Honecker, G. Mussardo and P. Pujol, Jour. Phys. A : Math. Gen. **30**, 8415 (1997).

[3] H. Nishimori, Prog. Theor. Phys. **66**, 1169 (1981) ; J. Phys. Soc. Jpn. **55**, 3305 (1986) ; Y. Ozeki and H. Nishimori, J. Phys. A : Math. Gen. **26**, 3399 (1993).

[4] A. Georges and P. Le Doussal, *unpublished preprint* (1988), P. Le Doussal and A. B. Harris, Phys. Rev. Lett. **61**, 625 (1988), Phys. Rev. **B 40**, 9249 (1989).

[5] I. A. Gruzberg, N. Read and A. W. W. Ludwig, Phys. Rev. **B 63**, 104422 (2001).

Universality Class of the Nishimori Point in the 2D $\pm J$ Random-Bond Ising Model

A. Honecker,[1] M. Picco,[2] and P. Pujol[3]

[1]*Institut für Theoretische Physik, TU Braunschweig, Mendelssohnstrasse 3, 38106 Braunschweig, Germany*
[2]*LPTHE,* Université Pierre et Marie Curie, Paris VI, Université Denis Diderot, Paris VII Boite 126, Tour 16, 1er étage, 4 place Jussieu, 75252 Paris Cédex 05, France*
[3]*Laboratoire de Physique,† Groupe de Physique Théorique, ENS Lyon, 46 Allée d'Italie, 69364 Lyon Cédex 07, France*

(Received 11 October 2000; published 5 July 2001)

We study the universality class of the Nishimori point in the 2D $\pm J$ random-bond Ising model by means of the numerical transfer-matrix method. Using the domain-wall free energy, we locate the position of the fixed point along the Nishimori line at the critical concentration value $p_c = 0.1094 \pm 0.0002$ and estimate $\nu = 1.33 \pm 0.03$. Then, we obtain the exponents for the moments of the spin-spin correlation functions as well as the value for the central charge $c = 0.464 \pm 0.004$. The main qualitative result is the fact that percolation is now excluded as a candidate for describing the universality class of this fixed point.

DOI: 10.1103/PhysRevLett.87.047201 PACS numbers: 75.50.Lk, 05.50.+q, 64.60.Fr

In the past years, the subject of disordered systems has shown a huge renewal of interest in the condensed matter and statistical mechanics community. Among these disordered models, two-dimensional (2D) systems are of particular interest. Since the discovery of the unitary series of conformal field theory (CFT) in 1984 [1], exact values for the exponents of many well-known models of statistical mechanics have been given. However, an equivalent classification for universality classes of such systems in the presence of impurities is still missing. A first big step towards a more general classification was done recently as a random matrices classification [2]. The data for critical exponents in most of the experimental relevant fixed points for impure system are, however, still not available.

The Ising model on a square lattice is one of the most popular two-dimensional systems. It is specified by the energy of a spin configuration

$$E(\{S_i\}) = \sum_{\langle i,j \rangle} J_{i,j} \delta_{S_i,S_j}\,, \tag{1}$$

where the sum is over all bonds and the coupling constants $J_{i,j}$ are bond dependent. We consider here the $J_{i,j} = \pm 1$ random-bond Ising model (RBIM) with the following probability distribution:

$$P(J_{i,j}) = p\,\delta(J_{i,j} - 1) + (1 - p)\delta(J_{i,j} + 1)\,. \tag{2}$$

Note that, with these conventions, the pure model ($p = 0$) is characterized by $J_{i,j} = -1$ and thus has a ferromagnetic ground state.

The RBIM is similar to other relevant disordered models such as the Chalker-Coddington random network model which was proposed originally in the context of the quantum Hall effect plateau transition [3]. However, it is important to stress that these systems have a different phase diagram and therefore their fixed points have no reason to be in the same universality class [4].

The topology of the phase diagram of the RBIM depends crucially on the type of disorder one considers. An instructive example is provided by a disorder having only two possible values for the bonds with equal signs and probabilities. It is by now well established [5] that the only nontrivial fixed points are located at the extrema of the boundary of the ferromagnetic phase, corresponding to the pure Ising fixed point and a zero-temperature fixed point which turns out to be in the percolation universality class. It is interesting to notice that percolation is also the universality class of the so-called spin quantum Hall model [6], another random network model.

When the distribution also contains bonds with different signs [as in (2)], the situation is more subtle. For a certain class of probability distributions, Nishimori has shown that a so-called "Nishimori" line exists, where many properties can be calculated exactly [7]. For the probability distribution (2), this line is given by

$$e^{\beta} = \frac{1 - p}{p}\,, \tag{3}$$

with $\beta = 1/T$. On the Nishimori line, the internal energy can be calculated exactly and an upper bound can be given for the specific heat. Also of interest is an equality of the moments of the spin correlation functions (see below). Nishimori has further proven inequalities for the correlation functions which yield important constraints on the topology of the phase diagram which is shown in Fig. 1 for the $\pm J$ RBIM [8]. Since the Nishimori line is also invariant under renormalization group (RG) transformations [10], the intersection of the Nishimori line and the Ferro-Para transition line must be a fixed point. This so-called Nishimori point (N) corresponds to a new universality class belonging precisely to the family of strong disorder fixed points. The bold line in the phase diagram (Fig. 1) is the phase boundary between the ferromagnetic and paramagnetic regions. At zero temperature the model

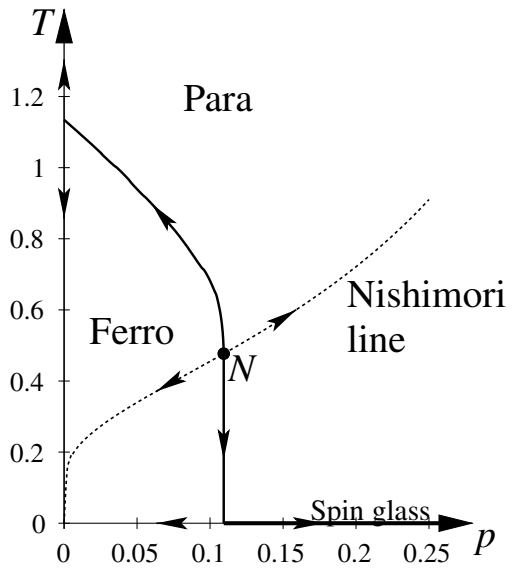

FIG. 1. Phase diagram of the two-dimensional $\pm J$ random-bond Ising model.

has a spin glass phase [11]. The three nontrivial fixed points along the bold line are the pure Ising fixed point, the Nishimori point at the crossing with the Nishimori line (dotted line), and the zero-temperature point, separating the ferro and the spin glass phases. The properties of the latter point are still mostly unknown. This point will be the subject of future investigations [12].

In the past years, many numerical and analytical efforts have been made in order to identify the universality class of the Nishimori point. Very recently, an analytic approach suggested that it is governed by an $Osp(2n + 1|2n)$ symmetry [and maybe $Osp(2n + 2|2n)$ [9]], but, unfortunately, the classification of CFTs with such symmetries is still missing. From a numerical point of view, there is by now a long list of results [13–17]. An important observation is that all the numerical results for the critical exponents tend to suggest that this point is in the percolation universality class. Because of the importance of the statistical model on its own and its relevance for understanding the plateau transition in the quantum Hall effect, it is crucial to elucidate the similarity to percolation and the relation to the supersymmetric CFT proposed in the literature.

In this Letter we provide results of extensive numerical transfer-matrix calculations of the Nishimori point with the binary distribution (2) for bonds on the square lattice. We use the domain-wall free energy to accurately locate the critical concentration of disorder p_c and to estimate the exponent ν. We then analyze the spin correlation functions and the scaling of the free energy, giving accurate and novel results for the magnetic exponent η and central charge c. Apart from improving the identification of this universality class (providing, in particular, values for the central charge which have never been measured before), our main result is that percolation is excluded as a possible candidate for describing this fixed point.

We use the free energy of a domain wall [13] to locate the critical point. For a strip of width L the domain-wall free energy d_L is defined as [18]

$$d_L = L^2(f_L^{(p)} - f_L^{(a)}), \tag{4}$$

where $f_L^{(p)}$ is the free energy *per site* of a strip of width L with *periodic* boundary conditions, and $f_L^{(a)}$ is the corresponding one with *antiperiodic* boundary conditions. d_L is an observable which can be used directly to study the RG flow under scale transformations. In particular, it is constant at a fixed point.

We have computed $f_L^{(p)} = \frac{\ln Z^{(p)}}{LN}$ and $f_L^{(a)} = \frac{\ln Z^{(a)}}{LN}$ by employing a standard transfer-matrix technique with sparse matrix factorization (see, e.g., [19]) on strips of length $N = 10^6$. Since randomness is strong, care must be taken to reduce fluctuations even if the free energies are self-averaging. Therefore, we have fixed the concentration of bonds p globally on a sample and computed $f_L^{(p)}$ and $f_L^{(a)}$ on the same sample. Still, one needs about 1000–4000 samples of $L \times 10^6$ strips to obtain sufficiently small error bars for $L \leq 12$. Even on modern computers this needs an amount of CPU time which precludes the analysis of wider strips. However, since we are looking for a fixed point, no crossover effects are expected and it is legitimate to use small system sizes.

The inset of Fig. 2 shows $d_L(p)$ along the Nishimori line (3) in the vicinity of the critical concentration p_c. A finite-size estimate for p_c is given by the crossing points $d_{L_1}(p_c) = d_{L_2}(p_c)$. After extrapolation to an infinitely wide strip (details will be given elsewhere [12]), one obtains

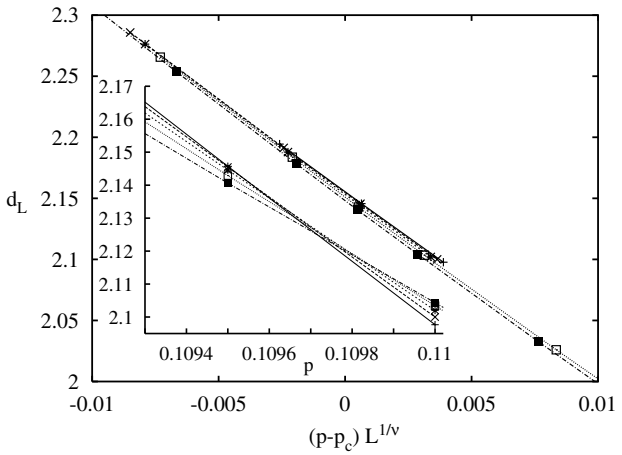

FIG. 2. Domain-wall free energy. The inset shows the raw data and the main panel shows the scaling collapse with $p_c = 0.1094$ and $\nu = 1.33$. The symbols are for $L = 8$ (filled boxes), $L = 9$ (open boxes), $L = 10$ (▫), $L = 11$ (×), and $L = 12$ (+). Error bars are much smaller than the size of the symbols.

$$p_c = 0.1094 \pm 0.0002\,. \tag{5}$$

This estimate improves upon the accuracy of earlier estimates [14–17]. It agrees perfectly with the transfer-matrix computations [14,17], while we find a slightly smaller value of p_c than [15,16]. We would like to mention that (5) is confirmed by standard Monte Carlo simulations on systems up to 32×32 sites [12]—the present estimate is just more accurate.

One can also extract the correlation length exponent ν from d_L if one assumes the scaling form

$$d_L(p - p_c) = d[(p - p_c)L^{1/\nu}]. \tag{6}$$

Again, we omit details [12] and quote just the final result

$$\nu = 1.33 \pm 0.03\,. \tag{7}$$

The main panel of Fig. 2 demonstrates that d_L follows indeed the scaling form (6) with the parameters (5) and (7).

The result (7) is in complete agreement with $\nu = 1.32 \pm 0.08$ obtained by high-temperature series [15] as well as the value $\nu = 4/3$ for percolation (see, e.g., [20]).

Another important quantity is the magnetic exponent η. This exponent can be measured, for example, by computing spin-spin correlation functions. As mentioned earlier, all along the Nishimori line the moments of these correlation functions are equal two by two:

$$[\langle S(x_1, y_1)S(x_2, y_2)\rangle^{2k-1}] = [\langle S(x_1, y_1)S(x_2, y_2)\rangle^{2k}] \tag{8}$$

for any integer k. Here $[\cdots]$ represents the average over the disorder. Assume now that the correlation functions (8) decay algebraically on a plane and define by x, y the coordinates on the infinite cylinder of circumference L, with $x \in [1, L]$ and $y \in]-\infty, +\infty[$. Using a conformal mapping, one infers then the following behavior of the correlation functions on the cylinder:

$$[\langle S(x_1, y)S(x_2, y)\rangle^n] \propto \left[\sin\left(\frac{\pi(x_2 - x_1)}{L}\right)L\right]^{-\eta_n}. \tag{9}$$

For a pure system, one has $\eta_n = n \times \eta$. On the other hand, in the case of percolation over Ising clusters, it is easy to see that the moments of spin correlation functions are all equal (and not only two by two). Then, if the Nishimori point is in the percolation universality class, the exponents for the correlation functions in (9) should collapse to a unique value $\eta_n = \eta$ at the critical point.

In order to verify this we have calculated the spin-spin correlation functions on cylinders of width L and length $400 \times L$, (i.e., with the length $\gg L$) for L up to 20. We have checked that, for width $L = 12$, lattice and finite-length corrections are of order 1%. One example of these correlation functions can be seen in Fig. 3 (with $x_1 = y = 0$ and $x_2 = x$) on a doubly logarithmic scale. One observes that the correlation functions nicely obey the power law (9), thus verifying both the correct location of the critical point as well as the functional form of the spin-spin correlation function in a finite strip.

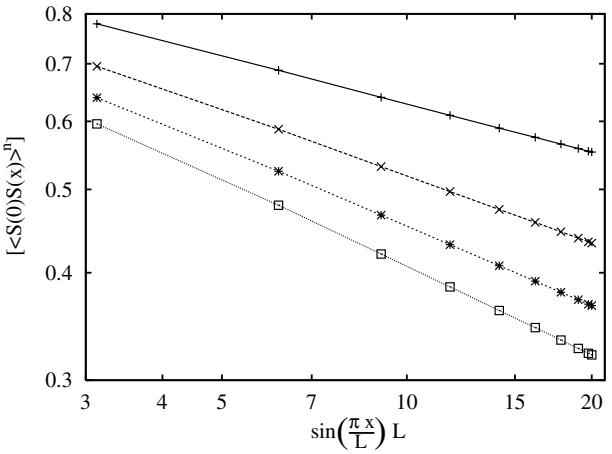

FIG. 3. Moments of the spin-spin correlation function for $p = 0.1095$ and $L = 20$. We only show the odd moments: $n = 1$ (+), $n = 3$ (×), $n = 5$ (▫), and $n = 7$ (open boxes). Error bars are smaller than the size of the symbols. The values of the exponents are given in (10).

We can then fit the exponent by studying the dependence with the distance of the correlation functions (9) or by studying the dependence with L for the fixed location $x = L/2$. The first method has proven to give smaller error bars and we obtain for the family of exponents η_n, for $p_c = 0.1095$ and $L = 20$,

$$\begin{aligned} \eta_1 &= \eta_2 = 0.1854\,, \\ \eta_3 &= \eta_4 = 0.2561\,, \\ \eta_5 &= \eta_6 = 0.3015\,, \\ \eta_7 &= \eta_8 = 0.3354\,, \end{aligned} \tag{10}$$

with relative errors, at most, of the order of 1%.

One immediately notices two things: (i) The value for η_1 differs considerably from the value of percolation $\eta = 5/24 \approx 0.2083$ (see, e.g., [20]), and (ii) the exponents for higher moments are also considerably different from η_1 which is also clear from inspection of Fig. 3.

These results are compatible with the behavior of the magnetic susceptibility that will be presented elsewhere [12]. We have also calculated estimates for the exponents assuming different values for p_c, namely, $p_c = 0.109$ and 0.110 and the results are still distinct from the ones of percolation [we obtain $\eta_1 = 0.180(1)$ for $p = 0.109$ and $\eta_1 = 0.190(1)$ for $p = 0.110$]. Moreover, it is only in the region very close to $p = 0.1095$ that we obtain a stable estimate for η_1 as we increase the width L of the lattices. One can then conclude from the exponents controlling the algebraic decay of the correlation functions that the Nishimori point is not in the percolation universality class.

Finally, we discuss the (effective) central charge c. It characterizes the number of gapless degrees of freedom at

the critical point and appears as the universal coefficient of the first finite-size correction to the free energy for periodic boundary conditions [21]

$$f_L^{(p)} = f_\infty^{(p)} + \frac{c\pi}{6L^2} + \ldots . \tag{11}$$

The leading term $f_\infty^{(p)}$ is not universal and does indeed already change when we modify the conventions for the model (1). There are higher-order finite-size corrections to the free energy, including terms of the form L^{-4}. The central charge is an important quantity identifying the CFT description [1] of a fixed point. One has $c = 1/2$ for the critical point of the pure Ising model, but it has not yet been determined for the Nishimori point.

In the process of computing d_L we have also obtained estimates of $f_L^{(p)}$ for different values of p. One can either fit these values for $f_L^{(p)}$ exactly by (11) ignoring further corrections, in which case the data for the smallest values of L should not be used, or one includes a correction term of the form L^{-4} which improves the convergence with system size. These two approaches yield consistent estimates for a given p. In addition, one can test that the result does not change significantly if other higher-order corrections are added. It should also be noted that the sensitivity of the estimates for c with respect to the location of p_c is negligible in comparison with the errors coming from the finite-size analysis. The final result is that the following is a safe estimate for c at the Nishimori point of the $\pm J$ RBIM (more details will be given in [12]):

$$c = 0.464 \pm 0.004 . \tag{12}$$

Assuming again the universality class of percolation, we would expect the value for percolation in the Ising model $c = \frac{5\sqrt{3}\ln 2}{4\pi} \approx 0.4777$ [5]. Even if our result (12) is close to this value, it can still be distinguished safely from percolation. This finding is one more argument that the Nishimori point is *not* in the universality class of percolation, at least the one expected from Ising clusters. Notice also that the central charge does not rely on a choice of observables, and this argument can then be considered as the most general one.

The results presented in this Letter provide new insight into the 2D $\pm J$ RBIM and the Nishimori point. The main result is that, according to the magnetic exponent and the behavior of the higher moments of the correlation functions, the universality class is different from the one of percolation, at least when considering the Ising spin variables as fundamental observables. This conclusion is supported by the central charge which is independent of the choice of observables and was measured here for the first time. These results and a detailed study of the zero-temperature fixed point will provide general and complete control of the RBIM, which one could consider as the simplest, but most fundamental, model for disordered systems in 2D.

We thank S. Franz, J. L. Jacobsen, J. M. Maillard, G. Mussardo, N. Read, and F. Ritort for useful discussions and comments.

*Unité Mixte de Recherche CNRS UMR 7589.
†URA 1325 du CNRS associée à l'Ecole Normale Supérieure de Lyon.

[1] A. A. Belavin, A. M. Polyakov, and A. B. Zamolodchikov, Nucl. Phys. **B241**, 333 (1984); J. Stat. Phys. **34**, 763 (1984).
[2] M. R. Zirnbauer, J. Math. Phys. **37**, 4986 (1996); A. Altland and M. R. Zirnbauer, Phys. Rev. B **55**, 1142 (1997).
[3] S. Cho and M. P. A. Fisher, Phys. Rev. B **55**, 1025 (1997).
[4] J. T. Chalker, N. Read, V. Kagalovsky, B. Horovitz, Y. Avishai, and A. W. W. Ludwig, cond-mat/0009463.
[5] J. L. Jacobsen and J. L. Cardy, Nucl. Phys. **B515**, 701 (1998).
[6] I. A. Gruzberg, A. W. W. Ludwig, and N. Read, Phys. Rev. Lett. **82**, 4524 (1999); J. Cardy, Phys. Rev. Lett. **84**, 3507 (2000).
[7] H. Nishimori, Prog. Theor. Phys. **66**, 1169 (1981); J. Phys. Soc. Jpn. **55**, 3305 (1986); Y. Ozeki and H. Nishimori, J. Phys. A **26**, 3399 (1993).
[8] Different variants of the phase diagram Fig. 1 have been presented before, in particular in [9] which we refer to for further comments and references regarding global properties of the phase diagram.
[9] I. A. Gruzberg, N. Read, and A. W. W. Ludwig, Phys. Rev. B **63**, 104422 (2001).
[10] A. Georges and P. Le Doussal, report, 1988 (unpublished); P. Le Doussal and A. B. Harris, Phys. Rev. Lett. **61**, 625 (1988); Phys. Rev. B **40**, 9249 (1989).
[11] I. Morgenstern and K. Binder, Phys. Rev. B **22**, 288 (1980); I. Morgenstern and H. Horner, Phys. Rev. B **25**, 504 (1982); W. L. McMillan, Phys. Rev. B **28**, 5216 (1983).
[12] A. Honecker, M. Picco, and P. Pujol (unpublished).
[13] W. L. McMillan, Phys. Rev. B **29**, 4026 (1984).
[14] Y. Ozeki and H. Nishimori, J. Phys. Soc. Jpn. **56**, 3265 (1987).
[15] R. R. P. Singh and J. Adler, Phys. Rev. B **54**, 364 (1996).
[16] Y. Ozeki and N. Ito, J. Phys. A **31**, 5451 (1998).
[17] F. D. A. Aarão Reis, S. L. A. de Queiroz, and R. R. dos Santos, Phys. Rev. B **60**, 6740 (1999).
[18] We omit a factor β since it is not important at finite temperature.
[19] M. P. Nightingale, in *Finite Size Scaling and Numerical Simulations of Statistical Physics,* edited by V. Privman (World Scientific, Singapore, 1990), pp. 287–351.
[20] D. Stauffer and A. Aharony, *Introduction to Percolation Theory* (Taylor & Francis, London, 1994), 2nd ed.
[21] H. W. J. Blöte, J. L. Cardy, and M. P. Nightingale, Phys. Rev. Lett. **56**, 742 (1986); I. Affleck, Phys. Rev. Lett. **56**, 746 (1986).

2.2.2 Systèmes avec contraintes et dynamique lente sans désordre

Les systèmes avec des contraintes forment un domaine de la mécanique statistique qui suscite de plus en plus d'intérêt. Dans cette section nous allons discuter un modèle qui met en évidence les divers comportements inhabituels que l'on peut trouver dans de tels systèmes. La présence de contraintes peut tout d'abord donner lieu à un espace de phases de topologie ou connectivité hautement non-triviale. Ceci peut entraîner à son tour un comportement statique, d'équilibre, très exotique. Finalement, un diagramme de phase trop intriqué aura aussi des conséquences sur le comportement dynamique du système qui peut se retrouver hors équilibre, comme dans les systèmes désordonnés. Cependant, le comportement hors équilibre que nous trouvons dans ce genre de systèmes est obtenu sans la présence d'impuretés, mais à cause de raisons topologiques dues aux contraintes.

Considérons le réseau hexagonal où à chaque lien on associe une couleur, qui peut être rouge, bleu ou vert (ou A, B et C). Nous allons imposer que sur les trois liens qui rejoignent chaque vertex, les trois couleurs doivent être présente (voir figure (6)). Il est très facile de se convaincre qu'il existe plusieurs façon de colorer le réseau tout en respectant la contrainte à chaque vertex. De façon plus précise, Baxter [1] a montré que le nombre de configurations possibles augmente avec le nombre de sites N comme W^N avec $W = 1.2087....$ Cette entropie extensive du système a des conséquences très intéressantes : par une description en termes d'un modèle de hauteurs à deux composantes [2], on peut montrer que la description à grandes échelles du système est une théorie conforme, plus précisément un modèle de WZNW $SU(3)_1$ dont la charge centrale est 2. La présence de degrés de liberté critiques peut être mise en évidence en calculant, par exemple, des fonctions de corrélation. Imaginons que nous prenions un chemin formé par des liens rouges et bleus successifs. Il est clair que, vue la contrainte imposée sur chaque vertex, ce chemin doit forcément être une boucle fermée. Imaginons maintenant que dans cette boucle, nous fixons deux points, comme dans la figure (7), et permutons les couleurs rouge et bleu dans seulement un coté de la boucle. Ces deux points $\vec{r}_1$ et $\vec{r}_2$ vont alors correspondre à des vertex où la contrainte n'est pas satisfaite, le premier aura deux liens bleus et le second aura deux liens rouges, on dira qu'ils correspondent à des défauts. Nous pouvons ensuite définir une fonction de partition où l'on compte toutes les configurations de coloriage possibles dont tous les vertex satisfont à la contrainte, sauf les deux vertex où se situent les défauts $Z(\vec{r}_1, \vec{r}_2)$. Si nous définissons ensuite la fonctions de corrélation défaut-défaut comme le rapport entre $Z(\vec{r}_1, \vec{r}_2)$ et la fonction de partition du modèle sans défauts Z (*i.e.* W^N), nous obtenons une décroissance algébrique avec la distance entre les deux défauts pour $|\vec{r}_1 - \vec{r}_2| \to \infty$:

$$\frac{Z(\vec{r}_1, \vec{r}_2)}{Z} \propto \frac{1}{|\vec{r}_1 - \vec{r}_2|}. \tag{47}$$

ce résultat est un exemple parmi d'autres qui mettent en évidence la présence

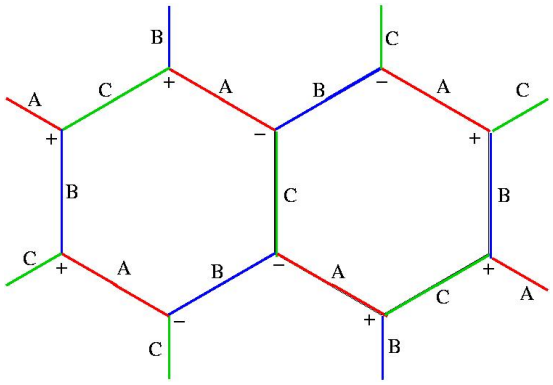

FIG. 6 – Le coloriage du réseau hexagonal avec trois couleurs. Dans chaque vertex, en fonction de la parité dans l'ordre tournant des couleurs, on peut définir un spin d'Ising $\pm$. Ces spins doivent satisfaire à la contrainte que l'aimantation totale de chaque hexagone soit $0,\ \pm 6$.

sous-jacente d'une théorie conforme, due uniquement au caractère entropique de notre système.

Examinons maintenant un coloriage particulier du réseau pour remarquer que, à chaque vertex, on peut associer un spin d'Ising ± 1 en fonction de l'ordre horaire ou anti-horaire des couleurs autour de ce vertex (voir figure 6). Il est clair que, à une valeur du spin correspondent trois configurations de couleurs associées aux permutations cycliques que l'on peut faire sur celles-ci. D'un autre coté, toute configuration de spins que l'on peut construire dans le réseau ne correspond pas à une configuration de couleur particulière (modulo $\mathbb{Z}_3$). En effet, les spins construits à partir des couleurs satisfont à une contrainte pour chaque hexagone qui est :

$$\sum_{i=1..6} \sigma_i = 0,\ \pm 6 \tag{48}$$

où l'indice i étiquette tous les spins autour d'un hexagone. Nous donnons dans l'article présenté dans cette section une preuve de ce résultat basée sur une description en termes d'un champ de jauge et de quantification du flux magnétique pour que la distribution de couleurs soit auto-cohérente.

Jusqu'à présent l'intérêt de notre modèle est basé sur une entropie extensive et nous n'avons introduit aucun terme d'énergie. Nous allons le faire maintenant par l'intermédiaire des spins de chiralité et discuterons plus tard pourquoi ce choix est le plus pertinent pour les conditions expérimentales que nous voulons décrire avec ce modèle. Nous proposons alors le Hamiltonien :

$$H = -J \sum_{<ij>} \sigma_i \sigma_j \tag{49}$$

où la somme se fait sur les couples de sites $< ij >$ plus proches voisins sur le

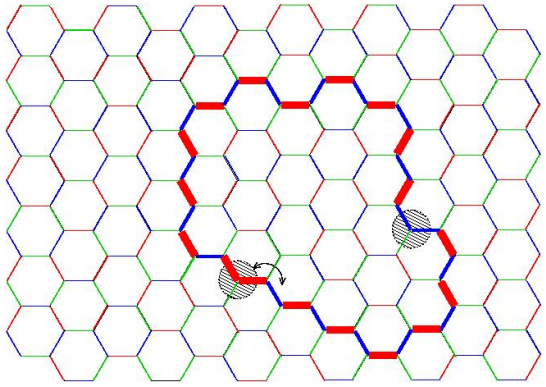

FIG. 7 – Création d'une paire de défauts dans le modèle de couleurs, en permutant les couleurs dans une boucle rouge-bleu uniquement dans une section incomplète de la boucle.

réseau. Pour $|J/T| << 1$ nous pouvons utiliser la description de théorie conforme pour discuter le comportement du système en présence de ce terme d'énergie. Dans l'article nous discutons comment ce terme introduit une perturbation marginale pertinente pour $J < 0$ (couplage AF) et marginale non-pertinente pour $J > 0$ (couplage Ferro). De ce fait, pour $J < 0$, le système développe un ordre AF à toute température finie, alors que pour $J > 0$ le système reste critique. Cette approche est perturbative et valable pour $|J/T| << 1$ et ne peut nous renseigner sur le comportement pour $|J/T|$ plus grand.

Pour étudier le régime de plus basses températures nous devons donc abandonner l'approche perturbative à partir de la théorie conforme et utiliser une technique de champ moyen adaptée aux systèmes avec contraintes [3]. Cette technique correspond à une généralisation du champ moyen standard. Au lieu de considérer un seul spin couplé à un champ moléculaire nous allons considérer un cluster, qui dans ce cas correspond à un hexagone, et calculer la fonction de partition de cet amas de spins en fonction d'un champ effectif représentant le couplage au reste du réseau. Cette technique s'avère être très précise ; elle permet par exemple de donner une estimation de l'entropie de Baxter pour $T \to \infty$: 1.1726 (comparer avec la valeur exacte 1.2087), et plus important encore elle prédit une transition de phase du premier ordre vers une phase d'ordre Ferro à la température $T \sim 9.872J$. Le réseau hexagonal étant bipartite, en l'absence de contrainte sur les spins le comportement pour J positif et négatif est équivalent, avec une transition du deuxième ordre à la même température des deux cotés. Or ici, à cause des contraintes, le système AF s'ordonne pour toute température finie alors que le cas Ferro présente une transition du premier ordre. ce comportement est d'autant plus exotique que la phase ordonnée du cas Ferro est très particulière. En effet, pour toute température $T < T_c$, le système a un ordre ferromagnétique parfait, ou saturé $< M >= 1$. Pour comprendre la raison de ce

comportement assez anti-intuitif, il suffit de se placer sur l'un des deux états de plus basse énergie (*i. e.* parfaitement ordonné) et essayer de créer une excitation pour comparer le gain entropique et la perte énergétique. Créer une excitation élémentaire tout en respectant la contrainte consiste à choisir une boucle de couleur, disons rouge-bleu, et de changer le signe de tous les spins présents dans cette boucle. Or, dans l'état parfaitement ordonné, on peut se convaincre facilement que les boucles de couleurs sont des chemins droits qui partent à l'infini, ou dans un système avec des conditions aux bords périodiques (un tore) s'enroule autour du tore. Une excitation fondamentale coûtera donc un prix énergétique de l'ordre de grandeur L, la taille linéaire du système. D'autre part, le système possède L de ces boucles que l'on peut créer comme excitation, ce qui donne une entropie de l'ordre de $ln(L)$. On voit donc que, contrairement aux cas du système sans contraintes où, à toute température non-nulle il sera toujours pour des raisons d'entropie favorable de créer des excitations, ici, dans la limite thermodynamique, le coût énergétique l'emportera toujours sur le gain entropique, et il ne sera donc pas favorable de créer des excitations même à température non-nulle. Une fois atteinte la température T_c, il sera plus favorable de désordonner complètement le système plutôt que de créer un nombre fini d'excitations, et le système basculera donc de l'ordre parfait au désordre complet. Cette particularité de l'état thermodynamique du système à $T < T_c$ nous permet d'obtenir une estimation très précise de la température critique. En effet, dans la phase désordonné le système s'équilibre facilement et l'on peut tracer sans problèmes la courbe de l'énergie interne en fonction de la température. En intégrant cette courbe on obtient donc la valeur de l'énergie libre en fonction de T. D'un autre coté, l'énergie libre pour $T < T_c$ est tout simplement donnée par l'énergie interne de l'état complètement ordonné. En comparant les deux courbes d'énergie libre on obtient le point de croisement qui nous donne : $T_c \sim 9.6J$, résultat très proche de celui obtenu par la méthode de champ moyen de clusters.

Les propriétés à l'équilibre statique du système permettent d'envisager un comportement dynamique assez intéressant. Pour envisager une dynamique de type Monte Carlo, le premier pas consiste à identifier la mise à jour microscopique, ou élémentaire dans notre dynamique de MC. Sachant que la contrainte sur chaque vertex doit être satisfaite à chaque mise à jour, il est clair que l'algorithme naturel pour les mises à jour est de repérer de façon aléatoire des boucles de couleur et de permuter les couleurs dans celles-ci, ce qui revient à inverser tous les spins parcourus par cette boucle. Bien que ces mises à jour soient hautement non-locales, nous montrerons dans la suite qu'elles correspondent à une dynamique accélérée de la réalisation expérimentale que nous discutons plus bas. De ce fait, tout phénomène de dynamique lente présent dans les simulations MC le sera déjà dans le cadre d'une dynamique accélérée par rapport au comportement microscopique du système réel.

Le comportement dynamique ainsi étudié est très riche et tous les détails peuvent être trouvés dans l'article inclus dans cette section. Si l'on fait une ex-

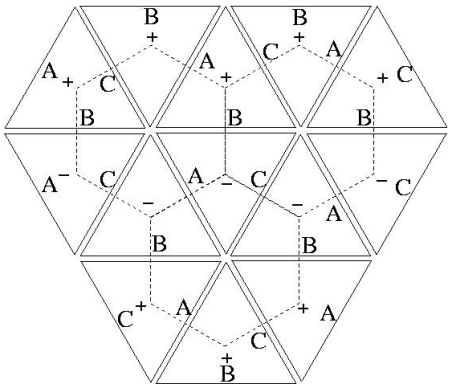

FIG. 8 – Une matrice formée de pastilles triangulaires couplées par des jonctions Josephson. Les spins de chiralité sont situés au centre des pastilles triangulaires et le réseau hexagonal dual est représenté en pointillés.

périence de refroidissement à partir d'un régime de haute température avec différents taux de refroidissement on observe le comportement suivant : Une mesure du paramètre d'ordre d'aimantation nous dit que le système ne s'aimante pas, même pour des températures très basses et avec un taux de refroidissement très lent. Si en revanche on s'intéresse à l'énergie interne, on observe, toujours pour des taux de refroidissement lents, une chute assez rapide au voisinage de T_c avec un comportement hystérétique assez typique des transitions du premier ordre. Cependant, même pour les taux de refroidissement les plus lents utilisés dans cette simulation, la valeur de l'énergie interne n'atteint jamais sa valeur d'équilibre, qui comme nous l'avons dit correspond à sa valeur minimale pour $T < T_c$. Si l'on fait une "photographie" du système à $T = 0$ après un refroidissement lent, comme nous en montrons plusieurs dans l'article, nous observons que la configuration d'ordre parfait n'est pas atteinte, mais en revanche, une configurations de quasi-cristaux peut être observée. Le système reste gelé dans une configuration où des domaines de spins + et − ont une forme de diamant avec des parois de domaines de forme rectiligne. La forme très particulière des ces domaines est clairement due à la contrainte d'aimantation $\pm 6,\ 0$ qui doit être satisfaite sur chaque hexagone. Malgré l'absence de désordre, nous avons donc un comportement hors équilibre du système exclusivement due à la faible connectivité de l'état de plus basse énergie avec le reste de l'espace de phases. Pour comprendre pourquoi ces domaines restent 'gelés' dans cette configuration il faut voir quel type de mise à jour intervient pour faire évoluer le système. Une fois cette configuration quasi-cristalline atteinte, les boucles bicolores que l'on doit suivre pour permuter tous les spins qui y sont présent forment des chemins qui traversent au moins trois domaines et dont la longueur est du même ordre de grandeur que la taille de ceux-ci. La mise à jour de cette seule boucle donnera une configuration d'énergie plus haute et il faudra donc renverser les spins de plusieurs de ces boucles avant

d'obtenir une configuration d'énergie plus basse que celle de la configuration initiale. En d'autre termes, pour faire nucléer plusieurs domaines en un seul (et faire ainsi croître la taille des domaines) il faut franchir une barrière énergétique qui augmente avec la taille des domaines. Ce phénomène donne lieu à une croissance très lente des domaines, typiquement logarithmique, et ceci dans le contexte de la dynamique de mise à jour de boucles qui peut être considérée déjà comme une dynamique accélérée.

La description du comportement statique et dynamique de ce modèle ayant été faite, nous pouvons discuter des réalisations expérimentales possibles. Un premier exemple que nous ne mentionnons que très rapidement correspond à un réseau de kagomé supraconducteur de fil d'Aluminium à 2^oK [4], en présence d'un champ magnétique réglé de telle façon que le flux traversant chaque triangle de kagomé soit un demi quantum de flux. Il est clair qu'un courant va se produire dans les fils de façon a compenser ou compléter ce flux et obtenir, soit zéro, soit un quantum de flux (voir [4] pour les détails). On peut donc définir un spin de chiralité au centre de chaque triangle formant ainsi le réseau hexagonal. Dans ce contexte, la contrainte sur l'aimantation des hexagones $0, \pm 6$ correspond à la quantification du flux magnétique traversant les hexagones du réseau de kagomé formé par les fils. Bien que notre modèle donne une idée très proche du comportement de cette réalisation expérimentale, le terme d'énergie et l'évolution dynamique de celle-ci ne correspondent pas tout à fait à celle que nous avons choisie pour notre modèle. Ce système présente toute fois un comportement de dynamique lente que l'on peut parfaitement comprendre grâce à l'étude de notre système.

Une réalisation expérimentale que nous prétendons être plus proche de notre modèle, aussi bien pour le Hamiltonien que pour le comportement dynamique, correspond à un arrangement de pastilles supraconductrices faites de Sr_2RuO_4, un matériau qui a un paramètre d'ordre supraconducteur du type $p_x \pm ip_y$. Imaginons que nous prenons des pastilles triangulaire de ce matériau (voir figure (8)) que nous couplons avec des jonctions Josephson. En parcourant le périmètre de chaque pastille nous verrons donc l'argument du paramètre d'ordre changer de 0 à 2π dans le sens horaire ou anti-horaire. En passant du centre d'une arête du triangle à celui de l'arête suivante, nous aurons donc une différence d'angle dans la phase du paramètre d'ordre de $\pm 2\pi/3$. Nous montrons dans l'article présenté ici comment le terme dominant du tunneling à travers la jonction impose que la phase du paramètre d'ordre de chaque coté de la jonction soit la même. Considérant cette phase au centre de l'arête du triangle, nous voyons donc que, modulo une rotation $U(1)$ globale de la phase de tous les triangles nous pouvons définir trois couleurs A, B et C, correspondant aux angles 0, $2\pi/3$ et $-2\pi/3$ et qui coïncident de chaque coté de la jonction. A l'aide de la figure (8) nous pouvons donc voir que nous avons une réalisation de notre modèle de couleurs dans le réseau hexagonal. Le terme sous-dominant du tunneling à travers la jonction donnera un couplage entre les spins de chiralité de chaque triangle qui est celui que nous avons considéré dans notre modèle. La contrainte sur les hexagones apparaît en-

core une fois de façon naturelle comme la condition sur le paramètre d'ordre supraconducteur pour être univalué. Au delà du comportement statique, nous présentons dans l'article les défauts toplogiques (vortex) qui peuvent être formés le plus facilement dans cet arrangement supraconducteur. Ils correspondent justement aux défauts de boucles que nous avons présentés auparavant et sont précisément les générateurs des mises à jours de boucles que nous utilisons dans notre évolution dynamique de Monte Carlo. Notre algorithme correspond donc à une dynamique accélérée de celle de ce système et le comportement aussi bien statique que dynamique que nous avons présenté est donc réaliste pour cette réalisation expérimentale en absence de défauts. Il est clair que des défauts seront toujours présents, ce qui correspond à des violations de la contrainte d'hexagones occasionels, ce qui à son tour lissera le comportement statique si exotique que nous avons présenté ici. Par ailleurs, pour des ordres de grandeur de temps plus importants, le système ne restera pas gelé mais évoluera par la prolifération de défauts topologiques jusqu'à l'obtention d'une configuration d'équilibre. On aura en fait un passage du régime de temps 'courts', où la dynamique est gelée, à celui des temps très longs, avec une croissance de domaine traditionnelle, et où, pour des échelles de temps intermédiaires, on aura un comportement dynamique encore plus semblable à celui des verres structurels qui présentent du vieillissement. L'extension de cette étude au cas où la contrainte forte est remplacée par un terme énergétique qui rend possible, à des échelles de temps très grandes, la prolifération de défauts, nous permettrait alors de décrire les différents régimes de fragilité de notre système à dynamique lente.

Références

[1] R. J. Baxter, J. Math. Phys. **11**, 784 (1970).

[2] J. Kondev and C. L. Henley, Nucl. Phys. **B 464**, 540 (1996) ;
J. Kondev, J de Gier and B. Nienhuis, J. Phys. A : Math. Gen. **29**, 6489 (1996).

[3] V. G. Vaks *et al.*, Sov. Phys. Usp. **26**, 1059 (1984).
V. G. Vaks and V. I. Zineko, J. Phys. C : Solid State Phys. **19**, 3083 (1986).

[4] M. J. Higgins *et al.*, Phys. Rev. **B 61**, R894 (2000).
K. Park and D. A. Huse, Phys. Rev. **B 64**, 134522 (2001).

Dynamical obstruction in a constrained system and its realization in lattices of superconducting devices

Claudio Castelnovo,[1] Pierre Pujol,[1,2] and Claudio Chamon[1]
[1]*Physics Department, Boston University, Boston, Massachusetts 02215, USA*
[2]*Laboratoire de Physique, Groupe de Physique Théorique de l'École Normale Supérieure, Lyon, France*
(Received 13 November 2003; published 29 March 2004)

Hard constraints imposed in statistical mechanics models can lead to interesting thermodynamical behaviors, but may at the same time raise obstructions in the thoroughfare to thermal equilibration. Here we study a variant of Baxter's three-color model in which local interactions and defects are included, and discuss its connection to triangular arrays of Josephson junctions of superconductors with broken time-reversal symmetry and *kagomé* networks of superconducting wires. The model is equivalent to an Ising model in a hexagonal lattice with the additional constraint that the magnetization of each hexagon is ± 6 or 0. Defects in the superconducting models correspond to violations of this constraint, and include fractional and integer vortices, as well as open strings within two-color loops. In the absence of defects, and for ferromagnetic interactions, we find that the system is critical for a range of temperatures (critical line) that terminates when it undergoes an exotic first-order phase transition with a jump from a zero magnetization state into the fully magnetized state at finite temperature. Dynamically, however, we find that the system becomes frozen into domains. The domain walls are made of perfectly straight segments, and domain growth appears frozen within the time scales studied with Monte Carlo simulations, with the system trapped into a ''polycrystalline'' phase. This dynamical obstruction has its origin in the topology of the allowed reconfigurations in phase space, which consist of updates of closed loops of spins. Only an extreme rare-event dominated proliferation of confined defects may overcome this obstruction, at much longer time scales. Also as a consequence of the dynamical obstruction, there exists a dynamical temperature, lower than the (avoided) static critical temperature, at which the system is seen to jump from a ''supercooled liquid'' to the polycrystalline phase within our Monte Carlo time scale. In contrast, for antiferromagnetic interactions, we argue that the system orders for infinitesimal coupling because of the constraint, and we observe no interesting dynamical effects.

DOI: 10.1103/PhysRevB.69.104529 PACS number(s): 74.81.Fa, 64.70.Pf

I. INTRODUCTION

Systems with hard constraints often display interesting thermodynamic properties such as infinite-order phase transitions or, on the contrary, very sharp first-order phase transitions. Many of these models can be described in terms of vertex models and some of them are exactly solvable. Examples of such systems are given by dimer models,[1] the planar ice model,[2] or the three-coloring model of the hexagonal lattice.[3]

It is very natural to ask whether the hard constraint, which leads to the interesting thermodynamics, may at the same time pose obstructions in the (possible) path to thermal equilibration. In essence, equilibrium properties require averages over all the configurations allowed by the constraint, weighted in accordance with the appropriate Boltzmann-Gibbs distribution. Dynamically, the system must sample the different allowed states in a manner that satisfies detailed balance. However, leaping from an allowed configuration to another might require large rearrangements, and physically one must investigate which mechanisms could possibly lead to these moves in phase space and what are the corresponding time scales. Sometimes the constraint forbids any local rearrangement of the system (as in the present case), and it ought to be softened in order to allow for a local dynamics. The system then evolves by formation of constraint-violating defects that propagate and recombine.

Plenty of issues arise regarding the dynamical generation and recombination of defects, which depend on the microscopic details of the physical system, and the energetics of the states outside the manifold of constraint-satisfying states. For example, paying the energy cost to create a defect already slows down the dynamics; however, this waiting for the defect generation simply rescales the time scales for dynamical evolution in a trivial way. More interesting are those issues related to the possible energy costs for moving defects around. In particular, if the microscopics are such that the defects (when created in pairs) are confined, one would expect further and nontrivial slowing down of the dynamics.

Glassy behavior in constrained three-color models with infinite range interactions has indeed been recently found by Chakraborty, Das, and Kondev.[4] This is an interesting example of glassy behavior in a Hamiltonian model without quenched disorder, where it was found that the characteristic time scales obeyed a Vogel-Fulcher law as the temperature approached a dynamical transition temperature, mimicking fragile structural glasses. In order to maneuver within the phase space of allowed states, nonlocal loop dynamics was implemented.

In this paper, we study variations of the Baxter three-color model with short-range interactions and discuss the possible mechanism for defect motion. In particular, we argue that the loop updates used by Chakraborty *et al.*[4] correspond to the unbinding of certain defect pairs that are deconfined, and thus they are the least costly mechanism for dynamical evo-

lution. We find that finite range ferromagnetic interactions lead to a frozen ''polycrystal,'' as opposed to a fragile glass as in the case of infinite range interactions. We present two possible experimental realizations using lattice arrays of superconducting devices that could in principle be experimental settings for studying sluggish relaxation or nonequilibrium effects in Hamiltonian systems without quenched disorder.

In Sec. II we present in detail the three-color model, and show that it is equivalent to an Ising model on a hexagonal lattice, with the constraint that the magnetization of each hexagon must be ± 6 or 0. In the Ising language the extra interaction that we add to the three-color model has a simple form: it is a nearest-neighbor spin-spin interaction. Such interaction is present in the possible experimental realizations of the model in two different two-dimensional (2D) superconducting geometries. Because of the constraint imposed on the plaquettes, the system is critical in the absence of two-spin interactions ($J=0$) and is described by a $c=2$ conformal field theory (CFT).[5] In Sec. III, we use this description to argue about the behavior of the model in the presence of nonzero two-spin interactions. While for arbitrarily small antiferromagnetic coupling ($J<0$) the system orders, it remains critical for small ferromagnetic coupling ($J>0$). The CFT description near the $J=0$ point is ill suited for strong couplings. In this regime we use instead a cluster mean-field method (CMFM) which has proven to be very accurate in describing constrained system such as the ice model.[6] We find a strong first-order phase transition where the system jumps from the disordered configuration to the fully magnetized ferromagnetic state (FMFS).

When the hard constraint is softened, defects are allowed in the system at a high-energy scale U, which enters in the defect formation energy and in the defect pair interactions. In Sec. IV, we discuss the role of these defects and their implications in the dynamics of the system. In the superconducting realizations there are a number of different defects: fractional vortices, integer vortices, and open segments of closed two-color loops. Integer and fractional vortices can be shown to be confined below a Kosterlitz-Thouless transition temperature that can be rather high depending on the energy scale U. Thus, these defects are rather ineffective as a mechanism to move from one allowed state to another. We show, on the other hand, that the end points of open segments of closed loops made of two alternating colors are deconfined, they can move around and travel a whole closed loop, and therefore they are the main actors for the evolution of the system. For defect formation rates much smaller than the defect recombination rates, this evolution corresponds essentially to the loop dynamics that we use in the present paper.

In Sec. V we study the dynamics of the constrained system. By fitting the value of the free energy for the disordered state as a function of temperature and comparing it to the one of the ordered state we first obtain an accurate estimate for the transition temperature, which is in good agreement with the result from the CMFM. We then show that there is no sign of the above-mentioned thermodynamic transition to the FMFS. The system instead becomes supercooled and undergoes a lower-temperature nonequilibrium transition from the supercooled liquid phase to a frozen ''polycrystalline'' phase. The transition shows features that are characteristic of first-order phase transitions, such as a hysteretic behavior as a function of temperature. The underlying physics behind this phenomenon is understood by studying the spin-spin autocorrelation function as well as the evolution of the internal energy and other physical quantities when we cool the system at different cooling rates or after a quench from infinite temperature.

II. THE MODEL AND ITS POSSIBLE EXPERIMENTAL REALIZATIONS

In this section we review Baxter's three-color model, and present two of its possible experimental realizations in lattices of superconducting devices in some detail. We show that the three-color model and these two realizations can be described as an Ising model on a hexagonal lattice, with a plaquette constraint of $\pm 6,0$ for the sum of the spins around each hexagon. It is important to notice that while the three-color model is only $\mathbb{Z}_2$ symmetric in the Ising spin representation, the superconducting realizations have a larger $\mathbb{Z}_2 \times \mathrm{U}(1)$ symmetry due to the superconducting phase. This difference is particularly relevant for the possible defects that can originate in an allowed configuration and for their dynamic behavior.

The one extra ingredient that we add to Baxter's three-color model is a local interaction. In the Ising spin representation, this interaction takes the form of a nearest-neighbor spin-spin interaction. It has the effect, in the three-color model, of favoring or opposing to the alignment of bonds of the same color on neighboring sites. The extra interaction is responsible for all the interesting thermodynamical and dynamical effects that are studied in this paper. Moreover, in the lattices of superconducting devices these interactions are always present.

A. The three-color model

The three-color model consists of vertices having three bonds of different colors: A, B and C. These different colors can be thought of as three different phases differing pairwise by $\pm 2\pi/3$, which is how we will later connect the model to arrays of superconducting devices. One can naturally associate to each vertex a chirality spin ± 1 depending on the counterclockwise or clockwise ordering of the phases, as shown in Fig. 1. A hexagonal lattice is constructed with these vertices by connecting the bonds, where the connected bonds must share the same color. As we show below, the chirality spins cannot adopt an arbitrary configuration. Indeed, the spins must satisfy the constraint that their sum around any hexagon of the lattice is $\pm 6,0$. On the other hand, given an allowed configuration of the spins, there are clearly three different corresponding color configurations, since any global even permutation of the colors in the lattice gives rise to the same spin configuration. In the absence of any kind of interaction this model corresponds to the Baxter's three-coloring model on the hexagonal lattice. The partition function Z has a purely entropic origin and its value is given by

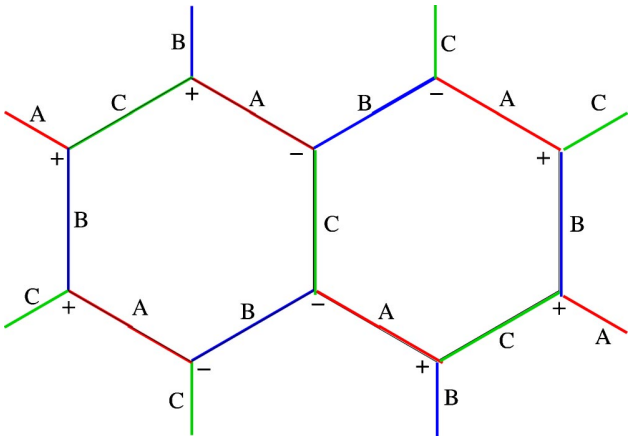

FIG. 1. (Color online) The gluing of the ABC vertices gives Baxter's three-coloring model on the hexagonal lattice. To every vertex we can associate a chirality spin depending on the order in which the three colors appear counterclockwise around the vertex: $+/-$ for even/odd permutations of the sequence ABC.

the number of ways of coloring the bonds of the hexagonal lattice. This number is known to grow exponentially with the system size. Indeed, Baxter solved exactly this model and showed that $Z=W^N$ for large values of the number of sites N, where $W=1.2087\ldots$ is the entropy per site.[3]

It is worth discussing in detail how the system can rearrange from one allowed configuration to another. No single-bond flip or double-bond exchange is allowed without violating the constraint in the neighboring vertices. However, we can notice that by choosing one vertex and two colors, say A and B, we can uniquely define a loop by taking the sequence of ABAB . . . bonds starting from the chosen vertex. The loop must be non-self-intersecting and closed, the last property holding only if the system has periodic boundary conditions. Clearly, if we pick one such loop and we flip the color sequence, say ABAB . . . to BABA . . . , the color constraint is preserved. These loop flips (or updates) provide a mechanism for the system to move around the phase space of allowed configurations. In Sec. IV we will show how the loop updates originate from local constraint-violating defects.

Notice that, given any allowed configuration, every vertex belongs to one and only one of such loops. Thus, by simply removing all the bonds of one of the three colors (say C), we realize one of the three possible simultaneous mappings of the system to a fully packed loop configuration on the hexagonal lattice which, at large scales, can be described by an SU(3) level 1 Wess-Zumino-Novikov-Witten (WZNW) model.[5]

The three-color model becomes even richer when we introduce a nearest-neighbor spin-spin interaction in the Ising representation, which we do in Sec. II E, after we discuss the experimental realizations right below.

B. The Josephson-junction array of superconductors

A possible experimental realization of the model is given by a Josephson-junction array of triangles of a superconductor with broken time-reversal symmetry. For example, there is experimental evidence of a $p_x \pm ip_y$ order parameter in the compound Sr_2RuO_4;[7,8] here the two possible states $p_x \pm ip_y$ correspond to the chirality spin ± 1 defined above. The same geometry we propose here with $p \pm ip$ states has also been studied by Moore and Lee, who in addition to the p-wave states have also looked at $d \pm id$ superconductors,[9] believed to be realized by the recently discovered hydrated cobalt oxide compounds. In their work, they have also discussed other type of arrays in triangular and square lattices.

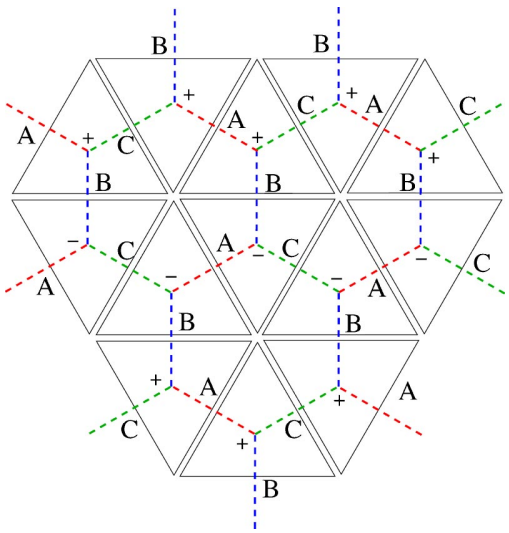

FIG. 2. (Color online) An example of the correspondence between the Josephson-junction array and the three-color model, provided we identify the three colors with the values of the phases of the order parameter in the middle of each triangle edge. Notice that ferromagnetic order among nearest-neighboring spins corresponds to aligning the bonds with the same color along the same direction.

In the $p_x \pm ip_y$ Josephson-junction arrays, the three colors correspond to the three relative phases of the order parameter in the middle of each of the edges of the triangles, which differ by $\pm 2\pi/3$ (see Fig. 2). (To be precise, the phase of the order parameters is defined in momentum space; but, as it can be deduced from the analysis carried out in the Appendix, one can think in real space by considering the phases for the momenta that point along the directions perpendicular to the three faces of each triangle.) The superconducting order parameter of each triangle has also an overall U(1) degree of freedom. Therefore, at the center of each of its three edges, one can define a phase $\theta_{i,a}=\theta_i \pm (2\pi/3)a$ for the triangle at site i, along its ath edge ($a=0,1,2$), where the edges are labeled counterclockwise starting from the horizontal one (see Fig. 3). The $\pm$ sign corresponds to the chirality $\sigma_i = \pm 1$ of the $p_x \pm ip_y$ state at site i. The Josephson coupling $-U\cos(\theta_{i,a}-\theta_{j,a})$ along an edge shared by two neighboring triangles tends to align the phases $\theta_{i,a}$ and $\theta_{j,a}$. In the $U \to \infty$ limit one recovers Baxter's three-coloring model, modulo a global U(1) phase. Notice that, in this infinite U coupling limit, the only difference between this system and the three-color model (in the spin representation) described in the preceding section is a $\mathbb{Z}_2 \times U(1)$ symmetry instead of a simple $\mathbb{Z}_2$ symmetry. We will show in Sec. IV how this dif-

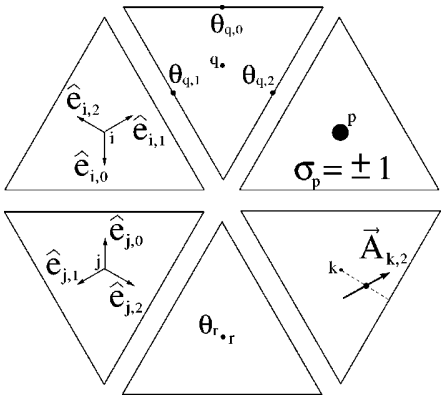

FIG. 3. Labeling of the edges of the up and down triangles, with the relative unit vectors $\hat{e}_{i,a}$. While the chirality spins σ_p sit at the centers of the triangles, the ''gauge'' fields (an example of which is shown in one of the triangles) sit at the midpoints of the segments joining the centers of the triangles to the corresponding edges. Examples of the U(1) phase θ_r and of the edge phases $\theta_{q,a}$, $a=0,1,2$ are also shown.

ference allows for a wider variety of defects in the Josephson-junction array rather than in the three-coloring model.

C. The kagomé network of superconducting wires

Another (related) realization of the three-color model is given by a superconducting *kagomé* wire network in the presence of a magnetic field[10–12] such that the magnetic flux per triangular plaquette is one-half of a flux quantum ($f=1/2$). Using a Ginzburg-Landau analysis, Park and Huse[12] showed that the possible superconducting phases must have a gauge-invariant phase change around each elementary triangle equal to $\pm\pi$ and a gauge-invariant phase change along each wire segment equal to $\pm\pi/3$. They also show that the allowed minimum free-energy states of this model are equivalent to ground states of the XY kagomé antiferromagnet, which are in one-to-one correspondence to the three-color model configurations, modulo a U(1) phase analogous to the one in the Josephson-junction array. The ±1 chirality spin can be immediately read from the value of the (counterclockwise) phase change around each triangle $\pm\pi$, i.e., from the value of the induced flux through each triangle: 0 or 1 flux quantum. Even though this realization seems quite similar to the previous one, there are differences that arise mainly from the fact that time reversal is explicitly broken by the external field in the wire networks. For example, the $\pm\pi$ chiralities do not have the same energy in the case of wires of finite width. We refer the reader to the thorough discussion of the energetics by Park and Huse.[12]

D. Mapping to a constrained Ising model

The hard constraint of the three-color model imposes a hard constraint in the allowed configurations of the chirality ±1 Ising spins. Here we show that in the spin representation the hard constraint requires that any elementary hexagonal plaquette P must have total magnetization:

$$\sigma_P^{\hexagon}=\sum_{i\in P}\sigma_i=\pm 6,0. \tag{1}$$

A similar result was obtained by Di Francesco and Guitter when connecting the folding problem in the triangular lattice to the three-coloring model.[13] In our proof, we make use of phases accumulated along paths on the hexagonal lattice, requiring that these phases are single valued. This approach is more appropriate to the discussion of superconducting systems and their defects (integer and fractional vortices) that we present in this paper.

Indeed, as we show, one can obtain a simple interpretation of the hard constraint by identifying the accumulated phase around any loop lying on links of the hexagonal lattice with the circulation of a vector potential. For concreteness, we will use the example of the Josephson-junction array in the discussion, but the argument is general.

The phase $\theta_{i,a}$ on the edge a of the superconducting triangle i can be written as

$$\theta_{i,a}=\theta_i+\hat{e}_{i,a}\cdot\vec{A}_{i,a}, \tag{2}$$

where $\hat{e}_{i,a}$ is the unit vector that points from the center of triangle i to its ath edge, and the ''gauge'' potential $\vec{A}_{i,a}$ is defined at the center of such segment (see Fig. 3).

The phase difference across a face a between triangles i and j is

$$\theta_{i,a}-\theta_{j,a}=\theta_i-\theta_j+[\hat{e}_{i,a}\cdot\vec{A}_{i,a}-\hat{e}_{j,a}\cdot\vec{A}_{j,a}]. \tag{3}$$

The last term is simply the discrete sum equivalent of $\int d\vec{\ell}\cdot\vec{A}$ (notice that for neighboring sites i,j the unit vectors are opposed, $\hat{e}_{i,a}=-\hat{e}_{j,a}$).

Now recall that one can write $\theta_{i,a}=\theta_i+(2\pi/3)a\,\sigma_i$ and hence the vector potential is such that

$$\hat{e}_{i,a}\cdot\vec{A}_{i,a}=\frac{2\pi}{3}a\sigma_i. \tag{4}$$

What is the corresponding magnetic field? This is simple to answer, by looking at the accumulated phase around a loop. Consider an elementary counterclockwise hexagonal loop. The loop visits six triangles, and the portion of the loop within each triangle enters through face a and exits through face $a-1$ (mod3), so that the accumulation of the vector potential along that portion of the loop is

$$\hat{e}_{i,a-1}\cdot\vec{A}_{i,a-1}-\hat{e}_{i,a}\cdot\vec{A}_{i,a}=\frac{2\pi}{3}(a-1)\sigma_i-\frac{2\pi}{3}a\sigma_i$$

$$=-\frac{2\pi}{3}\sigma_i. \tag{5}$$

The above result, that each of the six sites visited by an elementary hexagon loop contributes $-(2\pi/3)\sigma_i$ to a counterclockwise accumulation of phase around the loop, has a very simple interpretation. Each Ising spin $\sigma_i=\pm1$ corresponds to a $\mp2\pi$ vortex sitting at a vertex of the hexagonal lattice. Each vertex is shared by three hexagons; hence each hexagon can be thought to contain 1/3 of that vortex, as

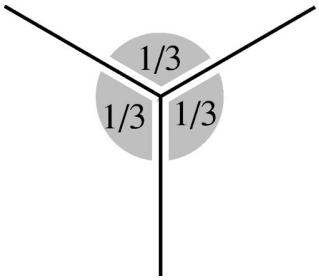

FIG. 4. A vortex sitting at each vertex in the hexagonal lattice is shared by three hexagons. Hence, the contribution to a counterclockwise accumulation of phase around a hexagon encloses one-third of each of the six vortices sitting at the six vertices in the loop.

depicted in Fig. 4. This is why the contribution from the hexagonal path going through vertex i picks up the phase $-(2\pi/3)\sigma_i$ as shown above. Basically, the vortex is divided equally among the three neighboring hexagons sharing the common vertex.

Using Eq. (5) we can now compute the flux encircled by an elementary hexagon on plaquette P; it is given by

$$\Phi_P^{\hexagon} = -2\pi/3 \sum_{i \in P} \sigma_i = -2\pi/3 \sigma_P^{\hexagon}. \tag{6}$$

Therefore the flux enclosed by an elementary hexagonal loop is just 1/3 of the sum of the vorticities in the six sites. Now, matching the color scheme after going around any closed loop requires the phase around any hexagon to be uniquely defined $(\mathrm{mod}2\pi)$, which in turn requires the flux to be a multiple of 2π: $2\pi/3\,\sigma_P^{\hexagon}=0\ (\mathrm{mod}2\pi)$, that is, $\sigma_P^{\hexagon}=\pm 6,0$ (notice that $\sigma_P^{\hexagon}$ is even). Since the total flux inside any loop is given by the sum of the fluxes through each elementary hexagon, then the condition $\sigma_P^{\hexagon}=\pm 6,0$ grants the phase to be uniquely defined $(\mathrm{mod}2\pi)$ around any loop.

Once the $\sigma_P^{\hexagon}=\pm 6,0$ constraint is satisfied, there is a one-to-three mapping of any spin configuration to a configuration of the color model, since there are three even permutations of the colors that produce the same chirality spin configuration.

In the case of the kagomé wire networks at half-flux *per* triangle (or vertex of the hexagonal lattice), each triangle will accommodate either 0 or 1 vortex. So instead of $\sigma_i=\pm 1$ one has a variable $n_i=0,1$. Still, the vortices are split equally into three pieces, and the circulation around a hexagonal plaquette P going through the centers of the kagomé triangles is $(2\pi/3)N_P^{\hexagon}=(2\pi/3)\Sigma_{i\in P}n_i$. The circulation is a multiple of 2π if $N_P^{\hexagon}=6,3,0$. Indeed, the fact that the vortices in the elementary triangles are shared by three sites was used by Park and Huse[12] in their argument for fractionalized vortices in the kagomé superconducting wire networks.

For finite U, there are defects that violate the $\sigma_P^{\hexagon}=\pm 6,0$ constraint; we shall discuss these defects in detail in Sec. IV, where we study integer and fractional vortices, as well as open segments of closed two-color loops. We analyze whether these different defects are confined or deconfined, and their importance in determining the ilk of the processes responsible for the dynamics.

E. Interactions

Each experimental realization of our model contains subdominant effects that may lead to a degeneracy lifting of the ground state. In this paper we concentrate on the effect produced by nearest-neighbor interactions between the chirality spins:

$$H = -\sum_{\langle i,j \rangle} J\sigma_i\sigma_j, \tag{7}$$

where the coupling J depends on the microscopic details of the problem. Such a coupling can arise, for example, if one considers the higher-order effects of having an extended Josephson-junction barrier between two neighboring triangles in the array geometry. In the Appendix we show how to derive the constants U and J from a microscopic Hamiltonian for the array of Josephson couplings and we discuss the conditions for having $U \gg J$. The sign of the J coupling is positive in this case.

This nearest-neighbor interaction leads, in the color language, to an aligning or antialigning interaction between the bonds, depending on the sign of the coupling constant J as it can be easily seen with the help of Fig. 2. For J positive, the spin interaction is ferromagnetic and the zero-temperature ground state (g.s.) of the system has all the bonds with the same color aligned in the same direction. We will refer to this translation invariant state as the FMFS state or single crystal state. For J negative, the spin interaction is antiferromagnetic and the zero-temperature g.s. of the system is a configuration where the six bonds in every hexagon form a sequence of only two alternating colors, which is simply the Néel order in the hexagonal lattice.

In the following section, we discuss the thermodynamics of this system considering only the phase space of the configurations allowed by the ABC coloring constraint or, equivalently, by the $\sigma_P^{\hexagon}=\pm 6,0$ constraint.

III. THERMODYNAMICS OF THE DEFECT-FREE MODEL

A. Small J and the CFT description

Since the model without interactions can be described by a WZNW CFT, it is tempting to use this technique to analyze its behavior for small values of the spin-spin interaction.

The first step is to represent the system by a height model (see Kondev *et al.* for details[5]). Flat configurations of this height model correspond to the different Néel states of the system. In terms of the colors there is a total of six of those configurations which are arranged to form an hexagonal lattice. The coarse-grained version is described by two fields $\vec{h}=(h_1,h_2)$ and a locking potential $V(\vec{h})$ that favors the fields to lie in one of the flat configurations; this potential has then the periodicity of the hexagonal lattice. The action reads

$$S = \int d^2x \left(\frac{\pi}{2} \left| \nabla \vec{h} \right|^2 + V(\vec{h}) \right). \tag{8}$$

In this language, the spin-spin interaction introduces a perturbation which is proportional to the ''locking potential'' since, depending on the sign of J, it favors or opposes the

locking in one of the flat configurations. In the WZNW language, the locking potential can be written as a current-current perturbation of the underlying WZNW model.[5]

When the spin-spin interaction is turned on, we can use this description to propose an action for the perturbed CFT. Since the A,B,C permutation symmetry is preserved, we can argue that the perturbing term to the pure CFT action should read

$$\int d^2x\left[\lambda_H\left(\sum_{i=1}^{2} J_R^{H_i}J_L^{H_i}\right)+\lambda_E\left(\sum_{j=1}^{3} J_R^{\alpha_j}J_L^{-\alpha_j}+J_R^{-\alpha_j}J_L^{\alpha_j}\right)\right], \tag{9}$$

where α_j's are the generators of the root lattice of su(3), and the Cartan generators J^{H_i} are simply given by the derivatives of the height fields ∂h_i. The case $\lambda_E=\lambda_H$ corresponds to the SU(3) symmetric case. The one-loop renormalization-group (RG) equation in this case reads

$$\dot{\lambda}=-\frac{3}{2\pi}\lambda^2, \tag{10}$$

and for $\lambda>0$ the flow is toward the unperturbed level 1 SU(3) WZNW model, which can be identified with the $J=0$ case. In general, however, we just have the A,B,C permutation symmetry, and we cannot exclude the possibility of $\lambda_H\neq\lambda_E$. Defining $\delta\lambda=\lambda_H-\lambda_E$, the RG is now

$$\delta\dot{\lambda}=\frac{1}{\pi}\ \delta\lambda\ \ \lambda_E,$$

$$\dot{\lambda}_E=-\frac{3}{2\pi}\lambda_E^2-\frac{1}{\pi}\ \delta\lambda\ \ \lambda_E, \tag{11}$$

where, at least for a small spin-spin interaction, we assume $|\delta\lambda|\ll\lambda_E$. The RG flow is as follows (see Fig. 5). For $\delta\lambda>0$, the system flows to the line of fixed points $\lambda_E=0$. While the SU(3) symmetry is broken, the system remains critical. We propose that this case corresponds to a ferromagnetic interaction, since it is equivalent to a decrease of the locking potential. This result is valid for small interspin couplings. As we show below, for large enough couplings a first-order phase transition takes place. Since this is highly nonperturbative in the CFT language, this scenario is much better described by the cluster mean-field method that we explain below. For an antiferromagnetic coupling, $\delta\lambda<0$ and the flow goes toward strong coupling, bringing the system off criticality and forcing the system into antiferromagnetic ordering, as was argued by Huse and Rutenberg[14] in their studies of the related classical kagomé *XY* model.

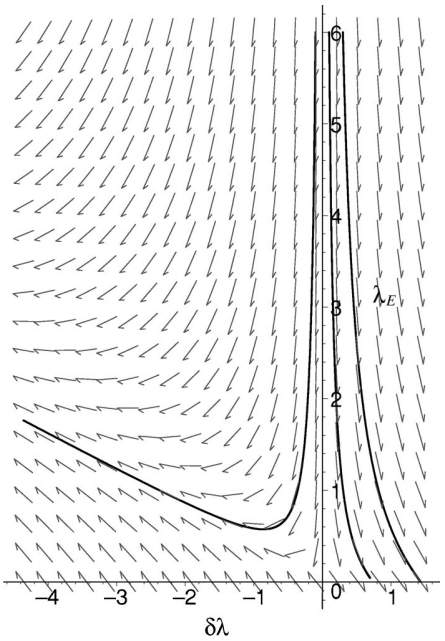

FIG. 5. Diagram of the RG flow for our model, where the horizontal axis corresponds to $\delta\lambda$ and the vertical to λ_E. The solid lines are numerical solutions of the system of equations (11) for three different initial conditions, and are drawn for visualization purposes only.

B. The cluster mean field method: General approach

The CMFM is a technique that has proven to be very powerful in studying structural phase transitions in crystals and the thermodynamics of vertex models.[6] When a system is constrained, fluctuations are considerably reduced and an appropriate mean-field treatment can give very good results if the constraint is taken into account. The idea is to consider as the fundamental entity coupled to a ''molecular'' field, instead of a single spin, a cluster in which the allowed spin configurations are restricted by the constraint. The bigger the cluster, the more accurately fluctuations and constraints are taken into account. This method has given very precise results for the ice model[6] and is a good candidate for giving an accurate picture of our constrained spin model in the hexagonal lattice.

It is particularly simple to introduce the CMFM in the case of a corner sharing plaquette[15] lattice with Hamiltonian

$$H=\sum_{i,j} J_{i,j}\sigma_i\sigma_j+h\sum_i \sigma_i, \tag{12}$$

where the range of the $J_{i,j}$ interaction is shorter than the distance between the two farthest spins in a plaquette. This is the case for the present system. Let us assume that the lattice has N spins and $2N/S$ plaquettes, where each plaquette has S sites. The sums in the Hamiltonian can be rearranged as

$$H=\sum_P\left[\sum_{i,j\in P} J_{i,j}\sigma_i\sigma_j+h\sum_{i\in P}\sigma_i\right]-h\sum_i \sigma_i, \tag{13}$$

where the first sum is over all plaquettes P and the last term compensates for the double counting of the site energy term. The mean-field approximation is obtained by considering each term as the sum over an elementary cluster (of S and 1 spins, respectively) coupled to an effective field representing the interaction with the rest of the lattice:

$$H \simeq \frac{2N}{S}\left[\sum_{i,j\in P} J_{i,j}\sigma_i\sigma_j + (h+\phi_{ext})\sum_{i\in P}\sigma_i\right] - N[(h+\phi)\sigma_i]$$

$$= \frac{2N}{S}H_S - NH_1, \tag{14}$$

where H_S and H_1 are the S- and 1-spin cluster Hamiltonian, respectively. Here, ϕ and ϕ_{ext} are proportional to the number of spins that are external to the cluster but connected to the internal spins. Since for the 1-spin clusters such number of external spins is twice the number for the S-spin clusters, we have $\phi = 2\phi_{ext}$. Let us now define the effective internal energy per spin

$$\varepsilon = \frac{2}{S}\langle H_S\rangle_S - \langle H_1\rangle_1, \tag{15}$$

where $\langle\cdots\rangle_S$ and $\langle\cdots\rangle_1$ are the thermal averages computed with H_S and H_1, respectively. Integrating then over the inverse temperature β we get an effective free energy:

$$\beta F = -\frac{2}{S}\ln Z_S + \ln Z_1, \tag{16}$$

where $Z_i = \mathrm{Tr}\{\exp(-\beta H_i)\}$, $i = S,1$, and the integration constant has been chosen such that in the case of unconstrained spins we get the trivial entropy ln(2) at infinite temperature. Minimizing the effective free energy with respect to ϕ:

$$\frac{\partial F}{\partial \phi} = 0 \tag{17}$$

is equivalent to imposing the self-consistency equation for the magnetization:

$$\langle\sigma\rangle_S = \langle\sigma\rangle_1 \tag{18}$$

and it gives us the optimal value for the field ϕ, which determines the behavior of the system at a given temperature. An important benefit of this method is the fact that it can be extended to larger and larger clusters. This allows us to improve systematically the accuracy of the results.

C. Application of the CMFM to the defect-free model

In order to be able to apply the CMFM to our problem in a straightforward way, it is convenient to switch to a bidual representation and describe our system in terms of spins $S_{ij} = \pm 1$ sitting on the links of the hexagonal lattice (see Fig. 7). These spins are given by the product of the original chirality spins σ_i at the two vertices of each link: $S_{ij} = \sigma_i\sigma_j$. Obviously, the number of configurations of the S spins is half the number of original σ spin configurations, due to the $\mathbb{Z}_2$ invariance of the product $\sigma_i\sigma_j$. The advantage of this mapping is that our lattice becomes now the (corner sharing hexagons) kagomé net in which each spin S_i is shared by two elementary plaquettes. In this description, the Hamiltonian (7) restricted to the nearest-neighbor interaction reads simply

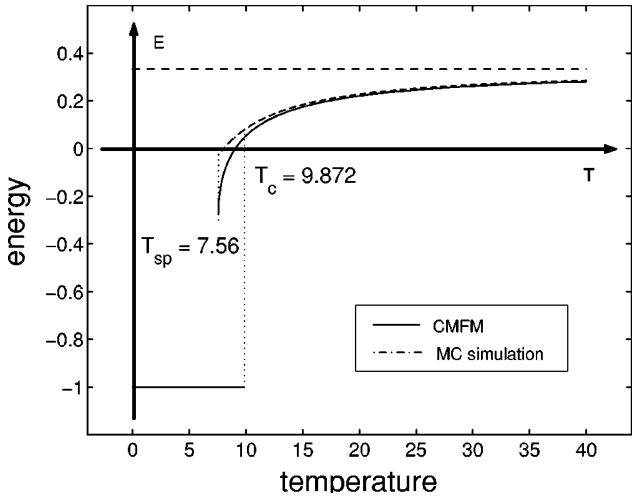

FIG. 6. Plot of the internal energy per link as a function of the temperature (in units of the coupling constant J). The solid line is the prediction from the CMFM and the doted-dashed line is the result from the numerical simulation.

$$H = -J\sum_{\alpha} S_\alpha, \tag{19}$$

where the index α refers to a link of the hexagonal lattice or a site of the bidual kagomé lattice. The CMFM implementation is particularly easy since in this picture we just have an effective magnetic field J in Eq. (12). The clusters that we use are the single-spin cluster and the elementary hexagon cluster (with 11 different configurations for the S spins), and the corresponding partition functions are given by

$$Z_1 = ax^2 + 1/(ax^2),$$

$$Z_6 = a^6x^6 + a^{-6}x^{-6} + 3(ax)^2 + 6/(ax)^2, \tag{20}$$

where $a = e^{\beta J}$ and $x = e^{\beta\phi/2}$. We can now obtain the values ϕ_{opt} corresponding to the minima of the effective free energy. Notice that ϕ_{opt} determines the equilibrium value of $\langle S\rangle$, i.e., of the internal energy per link of the original system. This method predicts the following scenario: for $T \to \infty$ we have $\langle S\rangle = 1/3$, which corresponds to an antiferromagnetic coupling in the system solely due to the constraint. This nontrivial value of the energy density is very close to the result obtained with the numerical method (see Sec. V). The cluster mean-field method also gives a reasonable estimate for Baxter's entropy in the limit $T \to \infty$. Substituting Eq. (20) into Eq. (16) and taking the limit $T \to \infty$ we obtain the entropy per site $S = \ln(11/8)/2 \simeq 1.1726$, while the exact value is 1.2087 . . . . Since the analytical expressions for the forthcoming quantities are too cumbersome, we just mention here their numerical values. At $T \simeq 9.872J$ the system undergoes a first-order phase transition in which the energy density jumps from $\langle S\rangle \sim 0.05$ to a fully polarized state in which $\langle S\rangle$ is exactly -1 (see Fig. 6). This transition has been first noticed via transfer matrix analysis by Di Francesco and Guitter[16] in the context of a folding transition. Our CMFM result is very close to their estimated critical temperature

$(9.1J)$ and even closer to our Monte Carlo estimate $9.6J$ (see Sec. V A 1). In terms of the original spins, this behavior corresponds to the exotic scenario in which the magnetization jumps from 0 to the fully saturated value 1 at the critical point, as was argued by Di Francesco and Guitter.[16] A similar kind of transition is also found in a frustrated spin model on the triangular lattice,[17] which turns out to be equivalent to a dimer model on the hexagonal lattice. Such kind of transition is accompanied by slow dynamics and aging. As we will see below, slow dynamics is also a central issue in our case.

Another temperature that we can compute via the CMFM is the spinodal temperature of the system. This is typical of first-order phase transitions, where an appropriate fast cooling process can avoid crystallization and bring the system into a supercooled liquid phase. The spinodal temperature T_{sp} is the temperature at which the supercooled liquid becomes unstable due to the crystal nucleation process. In this case, we can study the shape of the CMFM effective free energy as a function of ϕ for different temperatures. Starting from $T\sim\infty$ and lowering the temperature, the minimum corresponding to the liquid phase first becomes a local minimum (metastability) and eventually disappears. This metastability limit corresponds to the spinodal temperature $T_{sp}\simeq 7.56$ of the present model.

The choice of the bidual spin representation to implement the CMFM is due to the fact that the system becomes a model for which the CMFM is particularly suitable. Indeed, in terms of the bidual spins, the system becomes a kagomé lattice seen as an array of corner sharing hexagons, in which now the new spins are sitting at the vertices. By associating to each of the 11 configurations for each hexagon its corresponding energy, the model can also be described as an 11 vertex model on the triangular lattice dual to the hexagonal. This choice of variable usually limits the analysis since it does not allow us to measure the magnetization of the system, which is the typical order parameter used to study phase transitions. In the present case however the energy density variable gives very good results in the characterization of the system since the transition is first order. For continuous phase transitions the situation is different. Even though the CMFM still gives a quite accurate result for the numerical value of the energy density (in contrast to the normal mean-field method), it may fail in reproducing a subtle behavior such as an infinite slope point at T_c in the energy vs temperature curve. In this case, measuring the magnetization of the system is a much more powerful tool to detect and study the second-order phase transition. Thus, one needs to get back to the original spins instead of the bidual ones. Implementing the CMFM technique within the context of the real spins has two main disadvantages in our case. On one hand, the spins do not form corner sharing plaquettes, and relating the mean fields acting on the one-spin cluster and on the six-spin cluster becomes more difficult. On the other hand, since the coupling J is a two-spin nearest-neighbor interaction, a single variational mean field cannot take simultaneously into account both the J interaction (for which each spin interacts with its three neighbors) and the effective interaction due to the constraint (for which each spin interacts with all the 12 spins belonging to the three adjacent hexagons).

D. Free-energy argument for a first-order phase transition

The key point for understanding this particular phase transition is to understand the very peculiar nature of its FMFS ground state. As we already discussed before, in the FMFS state all the bonds of the same color are aligned in the same direction. As a result, any two-color loop is maximally straight and winds around the whole system. Thus, the smallest possible rearrangement of the FMFS configuration that produces another allowed configuration is the update of one of such loops. This is a striking feature of the ferromagnetic three-coloring model: the g.s. is separated from the first (1-loop) ''excited'' state by a system-spanning update which costs an energy: $E_{1\text{-loop}}-E_{\text{FMFS}}=2JL$, where $E_{\text{FMFS}}=-3JL^2$ and L is the system size ($2L^2$ sites, $3L^2$ bonds). Notice that if one prepares the system in the $T=0$ FMFS and starts to heat, the system is likely to remain in that state even for $T\to\infty$ for fast enough heating rates. Indeed, such an energy separation is likely to make the FMFS state metastable even for $T\to\infty$, in the thermodynamic limit. Since the FMFS state has zero entropy and the entropy of a straight winding loop is $\ln(3L)$, we can write the free energies of the two states

$$F_{\text{FMFS}}=-3JL^2,$$

$$F_{1\text{-loop}}=-3JL^2+2JL-T\ln(3L). \tag{21}$$

Clearly in the thermodynamic limit the energy cost $\Delta E\sim L$ overwhelms the entropic gain $\Delta S\sim\ln L$ and the excited state will never be favored over the FMFS state at any temperature. A similar argument applies to higher excited states, as long as their entropy is not exponential in the system size. The system is incapable (at equilibrium) to move out of its ground state in a ''smooth way.'' In terms of configurations, it has to jump from a fully ordered state into a state with finite-domain size. Since it is reasonable to assume that a finite-domain-size configuration has negligible magnetization, we can intuitively understand the origin of the complete first-order phase transition observed with the CMFM.

The peculiarity of this transition and the relatively small variation of the internal energy in the disordered phase make it possible to obtain an estimate for the transition temperature by comparing the free energy of the FMFS configuration with the free energy of the disordered configuration. In order to compute the free energy of a disordered configuration, we use the average infinite-temperature internal energy of the system $E_\infty=JL^2$, an estimate derived via the CMFM in the preceding section and confirmed by the numerical results (see Sec. V). Then, we can use Baxter's exact result for the residual entropy as an estimate of the entropy and obtain the free energy of a disordered state at all temperatures:

$$F_{\text{disordered}}=JL^2-T2L^2\ln(1.2087). \tag{22}$$

By comparing the free energy of the FMFS state $F_{\text{FMFS}}=-3JL^2$ with $F_{\text{disordered}}$ we obtain an estimate for the tran-

sition temperature $2J/(\ln 1.2087) \simeq 10.55J$, which is reasonably close to the result from the CMFM $T_c \simeq 9.872J$.

IV. DEFECTS AND THEIR ROLE IN THE DYNAMICS

In this section we discuss the importance of defects in determining how the system can, dynamically, move from one of the allowed low-energy configurations to another. For concreteness, let us start by discussing the Josephson-junction arrays, i.e., the case of $\mathbb{Z}_2 \times \mathrm{U}(1)$ symmetry.

A. Integer vortices

For finite U, it is best to understand the system in terms of the chirality Ising spins, plus XY spin waves of the U(1) sector. The lowest-energy excitations over any configuration with Ising spins satisfying $\sigma_P^{\hexagon} = \pm 6,0$ are topologically trivial (no vortices) XY spin waves.

When $\sigma_P^{\hexagon} = \pm 6,0$ is preserved, vortices of the U(1) sector can only have vorticity that is an integer multiple of 2π. These vortices cost an energy of order of magnitude U, the vortex core energy. The U(1) phase twist leads to the usual logarithmic interaction between a vortex/antivortex pair,

$$\mathcal{E}_1 \propto U 2\pi \ln R. \tag{23}$$

and these pairs are confined below a Kosterlitz-Thouless-type transition at a temperature scale $T_{KT}^{(1)} \propto U$. Since we are interested in the regime of temperatures $T \ll U$ such that the three-color constraint is enforced, these integer vortices will be confined.

Now, what are the accessible excitations that break the $\sigma_P^{\hexagon} = \pm 6,0$ constraint?

B. Fractional vortices

A fractional vortex excitation is illustrated in Fig. 7. Such fractional vortices are always created in pairs via a nearest-neighbor exchange of opposite pointing spins and they have been discussed by Park and Huse[12] in the case of the superconducting kagomé network. A fractional vortex excitation corresponds to a single hexagon that violates the $\sigma_P^{\hexagon} = \pm 6,0$ constraint. We define its fractional vorticity as $\Gamma = 2\pi\nu = (2\pi/3)\sigma_P^{\hexagon} \ (\mathrm{mod} 2\pi)$. Thus, we have $\nu = \pm 1/3$ for $\sigma_P^{\hexagon} = \mp 2$ or $\sigma_P^{\hexagon} = \pm 4$.

The presence of defects causes a fractional accumulation of the link sum of the vector potential $\vec{A}_{i,a}$, the equivalent of $\oint d\vec{\ell} \cdot \vec{A}$ in the continuum limit, that equals $\pm 2\pi/3 \ (\mathrm{mod} 2\pi)$. Once again it is useful to resort to the picture in Fig. 4 to understand that only one-third of the vorticity associated to an Ising spin at a vertex is included in the circulation around an elementary hexagon, and hence the flux is $\frac{1}{3} 2\pi \sigma_P^{\hexagon}$.

To minimize the energy cost across the Josephson junctions, the superconducting phases θ_i in the triangles must adjust accordingly to pick this extra phase difference $\pm 2\pi/3$. Hence, an excited state that breaks the $\sigma_P^{\hexagon} = \pm 6,0$ constraint in the Ising sector must be accompanied by a U(1) phase twist that scales with the distance r from the defect as $1/(3r)$ (in units of the lattice spacing).

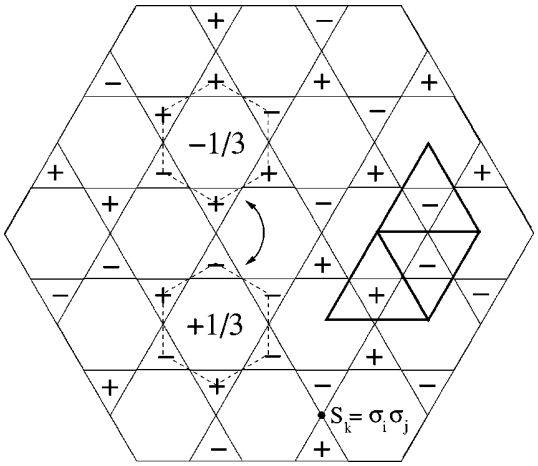

FIG. 7. A pair of $\pm 1/3$ vortices created by a nearest-neighbor spin exchange. The solid-line lattice represents the kagomé network considered by Park and Huse (Ref. 12). The Josephson-junction triangular array is represented instead by the bold triangles. The corresponding hexagonal lattice in our model is shown only around the two defects (dashed line). In the bottom right part of the picture we show the mapping to the bidual representation used in the CMFM.

The U(1) phase twist leads to a logarithmic interaction between a fractional vortex/antivortex pair a distance R apart:

$$\mathcal{E}_{1/3} \propto U \frac{2\pi}{3^2} \ln R. \tag{24}$$

Thermodynamically, there is an entropic contribution to the free energy, which was calculated by Moore and Lee,[9] and shown to also be logarithmic. Therefore, there is a confining transition of the Kosterlitz-Thouless-type at a temperature $T_{KT}^{(1/3)} \propto U/9$. If the Josephson coupling U is large compared to the temperature T, which is the regime we are interested in, then one is deep in the confined phase, and fractional vortices are rather ineffective as a source of phase-space reconfigurations.

C. Open segments of closed two-color loops

There is a special way to flip Ising spins along certain strings lying on the hexagonal lattice that, while violating the $\sigma_P^{\hexagon} = \pm 6,0$ constraint, only costs energy at the extremities of the string, irrespective of its length.

To understand these excitations, let us start by looking at the simple case of a single spin flip that violates the constraint on three neighboring hexagons. In terms of the color model, all colors remain perfectly well defined, with the exception of the one vertex where the spin flip occurred. The energy cost of this defect is of order U. It is possible that locally adjusting the U(1) phase near the defect might slightly relieve this cost, but we have not investigated this

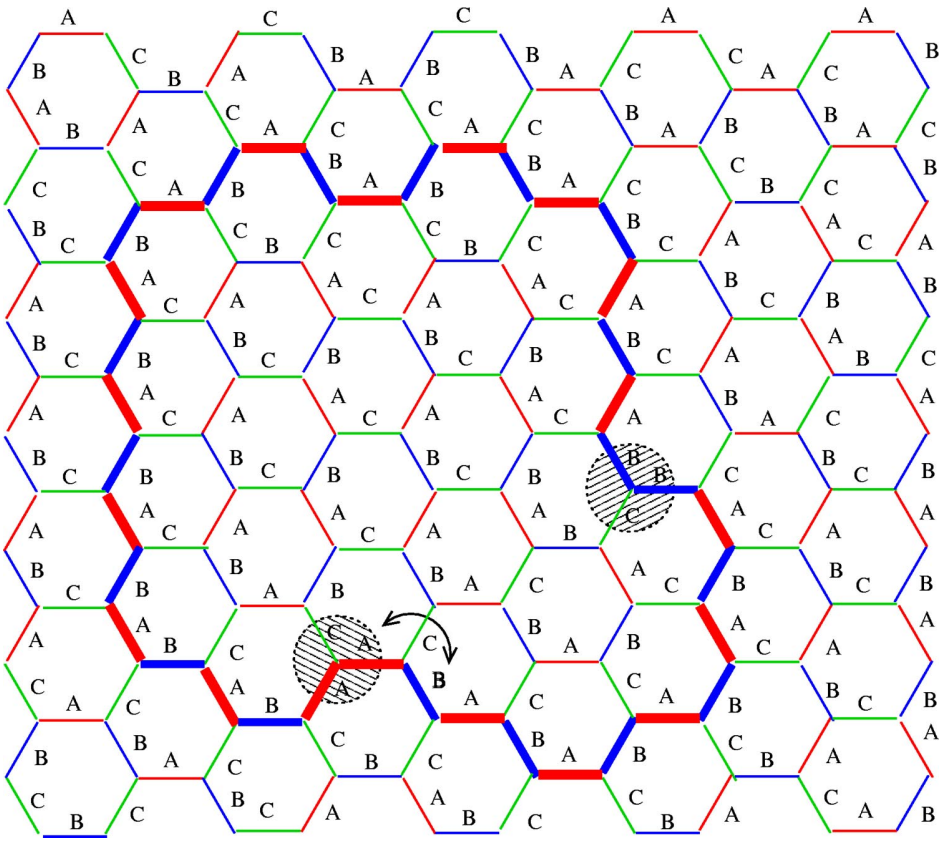

FIG. 8. (Color online) Defect pair at the end points of an open string, with end points highlighted (shaded circles) and the relative two-color path (bold links) shown in a configuration of the three-color representation of the model. The end points can travel freely along the path via nearest-neighbor color exchanges, such as the one outlined by the double arrow. Eventually, the two end points recombine by either exchanging all the bonds along the path or by leaving them all unchanged.

issue. A single spin flip could split into a $+1/3$ and $+2/3$ (or equivalently, a $-1/3$) fractional vortex pair. These, however, are confined together at low temperatures compared to U, as we argued above.

In the three-coloring model, this spin-flip defect corresponds to the initial step of creating an open segment defect described hereafter. Out of the three bonds departing from the spin-flipped site, two must have exchanged color (in order to change the chirality of the vertex), thus violating the color matching with the corresponding two neighboring sites. If we now move these two color defects starting from the two neighboring sites and performing the same original color exchange, we can propagate the defects at zero energy cost along a predefined path. Indeed, every color exchange will fix the previous color mismatch and create a new one, one lattice spacing apart. Notice that this process will flip all the spins between the two end points along the path. It is useful to recall the color description of the allowed low-energy states. Imagine one follows an ABAB . . . sequence that always forms a closed loop in an allowed configuration. We have already seen that flipping the whole loop to BABA . . . maintains the system in an allowed configuration. It is also trivial to show that this update flips all Ising spins visited by the loop. While this is a rather nonlocal move, starting from a single spin flip (color exchange) and propagating the color defects as above, we can realize this move through a sequence of local updates. Instead of flipping the whole loop at once, one can do it in steps, flipping the spins along a piece of the loop sequentially. Notice that the energy cost of this string is paid only at the end points and is of order U, as long as the sequence of spin flips moves on its two-color track. The end points can be thought of as a defect pair connected by a string. This special path is hidden in the constrained Ising representation, but is clear in the three-color one (see Fig. 8). The defect pair, once formed, can diffuse around the one-dimensional loop, and it has two channels to decay back into an allowed state: either the defects recombine by going around the whole loop, leading to the BABA . . . configuration, or they recombine without winding around the loop back to the original ABAB . . . configuration. These are the defects considered by Kondev *et al.*[5] In the CFT description, they correspond to vertex operators with conformal dimension 1/2. While, as we mentioned, for a fixed configuration of colors there is no confining force between pairs, an effective interaction appears because of entropic reasons, producing an algebraic decay with the separation distance for the partition function in the presence of such defects. However, for the dynamics one is really interested in the cost for a given configuration. Therefore, the formation and recombination of these defect pairs constitute the main mechanism responsible for the dynamical evolution of the system.

The defect formation time just enters as an overall rescaling of the time steps for loop updates. Also, since the time it takes for the defects to move diffusively around the 1D loop is algebraic in the loop length (and not exponential), we can neglect this correction and simply treat the whole loop update as a nonlocal elementary move, now with a justified local origin.

V. DYNAMICS

In order to study the dynamic properties of the system, we use Monte Carlo (MC) simulation techniques of an $N=2L^2$-site hexagonal lattice ($3L^2$ bonds) with periodic boundary conditions. As we discussed in Sec. II, the choice of the single-step update is nontrivial due to the color constraint. In Sec. IV we argued that the open segments of closed two-color loops are the main actors in the dynamical evolution of the system, based on energy and confinement considerations. Thus, without loss of generality, we consider only loop updates as single-step updates of our MC technique. We also assume that the rate of formation of the open segment defects is low enough not to allow for defect proliferation (i.e., for the intersection of two different open segments before they recombine).

To implement a loop update we proceed as follows: we first choose one site and two colors at random; then we compute the energy difference in the system for the update of the corresponding loop; eventually we accept or reject the update based on the usual Boltzmann probability. Notice that, with this choice of the single MC step, the update of a loop takes one unit of time, independent of its length. In a possible experimental realization we expect the two ends of an open segment defect to walk randomly along the corresponding closed path, until they recombine. Thus, our MC dynamics is accelerated and the rescaling of our MC time with respect to a possible ''real'' time is highly nontrivial. Since we are interested in studying the slowing down and freezing of the dynamics in the three-coloring model, we choose to use the accelerated loop dynamics in order to be able to sample much longer time scales, otherwise inaccessible with a realistic update mechanism based on defect formation and recombination.

In terms of the loops, one can notice that the two ordered configurations FMFS and Néel (ferromagnetic and antiferromagnetic, respectively) correspond to the two extrema in loop curvature. In the FMFS configuration, the loops are completely straight loops, winding around the whole system. In the Néel configuration, the loops are maximally curved into single-hexagon loops. For these reasons, we expect an entropic jamming in the approach to the FMFS state, for a ferromagnetic choice ($J>0$) of the interaction, as discussed in the case of infinite range interactions by Chakraborty *et al.*[4] Indeed, entropy favors rough and entangled loops, which in the infinite-temperature limit have a fractal dimension equal to 1.5.[5,18] This creates a phase-space bottleneck due to the small number of configurations that allow the system to reach the FMFS state with straight, packed loops. On the other hand, the approach to the Néel state in the antiferromagnetic interaction case ($J<0$) is much smoother for the system. Even though this state has zero entropy by itself, single-hexagon flips allow the system to achieve a gain in entropy of the order of $\ln L^2$ with an energy cost of the order of $6J$. Indeed the Néel state corresponds to the *ideal states* defined by Kondev and Henley,[5] which have maximum entropy density in the sense that they allow for a maximum number of local rearrangements of the spins in accord with the constraint. Thus, we do not expect any jamming phenomena to play a role in this case.

In this section we consider only the case of ferromagnetic interactions and we set $J=1$ as the unit of measure of energies and temperatures. In order to be able to access large simulation times, we choose the smallest system size for which our results do not show a significant dependence on system size ($L=18$).

A. Transition temperatures

1. Estimate of the thermodynamic transition temperature

The first result that we observe both in cooling/heating simulations and in quenching simulations is the phase-space ''isolation'' of the single-crystal phase or FMFS. Even though at equilibrium the system must eventually favor the FMFS, we were unable to reach it within any simulation time, up to 10^7 MC steps. The system prefers to settle into a frozen polycrystalline (P-xtal) phase with zero or close to zero average magnetization, and with very slow, event-dominated dynamics. In Fig. 9 we show the time evolution of the system after a quench in temperature from $T\sim\infty$ to $T=6.0$. After a single MC iteration [Fig. 9(a)], only a few small crystalline seeds are visible in a disordered liquid background. These seeds quickly develop into well-defined domains [Fig. 9(b)], whose size grows with time until the system becomes frozen into the P-xtal phase [Fig. 9(d)]. Notice the domain boundaries following the ''crystalline planes'' of the hexagonal lattice in the polycrystal. The dependence of the crystalline mass m on time t reflects the remarkable slowing down in the dynamics once the system enters the polycrystalline phase.

Even melting simulations starting from the FMFS phase and increasing the temperature are not useful to estimate the transition temperature. Indeed, they result in a large overestimate of T_c, since the melting time remains much larger than the simulation time well above T_c.

The only measure we can achieve of the thermodynamic transition temperature T_c is by computing the free energy in the liquid and crystal phases by integration of the internal energy. For a single crystal we know that $f_{\mathrm{FMFS}}=-1$ at all temperatures, where $f=F/(3L^2)$ is the free energy per bond. For the liquid phase, we use the curves in Fig. 13 showing the dependence of the internal energy on the temperature. Notice that the asymptotic value of the internal energy at infinite temperature is different than zero. This is purely due to the constraint, which appears to be slightly antiferromagnetic in nature. A simple way to visualize this effect is to look at an infinite-temperature configuration after performing a spin-flip operation on one of the two sublattices of the hexagonal lattice. The result is shown in Fig. 10.

An appropriate fit of the common high-temperature region of the internal energy (per bond) curves,[19]

$$\mathcal{E}_{\mathrm{liquid}}(T)=c-a/T^b \tag{25}$$

gives $a\simeq 4.3$, $b\simeq 1.22$, and $c\simeq 0.336$. Notice that a naive high-temperature expansion in powers of $1/T$ may be plagued by the criticality at high temperatures. In this sense

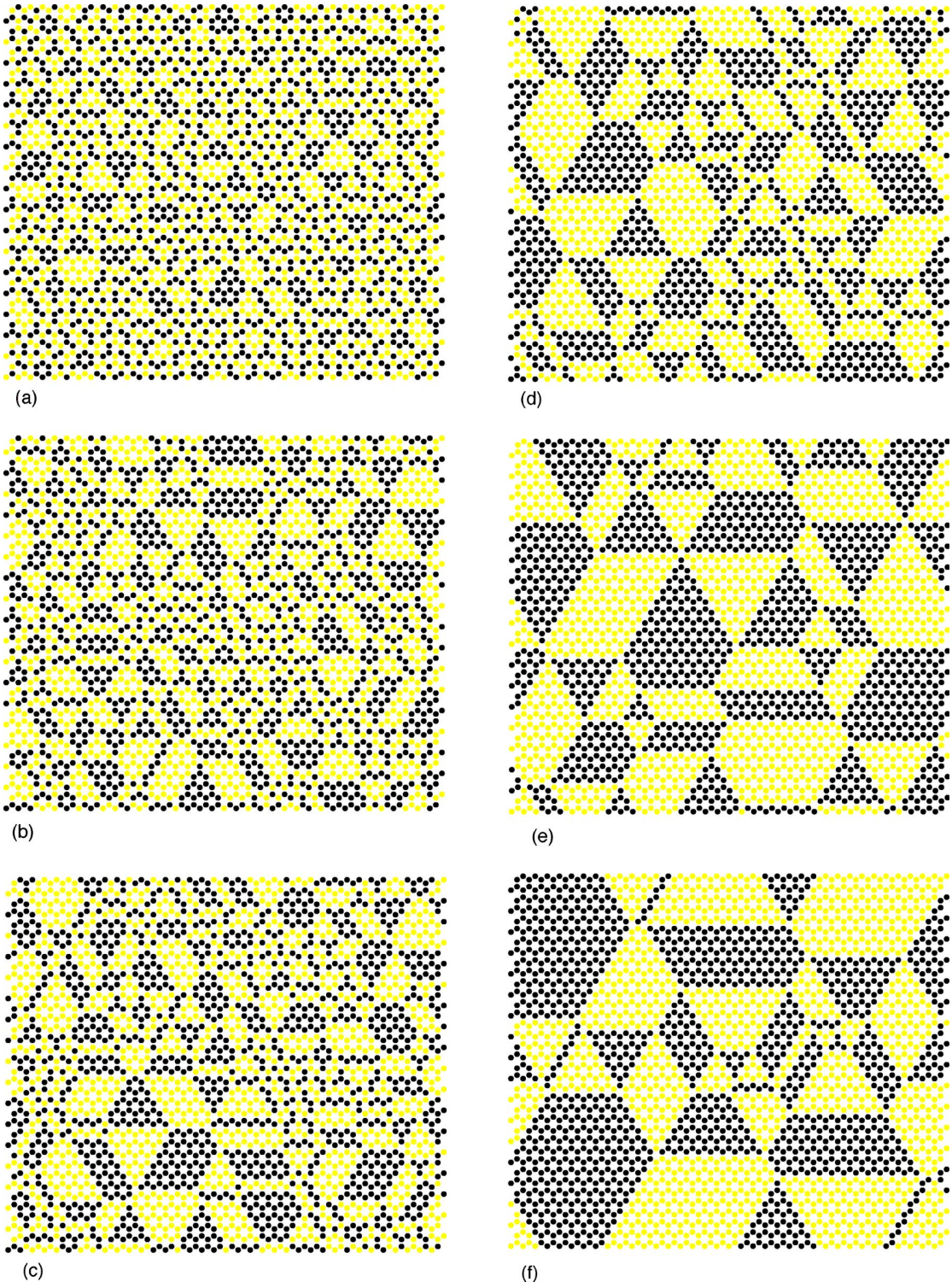

FIG. 9. (Color online) Time evolution snapshots of the system after a quench from $T\sim\infty$ to $T=6.0$ (at time $t=0$) below the transition temperature $T^*\simeq 8.1$. The dots represent the $2L^2$ vertices of the hexagonal lattice ($L=36$) and the two colors correspond to the two values of the chirality spin. The lattice is wrapped along the horizontal axis and along the 60° axis rotated counterclockwise above the horizontal. For each configuration, we report the measured crystalline mass m and the time t from the temperature quench: (a) $m=0.08$, $t=1$ MC step; (b) $m=0.24$, $t=28$ MC steps; (c) $m=0.32$, $t=49$ MC steps; (d) $m=0.50$, $t=192$ MC steps; (e) $m=0.68$, $t=5.7\times 10^4$ MC steps; and (f) $m=0.73$, $t=5.4\times 10^5$ MC steps.

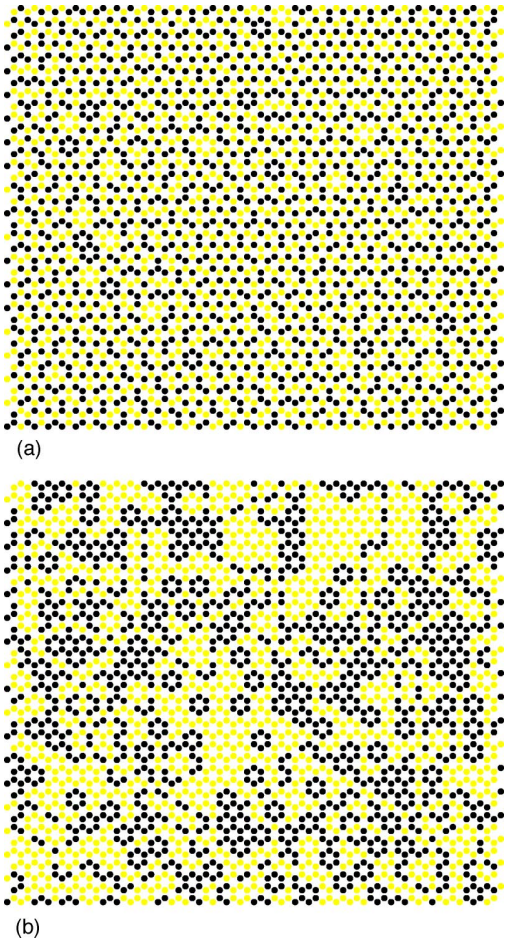

FIG. 10. (Color online) Two pictures of an $L=36$ system configuration at infinite temperature: (a) the original chirality spins; (b) the same configuration after we performed a spin-flip operation on one of the two sublattices. The antiferromagnetic correlations originating solely from the constraint are clearly visible.

the nontrivial exponent b may have an interpretation in terms of the CFT description at $T\to\infty$. We can then integrate to obtain the free energy:

$$\beta f(\beta)=\beta_0 f(\beta_0)+\int_{\beta_0}^{\beta} d\beta' \mathcal{E}(\beta'); \tag{26}$$

setting $\beta_0=0$ for the liquid phase and using the known residual entropy of the system, we obtain

$$f_{\text{liquid}}(T)=-\frac{2}{3}\ln(1.2087)T+c-\frac{a}{(b+1)T^b}, \tag{27}$$

where the 2/3 factor in front of the residual entropy comes from the fact that there are three bonds every two spins. Setting $f_{\text{liquid}}(T)=f_{\text{FMFS}}=-1$ gives the melting temperature $T_c=9.6$, in good agreement with the results from the CMF method.

Even though T_c is the actual thermodynamic transition temperature, we are unable to observe this transition due to the incredibly large time scales involved in the approach to the FMFS state. As it appears from the results below, the system seems to be completely unable to sample the phase-space region corresponding to the crystalline phase, at least on our simulation time scales, and it is confined to an ''effective phase space.''

2. The dynamic freezing transition

Instead of going through the thermodynamic transition, the system remains in a supercooled liquid state below T_c, until it reaches a temperature T^* where it evolves into a frozen polycrystalline state.

Looking at Fig. 9(f), we can clearly see that the polycrystallization is complete, in the sense that the domain boundaries are fully one dimensional, with almost no interstitial liquid left. While the size of these domains increases with longer waiting times, the growth becomes extremely slow, basically stopped within our Monte Carlo time scales before reaching the single-crystal configuration. This can be observed, for example, in the behavior of the zero-temperature saturation value of the energy in Figs. 13 and 14. The energy is in fact a measure of the area-to-perimeter ratio in the polycrystalline phase, provided complete polycrystallization has been achieved. This is clearly the case in the $T\to 0$ plateaus in Fig. 13. Instead of approaching the value -1, characteristic of the FMFS state, these plateaux seem to approach a limiting value $\mathcal{E}^{\text{P-}xtal}(T=0)\sim -0.74$ for larger cooling times.

The transition at T^* can be seen as a dynamic phase transition and does not have a thermodynamic origin. However, we can reasonably establish a correspondence of this transition to a ''true'' thermodynamic phase transition in a related, more constrained system. As we show with the following analysis, the origin of the dynamic transition at T^* resides in a free-energy barrier that prevents the system from visiting a phase-space region around the FMFS phase, at least within our simulation time scales. Since only winding loop updates can change the number of bonds per color per direction, it is possible to divide the phase space into topologically separated sectors by forbidding the update of winding loops. The FMFS configuration would then be in a topological sector by itself, and starting from an infinite-temperature configuration with equal number of bonds per color per direction it would be impossible for the system to reach its natural ground state. With this constraint, the system is expected to show a phase transition into a state which is not the FMFS, with a behavior analogous to the one observed in the present model.

This polycrystal transition is an intrinsic transition of the supercooled liquid phase, which would not exist in the infinite time limit. If we were able to wait infinite simulation times, we expect the dynamic transition at T^* to disappear, replaced by the equilibrium transition at $T_c>T^*$.

Since we cannot apply the same technique used above for T_c to the polycrystalline state, we have to measure T^* with a somehow more empirical method. We first prepare the system into an almost completely polycrystallized state by cooling it at very low rates. We then chose a particular value for the temperature T and let it evolve in time. If it eventually reaches the liquid state, then we conclude that $T>T^*$; conversely if it completes the polycrystallization process. The

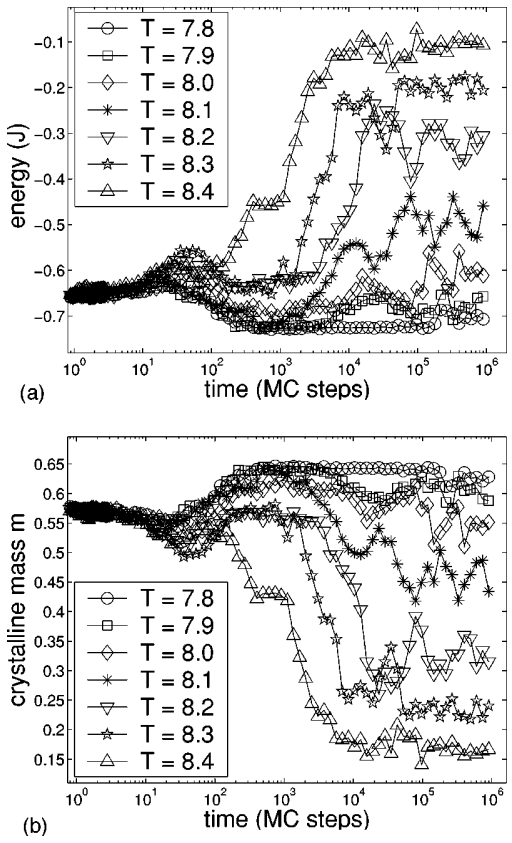

FIG. 11. Time evolution of the internal energy and crystalline mass, after the system has been prepared in an almost polycrystallized configuration. The curves correspond to different quenching temperatures (expressed in units of J) both above and below the transition temperature $T^* \simeq 8.1 \pm 0.1$. Note that all the temperatures are below the thermodynamic transition temperature $T_c \simeq 9.6$, while the system behaves as if it is incapable of visiting the favored FMFS configuration.

choice of the initial state closer to the polycrystalline state rather than to the liquid one is merely due to the stronger metastability of the liquid phase, as it appears from the asymmetry in the hysteretic process with respect to T^* [see Fig. 13(a)]. In Fig. 11 (top) we present the results in terms of time evolution of the energy. Even though we do not have a sharp distinction between the behavior above and below T^*, we can clearly identify a transition at $T^* \simeq 8.1 \pm 0.1$. When the system is set to a temperature $T > 8.2$, it quickly departs from the quasipolycrystallized initial state, while for $T < 8.0$ it completes the polycrystallization process, thus lowering its energy. It is interesting to notice that all the quenching temperatures are below the thermodynamic transition temperature $T_c = 9.6$, while the system behaves as if it is incapable of visiting the favored FMFS configuration.

Since the total magnetization of the system remains close to zero for all temperatures and time scales that we are able to sample, it cannot be used as an order parameter for this transition. A more appropriate order parameter is probably the crystalline mass m, shown in Fig. 11 (bottom). As proposed by Cavagna *et al.*,[20] the crystalline mass measures the fraction of crystallized spins independently of the size of the polycrystals. We first define the elementary crystal unit as the four-spin cluster composed of one spin and its three nearest neighbors. To avoid double counting, we choose the central spin exclusively in one of the two sublattices of the hexagonal lattice. Then, we define the (dimensionless) crystal mass density $m \in [0,1]$ as the number of these elementary units present in a given configuration, normalized by the total number of units L^2. Since we need to keep the elementary unit small enough to be sensitive to small amounts of crystal mass, we have a limited power of resolution. In fact, even a random configuration has a nonzero average crystalline mass $m_0 = 0.01$, which we consider as the effective zero of m. The results obtained by measuring the time evolution of m are in good agreement with the conclusion that $T^* \simeq 8.1 \pm 0.1$.

3. Some considerations on the dynamics of the polycrystal

The data shown in Fig. 11 are averages over 32 different histories starting from the same initial configuration. The reasons for the large time fluctuations and the lack of a sharp distinction between above-T^* and below-T^* behavior, as shown instead in the system studied by Cavagna *et al.*,[20] are to be found in the peculiar, rare-event-dominated dynamics of the polycrystalline phase. It is worth to analyze this dynamics in detail, as it helps understanding also the phase-space isolation of the thermodynamic g.s., i.e., the FMFS crystal.

With some simple reasoning about the colors and the chirality spins, one can see that within a single, ferromagnetically ordered domain, all the bonds of the same color are aligned in the same direction. Thus, any two-color sequence inside the domain follows a straight path from one side to the other along one of the three crystalline directions (or crystalline planes) of the hexagonal lattice. This high level of order is responsible for the first important difference with respect to usual domain growth: there are no small loops across the boundary of a domain (but for possible corner loops) and the domain is not capable of small rearrangements of its walls. While, for example, in a normal Ising model a domain can expand gradually, in our constrained Ising model a domain can only crack from side to side. It is important to notice that these cracks will almost always bring the system into an excited state with higher energy, the energy difference being proportional to the length of the crack.

If we now extend these considerations to the almost complete polycrystalline phase that the system is able to achieve below T^* (see Fig. 9), we can see that any loop has to cross a few domains before closing on itself. In fact, bending of the loops are allowed only at domain boundaries. Therefore, we have a second important difference with respect to usual domain growth: one domain cannot expand at the expenses of a single other domain; rather, the above cracks involve at least six domains (but for the case of winding loops), since every domain boundary corresponds to a 60° bending in the loop. One can easily convince oneself that the closer the system is to the polycrystalline phase, the more the dynamics become frozen, requiring entangled, multiple-domain cracking in order to move from one configuration to another. This behavior can be seen, for example, by looking at the behavior of the spin-spin autocorrelation function [see Eq. (29)],

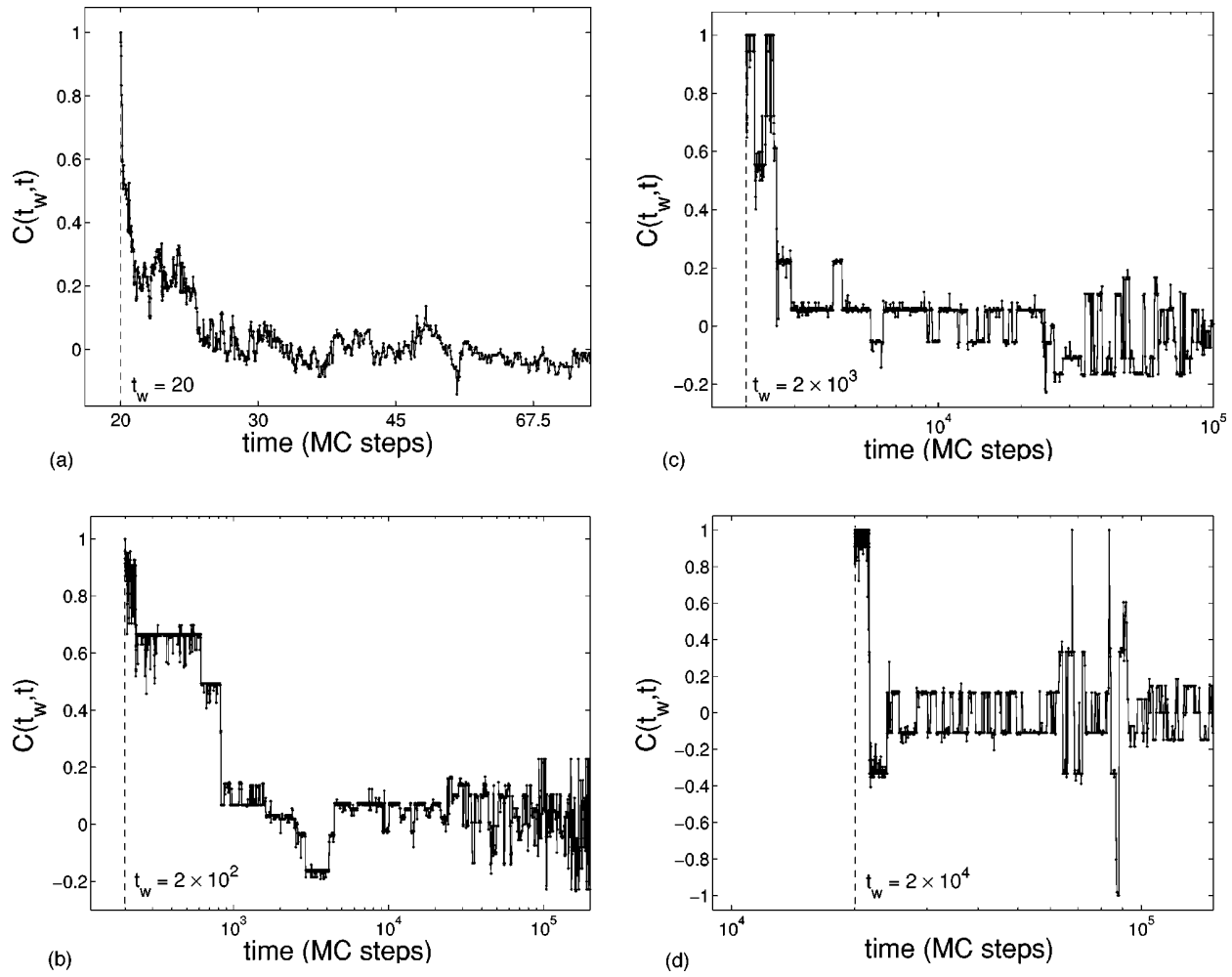

FIG. 12. Spin-spin autocorrelation function $C(t_w,t)$ for a single MC simulation and four different values of the waiting time t_w: (a) $t_w=20$ MC steps; (b) $t_w=2\times10^2$ MC steps. Note the rescaling of the time axis with respect to the previous figure; (c) $t_w=2\times10^3$ MC steps; and (d) $t_w=2\times10^4$ MC steps. The temperature is quenched at $t=0$ from $T=\infty$ to $T=6$, the same used in Fig. 9. At $t_w=20$, the system is still in a rapidly changing liquid phase [see Fig. 9(b)]. As the system gets deeper into the polycrystalline phase at $t_w=2\times10^3$ or even more at $t_w=2\times10^4$ [see Fig. 9(d)], the behavior of the correlation function becomes discontinuous, reflecting a rare-event dominated dynamics where the system undergoes highly nonlocal rearrangements. Notice the $\mathbb{Z}_2$ symmetry of the system [Fig. 12(c)]. When the dynamics become highly entangled in the polycrystalline phase [see Fig. 9(e)], the number of allowed configurations drops dramatically and rearrangements that bring the system from one configuration to its mirror image play a significant role in the evolution of the system.

shown in Fig. 12. For small values of t_w, the system is still in a rapidly changing liquid phase [see Fig. 9(b)], and the correlation function roughly follows the stretched exponential behavior with a very short relaxation time discussed in Sec. V B 2. As the system gets deeper into the polycrystalline phase for $t_w=2\times10^3$ or even more for $t_w=2\times10^4$ [see Fig. 9(d)], the behavior of the correlation function shows how the system now evolves mostly via rare events that are responsible of extended changes in the system configuration. Notice the $\mathbb{Z}_2$ symmetry of the system. When the dynamics become highly entangled in the polycrystalline phase [see Fig. 9(e)], the number of allowed configurations drops dramatically and rearrangements that bring the system from one configuration to its mirror image play a significant role in the evolution of the system [Fig. 12(c)].

It is important to underline the large energy cost of these updates, which scale with the linear size ξ of the domains. Indeed, we can interpret this energy difference as the activation energy $E_A(\xi)$ for domain growth. Processes where the activation energy depends on ξ, or more generally where freezing involves a collective behavior dependent on ξ belong to classes 3 and 4 for growth kinetics.[21] In the following paragraph, we will address this classification in greater detail.

Even if the system is able to overcome the activation energy barrier, the three-coloring constraint plays a new key role in preventing the system from reaching a new configuration. Let us consider an excited state after one loop has been updated in the polycrystalline phase. The system has then three types of updates available: the trivial repair of the crack, with consequent lowering of the energy; an independent update, which requires to overcome a similar activation energy; and the peculiar loop updates that are adjacent to the open crack. Clearly, since a loop update corresponds to flip-

ping all the spins along the loop, the latter update has a vanishing energy cost because the original crack crosses crystalline ordered domains. Thus, the system is able, via these adjacent loops, to expand or contract a crack with essentially equal probability. Indeed we expect this process to be similar in nature to a random walk, with two possible outcomes: the crack eventually contracts and closes on itself, or all the domains involved in the original crack get essentially flipped, with minimal structural change in the original configuration. Notice that the last update in this process is of the repair type, with the system getting back to a lower-energy state. The time to complete this process is the lifetime τ_d of a crack in the system, while the formation time of a new crack is determined by the activation energy barrier $\tau_f \sim \exp[-\beta E_A(\xi)]$. At low temperatures, τ_d is much shorter than τ_f; the system freezes into a specific polycrystalline configuration and the dynamics involve only rare events where entire domains are flipped simultaneously. At temperatures close to T^* instead, τ_d becomes comparable to τ_f and multiple cracks allow the system to deeply rearrange the domains. Notice, however, that it is still a rare-event dependent dynamics. In a typical process of configuration change, the system visits highly excited states with complete ''melting'' of extended areas of the polycrystal, before freezing again into a new polycrystalline configuration . These highly excited intermediary states easily become long lived due to the metastability of the liquid phase, which has instead very fast dynamics (see Fig. 15 and the results hereafter).

B. One-time quantities

1. Energy vs temperature and growth dynamics

In order to get a better insight in the dynamics of the model, we study the behavior of the system through temperature hysteresis with different cooling/heating rates. We vary the temperature from $T=40$, where the liquid phase is stable and equilibrates very easily, down to $T=0$ and up again to $T=40$, with a constant rate given by $r=\Delta T/\Delta t$, Δt being the total time to go from $T=40$ to $T=0$. During these simulations we measure all the relevant quantities in our system: the internal energy, the magnetization, the staggered magnetization, and the crystalline mass. Both magnetizations remain close to zero for any temperature and cooling/heating rate. The behavior of the internal energy is shown in Fig. 13 for some of the cooling/heating rates that we consider. The behavior of the crystalline mass is in agreement with the internal energy and does not provide any additional information.

The hysteresis observed in the energy curves is typical of first-order phase transitions. From Fig. 13 we can see that the hysteresis gets narrower for smaller values of r, indicating a transition temperature that is consistent with our previous estimate $T^* \simeq 8.1 \pm 0.1$ (that estimate is also confirmed by looking at the position of the peaks in the specific heat, measured from the energy fluctuations, for different cooling/heating rates). Notice the asymmetry of the hysteresis toward the liquid phase, particularly evident for large cooling/heating rates, due to the metastability of the liquid with respect to the polycrystalline phase. For large cooling rates,

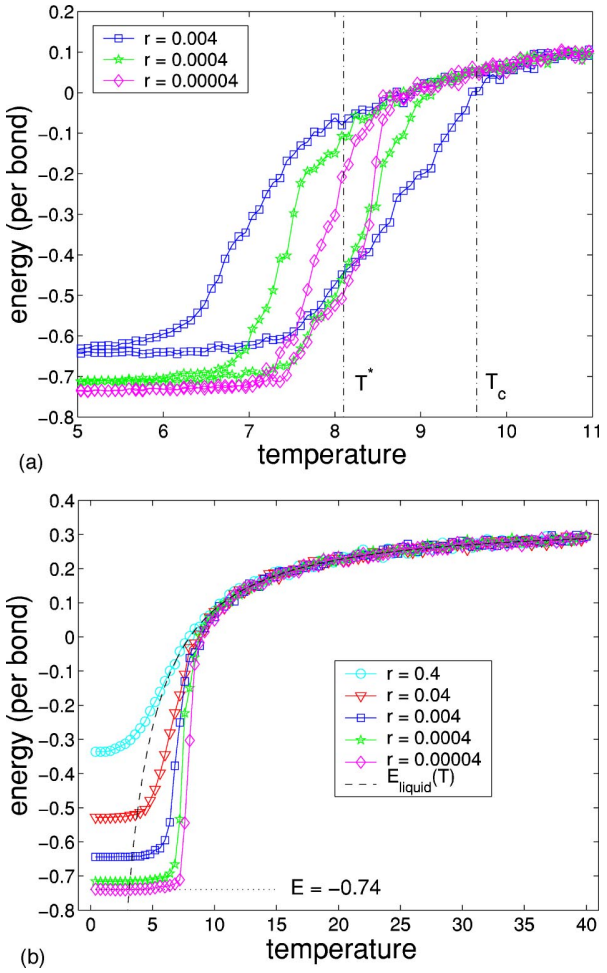

FIG. 13. (Color online) Internal energy vs temperature behavior for our system, in the temperature range $T \in (0,40)$: (a) temperature hysteresis for three different values of the cooling/heating rate: $r=0.04$, 0.004, and 0.00 004. The hysteretic behavior is typical of a first-order phase transition and it is in good agreement with our measure of T^*; (b) cooling curves for five different cooling rates: $r=0.4$, 0.04, 0.004, 0.0004 and 0.00 004. The dashed line is the extrapolated internal energy of the liquid phase [Eq. (25)]. Notice that, for $r=0.4$, the system stays in the liquid phase until $T=0$, since the energy curve remains above the dashed line at any temperature (Ref. 20). Energy and temperatures are in units of J, while the cooling/heating rates are expressed in units of J/MC step. These curves are obtained from simulations where the temperature is changed at a constant cooling/heating rate. For large temperatures ($T>15$), all the curves overlap and the system is at equilibrium in the liquid phase. Notice that there is no sign of the thermodynamic transition at $T_c=9.6$, as the system goes smoothly into the supercooled liquid phase.

see, for example, $r=0.4$ in Fig. 13, the energy curves never cross below the extrapolated $\mathcal{E}_{\text{liquid}}(T)$ curve (dashed line in the figure). Thus,[20] the system does not polycrystallize and it remains in a supercooled liquid phase with respect to the polycrystalline phase until $T=0$ (recall that the liquid is already supercooled with respect to the FMFS phase for $T<9.6$). This is confirmed also by the absence of a peak in the specific-heat curves. As the temperature is lowered to zero,

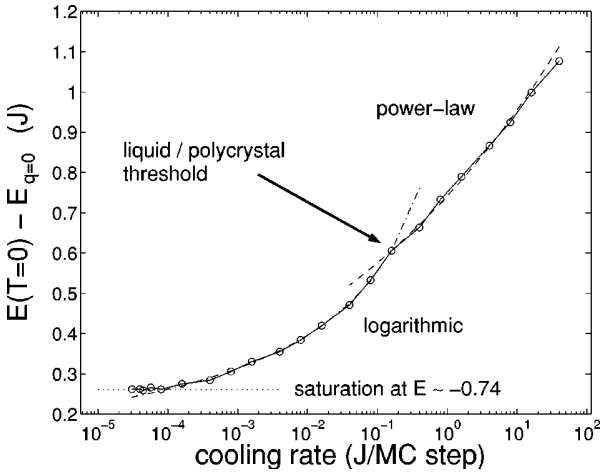

FIG. 14. Semilogarithmic plot of the plateau value of the internal energy with respect to the g.s. energy of the perfect crystal ($\mathcal{E}_{\mathrm{FMFS}}=-1$) vs the cooling rate $r=\Delta T/\Delta t$. Three distinct behaviors can be identified: a power-law behavior $\mathcal{E}\sim r^{0.11}$ for $r>0.2$, when the system remains in the liquid phase; a logarithmic behavior $\mathcal{E}^{-1}\sim\ln(1/r^{0.85})$ for $8\times10^{-5}\leqslant r\leqslant 0.2$; and a saturation plateau at $\mathcal{E}^{\text{P-}xtal}(T=0)\sim-0.74$ for $r<8\times10^{-5}$.

the curves reach a final value of the energy that decreases monotonically with smaller cooling rates. But for very large values of r (larger than 0.4), this final value of the energy is reached already at a finite temperature and the curves show a plateau typical of frozen or very slow dynamics. While we expect this behavior when the system enters the polycrystalline phase, we can notice that this plateau is also present for curves where the system remains in the supercooled liquid phase [e.g., see the curve for $r=0.4$ in Fig. 13]. A detailed analysis of this behavior is beyond the scope of the present paper and will be addressed in the future.

The dependence of the $T=0$ value of the energy on the cooling rate reflects the type of domain growth in the system. In particular, when the system enters the polycrystalline phase where domain boundaries are one dimensional, the energy difference $\mathcal{E}(T=0)-\mathcal{E}_{\mathrm{FMFS}}=\mathcal{E}(T=0)+1$ is proportional to the inverse of the linear size of the domains.[20] In Fig. 14 we show the behavior of $\mathcal{E}(T=0)-\mathcal{E}_{\mathrm{FMFS}}$ as a function of r.

As long as the system remains in the liquid phase, i.e., the energy curves never cross below the extrapolated $\mathcal{E}_{\mathrm{liquid}}(T)$ curve, the energy follows a power-law dependence on r: $\mathcal{E}-\mathcal{E}_{\mathrm{FMFS}}\sim r^{0.11}$. This is typical of class 1 growth kinetics, where freezing originates from local defects with activation energies independent of the domain size ξ.[20,21]

As we lower the cooling rate, we reach a threshold where the energy curves start crossing the extrapolated $\mathcal{E}_{\mathrm{liquid}}(T)$ curve and the system polycrystallizes. This threshold happens at $r_{\mathrm{th}}\simeq 0.2$ and $\mathcal{E}_{\mathrm{th}}\simeq-0.39$. Below this threshold, the behavior of the energy changes abruptly into a logarithmic form:

$$\mathcal{E}(T=0)-\mathcal{E}_{\mathrm{FMFS}}=\frac{1}{1+A\left[\ln\left(\frac{1}{r\tau_1}\right)\right]^m}. \tag{28}$$

From a fit of the results we obtain $m\simeq 0.85$, even though our numerical data do not have enough accuracy to exclude the case $m=1$. If our measurement of $m\neq 1$ is confirmed, it implies that the behavior of our system for $r\in[8\times10^{-5},0.2]$ belongs to class 4 growth kinetics.[21] Both class 3 (corresponding to the case of $m=1$) and class 4 kinetics are typical of processes that involve a ξ-dependent collective behavior in the frozen phase. As discussed above, we indeed expected the system to show this logarithmic behavior.

Eventually, for $r<8\times10^{-5}$ the energy saturates to a limiting value $\mathcal{E}^{\text{P-}xtal}(T=0)\sim-0.74$, in agreement with the entropic argument we provided before. The system behaves as if a whole region of phase space around the FMFS configuration is dynamically inaccessible due to a very large free-energy barrier.

To further confirm this peculiar free-energy landscape, we use again the CMFM described in Sec. III C. From the numerical results, we assume as a first-order approximation that the dynamically excluded configurations correspond to system energies smaller than the limiting value $\mathcal{E}^{\text{P-}xtal}(T=0)\sim-0.74$. We then impose appropriate constraints on the variational parameter such that the only allowed energies in the CMFM are larger than $\mathcal{E}^{\text{P-}xtal}(T=0)$. Under these constraints, the method predicts a first-order phase transition at $T^*\simeq 8.36$, in good agreement with the numerical value $T^*\simeq 8.1\pm0.1$, considering the approximations underlying this CMFM result.

2. Domain nucleation vs liquid relaxation

Here we study the equilibration time of the liquid phase in comparison to the nucleation time for the polycrystalline phase.

We measure the connected piece of the two-times autocorrelation function

$$\mathcal{C}(t_w,t)=\frac{1}{2L^2}\sum_i\langle\sigma_i(t_w)\sigma_i(t)\rangle, \tag{29}$$

where $\langle\cdots\rangle$ indicates the average over initial configurations of different MC simulations. Notice that $\Sigma_i\sigma_i(t)\simeq 0$ for all values of t within our simulation time scale, thus the disconnected piece of the autocorrelation function vanishes. Since we are interested in the relaxation time of the liquid phase at equilibrium, we quench the system from infinite temperature down to the target temperature T and we wait for it to equilibrate. The correlation function becomes time-translation invariant and depends only on the time difference $t-t_w$. At equilibrium, we adequately fit $\mathcal{C}(t-t_w)$ with a stretched exponential, which is the expected equilibrium behavior in supercooled liquids:[20]

$$\mathcal{C}(t)=\exp[-(t/\tau)^\beta]. \tag{30}$$

From the fit we obtain the relaxation time τ as a function of the quenching temperature, as shown in Fig. 15. We can extend the measurement of τ below T^* because of the metastability of the liquid phase. The system is able to equilibrate as a supercooled liquid well before the polycrystal transition takes place, at least for temperatures close enough to T^*.

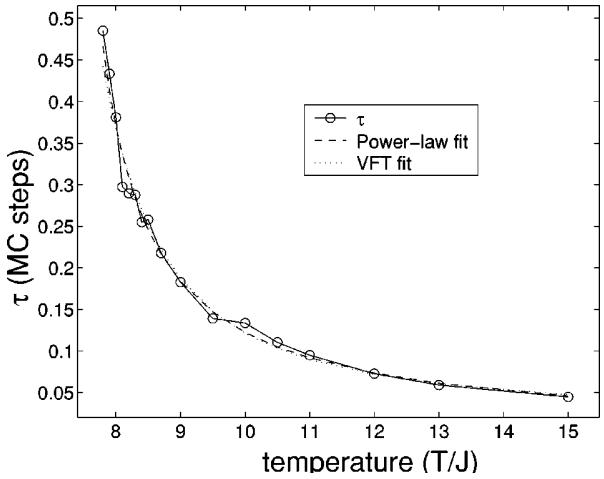

FIG. 15. Liquid phase relaxation time τ as a function of temperature, as measured from the stretched exponential fit of the autocorrelation function at equilibrium. The dashed line corresponds to a power-law fit while the dotted line corresponds to a Vogel-Fulcher-Tamman fit. Notice that there is no dynamic signature of the transition at temperature T^*.

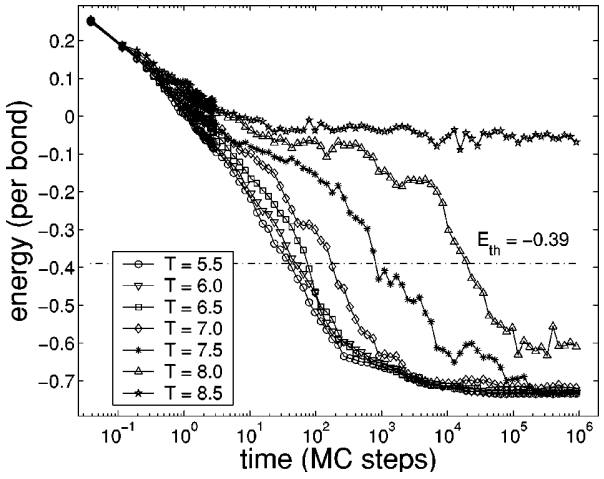

FIG. 16. Time evolution of the energy of the system, after a quench from infinite temperature down to a target temperature $T=5.5,6.0,6.5,7.0,7.5,8.0$, and 8.5 (both energy and temperature are measured in units of J). The horizontal line corresponds to the energy threshold for polycrystallization $\mathcal{E}_{\rm th}\simeq -0.39$, as identified above.

Notice that there is no dynamic signature of the polycrystal transition at T^* in the liquid relaxation time. The Kohlrausch exponent β of the stretched exponential fit decreases with temperature, as for realistic models of liquids. In Fig. 15 we show the fit of the τ data both with a power law,

$$\tau=\frac{A}{(T-T_c^{\rm lq})^{\gamma}},\quad T_c^{\rm lq}=7.0,\quad \gamma=1.0, \tag{31}$$

and with a Vogel-Fulcher-Tamman (VFT) form,

$$\tau=\tau_0\exp\left(\frac{\Delta}{T-T_0}\right),\quad T_0=4.4,\quad \Delta=11.1. \tag{32}$$

The results of these fits have to be considered with extreme care. Because of the accelerated nonlocal dynamics and because of the onset of polycrystal nucleation, the temperature range where we are able to measure the relaxation time of the liquid phase allows for τ to vary only over a narrow interval, from 0.05 to 0.5 MC steps. As a consequence, the values obtained for the fitting parameters lack in accuracy, since the fit spans a single decade of data. Moreover, a VFT behavior typically involves the large τ limit of the $\tau(T)$ curve, which is not accessible in the present system due to the rapid nucleation of the polycrystal. Indeed, our numerical data are the tail of a possible VFT behavior, and they suggest that a VFT behavior may be observed in the liquid phase of this system if the polycrystallization process were to be avoided.

Since the correlation function decays to zero in $\approx 20\tau$, we can take this value as the equilibration time for the liquid phase at a given temperature:[20] $\tau_{\rm eq}(T)=20\,\tau(T)$.

Measuring the nucleation time of the polycrystalline phase in this system is instead more complicated. Due to the frozen nature of the polycrystalline phase, we cannot compute its free energy as a function of temperature as we did for the liquid phase (see Sec. V A 1). Thus, methods such as the one in Cavagna *et al.*[20] are not applicable. More naively, we have to estimate $\tau_{\rm nucl}$ directly observing the time evolution of the system. In Fig. 16 we plot the energy dependence on time for quenches of the system from infinite temperature to the target temperature T. As we discussed above, the system polycrystallizes when the energy falls below a threshold value $E_{\rm th}\simeq -0.39$. Here we use this value in order to identify the onset of the polycrystallization process in the energy curves in Fig. 16. The time when the system starts developing a polycrystalline phase is indeed the nucleation time $\tau_{\rm nucl}$ we are interested in. We can see that $\tau_{\rm nucl}\simeq 800$ at $T=7.5$ while it drops to $\tau_{\rm nucl}\simeq 170$ at $T=7.0$.

Comparing these results with the ones of Fig. 15, provided we perform the rescaling $\tau_{\rm eq}=20\,\tau$, we can see that the crossover $\tau_{\rm eq}=\tau_{\rm nucl}$ will happen at a temperature T_{sp} close to $T_c^{\rm lq}$, where the liquid relaxation time shows a rapid growth. We can reasonably locate this crossover in the temperature range $7.0<T_{sp}<7.5$. This temperature is the spinodal temperature corresponding to the metastability limit of the liquid, when the liquid equilibration time scales become of the same order of the nucleation time scales and the liquid phase becomes unstable. The system reaches this limit in a time t_{sp} of the order of a few hundred MC steps.

VI. CONCLUSIONS

In this paper we have studied the very interesting properties of a model for describing the behavior, both static and dynamic, of different arrays of superconducting devices. Among the examples discussed, the main candidate to see such a rich phenomenology is a Josephson-junction array of triangular grains of superconductors with $p_x\pm ip_y$ order parameter. In the limit of very strong Josephson couplings, the system is equivalent to Baxter's three-color model in the hexagonal lattice. This model can in turn be represented by

an Ising model with a constraint on the total magnetization for each hexagonal plaquette, $\sigma_P^{\hexagon} = \pm 6,0$. In this paper we have presented a proof of this mapping based on the condition of the single valuedness of a superconducting order parameter. The Ising degrees of freedom correspond, in the Josephson arrays with *p*-wave islands, to the chirality of the $p_x \pm ip_y$ order parameter.

Within the constrained $\sigma_P^{\hexagon} = \pm 6,0$ space, the system is critical at infinite temperature but orders at any finite temperature if antiferromagnetic interactions between the Ising spins are present. For ferromagnetic interactions, it remains critical until a very particular first-order phase transition takes place, where the system orders completely. This behavior is due to the peculiar nature of the ordered state, which is isolated in phase space from any of its excitations by an energy of the order of the system size.

For a finite Josephson coupling strength, defects are present in the system, and there are violations of the color and, consequently, $\sigma_P^{\hexagon} = \pm 6,0$ plaquette constraint. A particularly interesting kind of defect is a fractional vortex pair. Within the context of the Josephson array of $p_x \pm ip_y$ superconducting islands, not only there is a large energetic cost to create these excitations, but they are also confined at low temperatures by logarithmic interactions. The other kind of interesting excitation is formed by flipping the spins along open segments of closed two-color loops. While there is also an energetic cost to create them, these defects can circulate on the lattice without further energetic cost, in contrast with the fractional vortices. Moreover, a new defect-free color configuration is obtained through the process of creation of a string of spin-flip excitations, the propagation of the defect along the two-color loop, and the recombination of the ends of the string after closing the loop. This mechanism is precisely the microscopic origin of the Monte Carlo dynamics that we implement in this paper.

Because of the constraint, the dynamics of the system is very peculiar. While the existence of a supercooled liquid phase is typical of first-order transitions, for our constrained system we find a whole temperature range in which such supercooled liquid is stable for extremely long time scales. Indeed, at all the time scales studied in this paper, the fully order phase cannot be reached and the system orders into a polycrystalline phase in which the global $\mathbb{Z}_2$ symmetry is unbroken. The transition from the liquid state to the polycrystal takes place at a critical temperature T^*, smaller than the static (avoided) critical temperature. This dynamical temperature T^* has been obtained both by studying the time evolution of the system after preparing it in a polycrystalline configuration, and by quenching the system from the liquid phase. The values obtained for T^* are in agreement with the naive estimate that we are able to obtain from the CMFM technique. The numerical analysis of the nucleation time and the liquid phase relaxation time allows us to give an estimate of the spinodal temperature of the liquid.

The rich phenomenology of the dynamics of this system is also reflected in the dependence of the difference between the final internal energy reached by the system and that of the fully ordered state on the cooling rate. While for very fast cooling rates this dependence shows a typical power-law scaling, the nucleation of the polycrystalline phase produces a logarithmic behavior until a total arrest in the domain growth is reached, meaning probably another logarithmic growth but with a much longer time scale. The origin of this scenario is the fact that the energy barriers through which the system has to pass to reach states with larger clusters grow with the size of the clusters. This places our system as one of the rare cases without randomness in which the dynamics is of class 3 or 4 in the classification of Lai *et al.*[21]

An important open problem concerns the possible mechanism to get out of the polycrystalline state. Proliferation of other (confined) type defects, such as fractional vortices, is a possible mechanism to help overcome the totally arrested dynamics in the polycrystalline phase. In this case, the large time-scale dynamics could be governed by the energetic cost of making a rather rare-event dominated proliferation and circulation of such (confined) defects. It is noteworthy that, in the polycrystalline phase, not only the fractional vortices are confined (logarithmically, with a prefactor of order *U*), but also the excitations that we argued are responsible for the microscopic dynamics, the open segments of closed two-color loops. The confinement of the two-color segments is proportional to the string length (linear) inside any ferromagnetically aligned domain, with a prefactor of order *J*. The example that we studied in this paper suggests an interesting scenario where defect confinement at the microscopic level is responsible for the slow dynamics and out-of-equilibrium behavior of a macroscopic system.

ACKNOWLEDGMENTS

We would like to thank H. Castillo and M. Kennett for enlightening discussions. We are particularly thankful to B. Chakraborty, D. Das, and J. Kondev for several stimulating discussions that greatly motivated our interest in this problem, and J. Moore for several discussions and correspondence on the issue of superconducting realizations of the model. This work was supported in part by the NSF Grant No. DMR-0305482 (C. Castelnovo and C. Chamon). P.P. would like to thank the warm hospitality of the Boston University Physics Department, where this work was carried out.

APPENDIX: MICROSCOPIC ORIGIN OF THE *U* AND *J* TERMS

In this appendix we estimate the relative values of *U* and *J* in terms of some microscopics for the tunneling through a Josephson barrier. Consider two neighboring triangles as in Fig. 3 sharing a common edge labeled by *a*. The microscopic tunneling Hamiltonian from a triangle labeled 1 to a neighboring triangle labeled 2 can be written as

$$H = -\sum_{\vec{k},\vec{q}} t_{\vec{k},\vec{q}}\; c_{\vec{k}}^{1\dagger} c_{\vec{q}}^{2} + \text{H.c.} \tag{A1}$$

Using second-order perturbation theory, we can estimate from this expression the Josephson coupling between the two superconductors in a standard way. The result is

$$E_J \sim -\sum_{\vec{k},\vec{q}} \frac{|t_{\vec{k},\vec{q}}|^2}{E_\Delta} \langle c^{1\dagger}_{-\vec{k}} c^{1\dagger}_{\vec{k}} \rangle \langle c^{2}_{\vec{q}} c^{2}_{-\vec{q}} \rangle, \tag{A2}$$

where we used $t_{\vec{k},\vec{q}} = t^*_{-\vec{k},-\vec{q}}$ and E_Δ is the superconducting energy gap.

It is useful to define the angles $\phi_{\hat{k}}$ and $\phi_{\hat{q}}$ as those formed by the vectors $\vec{k},\vec{q}$ and the reference unit vector $\hat{e}_{1,0}$. Notice that the ath unit vector $\hat{e}_{i,a}$ is normal to the side labeled by a (see Fig. 3 for the definition of these unit vectors).

The order parameters can be written as

$$\langle c^{1\dagger}_{-\vec{k}} c^{1\dagger}_{\vec{k}} \rangle = (\Delta^1_{\vec{k}})^* = \Delta e^{-i(\theta_1 + \sigma_1 \phi_{\vec{k}})}, \tag{A3}$$

$$\langle c^{2}_{\vec{q}} c^{2}_{-\vec{q}} \rangle = \Delta^2_{\vec{q}} = \Delta e^{i(\theta_2 + \sigma_2 \phi_{\vec{q}})}, \tag{A4}$$

where Δ is the order parameter magnitude, $\theta_{1,2}$ are the overall phases of grains 1,2, and $\sigma_{1,2}$ are the chiralities of the $p \pm ip$ order parameter in each grain.

As we show below, the constants U and J strongly depend on the behavior of $t_{\vec{k},\vec{q}}$, which is in general very difficult to obtain from first principles. For a flat interface, the component of momentum parallel to the junction is conserved, i.e., $k_\parallel = q_\parallel$. If the momenta involved are close to the Fermi momentum (and assuming for simplicity a spherically symmetric Fermi surface), then one has (approximately) that $k^2_\parallel + k^2_\square \approx k^2_F \approx q^2_\parallel + q^2_\square$; hence, $k_\square \approx q_\square$ or $k_\square \approx -q_\square$, corresponding to forward and backward scattering in the normal direction to the barrier, respectively.

There should be a strong suppression of tunneling when the vectors $\vec{k}$, $\vec{q}$ are not normal to the interface. The reason is that the smaller the perpendicular component, the more exponentially suppressed is the tunneling amplitude (for example, consider a WKB approximation: the smaller $k_\square$ and $q_\square$, the lower the particle energy is with respect to the barrier). If $\delta\varphi$ is a small angle that measures deviations from normal incidence and $\phi_{\hat{e}_{1,a}} = (2\pi/3)a$, one can show that the main contribution to the Josephson tunneling Hamiltonian comes from choosing any of the following four combinations:

$$\phi_{\hat{k}} = \frac{2\pi}{3} a + \delta\varphi \quad \text{or} \quad \phi_{\hat{k}} = \frac{2\pi}{3} a + \delta\varphi + \pi \tag{A5}$$

and

$$\phi_{\hat{q}} = \phi_{\hat{k}} \quad \text{or} \quad \phi_{\hat{q}} = \phi_{\hat{k}} + \pi - 2\delta\varphi, \tag{A6}$$

where the last choice corresponds to forward or backward scattering, respectively.

The Josephson coupling can be written in terms of these choices as

$$E_J \sim -\frac{\Delta^2}{E_\Delta} \int d\,\delta\varphi [|t_F(\delta\varphi)|^2 \cos\{\theta_{1,a} - \theta_{2,a} + (\sigma_1 - \sigma_2)\delta\varphi\} - |t_B(\delta\varphi)|^2 \cos\{\theta_{1,a} - \theta_{2,a} + (\sigma_1 + \sigma_2)\delta\varphi\}], \tag{A7}$$

where $t_F(\delta\varphi)$ and $t_B(\delta\varphi)$ are forward and backward small-angle scattering amplitudes (also, recall the definition $\theta_{i,a} = \theta_i + (2\pi/3)a\,\sigma_i$ from Sec. II).

Expanding around small $\delta\varphi$ before carrying out the angular integral, one obtains

$$E_J \sim -[U + J\sigma_1\sigma_2]\cos(\theta_{1,a} - \theta_{2,a}), \tag{A8}$$

where

$$U = \frac{\Delta^2}{E_\Delta} \int d\,\delta\varphi [|t_F(\delta\varphi)|^2 - |t_B(\delta\varphi)|^2](1 - \delta\varphi)^2 \tag{A9}$$

and

$$J = \frac{\Delta^2}{E_\Delta} \int d\,\delta\varphi [|t_F(\delta\varphi)|^2 + |t_B(\delta\varphi)|^2]\delta\varphi^2. \tag{A10}$$

As we discussed above, the barrier is more transparent for close to normal incidence, and can be engineered so that $\delta\varphi$ must remain small, and thus the ratio J/U as obtained above can be made controllably small. The precise condition for having $J \ll U$ depends on the details of $t_{F,B}(\delta\varphi)$. As a simple example, for tunneling through a square barrier in ordinary quantum mechanics, the ratio J/U will depend on the height of the barrier V and on $k_F a$, where a is the length of the barrier. The larger $k_F a$, the smaller J/U. This model may not capture in full detail the underlying physics of the Josephson coupling problem;[22] nevertheless, simple as it is, it shows how the structure of the barrier can be used to tune the ratio J/U.

If $J \ll U$, then in the temperature regime $J \ll T \ll U$ the system is effectively constrained to the three-color manifold of states: $\theta_{1,a} - \theta_{2,a} = 0 (\mathrm{mod} 2\pi)$. In this case, the effective Hamiltonian for the coupling between triangles 1 and 2 is simply

$$H_{1,2} = -J\sigma_1\sigma_2, \tag{A11}$$

with $J > 0$ (ferromagnetic coupling).

[1] P.W. Kasteleyn, J. Math. Phys. **4**, 287 (1963).
[2] E.H. Lieb, Phys. Rev. Lett. **18**, 1046 (1967).
[3] R.J. Baxter, J. Math. Phys. **11**, 784 (1970).
[4] B. Chakraborty, D. Das, and J. Kondev, Eur. Phys. J. E **9**, 227 (2002).
[5] J. Kondev and C.L. Henley, Nucl. Phys. B **464**, 540 (1996); J. Kondev, J. de Gier, and B. Nienhuis, J. Phys. A **29**, 6489 (1996).
[6] V.G. Vaks, V.I. Zinenko, and V.E. Schneider, Usp. Fiz. Nauk **141**, 629 (1983) [Sov. Phys. Usp. **26**, 1059 (1983)]; V.G. Vaks and V.I. Zinenko, J. Phys. C **19**, 3083 (1986).
[7] A.P. Mackenzie and Y. Maeno, Rev. Mod. Phys. **75**, 657 (2003).
[8] There have been recent proposals of order parameters for Sr_2RuO_4 that have nodes along the c axis, but this possibility should not affect the results we discuss in this paper if the c axis is perpendicular to the triangles in the array. The only change is that the superconducting phases θ_i in each triangle will accommodate the sign changes of the order parameter (the phases will change by π) as a function of the vertical distance, along the

c-axis direction. For recent work on the *c*-axis nodes, see M.E. Zhitomirsky and T.M. Rice, Phys. Rev. Lett. **87**, 057001 (2001); H. Won and K. Maki, Europhys. Lett. **52**, 427 (2000); Hae-Young Lee, Yong Baek Kim, and K. Maki, cond-mat/0309156 (unpublished).

[9] J.E. Moore and D.-H. Lee, cond-mat/0309717 (unpublished).

[10] M.J. Higgins, Y. Xiao, S. Bhattacharya, P.M. Chaikin, S. Sethuraman, R. Bojko, and D. Spencer, Phys. Rev. B **61**, R894 (2000).

[11] Y. Xiao, D.A. Huse, P.M. Chaikin, M.J. Higgins, S. Bhattacharya, and D. Spencer, Phys. Rev. B **65**, 214503 (2002).

[12] K. Park and D.A. Huse, Phys. Rev. B **64**, 134522 (2001).

[13] P. Di Francesco and E. Guitter, Europhys. Lett. **26**, 455 (1994).

[14] D.A. Huse and A.D. Rutenberg, Phys. Rev. B **45**, 7536 (1992).

[15] Here by plaquette we mean any closed polygon of spins. The case of more complex spin plaquettes (e.g., with internal spins) requires some nontrivial adjustments in the CMFM.

[16] P. Di Francesco and E. Guitter, Phys. Rev. E **50**, 4418 (1994).

[17] H. Yin and B. Chakraborty, Phys. Rev. Lett. **86**, 2058 (2001); Phys. Rev. E **65**, 036119 (2002).

[18] J. Kondev and C.L. Henley, Phys. Rev. Lett. **74**, 4580 (1995).

[19] The more usual expression $E_{LQ}=c-a\tanh(b/T)$, used, for example, by Cavagna *et al.* (Ref. 20), provides a worse fit than Eq. (25) for our numerical data. Nevertheless, the difference in the transition temperatures derived with the two expressions is less than 0.5.

[20] A. Cavagna, I. Giardina, and T.S. Grigera, J. Chem. Phys. **118**, 6974 (2003).

[21] Z.W. Lai, G.F. Mazenko, and O.T. Valls, Phys. Rev. B **37**, 9481 (1988).

[22] See, for example, G.D. Mahan, *Many-Particle Physics*, 3rd ed. (Kluwer Academic, Dordrecht, 2000).